Inaugural dissertation

for

obtaining the doctoral degree

of the

Combined Faculty of Mathematics, Engineering and Natural Sciences

of the Ruprecht - Karls - University Heidelberg

Presented by

Encarnación Sánchez Salvador (M.Sc.)

born in: Moral de Calatrava, Spain

Oral examination: 05/12/2025

Implication of *N*-glycosylation in the maintenance and degeneration of photoreceptors in the Japanese rice fish *Oryzias latipes*

Referees: Prof. Dr. Joachim Wittbrodt

Prof. Dr. Britta Bruegger

Abstract

Glycosylation is a ubiquitous post-translational modification essential for protein folding, stability, and function. Defects in glycosylation pathways cause congenital disorders of glycosylation (CDGs), multisystem diseases with diverse symptoms. Among these, ocular defects are particularly pronounced, often resulting in photoreceptor degeneration and retinopathies. In a model for ALG2-CDG (Alpha-1,3/1,6-mannosyltransferase-CDG) in medaka (*Oryzias latipes*) it was observed that photoreceptors are especially sensitive to impaired glycosylation. Therefore, I hypothesize that specific glycoproteins are critical for maintaining photoreceptor stability, and that proper *N*-glycosylation is required for their folding, function, and the preservation of retinal structure and visual performance. To address this, I developed a multilayer workflow to identify candidate genes with retina-specific expression and potential *N*-glycosylation dependence. Candidates were prioritized through comparative database analysis and CRISPR-based functional analysis, and precise interventions at predicted glycosylation sites were designed. This strategy allowed to study how specific molecular perturbations affect protein function and retinal development. The analyses revealed that perturbation of potential *N*-glycosylation sequons can substantially alter protein conformation and photoreceptor organization. Even single amino acid substitutions propagated structural changes that influenced photoreceptor differentiation and outer nuclear layer organization. Computational simulations using AlphaFold and GlycoShape provided structural insight, showing how Asn→Gln substitutions can affect folding, polarity, and potential protein interactions, providing a first insight into the observed developmental defects. These findings highlight the essential role of *N*-glycosylation in photoreceptor homeostasis and demonstrate the utility of medaka as a versatile *in vivo* model for studying post-translational modifications. By integrating computational and experimental approaches this work provides a framework to link subtle molecular changes to structural and functional outcomes in the retina, offering insight into the mechanisms underlying retinal development and disease.

Zusammenfassung

Glykosylierung ist eine ubiquitäre posttranslationale Modifikation, die für die Faltung, Stabilität und Funktion von Proteinen unerlässlich ist. Defekte der Glykosylierungsenzyme verursachen angeborene Glykosylierungsstörungen (CDGs), Multisystemerkrankungen mit vielfältigen Symptomen. Unter diesen sind Augenfehlbildungen besonders ausgeprägt, die häufig zu einer Degeneration der Photorezeptoren und Retinopathien führen. In einem Modell für ALG2-CDG (Alpha-1,3/1,6-Mannosyltransferase-CDG) in Medaka (*Oryzias latipes*) wurde beobachtet, dass Photorezeptoren besonders empfindlich auf eine beeinträchtigte Glykosylierung reagieren. Daher nehme ich an, dass bestimmte Glykoproteine für die Instandhaltung der Photorezeptoren entscheidend sind und dass eine korrekte *N*-Glykosylierung für ihre Faltung, Funktion und die Erhaltung der Netzhautstruktur und Sehleistung erforderlich ist. Um dies zu untersuchen habe ich einen schrittweisen Prozess entwickelt, um Kandidatengene mit Retina-spezifischer Expression und potenzieller *N*-Glykosylierungsabhängigkeit zu identifizieren. Die Kandidaten wurden durch vergleichende Analyse von Datenbanken und CRISPR-basierte Funktionsanalysen priorisiert und präzise Eingriffe an vorhergesagten Glykosylierungsstellen wurden konzipiert. Dadurch konnte untersucht werden, wie bestimmte molekulare Störungen die Proteinfunktion und die Entwicklung der Retina beeinflussen. Die Analysen zeigten, dass Störungen potenzieller *N*-Glykosylierungssequenzen die Proteinkonformation und die Organisation der Photorezeptoren erheblich verändern können. Selbst einzelne Aminosäuresubstitutionen führten zu strukturellen Veränderungen, die die Differenzierung der Photorezeptoren und deren räumliche Anordnung beeinflussten. Simulationen mit AlphaFold und GlycoShape lieferten Erkenntnisse zur Proteinstruktur und zeigten, wie Asn→Gln-Substitutionen die Faltung, Polarität und potenzielle Proteininteraktionen beeinflussen können, was einen ersten Einblick in die beobachteten Entwicklungsstörungen ermöglichte. Diese Ergebnisse unterstreichen die wesentliche Rolle der N-Glykosylierung für die Homöostase der Photorezeptoren und zeigen Medaka als vielseitiges *in vivo*-Modell für die Untersuchung posttranslationaler Modifikationen. Durch die Integration virtueller und experimenteller Ansätze bietet diese Arbeit einen Rahmen, um subtile molekulare mit strukturellen und funktionellen Veränderungen in der Retina zu verknüpfen, und liefert Einblicke in die Mechanismen, die der Entwicklung und Erkrankung der Retina zugrunde liegen.

Abbreviations

A	adenine
ABE	adenine base editor
ACEofBASEs	a careful evaluation of base edits
ALG	Asn linked glycosylation
Asn	Asparagine
Asp	Aspartate
ATF	activating transcription factor
bp	base pair
C	cytosine
Cas9	CRISPR-associated system 9
CBE	cytosine base editor
CDG	Congenital Disorders of Glycosylation
cDNA	complementary DNA
CHOP	CCAAT/enhancer-binding protein homologous protein
CMZ	ciliary marginal zone
cone	Cone photoreceptor
COS	Centre for Organismal Studies
crispant	CRISPR/Cas9 edited embryos
CRISPR	clustered regularly interspaced short palindromic repeats
crRNA	CRISPR RNA
***cr/tr*RNA**	CRISPR tracer RNA
Cys	cysteine
DAPI	4’,6-diamidino-2-phenyindole
DNA	deoxyribunuleic acid
dNTPs	deoxynucleoside triphosphate
Dol	dolichol
Dol-P	dolichol phosphate
dpf	days post fertilization
dph	days post hatch
DBS	double-strand break
E. coli	*Escherichia coli*
E3	ubiquitin ligase
ECM	extracellular matrix
editant	base edited embryos

elovl4b	*Elongation of the very long fatty acid chain4*
ER	endoplasmic reticulum
ERAD	ER-associated protein degradation
ERG	electroretinogram
ERM	embryo rearing media
EtBr	ethidium bromide
F	generation
F0	injected generation
F1	first generation
fwd	forward
G	Guanine
GalNac	*N*-Acetylgalactosamine
GCL	Ganglion cell layer
gDNA	genomic DNA
GDP	guanosindiphosphat
GFP	green fluorescent protein
GlcNac	*N-acetylglucosamine*
Gln	Glutamine
Gly	Glycine
GPCR	G protein-coupled receptor
GPI	glycosylphosphatidylinositol
h	hours
HDR	homology-directed repair
Het	heterozygous
HF	homology flank
Hom	homozygous
I	inosine
Ile	Isoleucine
Indel	insertion/deletion
INL	inner nuclear layer
IdoA	iduronic acid
IPL	inner plexiform layer
IRE1	inositol requiring enzyme 1
KO	knockout
Leu	Leucine
LLO	lipid-linked oligosaccharide

Man	mannose
min	minute
ml	milliliter
mM	millimolar
MPI	mannose phosphate isomerase
mRNA	messenger RNA
n	sample number
N	Asparagine
ng	Nanogram
NHEJ	non-homologous end joining
OMR	optomotor response
O/N	overnight
oca2	*Oculocutaneous albinism II*
ol	*Oryzias latipes*
ONL	outher nuclear layer
OPL	outer plexiform layer
opn1sw	*Short wave opsin 1*
OST	oligosaccharyltransferase
P	phosphate
PAM	protospacer adjacent motif
PCDH	protocadherin
PCR	polymerase chain reaction
PERK	proteins kinase R-like ER kinase
POMT	protein O-mannosylation protein
Pro	Proline
PTM	post-translational modification
Q	Glutamine
rev	reverse
RFT1	oligosaccharid-Translocationsprotein RFT1 Homolog
RNA	ribonucleic acid
rho	*Rhodopsin*
rod	rod photoreceptor
RP	retinitis pigmentosa
RPE	retinal pigmented epithelium
rpm	rounds per minute
RT	retrotranscriptase

sd	standard deviation
T	thymine
TB	terrific broth
Thr	threonine
tnc	*tenacine*
tracrRNA	transactivating CRISPR RNA
Trp	triptophane
UPR	unfolded protein response
UV	ultraviolet
WT	wild-type
Xyl	xylose
Xxx	any aminoacid
µl	microliter
µM	micromolar
µm	micrometer

Table of Contents

1 Introduction 1

1.1 Glycosylation 1

1.2 ER-resident glycosylation 3

1.2.1 *N*-glycosylation 4

1.2.2 ER associated degradation and Unfolded Protein Stress 7

1.3 Congenital Disorders of Glycosylation 9

1.3.1 Neural vulnerability in CDG 10

1.3.2 Ocular involvement in CDGs 12

1.4 Development and structure of the vertebrate eye 13

1.4.1 Congenital eye diseases 15

1.4.2 Rhodopsin as a model for glycosylation in retinitis pigmentosa 16

1.5 Genome editing tools for perturbing *in vivo* gene and protein function involved in glycosylation and retinal homeostasis 16

1.5.1 Genome editing mediated by CRISPR-Cas9 induced DSBs 17

1.5.2 CRISPR-Cas9 Base Editors 18

1.6 Medaka as a model for human diseases 18

1.6.1 Glycosylation disorders modeled in medaka 19

1.6.2 Alg2 medaka model shows strong eye defects 20

2 Hypothesis and Aims 23

3 Results 25

3.1 Identification of glycosylation-dependent candidate genes in retinopathies 25

3.2 Precise CRISPR-Based Screening targeting the *N*-glycosylation sequon of the candidates 28

3.2.1 Precise targeting of the *N*-glycosylation site using Adenine Base Editors 28

3.2.2 HDR mediated mutation of the *N*-glycosylation motifs as an alternative route to candidate gene validation 30

3.2.3 opn1sw knockout impacts ONL integrity 33

3.2.4 *rhodopsin* mutants displayed severe defects in visual function 35

3.2.5 Morphometric workflow of retina photoreceptor populations 39

3.3 mRNA Rescue of CRISPR/Cas9 Knockouts to Assess Glycosylation in Medaka Retinal Development 44

3.3.1 Wild-Type *rhodopsin* mRNA restored rod photoreceptor stability during early development in *rhodopsin* KOs 45
3.3.2 mRNA rescue of *opn1sws* highlights the role of asn10 in retinal integrity....48
3.3.3 Functional analysis of *elovl4* via mRNA rescue indicates critical developmental roles independent of glycosylation....51
3.3.4 pikachurin mRNA rescue highlights critical roles in embryonic development and photoreceptor integrity 53

4 Discussion 57

4.1 Evaluating candidate genes and the constraints of CRISPR-based editing 58

4.2 Glycosylation in *rhodopsin* is essential for rod survival and ONL organization 60

4.3 Site-specific glycosylation in *opn1sw* shapes cone photoreceptor organization 61

4.4 Elovl4 glycosylation modulates photoreceptor layer structure 62

4.5 Pikachurin glycosylation coordinates photoreceptor differentiation and ONL integrity..63

4.6 *In silico* modeling provides mechanistic insight into glycosylation-dependent protein stability....64

4.7 Stable knockout lines demonstrate gene-specific contributions to retinal structure and visual function 66

5 Conclusions and Outlook 67

6 Materials & Methods....69

6.1 Materials....69

6.1.1 Bacteria 70
6.1.2 Plasmids 70
6.1.3 Primers....71
6.1.4 cr/trRNAs 73
6.1.5 Antibiotics 74
6.1.6 Enzymes and buffers 74
6.1.7 Chemical and reagents....75
6.1.8 Antibodies 76
6.1.9 Commercial kits....76
6.1.10 Buffer and solutions 76
6.1.11 Consumables 78
6.1.12 Equipment and Instruments....79
6.1.13 Sofware and online tools....80

6.2 Methods 80
6.2.1 Fish husbandry 80
6.2.2 Molecular cloning 81
6.2.3 Plasmid Preparation 84
6.2.4 mRNA *in vitro* synthesis 85
6.2.5 crRNA 86
6.2.6 Microinjections and phenotypes 87
6.2.7 Sanger sequence genotyping of crispants and editants 91
6.2.8 Functional and behavioural analysis of mutant stable lines 91
6.2.9 mRNA rescue injections 93
6.2.10 Immunohistochemistry of medaka hatchlings retina 94
7 Appendix 97
7.1 Supplementary data 97
7.2 Supplementary figures 129
8 References 141
Acknowledgements 162
Publication 166
Declaration 168
List of Figures 170
List of Tables 172

"Nothing in life is to be feared, it is only to be understood. Now is the time to understand more, so that we may fear less."
Marie Skłodowska-Curie

1 Introduction

Life relies on functional biomolecules, particularly proteins, which perform the vast majority of cellular tasks. To achieve proper activity and regulation, proteins undergo post-translational modifications, chemical changes that modulate their stability, localization, and interactions. More than 400 post-translational modifications have been described, reflecting the complexity of cellular regulation. Among these modifications, some, such as glycosylation, are highly prevalent and critical for cellular physiology, yet many aspects of their functional roles remain to be fully understood.

1.1 Glycosylation

Glycosylation is an essential posttranslational modification, in which different oligosaccharides, or glycans bind covalently to proteins or lipids. It is a very well conserved pathway within the different kingdoms in nature (Moremen et al., 2012). Glycosylation plays and key role in protein folding, stability, trafficking and signalling, as well as cell-cell adhesion and modulation of the immune recognition (Varki, 2017; S. Wang et al., 2020). To date glycan structures and their assembly is well understood, yet protein functionality linked to differential residue glycosylation remains elusive.

The glycans are formed by the attachment and combination of ten different monosaccharides, such as mannose (Man), fucose (Fuc), galactose (Gal), glucose (Glc), sialic acid (SA), N- acetylgalactosamine (GalNAc), N-acetylglucosamine (GlcNAc), glucuronic acid (GlcA), iduronic acid (IdoA), and xylose (Xyl). These

monosaccharides give rise to complex glycans, and enable more than thousands of different combinations to be created per cell. In mammalian cells, it is estimated that, out of 700 proteins capable of catalyzing reactions for glycan assembly, 200 are glycosyltransferases (Moremen et al., 2012; Schjoldager et al., 2020).

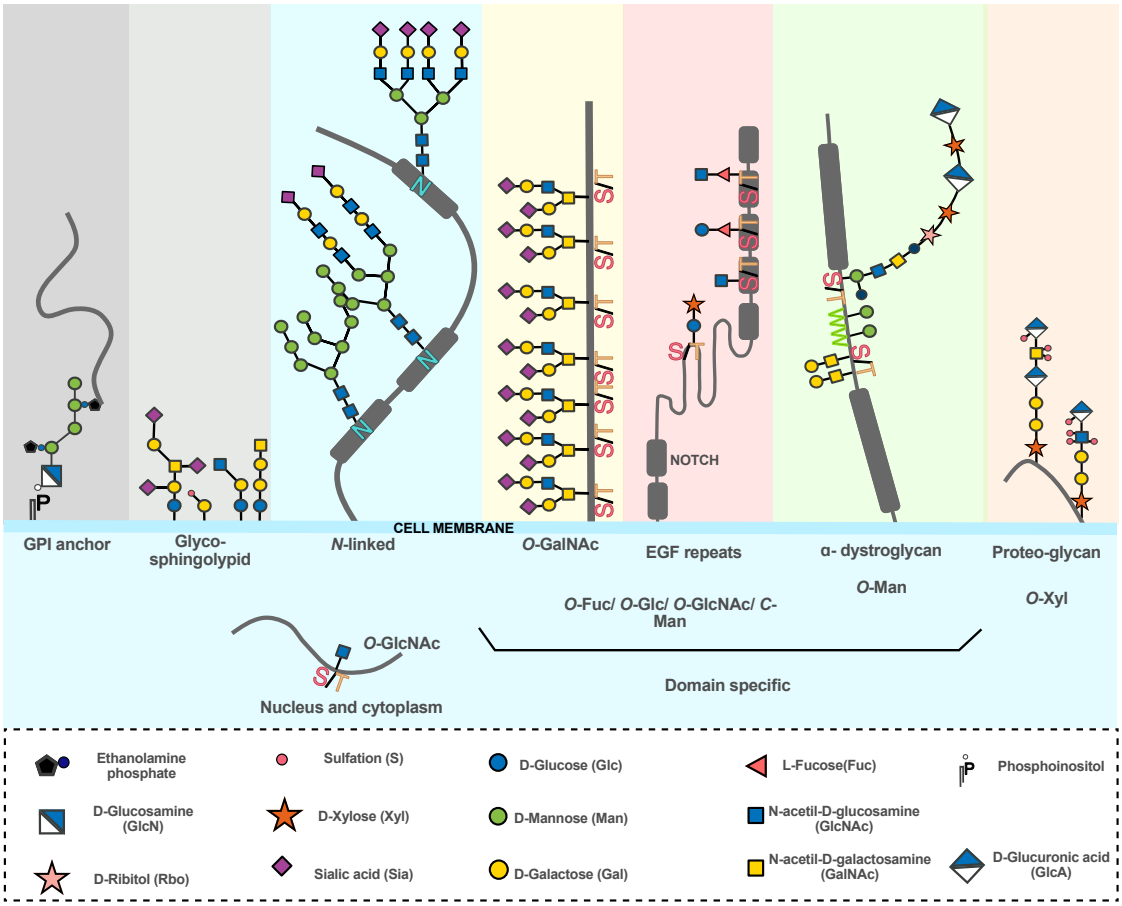

Figure 1. Schematic overview of major glycosylation types. Protein glycosylation primarily occurs as N-glycosylation, where glycans are attached to asparagine (N) residues, and O-glycosylation, which targets serine (S) or threonine (T) residues. Some O-glycosylated proteins are localized in the cytosol and nucleus, while others are anchored to the cell membrane via glycosylphosphatidylinositol (GPI) moieties. C-glycosylation, a relatively rare modification, involves mannose attachment to tryptophan (W) residues. Membrane lipids, such as sphingolipids, can be glycosylated to form glycosphingolipids. Adapted from *(Schjoldager et al., 2020).*

Six main types of glycosylation have been described based on the target residue and linkage with the glycan: *N*-linked, *O*-linked, and *C*-linked glycosylation, glypiation, and phosphoglycosylation as protein glycosylation, and sphingolipid glycosylation as lipid glycosylation (Moremen et al., 2012; Schjoldager et al., 2020) (Figure 1). *N*-linked glycosylation is the most common type of glycosylation, where the GlcNAc residue of the glycan is attached to the asparagine (Asn) of a nascent protein within the

consensus Asn-Xxx-Ser/Thr, (Xxx never beig proline (Pro); via amide (Nitrogen-Carbon) linkage (Reily et al., 2019; Varki et al., 2022). *O*-linked glycosylation is a diverse type of glycosylation, in which a variety of mono- and oligosaccharides(GalNAc, GlcNAc, Xyl, Man, glycosaminoglycans (GAG)) etc., bind through a glycosidic (Oxygen-Carbon) bond to serine (Ser) or threonine (Thr) and more rarely tyrosine (Tyr), Hydroxylysine (Hyl) or Hydroxyproline (Hyp) residues. This event takes place mainly in the cytoplasm and nucleus (Reily et al., 2019; Varki et al., 2022). Other types of glycosylation, which happened more rarely, are: *C*-linked glycosylation, which is a Carbon-Carbon linkage of a mannose to tryptophane (Trp); and *S*-linked glycosylation, where the linkage is a Carbon-Sulfur bond between the glycan and a cysteine (Cys) (Chen et al., 2023; Reily et al., 2019; Varki et al., 2022). Glypiation refers to the attachment of glycosyl-phosphatidylinositol (GPI) for the proper anchoring to the cell membrane (Roller et al., 2020). Phosphoglycosylation, is the attachment of carbohydrates to Ser residues by phosphodiester bond (Haynes, 1998) while lipid glycosylation can occur by the conjugation of glycans to lipids, such as glycosphingolipids, contributing to membrane architecture (Reily et al., 2019).
Collectively, these factors make glycosylation one of the most complex types of posttranslational modifications.

1.2 ER-resident glycosylation

Glycosylation is a very ubiquitous process, happening at different locations in the cell. The Endoplasmic Reticulum (ER) is a key place for glycosylation in which *O*-mannosylation, *C*-mannosylation and *N*-glycosylation are performed.
O-mannosylation is a highly conserved modification in eukaryotes(Hang et al., 2022), where the protein *O*-mannosyltransferase family (PMTs in fungi, and POMTs in vertebrates) catalyzes the transfer of a GDP-mannose to a Ser or Thr residue of a nascent protein. This Mannose can later be elongated in the ER or Golgi to more complex conformations (Neubert & Strahl, 2016; Praissman & Wells, 2014). The main substrate of this pathway is α-dystroglycan, cadherins, protocadherins, and plexins; key players in cell-cell recognition, signal transduction and cell migration(Hang et al., 2022).

C-mannosylation is the rarest glycosylation type that takes place in the ER. In this pathway an α-mannose is attached to the first Trp residue that forms the motif Trp-Xxx-Xxx-Trp/Cys, in the nascent protein. This reaction is catalyzed by the *C*-mannosyltransferases. The most common substrates for this type of glycosylation are the thrombospondin type I repeat (TSR) superfamily and the cytokine receptor type I family, having an important role in folding, sorting and secretion of those substate (Minakata et al., 2021).

1.2.1 *N*-glycosylation

N-glycosylation is the most complex, and abundant type of glycosylation that takes place in the ER. Of all proteins, around 70% are estimated to be glycosylated and of those 90% are *N*-glycosylated (Apweiler et al., 1999). *N*-glycosylation consists of the transfer of the lipid link oligosaccharides (LLOs) covalently to the nitrogen of an Asn residue, as part of the canonical motif Asn-Xxx-Ser/Thr (Xxx being any amino acid except proline) (Reily et al., 2019; Varki et al., 2022).

The assembly of the LLO is performed by different enzymes in a stepwise manner. It is initiated in the cytoplasm by the synthesis of the GDP-mannose, and elongated in the ER membrane with the dolichol-phosphate mannose (Dol-P-man) and dolichol-phosphate glucose (Dol-P-Glc). These are the main subtracts for the asparagine linked glycosylation (ALG) enzymes responsible to catalyse the stepwise extension of the LLO (Figure 2).

The initial steps of *N*-glycosylation occur on the cytoplasmic side of the ER. Here, *N*-acetylglucosamine-1-phosphate (GlcNAc-1-P) is linked to dolichol phosphate (Dol-P) by the glycosyltransferase DAPGT1, followed by the addition of a second GlcNAc residue mediated by the ALG13/14 complex. Once Dol-P-P-$GlcNAc_2$ is assembled, it is elongated with five mannose residues by ALG1, ALG2, and ALG11, yielding Dol-P-P-$GlcNAc_2Man_5$. This intermediate LLO is then translocated to the luminal side of the ER by the flippase RFT1. Subsequent elongation by ALG3, ALG9, and ALG12 adds four additional mannoses, generating the secondary branching of the LLO. The final assembly steps involve the attachment of three glucose residues by ALG6, ALG8, and ALG10, resulting in the fully assembled LLO, Dol-P-P-$GlcNAc_2Man_9Glc_3$ (Helenius & Aebi, 2004).

The mature LLO is subsequently transferred a consecutive aminoacid sequence, known as sequon, in the nascent polypeptides by the oligosaccharyltransferase (OST) complex, with the assistance of associated complexes such as the Sec61 translocon (Freeze et al., 2015; Price et al., 2011). Immediately after transfer, the terminal glucose residues and one mannose are removed, allowing the nascent glycoprotein to bind to the lectins calnexin and calreticulin. These chaperones facilitate proper protein folding and target the polypeptide for the ER quality control cycle (ERQC) (Q. Wang et al., 2015). Polypeptides that successfully pass ERQC are transported to the Golgi apparatus, where the glycans may undergo further maturation into complex structures (Fisher et al., 2019; Varki et al., 2022).

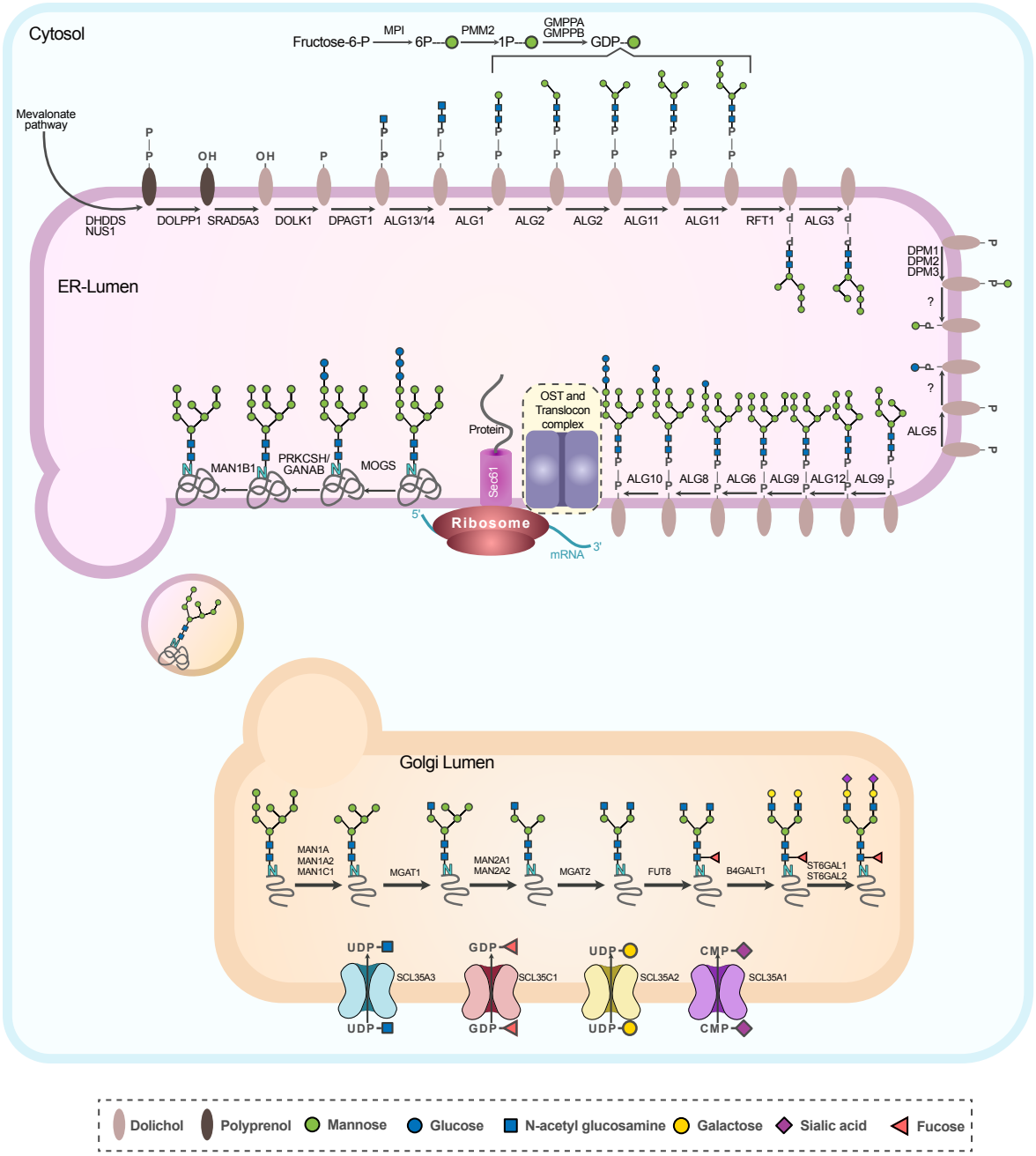

Figure 2. Schematic representation of the *N*-glycosylation pathway. The pathway depicts the sequential assembly of N-glycans and their transfer onto target proteins. *N*-glycosylation begins in the cytosol with the synthesis of GDP-mannose, which serves as a substrate for the indicated enzymes (shown in parentheses). The initial five mannose residues are added to form a lipid-linked oligosaccharide, which is then translocated into the ER lumen by the flippase RFT1. Subsequently, four additional mannose residues and three glucose residues are incorporated, forming the complete oligosaccharide that is transferred to the asparagine residues of nascent proteins. Proteins are then transported to the Golgi apparatus via vesicles, where N-glycans undergo further processing, including trimming and the addition of galactose, fucose, and sialic acid residues. P, phosphate; GDP, guanosine diphosphate; UDP, uridine diphosphate; CMP, cytidine monophosphate. Adapted from (Ng & Freeze, 2018)

1.2.2 ER associated degradation and Unfolded Protein Stress

Proper protein folding in the ER is essential for cellular function. Failure in this process for instance by mis- or reduced protein glycosylation leads to the accumulation of misfolded or unassembled proteins, which can disrupt ER homeostasis and compromise cell viability (Brodsky & Skach, 2011; Hao et al., 2025). To cope with the proteotoxic stress caused, the cell relies on mechanisms that detect, process and degrade aberrant proteins. This is for instance reassured by the Endoplasmic Reticulum-Associated Degradation (ERAD) pathway and the Unfolded Protein Response (UPR) (Panda et al., 2025).

ERAD is multistep mechanism, that starts with the recognition of the unfolded protein, by chaperons and lectins, including calnexin/calreticulin and ER mannosidases. Following detection, these are directed to the retrotranslocation complex. These complexes are found embedded in the ER membrane, like the Sec61 channel, which relocates the protein to the cytoplasm. Proteins fully embedded in the ER must undergo unfolding processes to be able to pass the lipid bilayer. Once the polypeptides have been relocated in the cytoplasm ubiquitination takes place. In those cases, where domains are already exposed to the cytoplasm, ubiquitination can happen before full relocation (Christianson & Carvalho, 2022; Helenius & Aebi, 2004; Kumari & Brodsky, 2021). Finally in the cytosol, the unfolded proteins are polyubiquitinated by the ER-associated E3 ubiquitin ligases, such as Hrd1, extracted from the ER by the AAA-ATPase p97/VCP (Cdc48 in yest), and immediately delivered to the 26S proteasome where degradation takes place (Figure 3) (Christianson et al., 2023; Christianson & Carvalho, 2022).

This pathway is not limited only to misfolded proteins, recent studies have shown that it also contributes to regulate the abundance of functional proteins, keeping a normal proteostasis in the cell (Dabsan et al., 2024; Oommen et al., 2020).

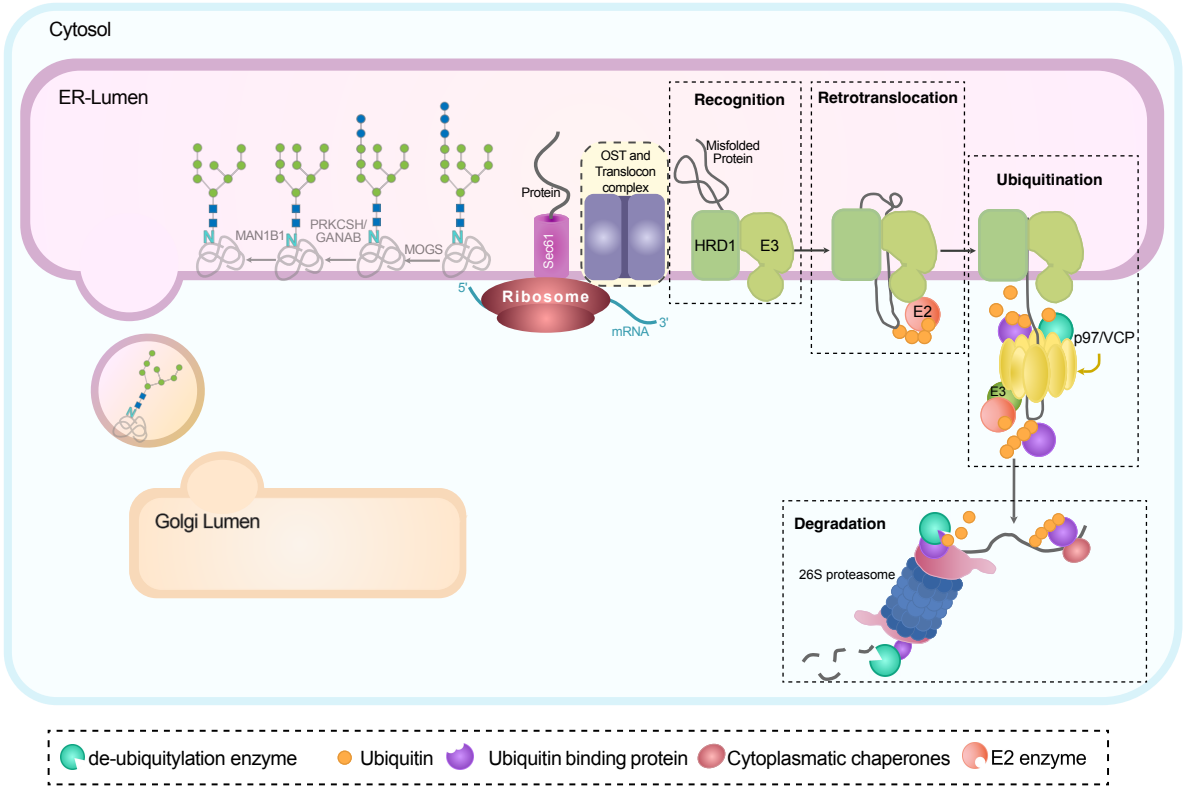

Figure 3. ER-associated degradation (ERAD) of misfolded polypeptides. Misfolded polypeptides are recognized for degradation by features such as prolonged association with folding enzymes, exposed hydrophobic regions, or specific N-linked oligosaccharide structures that act as degrons. Soluble proteins in the ER lumen are primarily directed to the HRD1 E3 ubiquitin ligase complex, while integral membrane proteins are processed through ERAD pathways. ER-membrane-bound E3 complexes facilitate retrotranslocation of polypeptides into the cytoplasm and attach polyubiquitin chains to mark them for degradation. Integral membrane proteins can be directly ubiquitylated on cytoplasmically exposed regions or on luminal domains once accessible. Polyubiquitylated substrates are extracted by the ubiquitin-dependent AAA-ATPase Cdc48/VCP, while ubiquitin-binding proteins prevent aggregation and assist in substrate delivery. Ubiquitin signals are further remodelled by chain-elongating and deubiquitylating enzymes, ultimately guiding the substrates to 26S proteasomes for degradation. Adapted from *(Christianson et al., 2023)*.

When ER capacities are exceeded by the demand of protein folding, an event known as ER stress starts. To handle this situation cells, activate an internal signalling cascade known as UPR. This process is led by three ER transmembrane sensors: inositol requiring enzyme 1 (IRE1); proteins kinase R-like ER kinase (PERK); and the activating transcription factor 6 (ATF6). The main function of this complex is to detect the accumulation of unfolded protein and to initiate an interconnected reaction (Dabsan et al., 2024; Kim, 2024).

IRE1 activates and splices the X-Box Binding Protein 1 (*xbp*1) mRNA, leading to the translation of the transcription factor that upregulates chaperones, ERAD components, and lipid synthesis genes (Dabsan et al., 2024; Wu et al., 2023). To reduce global translation of nascent protein into the ER, protein kinase RNA-like endoplasmic

reticulum kinase (PERK) phosphorylates eukaryotic initiation factor 2α (eIF2α). eIF2α can selectively start the translation of stress-response proteins such as activating transcription factor 4 (ATF4) (Dabsan et al., 2024; Ohno, 2014; Taniuchi et al., 2016). In parallel activating transcription factor 6 (ATF6) starts its translocation to the Golgi, as a response to ER stress, where it is cleaved. This results in the release of cytosolic fragments that triggers the activation of chaperones, ERAD machinery, and secretory pathway components (Dabsan et al., 2024; Koopman et al., 2019; J. Xu et al., 2019). Collectively, these responses aim to restore ER homeostasis by increasing folding capacity, enhancing degradation of misfolded proteins, and expanding the ER membrane (Koopman et al., 2019; Wu et al., 2023). If stress persists, ATF4 can activate the expression of the proapoptotic factor CCAAT/enhancer-binding protein homologous protein (CHOP) and GADD34. Coexpression of AFT4 and CHOP activates translation genes, which increase protein synthesis in the stressed cells, resulting in the production of reactive oxygen species and proteotoxicity and consequently cell death (Hetz et al., 2020; Koopman et al., 2019).
Importantly, ERAD and UPR are tightly interconnected. The interplay between these pathways is critical for maintaining ER homeostasis under both physiological and stress conditions, safeguarding cellular function and survival.

1.3 Congenital Disorders of Glycosylation

Disruptions in the glycosylation processes result in profound systemic consequences often incompatible with life. In rare cases, individuals with deficiencies in glycosylation are born and develop a wide clinical profile often with severe and multisystemic symptoms (Okamoto et al., 2025; Sparks & Krasnewich, 2017; Weixel et al., 2024).
Syndromes caused by defects in glycosylation are collectively referred to as Congenital Disorders of Glycosylation (CDGs), a group of systemic diseases with marked genetic and metabolic heterogeneity. These conditions may arise not only from mutations in enzymes that build glycans, but also from defects in those responsible for processing and attaching them to proteins. As a result, the clinical spectrum of CDGs is broad, with symptoms ranging from motor and cognitive developmental delay to complications such as hepatic or renal dysfunction. Altogether,

this reflects the essential role of glycosylation in sustaining human health. (Lefeber et al., 2022; Lopez et al., 2025).

CDGs are commonly classified according to the step of the glycosylation pathway that is affected. Within *N*-glycosylation, disorders are grouped into those in which glycan assembly is impaired (CDG-I) and those in which glycan transfer to the nascent protein and subsequent processing in the Golgi are disrupted (CDG-II) (Weixel et al., 2024).

A well-described example is Phosphomannomutase-2 deficiency (PMM2-CDG, CDG-Ia), which impairs the GDP-mannose biosynthetic pathway and leads to multisystemic symptoms including cerebral hypoplasia and coagulation defects (Del Medico et al., 2025; Grünewald, 2009). More severe examples include ALG2-CDG (CDG-Ii), which affects the first branching step during glycan assembly, and ALG6-CDG (CDG-Ic), that compromises the addition of glucose residues in the final steps of this process (Helenius & Aebi, 2004; Lefeber et al., 2011; Varki et al., 2022).

Recent advances in clinical glycomics, glycoproteomics, and next-generation sequencing (NGS) have substantially improved the diagnosis and molecular characterization of CDGs (Abu Bakar et al., 2018; Abu Bakar & Hamzan, 2025). These approaches have enabled the identification of more than 200 genes associated with glycosylation defects and have supported more precise patient stratification, often revealing subtle biochemical subtypes that correlate with distinct clinical outcomes (Ng et al., 2024; Weixel et al., 2024). Despite these improvements, a substantial proportion of CDGs remain poorly understood, and effective therapies are available for only a few subtypes, such as MPI-CDG, which can be treated with oral mannose supplementation (De Graef et al., 2022; Harms et al., 2002; Lu et al., 2023).

1.3.1 Neural vulnerability in CDG

Clinically, patients with CDGs often exhibit neurological impairments such as hypotonia, developmental delay, intellectual disability or epilepsy (Jaeken, 2013; Paprocka, 2023). All this reflects how glycosylation supports brain development, circuit assembly, and long-term maintenance. Across clinical and mechanistic surveys, abnormalities in *N*-glycosylation, *O*-mannosylation, and GPI-anchor biosynthesis consistently be linked to with broad neurological involvement (Freeze et al., 2015; Paprocka et al., 2021).

In neurons, highly polarized cells that depend on long-range trafficking, sustained activation of the UPR reprograms translation, disrupts calcium homeostasis and redox balance, and progressively limits the supply of synaptic proteins on which circuits rely. Consequently, the resilience of synaptic networks declines over time, even in the absence of a single focal lesion (Conroy et al., 2021).

Neuronal vulnerability of CDG patient brains also stems from changes in the way receptors and ion channels are handled. Glycosylation fine-tunes co-translational folding, ER export, synaptic delivery, clustering, and turnover of neurotransmitter receptors and voltage-gated channels. When fine tuning of neuronal connections fails, excitability and plasticity derives. This helps explain why seizures are common across diverse CDG symptoms, like patients with ALG13-CDG (Huo et al., 2020; Yoon et al., 2024).

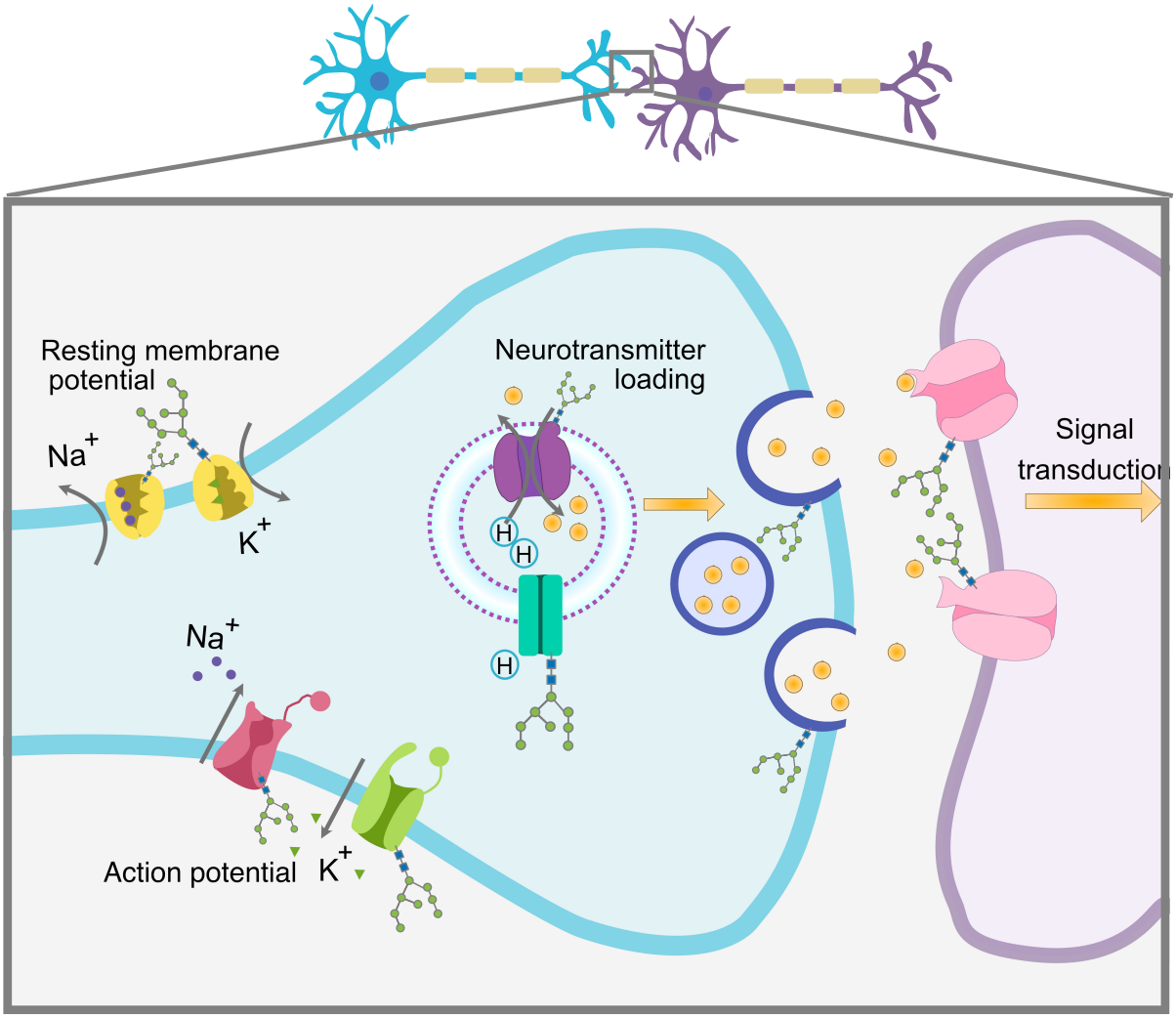

Figure 4. *N*-linked glycosylation in neuronal signaling. After Golgi processing, glycoproteins are packaged into carriers that deliver them to neuronal membranes. *N*-glycans then guide synaptic targeting and stabilize receptors and ion-channel complexes, modulating ligand binding and gating. Glycan-dependent endocytosis and recycling, adjust turnover and subunit composition, tuning

inhibitory–excitatory balance and plasticity. In parallel, *N*-glycosylation of presynaptic voltage-gated channels and adhesion complexes influences release probability and synapse stability. Disruption of these steps reduces functional receptor/channel availability and increases network instability. Adapted from *(Conroy et al., 2021).*

The neuronal context is not exclusively depending on *N*-glycosylated as for instance disrupted *O*-mannosylation weakens α-dystroglycan interactions with laminins and other ligands, disturbing neuronal migration and the integrity of cerebellar and cortical structures that raise baseline stress on developing and mature circuits (Dobson et al., 2013). The GPI-anchor pathway in addition is crucial as defects reduce the surface abundance of synaptic organizers, leading to developmental delay, seizures, and cerebellar anomalies (Castle et al., 2021; Jahncke & Wright, 2023).

In summary, the neurological symptoms in CDGs emerge from additive processes: persistent proteostatic stress, drifting excitability from receptor/channel mis-handling, compromised extracellular matrix (ECM) cues, and altered membrane organization. This multi-level stress environment may explain why heterogeneous genotypes converge on similar neural (Conroy et al., 2021; Paprocka, 2023).

1.3.2 Ocular involvement in CDGs

Due to their neural implications, CDGs are frequently accompanied by ocular disease like strabismus, nystagmus, delayed visual maturation, progressive myopia, and reduced vision; cataract, coloboma, glaucoma, retinal degeneration (including retinitis pigmentosa), ophthalmoplegia, and pallor/atrophy of the optic disc are reported across multiple CDGs subtypes (Kamarus Jaman et al., 2021; Sparks & Krasnewich, 2017). Electroretinography (ERG) abnormalities (affecting rod and/or cone pathways) have been described, consistent with photoreceptor dysfunction (Morava et al., 2009; Thompson et al., 2012).

Several pathways can account for this spectrum. Abnormalities in the dolichol/*N*-glycosylation axis, impaired dolichol synthesis or utilization compromises folding and trafficking of photoreceptor glycoproteins (e.g., rhodopsin), leading to rod-cone dystrophy and early severe visual impairment observed in DHDDS- and SRD5A3-related disease (Esfandiari et al., 2019; Kamarus Jaman et al., 2021; Ramachandra Rao et al., 2020). In *O*-mannosylation-CDG (dystroglycanopathy) spectrum, weakened α-dystroglycan-ECM interactions affect retinal and ocular basement-

membrane integrity and are associated with myopia, retinal dysplasia, and broader “muscle-eye-brain” features (Uribe et al., 2016). Beyond the retina, perturbed glycosylation at neuromuscular junctions and within oculomotor pathways possibly contributes to strabismus, nystagmus, and ophthalmoplegia, while altered glycosylation of lens and trabecular-meshwork proteins leads to cataract and pressure dysregulation. Together, these mechanisms provide a coherent basis for the heterogeneous yet recurring ophthalmic phenotype in CDGs (Morava et al., 2009).
These findings exemplify that the eye is an organ very sensitive to glycosylation defects during its embryonic development, physiological function and proper homeostasis. Further, its neural derivation, organ size, and confined structure renders the eye an interesting organ with direct experimental accessibility.

1.4 Development and structure of the vertebrate eye

Eye development in vertebrates results from coordinated interactions among the neuroectoderm, surface ectoderm, and neural crest-derived mesenchyme (Lachke & Maas, 2010; Sinn & Wittbrodt, 2013). Lateral evaginations of the forebrain form the optic vesicles, which contact the surface ectoderm and induce the lens placode formation (Hyer et al., 2003; Lachke & Maas, 2010; Martinez-Morales & Wittbrodt, 2009). A morphodynamic epithelial flow leads to cell sheet rearrangements and produces a bilayered optic cup: the inner layer becomes the neural retina, and the outer layer forms the retinal pigment epithelium (RPE) (Heermann et al., 2015). The lens vesicle then separates from the surface ectoderm, which later contributes the corneal epithelium (Jean et al., 1998; Magalhães et al., 2024), while neural crest cells populate the corneal stroma and endothelium, the sclera, and uveal tissues (Jean et al., 1998). Closure of the optic fissure establishes the optic nerve head and vascular entry (Cardozo et al., 2023; Heermann et al., 2015; Martinez-Morales & Wittbrodt, 2009).
Retinogenesis follows a conserved differentiation order . Retinal ganglion cells and cones arise early, followed by horizontal and amacrine interneurons; most bipolar cells and rods photoreceptors are generated later, with Müller glia appearing last. The mature neural retina comprises five principal layers intersected by limiting membranes: the ganglion cell layer (GCL, innermost), inner plexiform layer (IPL), inner nuclear layer

(INL), outer plexiform layer (OPL), and outer nuclear layer (ONL). Synaptic processing occurs in the plexiform layers: photoreceptor-bipolar/horizontal in the OPL, and bipolar-amacrine-ganglion in the IPL; while Müller glia span through all layers and provide structural and metabolic support (Marquardt & Gruss, 2002; Norden, 2023; Stevens-Sostre & Hoon, 2024) (Figure 5).

Although photoreceptor cell bodies lie in the ONL, their inner and outer segments extend outward; having the outer segments embedded in RPE microvilli (Cheng et al., 2006; Mahabadi & Khalili, 2023). The RPE acts as a support system to the photoreceptors by recycling visual pigment, maintaining the outer blood-retinal barrier, and regulating ion and water flux (Bandyopadhyay & Rohrer, 2010). Together, the photoreceptor-RPE pair functions as a single unit that sustains photoreceptor survival and stable visual signalling (Bandyopadhyay & Rohrer, 2010).

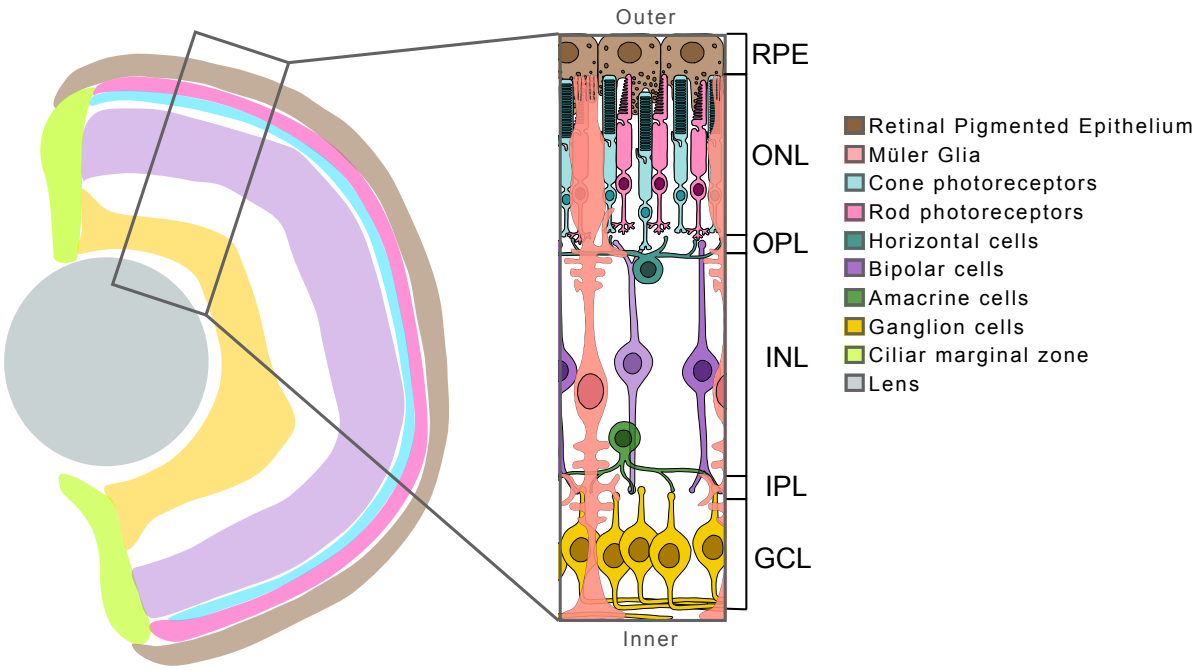

Figure 5. Layered architecture of the camera-type retina. From the inner, ganglion-cell side to the outer RPE/choroid, the neural retina forms five principal layers: the ganglion cell layer (GCL), inner plexiform layer (IPL), inner nuclear layer (INL), outer plexiform layer (OPL), and outer nuclear layer (ONL). Interneurons in the INL: bipolar, horizontal, and amacrine cells; route and shape signals between photoreceptors and ganglion cells, with synaptic exchange concentrated in the OPL (photoreceptor to bipolar/horizontal) and the IPL (bipolar to amacrine/ganglion). Photoreceptor cell bodies (rods and cones) lie in the ONL, while their inner and outer segments extend outward against the retinal pigment epithelium (RPE), which supports them structurally and metabolically.

In the camera type eye, the light is capture by the photoreceptors, which close cGMP-gated channels, hyperpolarizing and reducing glutamate release in their ribbon synapses. Photoreceptors react to different stimuli, rods favour dim-light sensitivity, while cones processes daylight vision, colour, and fine detail (Molday & Moritz, 2015; Yau & Hardie, 2009). Signals leave the photoreceptors in the OPL, and separate into ON (light increments) and OFF (light decrements) bipolar pathways (Ichinose & Habib, 2022; Puller et al., 2013; Snellman et al., 2008). Horizontal cells build centre-surrounded contrast before the signal reaches the inner retina (Thoreson & Mangel, 2012). Bipolar cells then connect with the amacrine cells in the IPL, to remain timing and gain (Bloomfield & Dacheux, 2001). At the end, ganglion cells integrate the inputs and encode the stimuli as an action potential to be send through the optic nerve to the brain (Ichinose & Habib, 2022).

1.4.1 Congenital eye diseases

Vision capacity depends the precise layering of the retina, in which photoreceptors, interneurons, ganglion cells, Müller glia and the RPE cooperate to capture, shape and deliver the light stimuli from sensing in the eye to processing in the brain (Mahabadi & Khalili, 2023; Marquardt & Gruss, 2002). When development is perturbed or pathogenetic variants alter its equilibrium due to genetic mutations, drugs or traumata, synaptic processing is compromised and vision is impaired (Garg & Tsang, 2024; W. Xu et al., 2022).

The most common developmental ocular diseases are: 1) congenital cataract, perturbing retinal image at youth. Although serious, this disease is treatable through surgery (Sheeladevi et al., 2016). 2) Primary congenital glaucoma which is caused by elevated intraocular pressure, often causing optic nerve damage if not treated early in life (Badawi et al., 2019). 3) Ocular coloboma, i.e. a condition in which the optic fissure closure is incomplete. This leads to segmental defects which can involve other layers like the iris or the RPE (Lingam et al., 2021). If the interaction of the RPE and photoreceptors is compromised, patients present profound visual dysfunction and show severely reduced or non-recordable full-field ERG, a condition known as Leber congenital amaurosis (den Hollander et al., 2008).

1.4.2 Rhodopsin as a model for glycosylation in retinitis pigmentosa

Retinitis pigmentosa (RP) is a heterogeneous group of inherited retinal dystrophies characterized by the progressive degeneration of rod and cone photoreceptors, typically presenting with night blindness and peripheral visual field loss before advancing to central vision impairment. RP affects approximately 1 in 3,000–5,000 individuals worldwide and is caused by pathogenic variants in more than 90 genes involved in photoreceptor structure, phototransduction, or retinal metabolism (Daiger et al., 2007; Hartong et al., 2006). Among these, rhodopsin (*rho*) was the first gene identified in autosomal dominant RP, and more than 150 disease-associated variants have been described, many of which compromise protein folding, trafficking to the outer segment, or structural stability (Jay, 1982; Mendes et al., 2005; Parmeggiani et al., 2011). Proper folding and correct localization of rhodopsin depend on *N*-glycosylation at two conserved asparagine residues (Asn-2 and Asn-15); disruption of these sites leads to endoplasmic-reticulum retention, impaired trafficking, and ultimately photoreceptor degeneration (Murray et al., 2009, 2015). This makes rhodopsin an informative reference for understanding how glycosylation regulates protein stability and contributes to retinal degeneration.

1.5 Genome editing tools for perturbing *in vivo* gene and protein function involved in glycosylation and retinal homeostasis

Multiple tools have been developed to precisely interfere with gene function, facilitating loss-of-function mutation across different model systems. At present, the most common methods employed are based on the Clustered regularly interspaced short palindromic repeats (CRISPR) / CRISPR-associated protein (Cas9) system for genome editing (Doudna & Charpentier, 2014; Hsu et al., 2014), complemented by RNA interference (Elbashir et al., 2001) or morpholino antisense oligonucleotides to block RNA splicing or translation (Moulton & Yan, 2008). These complementary tools perturb different layers of gene expression and provide functionality *in vivo* and *in vitro* (Hsu et al., 2014).

CRISPR-Cas9 systems derive from prokaryotic adaptive immune systems in which invader-derived spacers guide nucleases to matching sequences (Barrangou et al., 2007). For genome editing, Cas9 is directed by a guide RNA to cleave the target site adjacent to a protospacer adjacent motif (PAM), enabling precise, programmable DNA modification across organisms (Doudna & Charpentier, 2014; Hsu et al., 2014; Jinek et al., 2012).

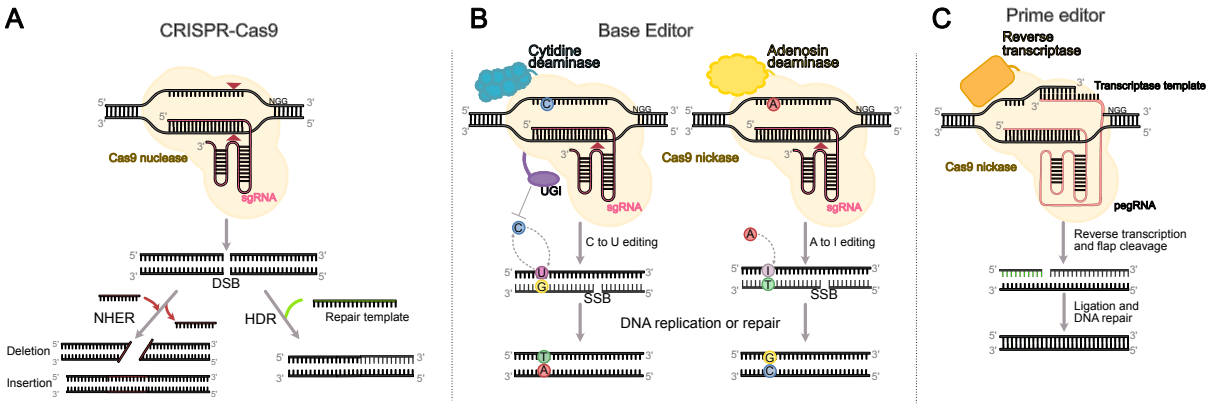

Figure 6. CRISPR-Cas genome editing mechanisms (A) Cas9 nuclease guided by a single-guide RNA (cr/trRNA) generates a site-specific double-strand break (DSB). Repair by non-homologous end *repair* (NHE*R*) creates indels suitable for knockout or homology-independent targeted integration *(*HITI*)* insertions; in the presence of a donor template, homology-directed repair (HDR) copies the encoded edit into the genome for precise correction/integration (edits in green). (B) Base editors (BEs) are fusion of *nickases Cas9 (*nCas9*)* and a deaminase. Cytosine base editors (CBEs) deaminate C→U within the R-loop; a fused UGI suppresses base-excision repair, and nicking of the opposite strand biases mismatch repair (MMR) so the U:G pair is resolved to T:A. Adenine base editors (ABEs) convert A→I, which pairs as G and is fixed to G:C after repair/replication. Together, CBEs and ABEs install the four transition mutations (C↔T, A↔G) without DSBs, within a PAM-constrained editing window. (C) Prime editor (PE) fuses nCas9 to a reverse transcriptase (RT) and uses a pegRNA carrying a primer-binding site (PBS) and an RT template. After nicking, the exposed 3′ end anneals to the PBS and is extended by RT to write the encoded change; flap equilibration, cleavage, and ligation incorporate the desired mutation without DSBs. Adapted from *(Zhao et al., 2023)*.

1.5.1 Genome editing mediated by CRISPR-Cas9 induced DSBs

CRISPR-Cas9 couples a targeted single-guide RNA (cr/trRNA) to the Cas9 endonuclease to bind a PAM-proximal target, form an R-loop, and cleave both DNA strands with its HNH and RuvC domains to generate a site-specific double-strand break (DSB) (Hsu et al., 2014; Jinek et al., 2012; Thumberger et al., 2022). Subsequently, the cells repair this lesion by end-joining pathways, predominantly non-homologous end joining (NHEJ) which may result in alleles containing random insertions/deletions (indels) (Helleday et al., 2007; van Overbeek et al., 2016).

When precise sequence changes are required, a co-supplied repair donor molecule can be used for targeted integration into the genome by homology-directed repair (HDR) (Ran et al., 2013) (Figure 6A). To prevent multimeric insertion of the donor cassette, the 5' ends of the DNA fragment can be occupied by large moieties like biotin (Gutierrez-Triana et al., 2018). Although precise, HDR events are less frequent than indel formation by NHEJ as the availability of the HDR machinery is limited to the S and G2 phase of the cell cycle while the NHEJ pathway is always available.

1.5.2 CRISPR-Cas9 Base Editors

As the CRISPR technology advanced, so-called base editors (BE) were invented that lead to transformation of single nucleotides with strongly reduced indel formation and which are not relying on the HDR machinery. A base editor is a fusion of a Cas9 nickase with a deaminase enzyme, that creates transit mutations without DSB formation (Rees & Liu, 2018). Two different types of BE are currently in use: Cytosine base editors (CBE) use cytidine deaminases to convert cytosines (C) into uracils (U); the edited U has a certain probability to being stably changed into thymine (T) after DNA repair (Komor et al., 2016; Rees & Liu, 2018); and adenine base editors using adenosine deaminases to convert adenines (A) to inosine (I), I pairs as guanines (G), and after repair allows the A to G change (Gaudelli et al., 2017; Rees & Liu, 2018) (Figure 6B).

CBEs and ABEs act within a position-defined editing window covering the 13th-17th nucleotides upstream of the PAM. DNA off-target effect with BEs is generally lower than with nucleases (Rees & Liu, 2018). Online design tools like ACEofBASEs are facilitating the choice of possible target sites by evaluating the introduced DNA mutations and analyse potential off-target sites in the genome (Cornean et al., 2022). Due to the limited and precise nature of editing coupled with the reported high efficiency, base editors seem to be the tool of choice when it comes to nucleotide-specific alterations of genomic loci.

1.6 Medaka as a model for human diseases

Animal models to study rare diseases such as congenital disorders of glycosylation (CDGs) are limited because many steps in glycosylation are essential, and severe loss-of-function alleles in mammals are frequently embryonically lethal; as a result, viable postnatal mutants are uncommon and in mammalian systems, embryos must often be recovered during gestation to obtain carriers of the desired mutations (Cacheiro et al., 2022; Thiel et al., 2006). In contrast, teleost fish, especially zebrafish (*Danio rerio*) and medaka (*Oryzias latipes*), represent particularly suitable vertebrate model systems with high conservation of their genes compared to humans (Howe et al., 2013; Kasahara et al., 2007). A feature that highlights fish models is their extrauterine development and transparent embryos, which allows to study embryonic features and development in the dish (Wittbrodt et al., 2002). Compared with zebrafish, medaka offers a smaller, more concise genome (~700 Mb, less than half of zebrafish), broad thermal tolerance (~10-40°C), and high inbreeding tolerance that allows the creation of near-isogenic lines, features that streamline genome editing, stable line generation, and reproducible phenotyping (Kasahara et al., 2007; Kirchmaier et al., 2015; Wittbrodt et al., 2002). Further, medaka has been used in previous studies to introduce human pathology for analysing.

1.6.1 Glycosylation disorders modeled in medaka

Especially for severe syndromes like CDGs, the extrauterine development of teleosts is well suited to investigate the onset and progression of phenotypes. Therefore, enzymes of the glycosylation machinery have been successfully targeted and mutant lines recapitulating the patient syndromes could be raised.

Modeling congenital disorders of glycosylation in mammals is often limited by early embryonic lethality when key enzymes are completely lost. For example, Pmm2 knockout in mice is lethal, and several knock-in approaches lead to high prenatal mortality or severe perinatal phenotypes, restricting their usefulness for mechanistic studies (Thiel et al., 2006). These limitations highlight the need for complementary vertebrate models that can tolerate partial loss of function.

In medaka, an auxin-inducible GFP-nanobody degron system has been used to generate a tunable Pmm2 hypomorphic phenotype, allowing dose-controlled depletion of the enzyme to reproduce patient-like hypomorphic states during embryogenesis

(Gücüm, 2021). This approach provided a practical alternative to lethal null alleles and enabled live imaging, biochemical assays, and rescue experiments to connect genotype with phenotype (Gücüm, 2021; Pakari et al., 2025).
A similar strategy was applied to model POMT2-related disease in medaka, this time using CRISPR/Cas9 and base-editing to generate a graded allelic series that was characterized through behavioral, biochemical, histological, and transcriptional analyses (Cornean, 2022). Pathological changes in the eye and brain were detected only when POMT-complex activity was substantially disrupted, supporting the idea that a minimal threshold of *O*-mannosylation is essential for tissue stability (Cornean, 2022; Taniguchi et al., 2006).

1.6.2 Alg2 medaka model shows strong eye defects

An ALG2 medaka mutant, resembling a patient-derived mutation was generated by CRISPR/Cas9 with an ssODN to introduce a premature stop at the patient site, yielding a rescuable hypomorphic model of hypo-*N*-glycosylation. The line recapitulates late-onset, multisystemic features that reflect the patient symptoms, including reduced *N*-glycan levels (Gücüm et al., 2021).
Proteomics analysis of enucleated eyes revealed a marked under-representation of phototransduction proteins, and histology demonstrated a failure to maintain rod photoreceptors accompanied by increased ONL apoptosis. In essence, the alg2-deficient eye displays with a RP-like, progressive degeneration of rod photoreceptors (Gücüm et al., 2021) (Figure 7). It remained elusive which factors are involved in progression of the phenotype and why some cell types are more affected by reduced *N*-glycosylation compared to others.

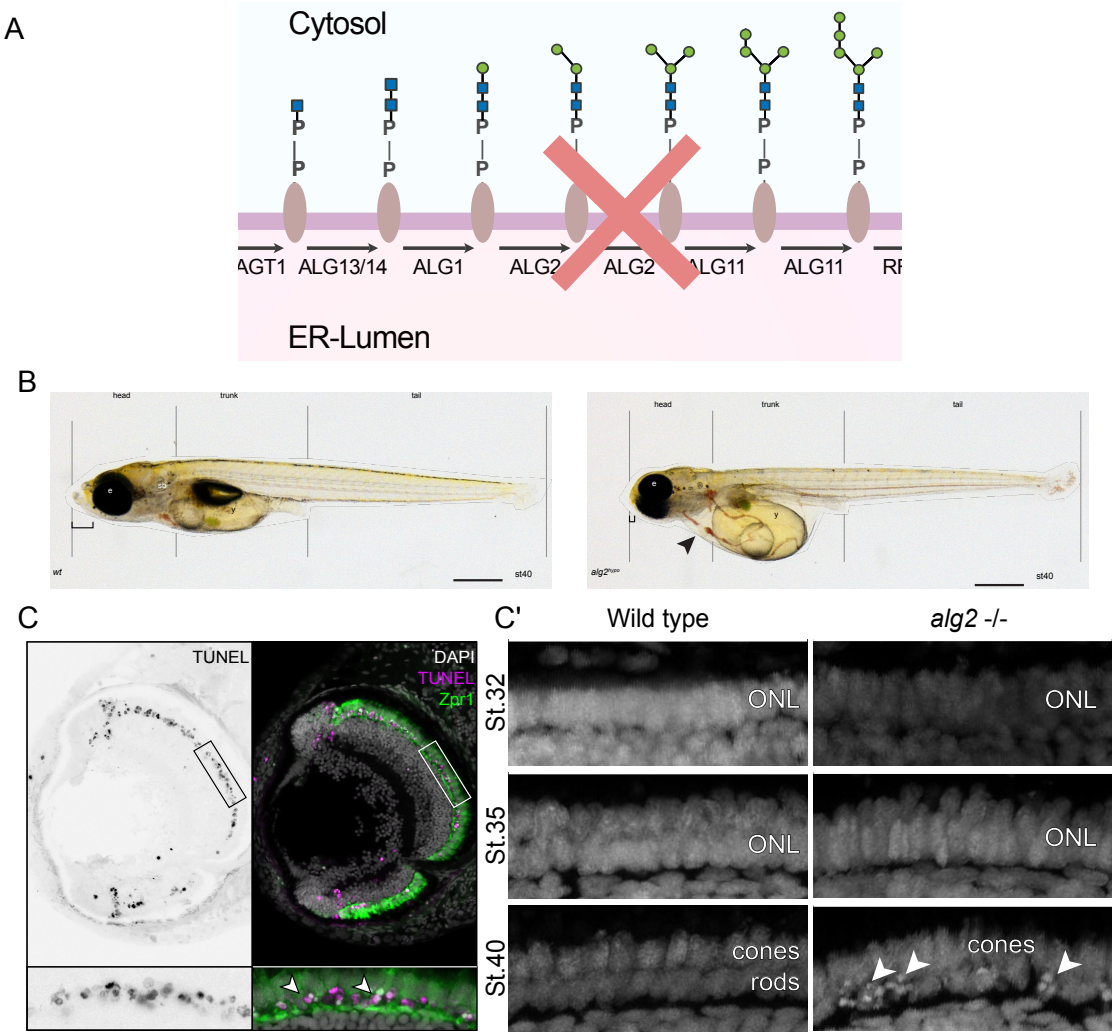

Figure 7. **alg2 mutants in medaka reveal systemic and retina-specific defects.** (A) Graphical representation of the lipid linked oligosaccharide synthesis at the ER membrane. Alg2 catalizes the addition of both mannoses used for the first branching. (B) Morphological comparison of hatchlings (WT vs *alg2* mutants) showing craniofacial dysmorphology, cardiac abnormalities, and hepatomegaly in mutants. (C) Retinal cross-sections from alg2 mutants with increased TUNEL signal indicating apoptosis, predominantly in rod photoreceptors. (C′) Developmental series of photoreceptors at medaka stages 32, 35, and 40 in WT and *alg2* mutants, illustrating delayed maturation/maintenance and progressive loss in mutants. Adapted from (Gücüm et al., 2021).

2

Hypothesis and Aims

Hypothesis

Glycosylation is a ubiquitous post-translational modification that regulates protein folding, stability, function and cell communication across all cell types. In hypoglycosylated conditions, such as reported in the Alg2-CDG medaka model, photoreceptors appear particularly vulnerable, highlighting their sensitivity to disruptions in this pathway. Based on this reoccurring phenotype, I hypothesize that besides rhodopsin, specific glycoproteins are critical for maintaining photoreceptor stability, and that proper *N*-glycosylation is required for their correct folding and function to preserve retinal structure and visual performance. To investigate this, I combine proteomics data derived from medaka CDG models, human expression atlas and single cell transcriptomics of wild-type medaka eyes available to the lab. I will analyse and validate these candidate glycoproteins in medaka and investigate how disruption of predicted *N*-glycosylation site mutation affects photoreceptor development, retinal organization, and visual function.

To this end, the following steps were considered:

I. **Identification of photoreceptor exclusive glycoproteins via database and *in silico* glycosylation profiling**
   comparing medaka CDG proteomics, medaka transcriptomics and patient data for potential evolutionarily conserved canonical *N*-glycosylation sequons, with predictive high probability of being *N*-glycosylated.

II. **Characterisation of candidate genes on implication with photoreceptor growth, maintenance and functionality**

using CRISPR/Cas9 genome editing and homology directed repair to substitute glycosylated asparagines within the predicted *N*-glycosylation sequeons, inhibiting candidates' glycosylation, and determining the impact by histological analysis of the retina.

III. **Study the importance of individual asparagines for their redundance or importance for the individual protein function**

providing mRNA variants that contain individual or combined N-glycosylation site mutation will be used to investigate the capacity to rescue the individual knockout scenario.

3

Results

To determine which genetic factors may be responsible for the onset of retinitis pigmentosa in the CDG-Alg2 model in medaka (Gücüm et al., 2021), candidate genes need to be identified. Even though glycosylation is a well-characterized process, its role in retinal disease is still not understood. Since glycosylation is mainly studied in the context of human diseases, most of the available databases are limited to mammalian models (Aoki-Kinoshita et al., 2024; Otaki et al., 2022). However, non-mammalian vertebrate systems allow for a more accessible way to study glycosylation in embryonic development. Therefore, the first step I took in this project was to develop a workflow for extracting glycosylation-dependent candidates, whose expression is restricted to the retina in the *Oryzias latipes*, medaka fish, model.

3.1 Identification of glycosylation-dependent candidate genes in retinopathies

To approach the first aim of this thesis I designed a workflow to obtain a list of candidate genes that fulfilled the following criteria: expression in medaka photoreceptors, downregulation in a hypoglycosylated scenario, their function has been related to retinopathies, conservation between medaka and human and presence of the AsnXxxSer/Thr sequon.

To identify potential gene candidates I used various databases containing proteomics and transcriptomics. These sources include comparative proteomics of the Alg2-CDG model in medaka vs wild-type medaka (Gücüm et al., 2021); comprehensive single cell transcriptomics of the medaka eye (Benjaminsen, Fuchs, Wittbrodt, unpublished); and finally, studies in humans of various previously described retinopathies (Hartong

et al., 2006; Vasireddy et al., 2010; Schneider et al., 2022). Obtaining a list of 87 genes (Supplementary Table 1) to select candidate genes according to the following criteria: their expression was downregulated in a hypoglycosylated scenario, they were exclusively expressed in the photoreceptors and/or their function has been related to retinopathies.

Although the complete medaka genome sequence is available (Kasahara et al., 2007b), the database repositories of medaka-related transcriptional and post-transcriptional data are incomplete. Thus, after obtaining potential candidate genes for medaka, I searched for their human orthologs, as post-transcriptional modifications in humans are extensively characterized (Kitamura & Galligan, 2023). To obtain these orthologs, I used the Ensembl database, specifically the BioMart tool, where the Ensembl ID, unique to each gene, was uploaded. The result was a comprehensive list of all possible human orthologs for each gene of interest, if present (Figure 8A).

Following this, I used publicly available tools, such as UniProt, to examine the presence of PTMs in each gene. UniProt describes whether PTMs are present, specifying the types of modifications such as glycosylation or phosphorylation, and whether they are experimentally confirmed or assigned through simulations based on the most current literature (Bateman et al., 2023). This process allowed me to filter the gene list, which I further analysed in GlyGen, a database that provides more detailed information on the presence of AsnXxxSer/Thr motifs in the protein sequence (York et al., 2020a). This motif is frequently found in protein sequences, although not all will undergo *N*-glycosylation. To filter down those not likely to be *N*-glycosylated, I used the tool NetNglyc to identify signal peptides in the amino acid sequence. Signal peptides are short amino acid sequences located in the N-terminus of a protein, crucial for the glycosylation pathway, as they direct the proteins into the ER (Gupta & Brunak, 2002; Pérez-Núñez et al., 2023). Additionally, NetNGlyc estimates the likelihood of *N*-glycosylation of Asn within the AsnXxxSer/Thr motif (Gupta & Brunak, 2002).

To determine if glycosylation is indeed regulating these candidates, I targeted Asn for a mutagenesis experiment, where sequence position and glycosylation probability were either equal or very similar in human and medaka, as glycosylation is a highly conserved PTM in vertebrates (Moremen et al., 2012b; Park & Zhang, 2011).

Once I identified all potential glycosylated motifs, I searched for the transcriptomic expression of the same candidates throughout the medaka embryonic development (Li et al., 2020).

To further adjust the candidate list to my objectives in investigating glycosylation-related retinopathies, I targeted genes related to the formation and differentiation of photoreceptors, which differentiate between developmental stages 36 and 38 (Iwamatsu, 2004; Mikula Mrstakova & Kozmik, 2024). To identify these gene candidates, whose peak of expression occurs at the stages of photoreceptor differentiation, I analysed transcriptional profiles along the medaka embryonic development, using glyceraldehyde-3-phosphate dehydrogenase (GAPDH), a housekeeping gene, to normalize the expression patterns (*GAPDH Glyceraldehyde-3-Phosphate Dehydrogenase [Homo Sapiens (Human)] - Gene - NCBI*, n.d.). The identified candidate genes, extracted from the presented workflow, shared overall different expression patterns, compared to each other. Yet, the highest transcriptomic expression, assigned to all of the genes, corresponded to the developmental stages of the retina (Figure 8C).

A

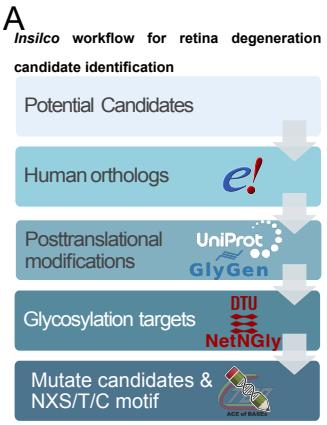

B

Gene name	EnsemblID medaka	EnsemblID human	Description
Rho	ENSORLG00000010599	ENSG00000163914	Rhodopsin
Opn1sw	ENSORLG00000019293	ENSG00000128617	Short-wave sensitive opsin1
Elovl4b	ENSORLG00000017019	ENSG00000118402	Elongation of very long chain fatty acidsprotein 4
EGFLAM	ENSORLG00000005499	ENSG00000164318	Pikachurin
Tena	ENSORLG00000002627	ENSG00000041982	Tenascinlike
PCDH8	ENSORLG00000011123	ENSG00000136099	Protocadherin 8
novel gene	ENSORLG00000000896	not found	Collagentype XIV alpha 1 chain
novel gene	ENSORLG00000013140	ENSG00000148702	Hyaluronanbinding protein 2
novel gene	ENSORLG00000024677	ENSG00000132639	Multifunctional fusionprotein
novel gene	ENSORLG00000025491	ENSG00000102003	Synaptophysin

C

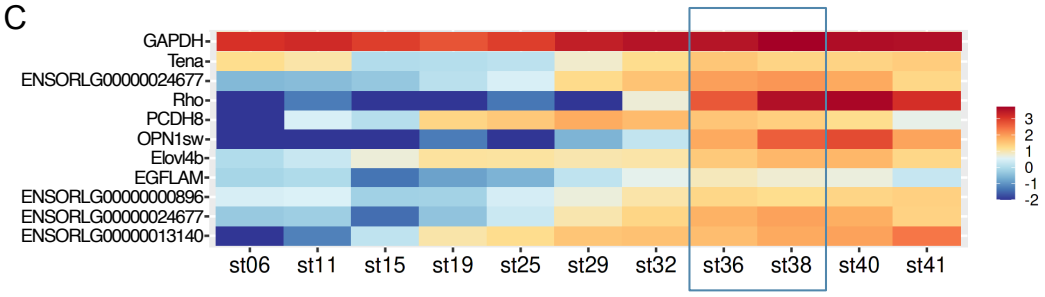

Figure 8. Methodological pipeline for glycoprotein-related candidate genes selection in retinal degeneration. (A) Schematics of the *in silico* workflow to identify potential gene candidates predicted to be glycosylated and associated with photoreceptor functionality and stability. (B) Candidate genes retrieved from the workflow. (C) Transcriptomic expression profiles of identified candidates found to be related with photoreceptor maturation throughout the medaka embryonic development. Box highlights the developmental stages (36-38), when photoreceptors are generated and undergo differentiation into cones and rods. GAPDH (top y-axis) was used as a control.

To validate candidate gene function for eye development and photoreceptor differentiation and maintenance, I opted for two strategies: 1) targeted genome editing to disrupt the gene function via the CRISPR/Cas9 system and 2) specific *N*-glycosylation sequon editing to interfere with *N*-glycosylation rather than disrupting the full protein.

3.2 Precise CRISPR-Based Screening targeting the *N*-glycosylation sequon of the candidates

3.2.1 Precise targeting of the *N*-glycosylation site using Adenine Base Editors

To precisely target the *N*-glycosylation site of the candidate genes, I used two types of base editors available: ABE and CBE. The Asn targeting was only feasible with the ABE type, because the codons of this amino acid are AAC and AAT. Depending on the position of the PAM motif and thus the limits of the base editing window, the first, second or both A of the Asn codon could be changed. Edits could thus lead to Asn>Ser (AAC>AGC or AAT>AGT), Asn>Asp (AAC>GAC or AAT>GAT) or Asn>Gly (AAC>GGC or AAT>GGT). With these substitutions the potential mis-glycosylation and functionality of the candidates in the retina should be studied in a F0 screening.
While designing the guide RNAs in silico, I came across cases where some Asn codons were not in the proximity of a PAM sequence. In these cases, I designed the cr/trRNAs to target the last amino acid of the *N*-glycosylation sequon. As mentioned in Chapter 1.1, Ser or Thr amino acids are reported to predominantly occupy that position of the sequon. Due to their codon sequences, I chose a CBE to cause the C-to-T conversions that would result in Ser>Phe/Leu or Thr>Ile (Figure 9B).

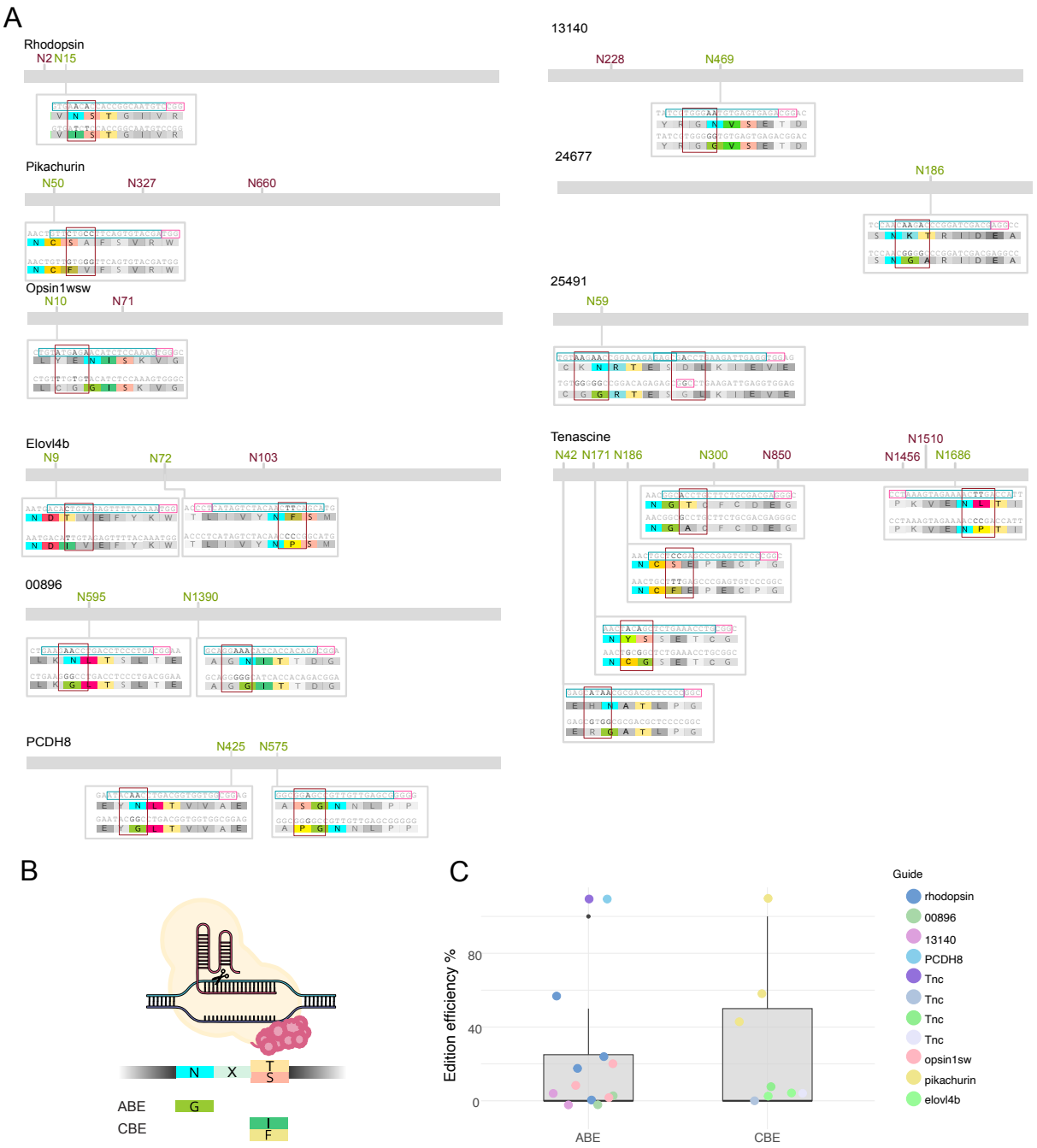

Figure 9. Design and outcome of base editing to disrupt NXS/T motifs reveal a trade-off between editing efficiency and embryonic viability. (A) Design of all guide RNAs used in this study. Each motif is highlighted within its surrounding amino acid context, with the target NXS/T residues highlighted in color and the expected amino acid substitutions shown. Color boxes indicate functional regions: fuchsia, PAM sequence; light blue, guide RNA sequence; and dark red, base editing window. (B) Schematic representation of the base editors used and the expected amino acid changes at AsnXxxSer/Thr motif. Adenine base editor (ABE) was applied to convert asparagine (N) residues to glycine (G), whereas cytosine base editor (CBE) was used to convert threonine (T) to isoleucine (I) and serine (S) to phenylalanine (F), thereby disrupting the canonical NXS/T glycosylation motif. (C) Boxplot showing editing efficiency of ABE and CBE, showing an average efficiency of ~20% for both editors. The highest editing efficiencies were associated with severe embryonic developmental defects, often incompatible with survival.

Among the injected embryos, lethality was observed within the first days post fertilization (dpf), though no altered effect on embryonic development was evident in the survivors. After frequent visual inspection of the embryo morphology was described. The success rate of the embryo injections was examined by the sequencing quality of the DNA extracted from individual or pooled embryos at 4dpf. After screening all potential guide RNAs, the editing efficiency of both ABE and CBE was lower than reported from other loci (Cornean et al., 2022). In this experimental setup, the majority of ABE conversions reached levels below 30% efficiency, whereas the CBE guide RNAs overall performed 15% better, but still not exceeding 50% (Figure 9B).

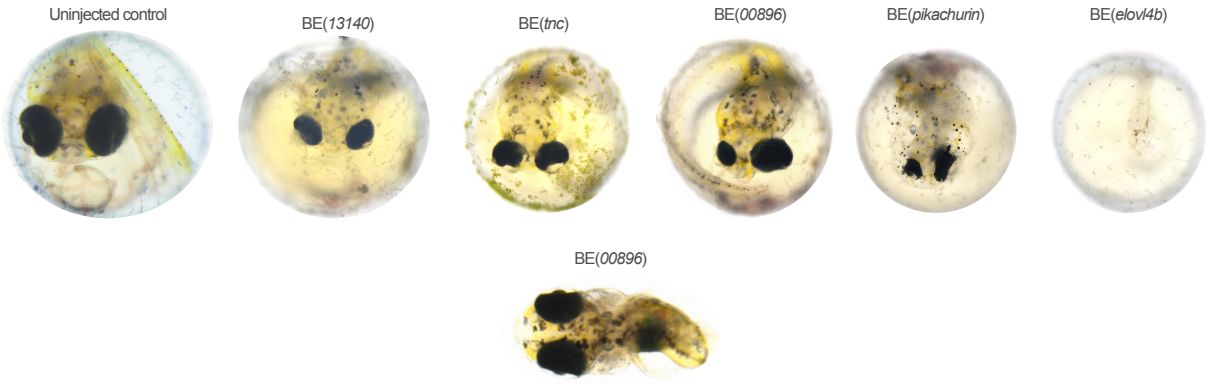

Figure 10. Base editor-mediated targeting of glycosylated Asn residues causes severe developmental delays. Representative images of 5 dpf embryos injected with adenine and cytosine base editors directed at predicted *N*-glycosylation sites. Embryos exhibit pronounced developmental delays, demonstrating that base editor-mediated disruption of glycosylated Asn residues can strongly affect early embryogenesis.

These results demonstrated that it was not feasible to screen the *N*-glycosylation mutation in the injected generation (F0). Further, these low levels impaired the efficient establishment of stable lines as embryos that showed stronger editing efficiency were those exhibiting severe developmental issues unable to be raised (Figure 10).

3.2.2 HDR mediated mutation of the *N*-glycosylation motifs as an alternative route to candidate gene validation

While base editing did not efficiently introduce point mutations within the glycosylation sequon of the candidate genes, an alternative approach for validation was envisaged. As an alternative strategy to create stable lines for mutations of glycosylation motifs I

chose to exploit the homology directed repair (HDR) pathway triggered upon DSB introduction (Figure 11A). BE limited the mutagenesis spectrum, as only adenines and cytosines are available to be changed. With HDR precise mutations can be designed and introduced, as the templates contains the mutations of interest. Having this in consideration, the mutations introduced in the glycosylation sequon were chosen to prevent structural and polarity changes, i.e. an amino acid replacement for asparagine was chosen to be least different. Thus, Asn was mutated to Gln (glutamine) in the repair donor sequence as both amino acids share similar polarity and structure (Figure 11A).

Donor constructs were designed for different candidate genes whose functionality had already been linked to the retina: *rhodopsin*, *opsin*, and *elovl4b* (Ma et al., 2022; Nwagbo et al., 2024; Sung et al., 1991). I synthesized the donor constructs containing the candidate sequences with all potentially glycosylated Asn replaced by Gln. Further, I introduced synonymous mutations to create restriction enzyme sites, facilitating the use of diagnostic digestion, and removal of the PAM sequence, inhibiting Cas9 activity upon insertion of the donor. These donors were designed with 150 bp homology arms on either side. To prevent potential concatemerization of the donors during integration, biotin moieties were added at both 5'-ends of the donor PCR fragment (Gutierrez-Triana et al., 2018) (Figure 11B).

After three rounds of injection, per gene, I visually inspected the injected embryos, which exhibited a wide range of eye-related phenotypes. Some paradigms included oedema, smaller eyes, and abnormal eye positioning , while other phenotypes included blood coagulation and microcephaly, all of which rendered embryonic development non-viable. Those embryos that did not show abnormalities in their development, Sanger sequencing only revealed DSBs pattern induced by CRISPR/Cas9 (Figure 11C; Supplementary Figure 1C; Supplementary Figure 2C). Viable embryos were raised until adulthood and progeny was used to determine successful insertion of the donors.

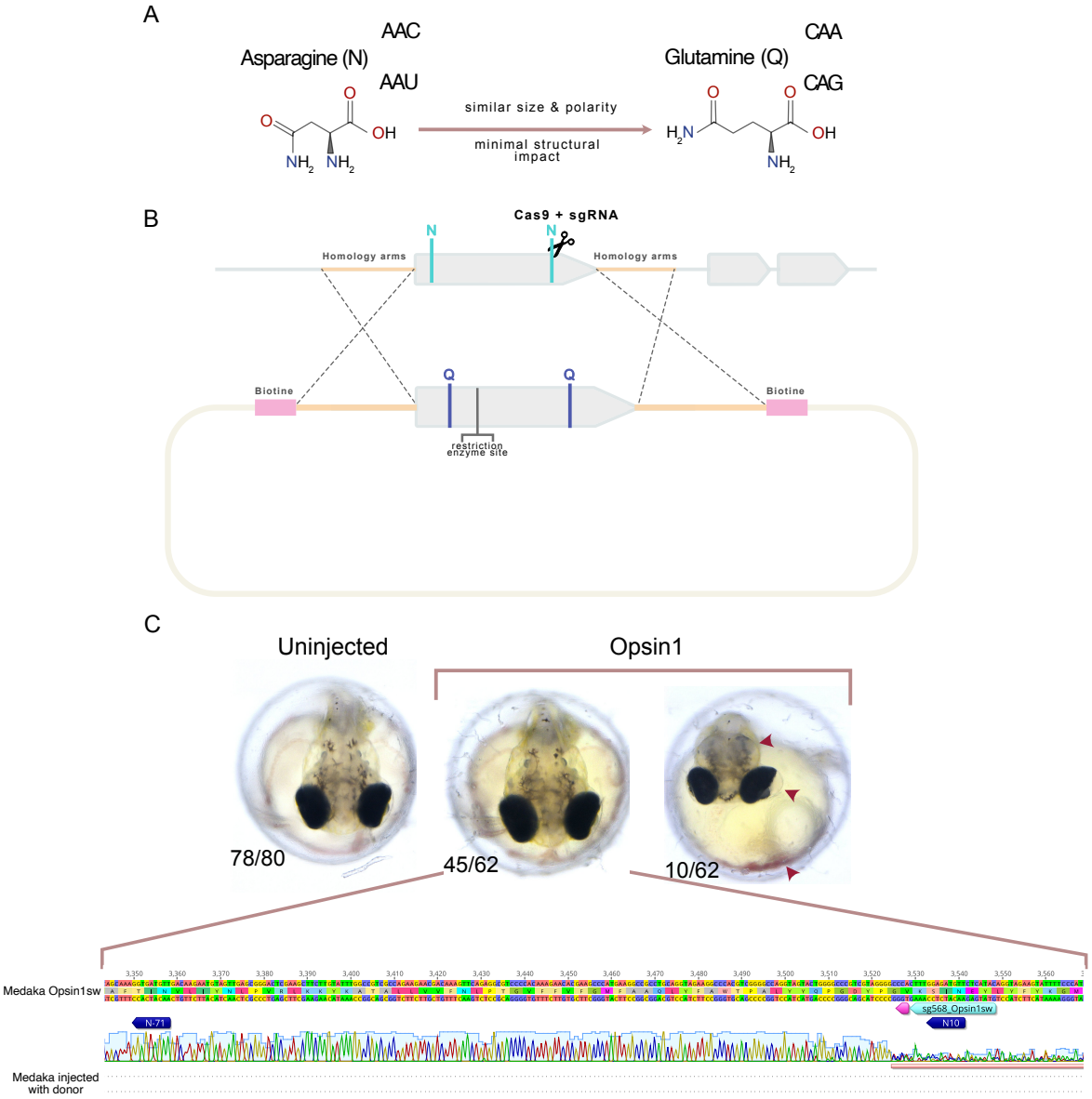

Figure 11. Experimental design for HDR-mediated donor insertion targeting *N*-glycosylation sites. (A) Substitution of asparagine (N) residues with glutamine (Q) was chosen to disrupt consensus N glycosylation motifs (NXS/T) while preserving side chain polarity and size, a change expected to minimize structural perturbations while abolishing glycosylation. (B) Schematic representation of the donor construct and HDR approach. The target region (top) was cleaved by Cas9 guided by a specific cr/trRNA, generating a double strand break (DSB). The donor sequence (bottom) contained glutamine (Q) substitutions at positions corresponding to predicted glycosylated asparagines (N). Homologous flanks (orange) promoted HDR mediated integration at the targeted locus (indicated by diagonal alignment lines), biotinylated ends (pink) prevented concatemer formation, and an engineered restriction site enabled diagnostic digestion. (C) Representative embryos from control (uninjected) and donor injected groups. While some injected embryos were phenotypically similar to controls, others exhibited severe developmental defects (microcephaly, ocular oedema, and blood coagulation; indicated by dark red arrows), which were incompatible with survival. Sanger sequencing of one phenotypically normal injected embryo showed no donor integration but clear evidence of double strand breaks (DSBs).

Unfortunately, no integrated donor sequence could be detected via genotyping and Sanger sequencing for all the HDR attempts. Knock-out founders were identified by sequencing for all the targeted genes, presenting indel mutations as a result of the DSB after CRISPR/Cas9 targeting (Figure 11C). I selected founders for the establishment of stable medaka fish lines to study the functional consequences of candidate gene loss.

3.2.3 opn1sw knockout impacts ONL integrity

To characterize the first generation of the *opn1sw* line, I performed genotypic profiling of the offspring (F1), with primers amplifying a 313 bp fragment of the target region of the cr/trRNA (Figure 12A). The *opn1sw* KOs presented an amplicon larger than the wild-type and heterozygote siblings (Figure 12A). Additionally, Sanger sequencing confirmed the presence of a double insertion: one of 20 bp upstream of the start codon and a second of 13 bp at the cr/trRNA target site (Figure 13A). These changes indicated a significant alteration in the genomic sequence, potentially affecting *opn1* function (Figure 13A).

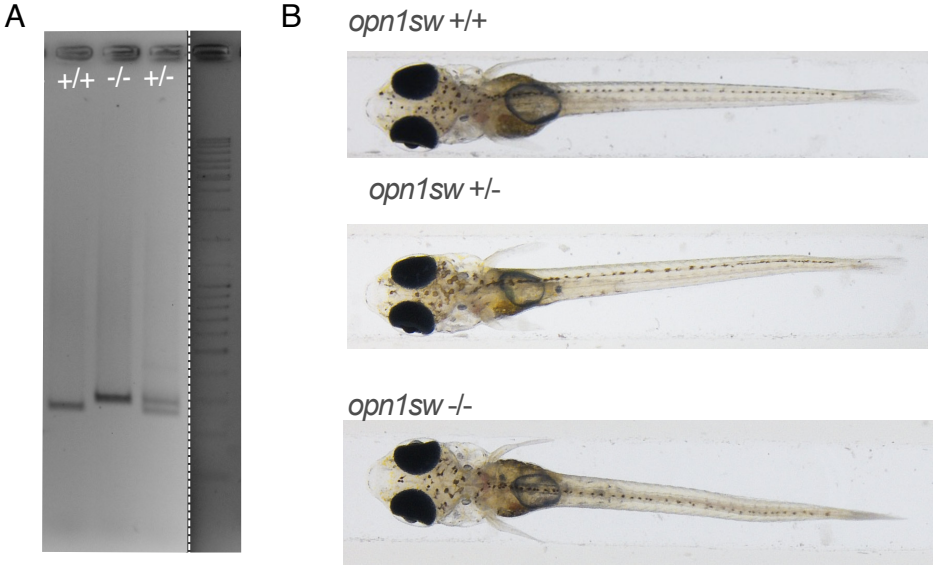

Figure 12. No gross morphological phenotype in *opn1sw* homozygous mutants (A) Genotyping of *opn1sw* heterozygous incross revealed individuals with wild-type (+/+) conditions (single band corresponding to the unmodified amplicon of 313 bp), homozygous mutants (-/-) displaying a larger amplicon (~350 bp) due to CRISPR/Cas9-induced indels and a heterozygous (+/-) individual with both bands. 2% agarose gel electrophoresis. (B) Representative image of hatchlings from the *opn1sw* stable line at 1dph, representing all the genotypes.

Downstream histological analysis of retina was performed to evaluate whether the *opn1sw* mutation impacted on its structural integrity.

Homozygous mutant (-/-) hatchlings exhibited disorganized ONL architecture (Figure 13B). As mentioned in 1.4, ONL is assembled by rods and cones tightly linearized in healthy wild-type fish. Compared to the retinas from wild-type and heterozygotes, *opn1sw* mutants, linear cell packing of the outer layers was disrupted, potentially impacted by non-fully differentiated photoreceptors (Figure 13B; arrow heads). In some regions, the ONL expanded to four cells in width rather than the typical two (Figure 13C; arrow heads). Nuclei of the ONL affected regions appeared more spherical, compared to +/+ or +/- siblings, suggesting structural alterations at the cellular level related to their spatial self-organization at the ONL region (Figure 13B).

To determine whether the observed morphological changes in the retina had functional consequences in the vision, electroretinography (ERG) was performed in collaboration with Dr. Jingjing Zang (University of Zurich). ERGs provide a robust electrophysiological measurement of the responses of specific photoreceptor populations from isolated retinas, exposed to controlled light stimuli (Chrispell et al., 2015). Opn1sw is a photopigment specialized in detecting short-wavelength light to measure reaction capacity of the photoreceptors, we exposed dissected retinas from 0 dph hatchlings of the *opn1sw* line were directly to blue/UV of a wavelength for 15 seconds.

ERG analysis indicated: wild-type and heterozygous retinas exhibited a logarithmic increase in b-wave amplitude with increasing light intensity, reflecting a normal activation of photoreceptors. In contrast, homozygous mutants displayed minimal changes in b-wave amplitude across light intensities, suggesting dysfunctionality among photoreceptor populations (Figure 13C).

These findings, together with the observed morphological defects, suggest that *opn1* is necessary for proper differentiation of photoreceptors and the detection of UV light.

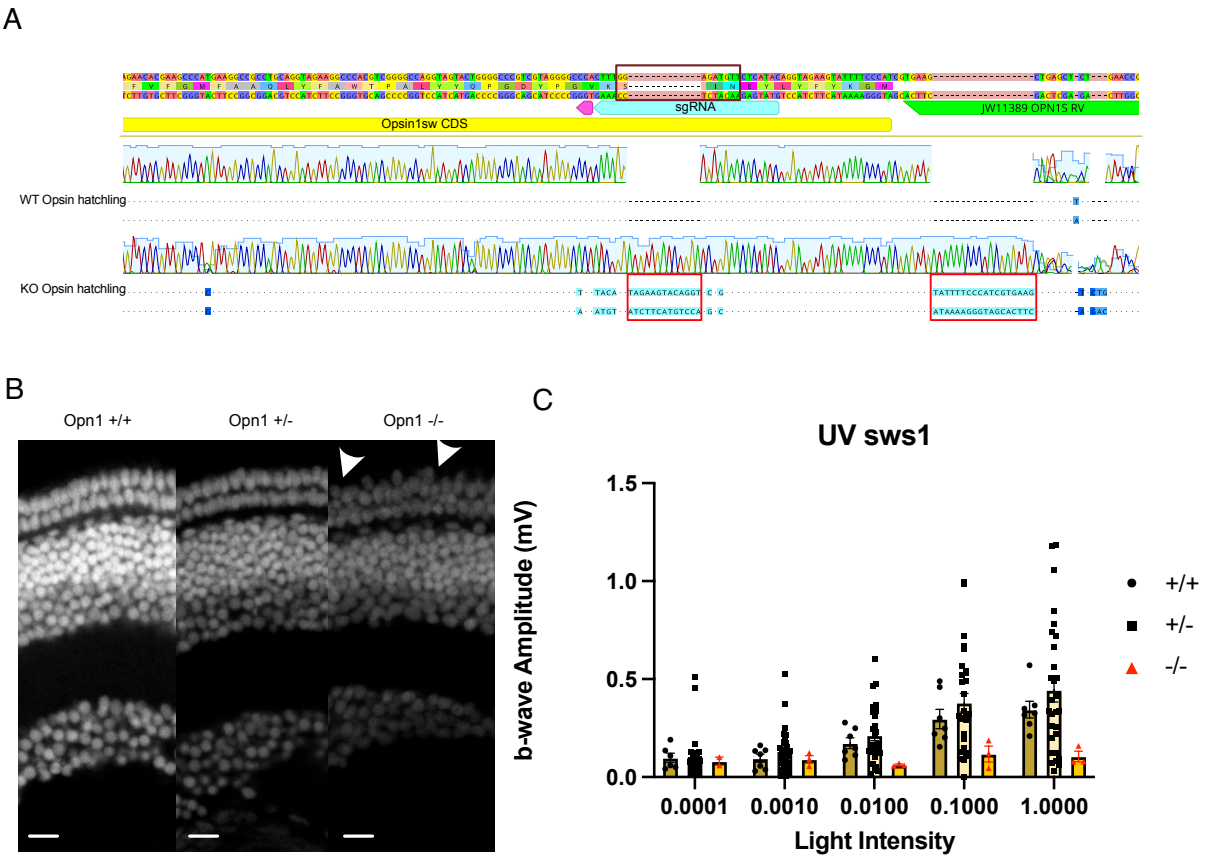

Figure 13. Characterization of a stable CRISPR/Cas9 edited *opn1sw* line. (A) Sanger sequencing validation of the opsin loci. The wild-type sequence perfectly matches the consensus reference, while the homozygous mutant sequence shows two insertions. Notably, a 13 bp insertion occurs within the designed mRNA editing window, disrupting a serine residue within a glycosylation motif, potentially altering protein function. An upstream insertion before the start codon does not affect the coding sequence. (C) DAPI-stained retinal sections showing photoreceptor organization. In wild-type (+/+) and heterozygous (+/-) retinas, the outer nuclear layer (ONL) is compact and well-organized, with clearly identifiable photoreceptor nuclei. In homozygous mutants (-/-), the ONL is disorganized with rounded nuclei and regions of cellular misalignment (arrow heads). Scale bar = 10 µm. (D) Column charts comparing the b-wave amplitude between the different genotypes in the *opn1sws* line. Wild-type and heterozygous retinas show a logarithmic response with increasing light intensity, whereas homozygous mutants exhibit no corresponding increase, indicating impaired photoreceptor responsiveness.

3.2.4 *rhodopsin* mutants displayed severe defects in visual function

Similarly, to *opn1sw*, the *rhodopsin* mutant stable line was generated. Adult medaka were genotyped to assess the extent of CRISPR/Cas9 mutagenesis. Genotyping revealed differences within the three genotypes: wild-type (650 bp), homozygous mutants (690 bp), and heterozygotes (three bands, including a heteroduplex formed during PCR) (Figure 14A). Follow-up Sanger sequencing identified a 9 bp deletion near the Cas9 cut site, together with a 41 bp insertion downstream (Figure 15A). This combination resulted in a frameshift and premature stop codon, likely leading to no functional Rhodopsin.

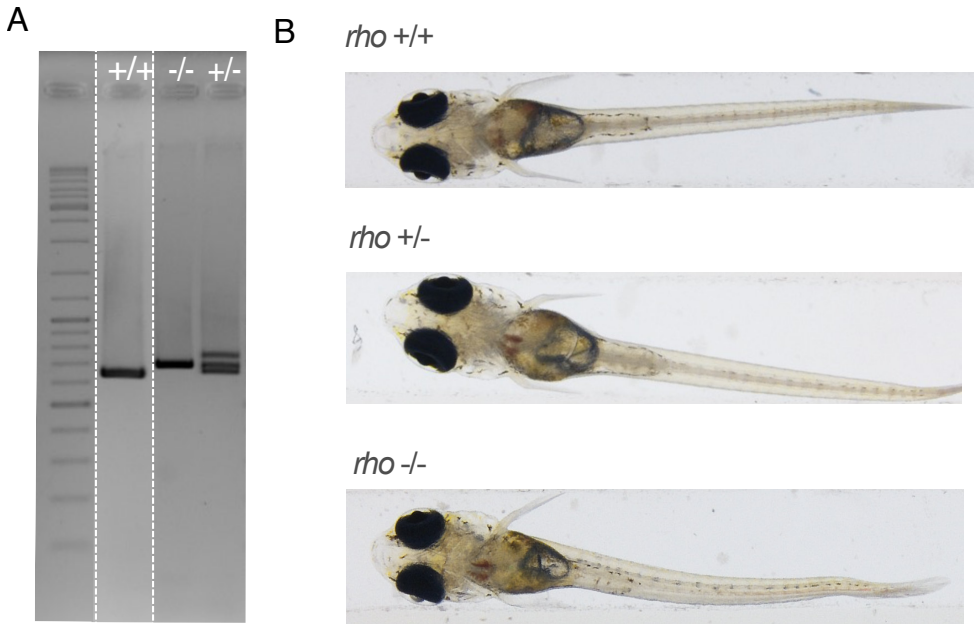

Figure 14. No gross morphological phenotype in *rhodopsin* homozygous mutants. (A) Genotypes of individual hatchlings from the stable *rhodopsin* line (heterozygous incross). Wildtype (+/+) hatchling display a single band of ~650 bp, homozygous mutants (-/-) show a single slightly larger amplicon (~690 bp) consistent with CRISPR/Cas9–induced insertions. Heterozygotes (+/-) exhibit three bands: the wildtype and mutant amplicons, plus an additional band likely resulting from heteroduplex formation. (B) Representative image of hatchlings from the *rho* stable line outcross at 1dph, representing all the genotypes.

Histological assessment of the retina revealed that *rhodopsin* +/+ and +/- hatchlings exhibited a physiological retinal structure, although the ONL in heterozygotes appeared slightly less compact. In homozygous (-/-) mutants, photoreceptor packing assembled similar to wild-type conditions, yet rod photoreceptors declined in numbers. Nucleus staining indicated an increase of apoptosis of photoreceptors, leading to near-complete loss of rod photoreceptors immediately after differentiation. This effect was observed across the entire retina (Figure 15B).

Consecutive ERG was performed by exposing dissected retinas from 0 dph hatchlings of the *rhodopsin* mutant line to white light, as Rhodopsin mediates black-and-white contrast detection. Increasing light intensities elicited robust and rapid responses in wild-type and heterozygous hatchlings (Figure 15C), further supporting the near-physiological conditioned morphology. Homozygous mutants exhibited delayed responses that required higher light intensities to elicit activation, indicating a loss of rod photoreceptor functionality (Parmeggiani et al., 2011; Tikidji-Hamburyan et al., 2017) (Figure 15C).

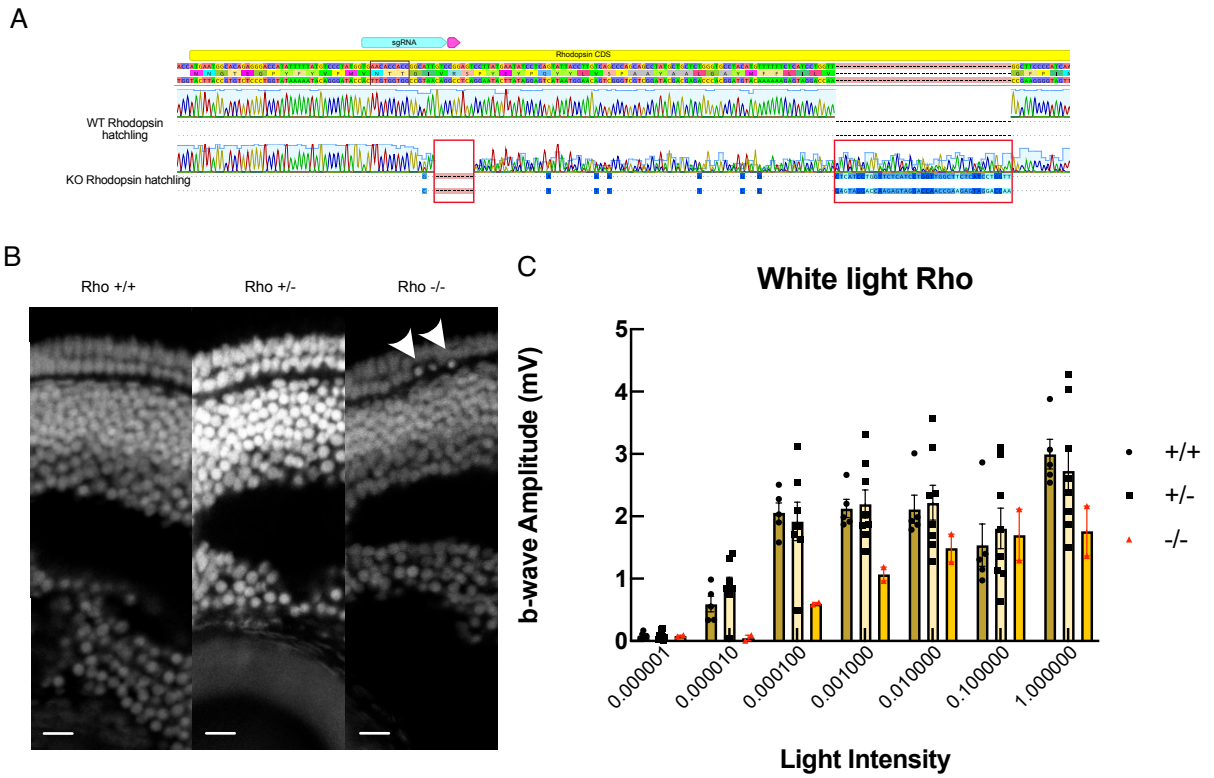

Figure 15. Loss of rod photoreceptors physiologically impacts on light sensitivity in rhodopsin mutants. (A) Sanger sequencing aligned to the Medaka *rhodopsin* consensus sequence. Wildtype sequences perfectly match the reference. In homozygous mutants, a 40 bp insertion occurs downstream of the guide RNA target site, accompanied by a 9 bp deletion at the Cas9 cleavage site. The canonical glycosylation site remains intact.(C) Retinal histology of the three genotypes stained with DAPI (scale bar: 10 µm). Both wildtype (+/+) and heterozygous (+/-) retinas show a well-organized ONL with clearly distinguishable rods and cones. In homozygous mutants (-/-), rod nuclei appear pyknotic (arrowheads) shortly after photoreceptor differentiation, and the ONL is reduced to a single disorganized layer, although cones (Zpr1-positive) remain present. (D) Electroretinography (ERG) Column charts comparing the b-wave amplitude between the different genotypes in the opn1sws line. Wild-type and heterozygous retinas show a logarithmic response with increasing light intensity, whereas homozygous mutants exhibit no corresponding increase, indicating impaired photoreceptor responsiveness.

To investigate whether reduced response to white light stimulus was reflected in mutant behaviour, OptoMotor Response (OMR) assay was conducted in collaboration with Dr. Risa Suzuki (Heidelberg University). Hatchlings (0dph) were placed in an so-called infinity pool in which a revolving stripe pattern as visual stimulus was projected on the surrounding walls. This allowed assessment of swimming behaviour, response latency, and visual acuity (Suzuki, 2025). The homozygous *rhodopsin* mutant hatchlings displayed significantly impaired tracking (0.02594098 ± SEM) of the visual stimulus compared with wild-type (0.03729552 ± SEM) and heterozygous (0.03513688 ± SEM) siblings (Figure 16C). While wild-type hatchlings responded to thin stripe stimuli (3 mm), mutants only responded reliably to thicker stripes (~6 mm).

Visual acuity, defined as the ability to follow the stimulus continuously over repeated trials, was significantly reduced in *rhodopsin* mutants (Supplementary Figure 4). In addition to the characteristic response of the mutant hatchlings, they exhibited increased overall activity, swimming faster during OMR trials than their wild-type counterparts (Figure 16C). This finding might explain the indecisive behaviour due to lower resolution of the stimulus, which potentially contributed to more movement.

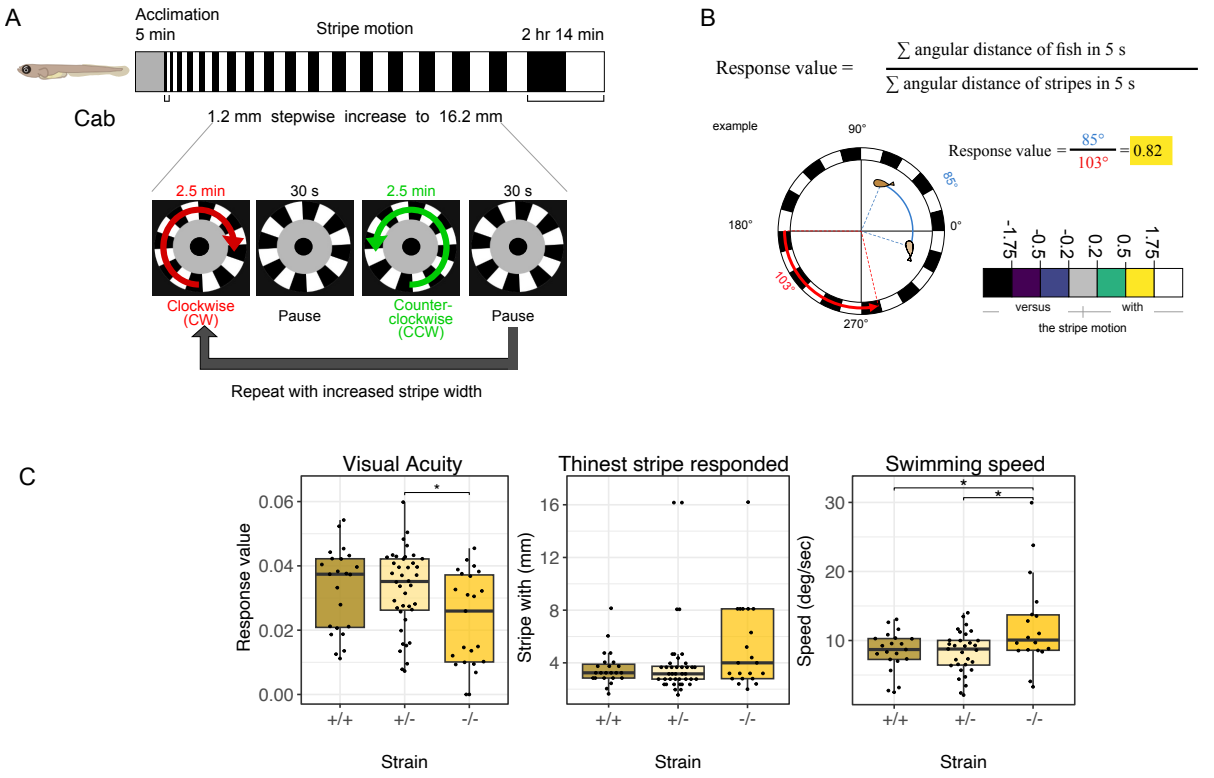

Figure 16. Optomotor response as a functional analysis for visual acuity in *rhodopsin* mutant line. (A) Schematical representation of the OMR Experimental procedure. After 5 minutes of acclimation, hatchlings were subjected to the stripe motion. Each set of stripe motions consists of 2.5 minutes of clockwise (CW) motion, 30 seconds of pause, 2.5 minutes of counterclockwise (CCW) motion, and 30 seconds of pause, which was followed by further sets of stripe motions with thicker stripes and speed. (B) Response value calculation. Dividing distance swam by the fish as an angle, by the movement of the stripe in 5s. (C) Boxplot representing the visual acuity, stripe response and swimming speed of the *rhodopsin* line in OMR. Wild-type and heterozygous hatchlings tracked moving visual stimuli (3 mm) consistently, while homozygous mutants required thicker stimuli (~6 mm) and could not maintain tracking, indicating reduced visual acuity (In collaboration with Dr. Risa Suzuki). Panels A & B adapted from (Suzuki, Wittbrodt 2025 unpublished).

Together, these results demonstrate that mutations in *opn1* and *rhodopsin* exert profound yet distinct effects on retinal integrity and visual performance. *Opn1sw* disruption primarily altered the compactness of cone photoreceptors, whereas *rhodopsin* mutation led to the rapid loss of rods shortly after differentiation. These structural abnormalities were directly reflected in functional characterization:

photoreceptor responses to light were diminished in mutants, and their ability to detect and track visual stimuli was impaired, as revealed by both ERG and OMR experiments. Collectively, these results highlighted the essential roles of *opn1sw* and *rhodopsin* in maintaining both the organization and survival of photoreceptors, and functional capacity of the retina, establishing a clear link between photoreceptor integrity and visual behavior in medaka hatchlings.

3.2.5 Morphometric workflow of retina photoreceptor populations

The opn1sw and rhodopsin mutant lines morphological and functional characterization demonstrated the impact of these candidate genes on the retina conformation and response to different light stimuli. The other candidate genes have not been phenotypically analyzed in medaka retinae.

To cover the understanding of the morphological impact of the candidate genes on the retina, I performed a quantitative analysis on photoreceptor distribution of hatchlings treated with CRISPR/Cas9 and cr/trRNA targeting for each of the candidate genes. Photoreceptor quantification was carried out manually using DAPI staining in combination with positional information within the retina, allowing reliable identification of individual cell types. Each stained nucleus was quantified for three selected regions in all retina layers: dorsal (green), central (cyan) and ventral (magenta, Figure 17A).

To standardise the obtained data, ratios of each photoreceptor population relative to the total number of cells counted in the respected region of the retina were calculated. Dorsal and ventral regions included a section of the retina close to the CMZ, yet with completed differentiation in all cell layers. The central region corresponded to a part of the retina as close as possible to the optic nerve with the nuclear layer structure defined. Since teleost retinal growth occurs through the addition of concentric rings at the periphery, regions closest to the CMZ correspond to the most recently generated tissue (Heermann et al., 2015; Miles & Tropepe, 2021). Conversely, the central region represents tissue formed earlier during embryonic development , potentially reflecting more clearly the cumulative effects of genetic mutations over time.

To standardize the quantification process, nuclei were used as proxy for cell shape and classified according to their shape and position within the ONL: cone photoreceptors were identified as elongated nuclei in the upper ONL; rod

photoreceptors as round nuclei situated beneath the cones; undetermined photoreceptors as nuclei with ambiguous morphology or localization; and pyknotic nuclei as small, intensely DAPI-stained cells indicative of apoptosis (Figure 17B).

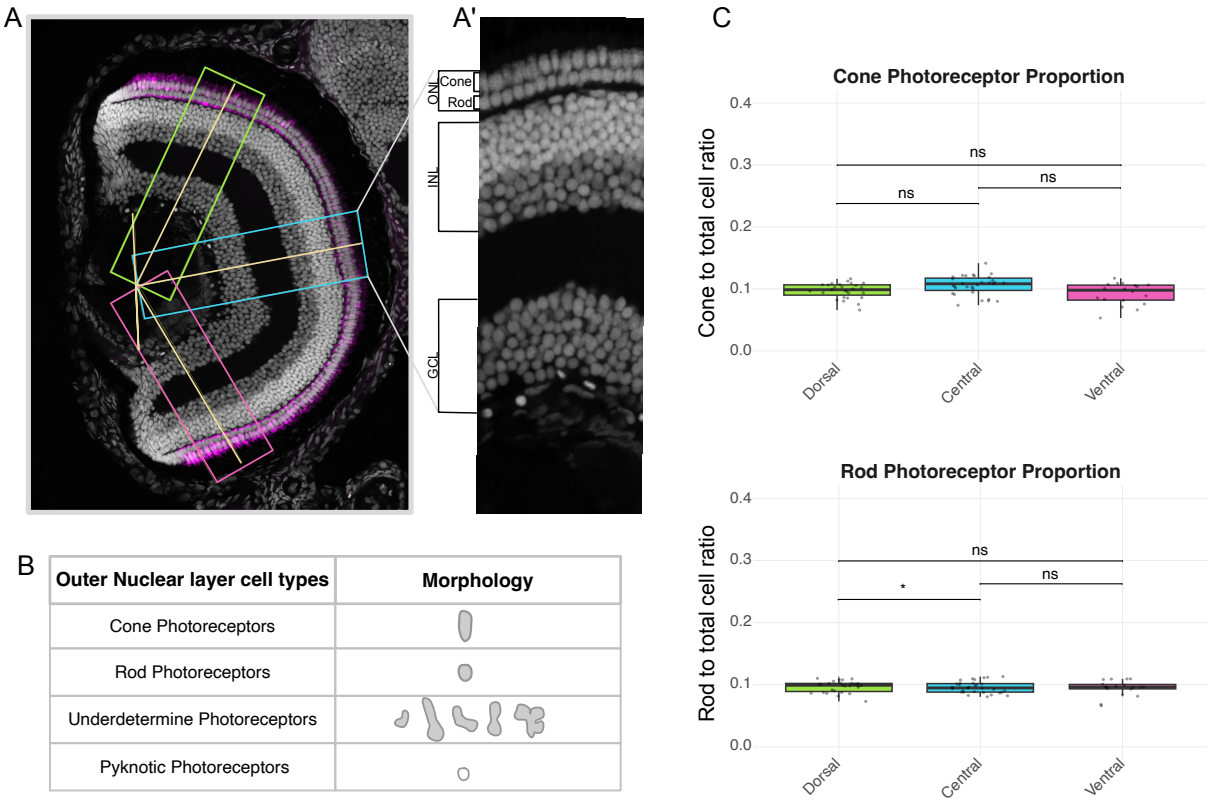

B

Outer Nuclear layer cell types	Morphology
Cone Photoreceptors	
Rod Photoreceptors	
Underdetermine Photoreceptors	
Pyknotic Photoreceptors	

Figure 17. Image acquisition and cell quantification strategy for photoreceptor analysis. (A) Transverse section of a 0 days post hatch (dph) medaka retina stained with DAPI (gray) to label nuclei and Zpr1 (magenta) as a cone marker. Three retinal regions (dorsal, central, and ventral) used for quantitative analysis are outlined. (A') Enlarged view of one selected region illustrating the retinal layers: ganglion cell layer (GCL), inner nuclear layer (INL), and outer nuclear layer (ONL). Within the ONL, two photoreceptor populations are distinguished by their position: rods, located deeper in the ONL with rounded nuclei, and cones, located more superficially with elongated nuclei. (B) Classification table summarizing the ONL cell types considered in this study: cones (superficial, elongated nuclei), rods (deeper, rounded nuclei), “indeterminate” cells (atypical morphology or unclear positional identity), and “pyknotic” nuclei (small, highly condensed DAPI signal). (C) Boxplots comparing the abundance of each photoreceptor cell type across dorsal, central, and ventral regions in wild type (WT) retinas. No regional differences were observed, supporting the use of the central retina for subsequent photoreceptor stability analyses. Statistical analysis was performed with two-tailed t-tests, corrected with Bonferroni, $p < 0.05$ N=35.

As a baseline analysis, I quantified the proportion of cone and rod photoreceptors found for each retina region in wild-type untreated hatchlings. Within the three regions, the cone-rod distributions were found to be identical, not significantly differing from one another (Figure 17C). For the central part being the oldest tissue within the forming retina and thus likely most affected by progressive effects, I focused on this area for

the following characterization of candidate gene mutant retinae (see appendix for dorsal and ventral regions for completeness).
Overall, the CRISPR-induced mutations of the candidate genes were expected to produce two main effects on the stable lines: induction of apoptosis in specific photoreceptor populations (Figure 15C), or changes in nuclear morphology and photoreceptor differentiation within the ONL (Figure 13C).

3.2.5.1 Impact of candidate gene loss of function on rod photoreceptors

Based on the morphometric workflow on retina photoreceptor populations, I assessed the remainder of the candidate genes by performing a CRISPR/Cas9-based screening in the injected generation. To rule out possible injection artifacts of Cas9 on retinal development, a cr/trRNA targeting *the oculocutaneous albinism 2 (oca2) gene* responsible for pigmentation in the medaka RPE, was used as a control.
Wild-type medaka hatchlings were injected at the one-cell stage with a mixture of Cas9 mRNA and the cr/trRNA targeting each gene of interest. Non-injected controls and *oca2* control guide-injected hatchlings shared similar composition in rod photoreceptors in the retina. Therefore, any alterations detected in the candidate genes KOs could be attributed to the gene-specific loss.
In the positive control, i.e. hatchlings injected with the guide RNA targeting *rhodopsin* showed the expected significant reduction in the rod photoreceptor population. Histological analysis revealed a high number of pyknotic nuclei in regions where rods would normally develop (Figure 18A), effectively recapitulating the phenotype observed in the stable rhodopsin line (Figure 15C). Further, hatchlings injected with the guide targeting *opn1* exhibited altered cellular organization in the ONL, with disrupted layer integrity, particularly affecting cones, where multiple nuclei were often observed occupying the same position (Figure 18B).
In the case of *elovl4*, the most pronounced effect was observed in the nuclear morphology of rod photoreceptors, which displayed elongated shapes rather than the typical round morphology and partially encroached on the space usually occupied by cones (Figure 18A).
Among the candidate genes, *pikachurin*, mutation revealed a global impact on medaka embryonic development, with increased embryonic fatality and body abnormalities.

Among injected embryos that reached a stage comparable to the wild-type, their retinas displayed severe abnormalities, including an increased presence of pyknotic nuclei (Figure 18A). In the ONL, the typical organization was highly disrupted, with no clear separation between rods and cones, and the characteristic nuclear morphology of the layer was largely unrecognizable (Figure 18A).

During the *in silico* screening for potential glycoprotein affectors of photoreceptor development and maintenance, several 'novel genes' were identified as well. Since their function was unknown, their implication with photoreceptor involvement was unclear. Two novel candidates, ENSORLG00000000896 and ENSORLG00000013140 were tested by targeted genome editing and only showed mild overall phenotypes including heart arrythmia small or ocular cysts during embryogenesis. Histological analysis of the retinas from these knockouts revealed no significant differences compared to the uninjected siblings as the ONL organized in two layers with regularly shaped nuclei and no indication of pyknotic cells (Figure 18 A&B).

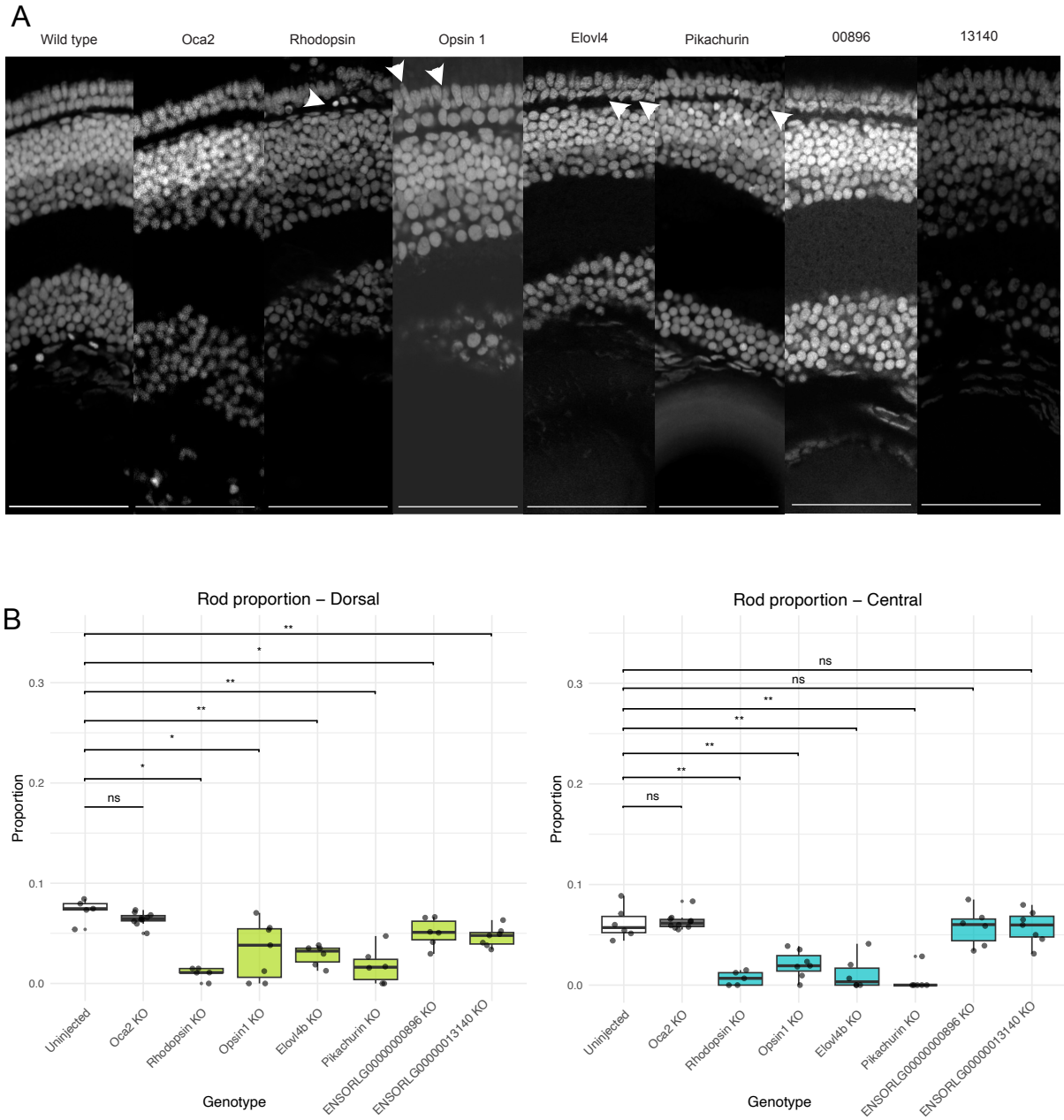

Figure 18. Knockout of candidate genes affects rod photoreceptor proportion in Medaka retina. (A) Representative transverse sections of the central retina from each knockout line stained with DAPI to visualize nuclear architecture. Scale bar: 50 µm. (B) Boxplot depicting the proportion of rods relative to the total number of cells in the dorsal and central retina for all knockout (KO) candidates generated using CRISPR/Cas9. Comparisons were made between knockout hatchlings and uninjected siblings at 0 days post hatch (dph). Rhodopsin, Elovl4 and Pikachurin showed a significance of $p < 0.001$, Opsin1 $p < 0.01$; ENSORLG00000000896 and ENSORLG00000013140 showed no significance Oca2 was used as injection control altering eye pigmentation but not the retinal cell composition. Asterisks indicate statistical significance compared with uninjected siblings. Statistical analysis was performed with two-tailed t-tests, corrected with Bonferroni, $p < 0.05$ N=9.

The morphological analysis together with the CRISPR/Cas9 screening provides robust evidence of the relevance of many of the selected candidate genes to photoreceptor development, morphology, and retina organization To take this mutant screening one

step further and investigate the impact of predicted *N*-glycosylation sites for the respective protein's function, I used a rescue scheme as detailed below.

3.3 mRNA Rescue of CRISPR/Cas9 Knockouts to Assess Glycosylation in Medaka Retinal Development

Since the applied genetic tools did not allow an efficient enough mutagenesis of asparagines (Asn) within the *N*-glycosylation sequon of the candidate genes, an alternative approach was applied. Knock-out mutations can be rescued by simultaneously injecting full length mRNA of the target gene. Usually, the rescue is most effective when mutations affecting early embryogenesis need to be reconstituted. Plasmids containing the full-length coding sequence of each candidate gene were established, and site-directed mutagenesis was used to replace the codons of predicted glycosylated asparagines with those of glutamine.

Further, different mRNA variants were prepared: a) wild-type, containing the coding sequence of the wild-type full-length transcript (*rho*→ ENSORLT00000013289.2*,* *opn1sw*→ ENSORLT00000024037.2*,* *elovl4b*→ ENSORLT00000021297.2*,* *pikachurin*→ ENSORLT00000027415.1), b) sequon mutant variant, where all predicted glycosylation Asn were substituted with Gln, and c) variants where individual Asn were individually mutated.

Cab embryos were injected at the one-cell stage with 150 ng/µl CRISPR/Cas9 mRNA, 4µM of the gene-specific cr/trRNA, the individual mRNA variants of each candidate (100ng/µl) and 10ng/µl *GFP* mRNA as injection tracer . Embryos were grown until hatching, and both developmental progress and survival were monitored for each condition. After hatching, a subset of hatchlings was collected for genotyping to confirm efficient Cas9 activity. To assess retinal phenotypes, a minimum of six hatchlings per condition were processed for analysis (Figure 19). The injections and subsequent genotyping of the embryos for the mRNA rescue experiment were performed with the assistance of Phoebe Karagianni (Heidelberg University).

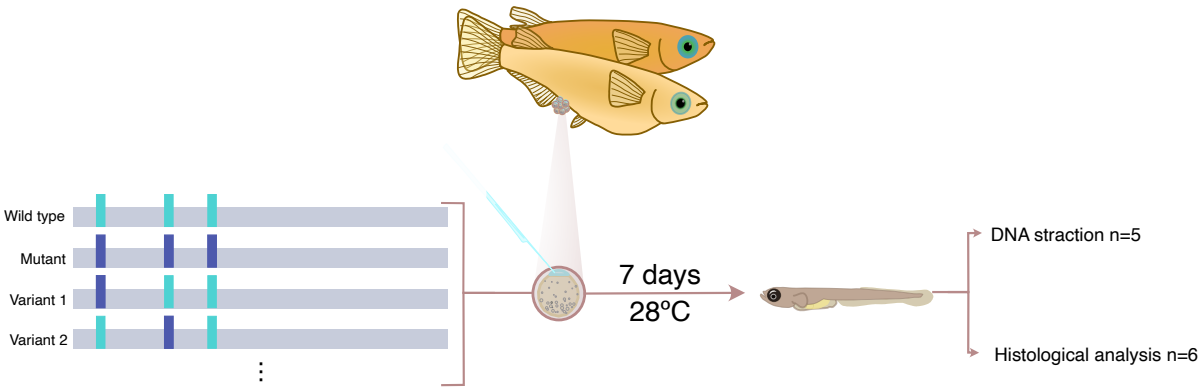

Figure 19. Experimental design for mRNA rescue assays. Schematic representation of the mRNA rescue experiment. At the one cell stage, *Oryzias latipes* embryos were injected with one of the following synthetic mRNAs in separate experimental groups: wild type mRNA (light blue, indicating the positions of all asparagine residues), mutant mRNA in which all asparagines were substituted by glutamines (dark blue), or variants in which individual asparagine residues were substituted by glutamine. Each injection also included Cas9 mRNA, a guide RNA targeting the gene of interest, and GFP mRNA as a tracer. Embryos were incubated under controlled conditions at 28 °C for 7 days until hatching. Five hatchlings per condition were collected for genomic DNA extraction, and the remaining hatchlings (minimum N = 6 per condition) were fixed in PFA for histological analyses.

Rescue experiments were evaluated based on multiple criteria beyond retinal histology. Mortality rates were carefully monitored, as inhibition of glycosylation in candidate proteins led to increased embryonic lethality. Additionally, only embryos that hatched successfully and developed comparably to uninjected controls were considered for analysis.

3.3.1 Wild-Type *rhodopsin* mRNA restored rod photoreceptor stability during early development in *rhodopsin* KOs

As a positive control Rhodopsin function was expected to be rescued by wildtype *rhodopsin* mRNA injection un parallel with a knock-out regime. Further, administration of mRNA variant mutant at the *N*-glycosylation motifs should not be able to reconstitute photoreceptor maintenance. Thus, two mRNA variants were designed: the wild-type version comprising the coding sequence of *rhodopsin* (ENSORLT00000013289.2) with both asparagines codons present at positions 2 and 15 of the protein, and a mutant version in which both codons were substituted (p.N2Q;N15Q) to encode glutamine (Figure 20A). As controls for the experiment, embryos were injected either with Cas9 and just the corresponding guide RNA, or just the synthesized mRNAs, to assess any potential toxic effects of the injections on embryonic development.

Baseline mortality in uninjected embryos was 27.9%, which increased to 37% upon injection of Cas9 with the *rhodopsin* guide alone (Figure 20B). Co-injection of wild-type *rhodopsin* mRNA with Cas9/guideRNA resulted in a similar lethality (39.1%), indicating that the WT mRNA is relatively well tolerated in the knockout context (Figure 20B). In contrast, embryos receiving the mutant *rhodopsin*$^{p.N2Q;N15Q}$ mRNA showed a striking increase in mortality, reaching 66.5% (Figure 20B). Control injections of WT and mutant mRNA alone produced lethality rates of 41.9% and 67%, respectively, demonstrating that the mutant mRNA is intrinsically more deleterious to embryonic development than the wild-type sequence (Figure 20B). These results highlight the critical role of the two asparagines in the reported *N*-glycosylation sequons for proper Rhodopsin function and more important also for embryonic viability upon systemic overexpression of the mRNA variants (Figure 20B).

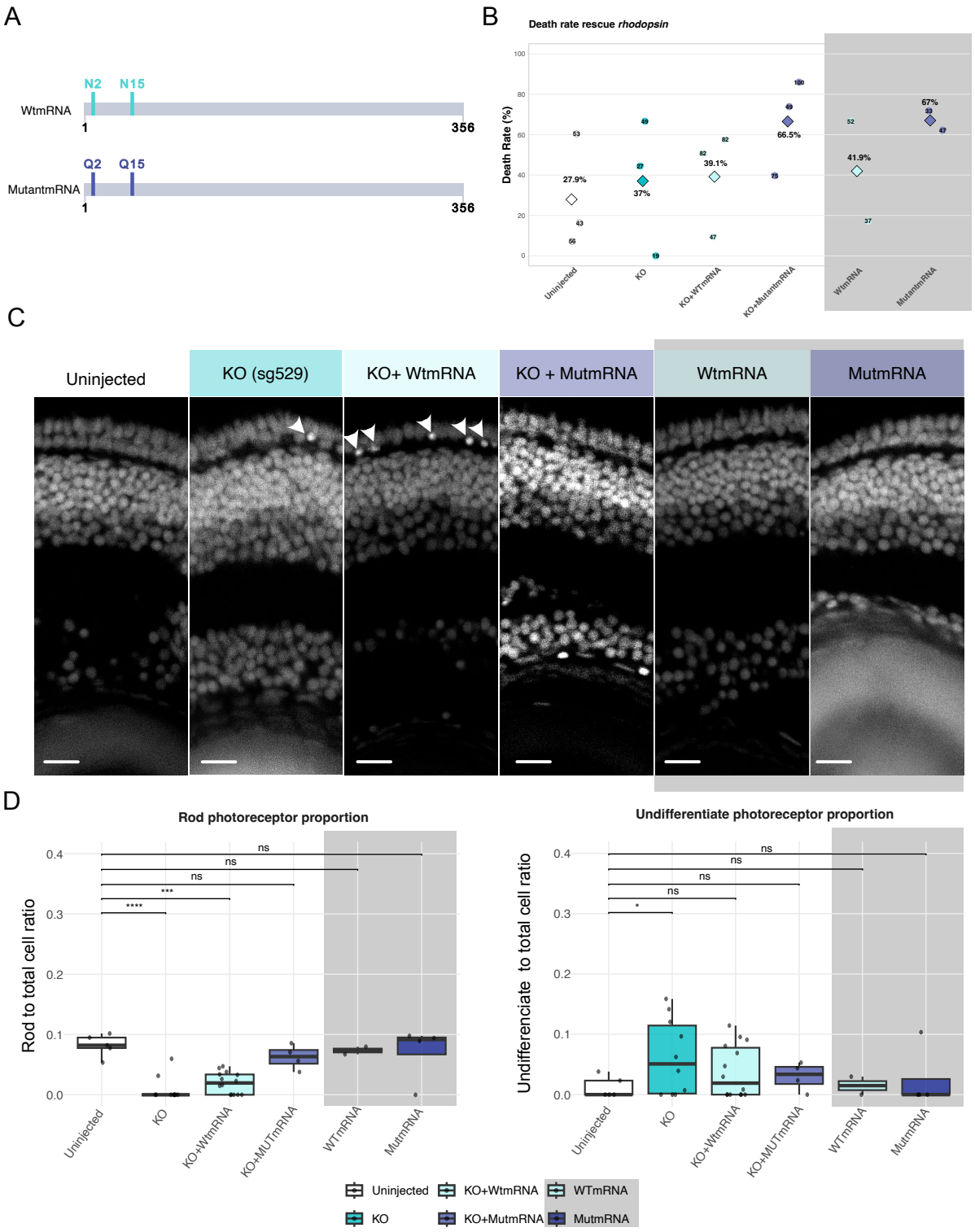

Figure 20. Reconstitution of wildtype but mutant Rhodopsin rescues knockout induced photoreceptor loss. (A) Schematic representation of the structure of the rhodopsin mRNA used in the study. Indicating in light blue the position of Asparagines (Asn) likely to be glycosylated; in the mutant Asn have been changed into Glutamine (Gln), indicated in dark blue.(B) Death rates observed following microinjection of each mRNA variant at the 1-cell stage (n ≥ 50 per condition; total number indicated in each dot).(C) Representative cryosections of retinas displaying the most common phenotype observed for each condition. Pointing arrows to pyknotic nuclei (bright DAPI signal). Scale bar = 10µm. (D) Quantification of photoreceptor cells in the retina at 0 dph. Left panel: proportion of rod photoreceptors relative to the total number of cells in central retinal region. Right: proportion of undifferentiated or unidentifiable cells based on DAPI staining. Each dot represents an individual retina. (N=6). Color code:

Uninjected (White), KO (Cyan), Wt (Ice Blue), Mut (dark blue). Bars represent mean ± SD. (two-tailed t-tests, corrected with Bonferroni, $p < 0.05$).

Histological examination confirmed a pronounced reduction in the rod photoreceptor population in the knockout hatchlings, accompanied by numerous pyknotic nuclei, indicating ongoing cell death (Figure 20C). A similar phenotype was observed in hatchlings co-injected with wild-type *rhodopsin* mRNA, where rod photoreceptor loss appeared even more pronounced than in the KO alone, suggesting partial rescue but persistent cellular stress (Figure 20C&D). In contrast, hatchlings injected with the mutant *rhodopsin*$^{p.N2Q;N15Q}$ mRNA showed no significant changes in retinal morphology compared to uninjected controls (Figure 20C&D). This apparent lack of effect is likely influenced by the high lethality observed in this group; the hatchlings that survived to hatching may represent escapers that were either not effectively injected or only displayed the residual impact of the KO. Importantly, embryos injected with either wild-type or mutant *rhodopsin* mRNA in the absence of Cas9 showed no alterations in retinal morphology, indicating that the mRNA itself does not affect retinal development (Figure 20C&D).

Taken together, these observations indicate that while wild-type mRNA can partially maintain rod integrity, disruption of glycosylation-sites in the mutant mRNA exacerbates embryonic lethality, limiting the number of individuals available for histological analysis and masking potential phenotypic effects (Figure 20C&D).

3.3.2 mRNA rescue of *opn1sws* highlights the role of asn10 in retinal integrity.

To investigate the role of asparagines in *opn1sws* on photoreceptor integrity, four variants of *opn1sw* mRNA were synthesized: the wild-type codon sequence of the ENSORLT00000024037.2, the variant missing both asparagine (N10Q;N71Q) codons present in predicted glycosylation sites, and two single-site variants in which either Asn10 or Asn71 was replaced by glutamine (Figure 21A). These mRNAs were injected into cab embryos at the one-cell stage in combination with CRISPR/Cas9 targeting *opn1sws*.

Lethality analysis revealed that uninjected embryos exhibited a baseline mortality of 8.1%, while knockout (KO) embryos had a similar rate of 8.9% (Figure 21B). Co-injection of wild-type mRNA with the KO increased lethality to 47.8%, whereas the

N10Q and N71Q single-site variants showed 81.3% and 89.6% lethality, respectively (Figure 21B). Injection of the fully mutated mRNA resulted in 67.3% lethality. Control injections of wild-type or mutant mRNA alone led to 8.6% and 30.8% lethality, respectively (Figure 21B).

Histological analysis showed that in the KO, the photoreceptor population was significantly reduced, with a marked increase in undifferentiated photoreceptors (Figure 21C&D). The outer nuclear layer appeared less compact compared to uninjected controls. Injection with wild-type mRNA produced a phenotype very similar to the KO (Figure 21C&D). In contrast, injection with the *opn1sw*$^{n10Q;N71Q}$ variant mRNA did not substantially reduce rod populations but resulted in a significant decrease in cones, accompanied by a large increase in undifferentiated photoreceptors (Figure 21C&D). Among the single-site variants, *opn1sw*^{N10Q} variant had the most pronounced effect on cone integrity and ONL organization, highlighting the potential role of Asp10 being glycosylated (Figure 21C&D). In all conditions, uninjected and only mRNA-injected controls displayed normal retinal morphology, indicating that the mRNA itself did not perturb development (Figure 21C&D).

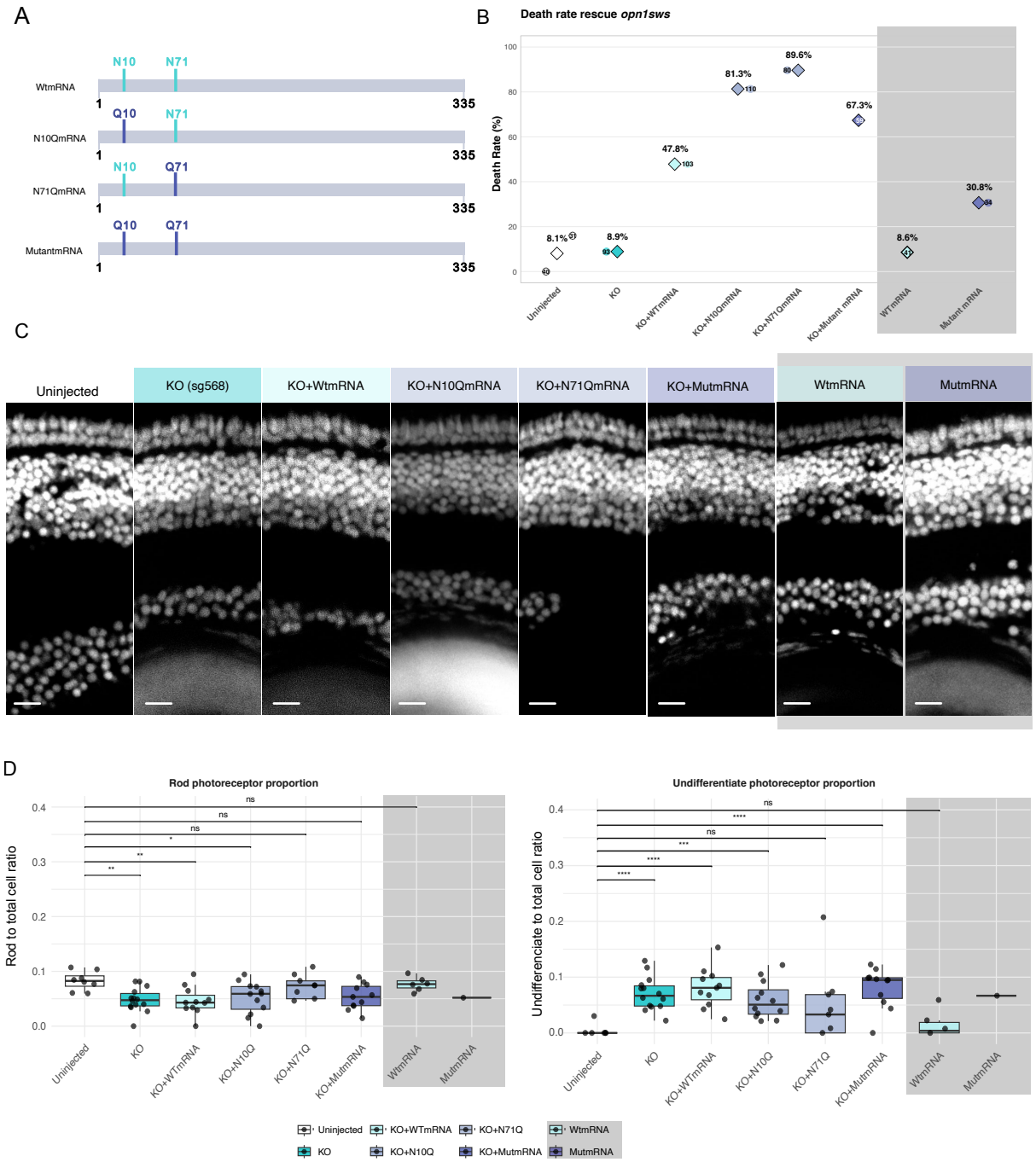

Figure 21. Histological and morphological evaluation of opsin mRNA rescue in medaka hatchlings. (A) Schematic representation of the structure of the mRNA used in the experiment. Indicating in light blue the position of Asparagines (Asn) likely to be glycosylated; different variants were generated were each Asn have been changed into Glutamine (Gln), indicated in dark blue.(B) Death rates observed following microinjection of each mRNA variant at the 1-cell stage (n ≥ 50 per condition).(C) Representative cryosections of retinas displaying the most common phenotype observed for each condition. Scale bar = 10µm. (D) Quantification of photoreceptor cells in the retina at 0 dph. Left pannel: proportion of Rod photoreceptors relative to the total number of cells in central retinal region. Right: proportion of undifferentiated or unidentifiable cells based on DAPI staining. Each dot represents an individual retina. (N=6). Color code: Uninjected (White), KO (Cyan), Wt (Ice Blue), Variants (Lavander). Bars represent mean ± SD. (two-tailed t-tests, corrected with Bonferroni, $p < 0.05$).

In summary, glycosylation at specific residues of opn1sws, particularly Asp10, is crucial for proper cone photoreceptor differentiation and for maintaining the ONL structural integrity.

3.3.3 Functional analysis of *elovl4* via mRNA rescue indicates critical developmental roles independent of glycosylation

To assess the role of *elovl4* in retinal development, five main mRNA variants were synthesized: the wild-type coding sequence of ENSORLT00000021297.2, a mutant variant, with three potential glycosylated Asn codons mutated into Gln, *elovl4b*$^{p.N9Q;N72Q;N116Q}$ and three additional variants where each individual asparagines were substituted with glutamines: *elovl4b*$^{p.N9Q}$, *elovl4b*$^{p.N72Q}$ and *elovl4b*$^{p.N116Q}$. Notably, the fully mutated mRNA was tested, but sequencing analysis did not confirm the presence of the intended mutations. Embryos were injected at the one-cell stage, allowed to develop until hatching, and subsequently analyzed for both lethality and retinal morphology (Figure 22A).

Lethality analysis revealed a pronounced impact of *elovl4* mRNA injections on embryo survival. Uninjected controls displayed a baseline mortality of 4.8%, while KO embryos alone showed 10.5% lethality. Co-injection of WT mRNA increased lethality substantially to 67.9%, with individual asparagine variants displaying similar high lethality: N9Q 69%, N72Q 82%, and N116Q 42.8%. These results indicate that embryos receiving *elovl4* mRNA, regardless of glycosylation status, were particularly sensitive to perturbations in this gene (Figure 22B).

Histological analysis of the central retina revealed a marked reduction in rod photoreceptor populations in KO embryos compared to uninjected controls. The ONL exhibited pronounced morphological changes, with small, rounded nuclei present in both rod and cone layers (Figure 22C&D). In embryos rescued with WT mRNA, the retinal phenotype was largely similar to the KO, albeit with an increased proportion of undifferentiated photoreceptors. Each of the single-asparagine mutant variants reproduced the KO-like phenotype, likely reflecting the high lethality observed in these groups (Figure 22C&D).

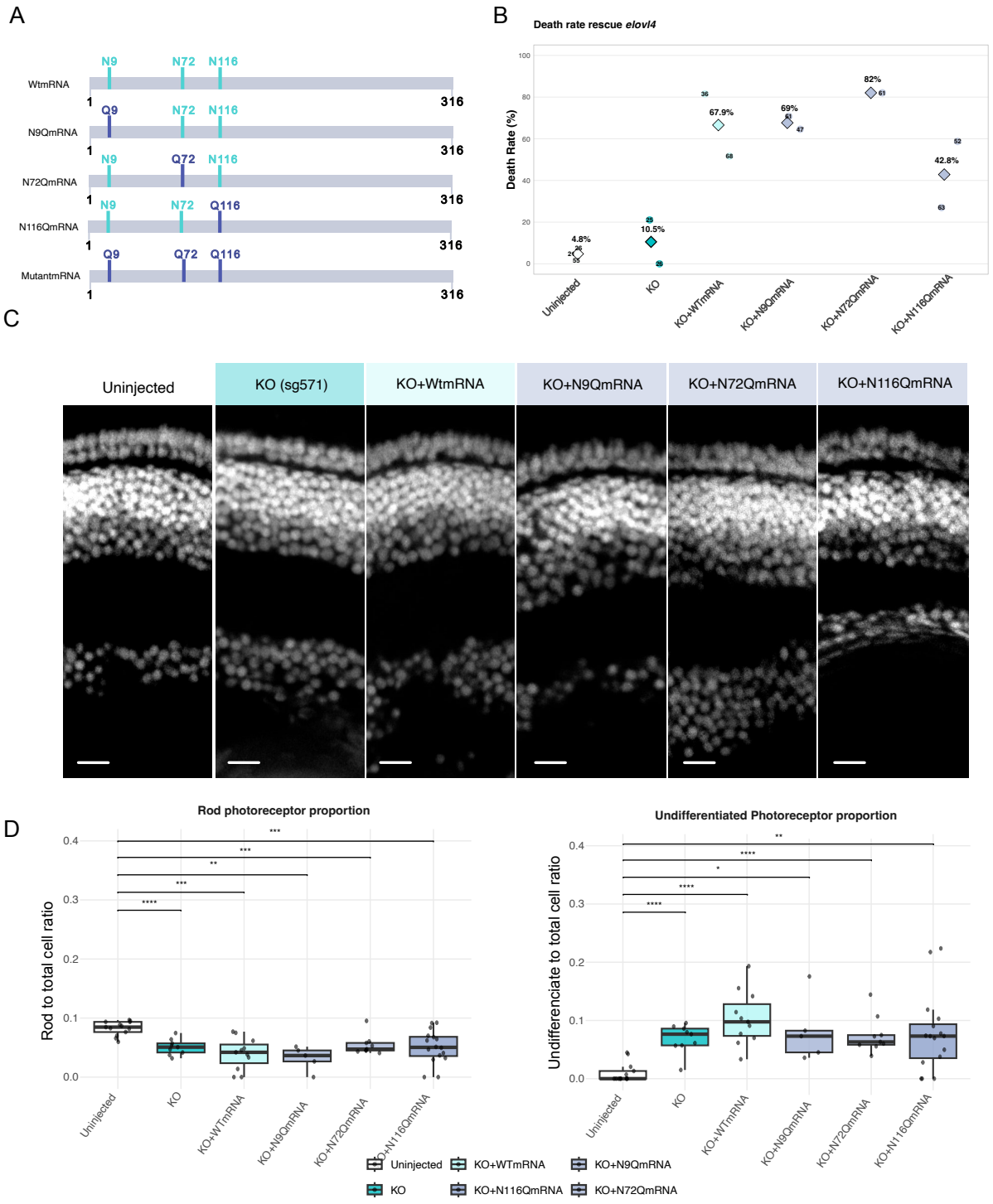

Figure 22. Histological and morphological evaluation of Elovl4 mRNA rescue in medaka hatchlings. (A) Schematic representation of the structure of the mRNA used in the experiment. Indicating in light blue the position of Asparagines (Asp) likely to be glycosylated; different variants were generated were each Asn have been changed into Glutamine (Glu), indicated in dark blue.(B) Death rates observed following microinjection of each mRNA variant at the 1-cell stage (n ≥ 50 per condition).(C) Representative cryosections of retinas displaying the most common phenotype observed for each condition. Scale bar = 10µm. (D) Quantification of photoreceptor cells in the retina at 0 dph. Left panel: proportion of Rod photoreceptors relative to the total number of cells in central retinal region. Right: proportion of undifferentiated or unidentifiable cells based on DAPI staining. Each dot represents an individual retina. (N=6). Color code: Uninjected (White), KO (Cyan), Wt (Ice Blue), Variants (Lavander). Bars represent mean ± SD. (two-tailed t-tests, corrected with Bonferroni, $p < 0.05$).

Overall, these results confirm the critical role of *elovl4* in retinal development and embryonic viability. The similarity of retinal phenotypes across WT and predicted sequon mutant mRNAs suggests that the observed effects are largely independent of potential glycosylation, highlighting the essential structural and functional contribution of Elovl4 protein during early embryogenesis.

3.3.4 pikachurin mRNA rescue highlights critical roles in embryonic development and photoreceptor integrity

To investigate the role of *pikachurin* in photoreceptor development, four mRNA variants were designed: the wild-type coding sequence of ENSORLT00000027415.1 and three asparagine mutants in which the Asn at corresponding aminoacid positions 50, 327, and 660 were substituted with glutamine codons (Figure 23A). These mRNAs were injected into cab embryos at the one-cell stage.

Lethality rates of the embryos ranged between 31.4% (KO+ N660Q mRNA) to 56.6% (KO + WT mRNA) in the knock-out co-injected with mRNAs. At similar rates, but less severe, uninjected (46.7%) and KO (39%) were found lethal (Figure 23A). Notably, the injection of WT and most mutant mRNAs led to a moderate increase in embryonic lethality compared to KO alone, reflecting the general toxicity of exogenous mRNA and/or the sensitivity of developing embryos to perturbations in *pikachurin* levels. The N660Q variant, in contrast, was associated with the lowest lethality among injected groups, suggesting either reduced effect, lower toxicity, or incomplete functional perturbation of the protein (Figure 23B).

These differences in survival rates were carefully considered in the downstream histological analyses, as higher lethality may bias the population of hatchlings that survive to hatching toward those less affected by the injections.

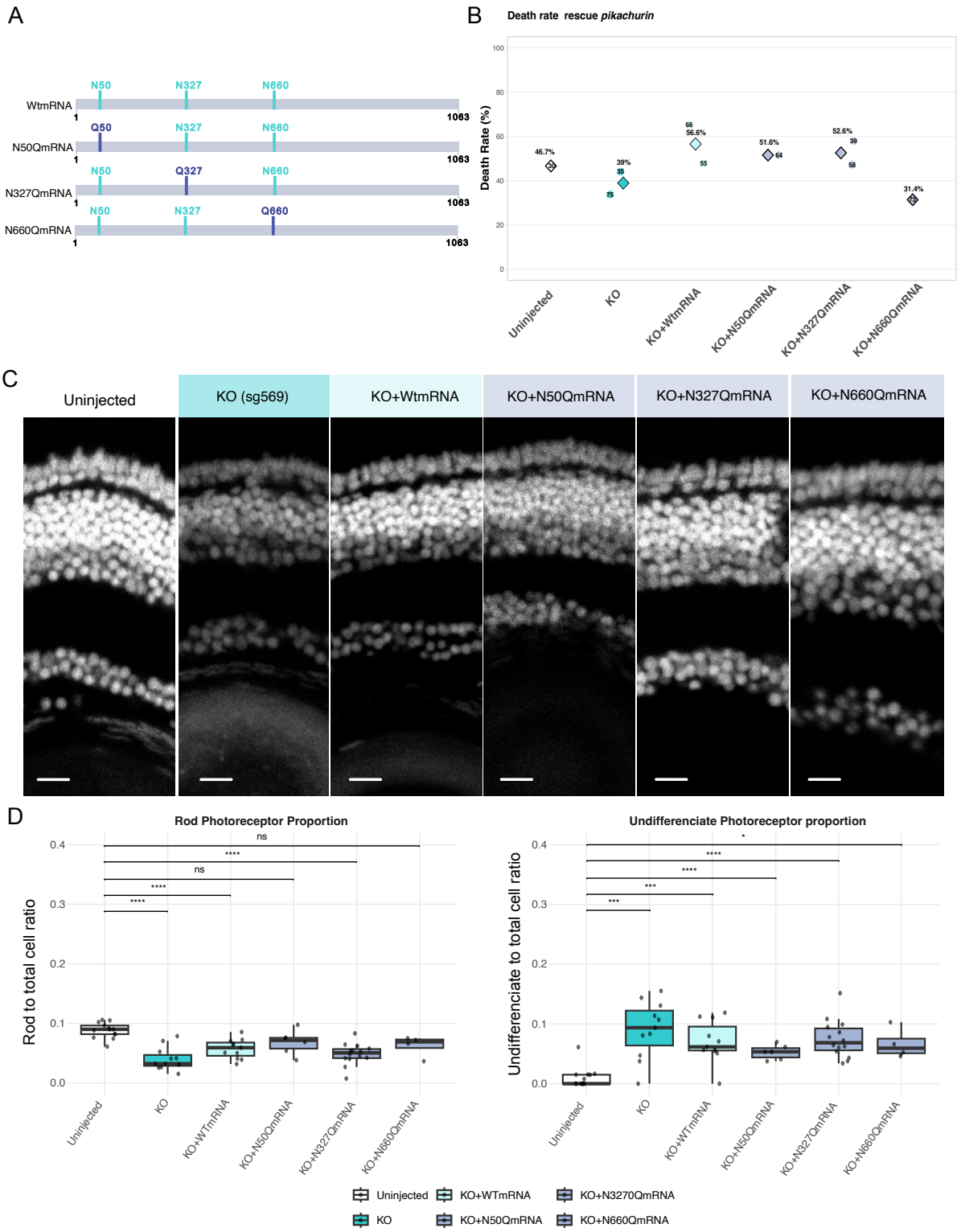

Figure 23. Histological and morphological evaluation of Pikachurin mRNA rescue in medaka hatchlings. (A) Schematic representation of the structure of the mRNA used in the experiment. Indicating in light blue the position of Asparagines (Asn) predicted to be glycosylated; different variants were generated in which all Asn have been changed into Glutamine (Glu), indicated in dark blue.(B) Death rates observed following microinjection of each mRNA variant at the 1-cell stage (n ≥ 50 per condition).(C) Representative cryosections of retinas displaying the most common phenotype observed for each condition. Scale bar = 10µm. (D) Quantification of photoreceptor cells in the retina at 0 dph. Left pannel: proportion of Rod photoreceptors relative to the total number of cells in central retinal region. Right: proportion of undifferentiated or unidentifiable cells based on DAPI staining. Each dot

represents an individual retina. (N=6). Color code: Uninjected (White), KO (Cyan), Wt (Ice Blue), Variants (Lavander). Bars represent mean ± SD. (two-tailed t-tests, corrected with Bonferroni, $p < 0.05$).

Histological analysis of the retinas revealed that the KO exhibited a marked reduction in rod photoreceptors, accompanied by a substantial increase in undifferentiated cells. The photoreceptor layer showed a complete disruption of its typical organization, with cones and rods indistinguishable from each other. Injection of WT mRNA partially restored photoreceptor differentiation, although the photoreceptor layer structure remained abnormal, with small nuclei failing to organize into the two distinct photoreceptor layers observed in controls. Among the glutamine substitution variants, N50Q closely resembled the WT mRNA phenotype, while N327Q displayed a more dispersed photoreceptor layer with less compact nuclei. Interestingly, the N660Q variant showed no significant differences compared to uninjected embryos, maintaining a relatively preserved rod population and a limited number of undifferentiated cells (Figure 23C&D).

Overall, these results indicate that pikachurin is critical for photoreceptor differentiation and organization, that its perturbation increases embryonic lethality, and that specific but not all potential glycosylation sites contribute differentially to the proteins' function during early retinal development.

Taken together, I could validate the function of 6 out of 15 candidate genes implicated with retina and photoreceptor development and maintenance by disrupting the open reading frame of these genes in the developing medaka embryo. Further, rescue experiments with mRNA variants in parallel to the CRISPR/Cas9 mediated knockout regime demonstrated that not all but certain asparagine residues were crucial for rescuing photoreceptor development and maintenance, suggesting a possible involvement of *N*-glycosylation or functional unit at the site of the respective asparagine. In addition, the systemic application of the different mRNA variants exhibited altered levels of embryonic lethality, indicative for cellular stress response in relation to the structure/function or even glycosylation variant.

4

Discussion

Glycosylation is a post-translational modification essential for proper protein folding, secretion, and function, and is therefore critical for the normal development of an organism (Haltiwanger & Lowe, 2004; Reily et al., 2019). Defects in the glycosylation machinery are generally incompatible with life; however, in rare cases, partial impairment of the machinery retains limited functionality, producing systemic effects. Individuals born with such defects suffer from CDGs (Lefeber et al., 2022; Reily et al., 2019). When mutations observed in these patients are modeled in animal systems such as medaka (*Oryzias latipes*), systemic effects at the organismal level are observed (Cornean, 2022; Gücüm, 2021).

Interestingly, the eye appears to be particularly sensitive in foremost one cell type, i.e. the rod photoreceptors show elevated vulnerability under these conditions (Gücüm et al., 2021). This raised the central question for this thesis: which factors are critical for maintaining rod photoreceptor homeostasis, and to what extent does the absence of potential glycosylation sites compromise their survival?

To address this question, I systematically identified glycosylation-dependent candidate genes that could contribute to rod photoreceptor vulnerability. Using a multi-level workflow integrating proteomic, transcriptomic, and human disease datasets, candidates were prioritized based on their retinal expression and potential dependency on glycosylation. CRISPR/Cas9-based mutagenesis, including base editors and homologous recombination approaches, was employed to disrupt predicted *N*-glycosylation motifs in these genes. Knockout embryos for *rhodopsin, opn1sw, elovl4*, and *pikachurin* exhibited variable effects on photoreceptor populations and the organization of the ONL. Additionally, mRNA rescue experiments were performed using both wild-type and asparagine substitution variants of the candidate genes to evaluate their effect on retinal morphology.

4.1 Evaluating candidate genes and the constraints of CRISPR-based editing

One of the major challenges I encountered during this study was the design and efficiency of CRISPR/Cas9-based base editing to target Asn residues within *N*-glycosylation motifs. The selection of suitable sgRNAs was constrained by the requirement for a PAM sequence at the correct distance, ensuring that the editing window contained the codons encoding the target Asn. The Cas9 systems used in this study are based on the *Streptococcus pyogenes* Cas9, thus relying on NGG PAM motif recognition, which prevented targeting all possible glycosylation sites, as some genes did not present a suitable NGG-PAM in the proper position. Even for those sites where the Asn codon could theoretically be targeted, the editing efficiency was insufficient to perform robust functional studies in the injected generation. This may have been influenced by two constraints: methodology and lethality of the genome-altered organism.

The base editing method relies on suitable nucleotide sequences surrounding the target nucleotide: the so-called dinucleotide context. It has been shown that the direct nucleotide leading the target one at the 5' site can have a predictive or random negative influence on the editability of the target nucleotide, depending of the base editor used (Cornean et al., 2022). When the target adenine is preceded by another adenine (AA dinucleotide context), the efficiency of conversion to guanine is significantly reduced compared to other contexts, such as cytosine-adenine (CA). Thus, in *N*-glycosylation motifs, the codons for Asn (AAC or AAT) are unavoidably comprising an AA dinucleotide context, reducing the editing efficiency. These observations are consistent with findings reported by Cornean et al., 2022, who demonstrated that ABE8e exhibits reduced activity in AA contexts. Additionally, similar limitations were reported by Nicole Jenkinson, (MD, PhD Johns Hopkins University; personal communication), who faced challenges when attempting to remove Asn in *N*-glycosylation sites in cancer cell culture using base editing approaches. Together, these factors highlight a general limitation of current ABEs for efficient manipulation of asparagine codons and thus glycosylation motifs *in vivo*.

To overcome the previously mentioned challenges, a more flexible and precise approach to manipulate *N*-glycosylation motifs would be needed. Prime-Editing has

emerged as a promising alternative, combining a Cas9 nickase with a reverse transcriptase and a an elongated guideRNA extending the desired nucleotide change as donor sequences at the 3' end of the guide RNA. This extension in turn serves as primer for the reverse transcriptase to on-spot generate donor DNA with a high likelihood of being inserted without indels. This system would allow specific point mutations, and medium size insertions, or deletions without constraints imposed by narrow editing windows, PAM proximity, or dinucleotide context (Zhao et al., 2023). Furthermore, Prime Editing could reduce the risk of undesired indels or off-target effects, providing a high-fidelity approach to investigate the role of glycosylation in rod photoreceptor homeostasis.

While the precision of Prime Editing offers clear conceptual advantages, its application *in vivo* has not yet been fully established and efficiencies are reported to be rather low as of now. HDR, in contrast, is a well-established method for introducing defined sequence changes via Cas9-induced DSBs and donor templates. Nevertheless, the resulting progeny displayed a wide spectrum of phenotypes as besides the desired integration, indels are frequently seen (Gutierrez-Triana et al., 2018). Whenever essential genes are targeted, there is a high risk in not obtaining the desired mutation due to (embryonic) lethality. Those surviving and maturing are often incompletely edited or escaped the genome targeting event entirely, without harboring and inheriting the desired allele. This variability complicated the identification of carriers in the F1 generation and, in some cases, restricted the analysis to functional evaluation rather than the establishment of stable lines.

To complement genome editing approaches and investigate the functional relevance of asparagines in predicted *N*-glycosylation sites, mRNA rescue was employed. Injection of WT or glycosylation-deficient mRNAs allowed direct assessment of the contribution of individual asparagine residues to rod photoreceptor differentiation, ONL organization, and cell survival. Taken together, HDR and mRNA rescue offer complementary strategies to probe structure/function and potential glycosylation-dependent mechanisms, each with distinct advantages and limitations, and provide the foundation for the gene-specific analyses presented in this thesis.

4.2 Glycosylation in *rhodopsin* is essential for rod survival and ONL organization

In the mRNA rescue experiments, knockout embryos lacking functional Rhodopsin exhibited a near-complete loss of rod photoreceptors, disrupted ONL organization, and an increased presence of undifferentiated photoreceptors. Injection of WT *rhodopsin* mRNA partially restored rod populations and improved ONL morphology, whereas *rhodopsin* mRNA encoding glycosylation-deficient Rhodopsin$^{p.N2Q;N15Q}$ failed to rescue these phenotypes. These observations suggest that glycosylation of Rodopsin at specific and evolutionarily highly conserved Asn residues is very likely affecting Rhodopsin function and is critical for rod survival and proper ONL organization, as previously reported by Tam & Moritz, 2009.

Rhodopsin is a G protein-coupled receptor (GPCR) expressed in rod photoreceptors, acting as the primary photopigment for detecting dim light (Palczewski, 2006). Photon absorption induces a conformational change that activates the visual transduction cascade, leading to rod hyperpolarization and signal transmission to downstream neurons (Lolley & Lee, 1990). Proper folding, trafficking to the outer segment, and incorporation into disc membranes are all dependent on post-translational modifications, particularly *N*-glycosylation (Murray et al., 2009; Sung et al., 1991). Miss-glycosylation disrupts these processes, leading to protein instability, ER stress, and photoreceptor degeneration, which aligns with the phenotypes observed in the knockout embryos (Chapple & Cheetham, 2003; Sung et al., 1994).

The inability of glycosylation-deficient mRNA to rescue the rods further underscores that these modifications are not merely structural but are essential for rhodopsin's functional interactions and the maintenance of retinal architecture. These findings are consistent with studies in other vertebrate models, where miss-glycosylated Rhodopsin leads to photoreceptor degeneration and retinitis pigmentosa (Palczewski, 2006; Sung et al., 1991, 1994). The results also suggest that specific Asn residues are crucial for protein stability, trafficking, and outer segment organization, highlighting the broader importance of *N*-glycosylation for photoreceptor homeostasis.

4.3 Site-specific glycosylation in *opn1sw* shapes cone photoreceptor organization

Knockout embryos lacking *opn1sw* displayed specific disruptions in cone photoreceptor organization. They also showed an increased proportion of undifferentiated cells. Injection of WT *opn1sw* mRNA partially restored cone structure and ONL organization, whereas mRNAs harboring mutations at predicted glycosylation sites produced variable phenotypes. Notably, mutation of Asn10Gln severely perturbed ONL organization despite largely normal protein expression, while Asn71Gln mutation led to increased embryonic lethality without causing pronounced retinal disorganization. These findings suggest that site-specific *N*-glycosylation is critical for cone photoreceptor stability and tissue architecture.

Opn1sw encodes a short-wavelength-sensitive cone opsin in medaka, mediating both blue and ultraviolet (UV) light detection (J. Wu et al., 2025). In cone photoreceptors, proper folding, trafficking to the outer segment, and disc membrane integration are essential for its function as a GPCR (Goth et al., 2020). While glycosylation is a well-characterized PTM for many GPCRs, including other rod and cone opsins, the glycosylation status of Opn1sw has not previously been explored in the context of retinal development (Goth et al., 2020; Salom et al., 2019). The findings from this study strongly supports that *N*-glycosylation at specific Asn residues is critical for Opn1sw folding and for maintaining photoreceptor structure and ONL organization.

The differing phenotypes observed upon mutation of Asn10 versus Asn71 suggest that these sites serve distinct biological functions. Potential glycosylation at Asn10 appears essential for proper protein–protein interactions within the outer segment and/or for engagement with chaperone proteins, whereas the lethality associated with Asn71 mutation likely reflects broader structural disruptions rather than the loss of glycosylation per se. These findings indicate that not all predicted glycosylation sites contribute equally to cone opsin function, emphasizing the critical role of precise *N*-glycosylation or at least sequon motifs in this position for cone photoreceptor differentiation and the maintenance of retinal architecture.

4.4 Elovl4 glycosylation modulates photoreceptor layer structure

Loss of *elovl4* function resulted in pronounced disorganization of photoreceptors within ONL, accompanied by an increased proportion of undifferentiated cells. Injection of WT *elovl4* mRNA partially restored photoreceptor structure, whereas mRNAs harboring mutations at predicted *N*-glycosylation sites produced variable effects. Specifically, mutations at Asn9, Asn72, and Asn116 led to differing degrees of ONL disorganization, indicating that Elovl4 function is highly sensitive to specific residues and that disruption of post-translational modifications compromises photoreceptor differentiation and retinal architecture.

elovl4 encodes a fatty acid elongase critical for the biosynthesis of very long-chain polyunsaturated fatty acids (VLC-PUFAs) in photoreceptors. VLC-PUFAs are essential for maintaining the structural integrity of outer segment discs, supporting disc membrane stability, and ensuring proper phototransduction (Agbaga et al., 2014; Barabas et al., 2013). Loss of *elovl4* disrupts these processes, resulting in abnormal disc morphology, impaired photoreceptor homeostasis, and ultimately retinal degeneration (Agbaga et al., 2014). The phenotypes observed in knockouts and potential glycosylation-site mutants indicate that even subtle alterations in the protein can significantly affect ONL organization and photoreceptor differentiation, emphasizing *elovl4*'s critical role in retinal architecture and visual function.

Mutations in the human *ELOVL4* gene are linked to autosomal dominant Stargardt-like macular dystrophy (STGD3), characterized by progressive loss of central vision due to retinal degeneration (Agbaga et al., 2014). These mutations often lead to mislocalization of ELOVL4 in photoreceptors, disrupting normal retinal structure and function (Agbaga et al., 2014). Similarly, *elovl4b* knockout zebrafish models demonstrate altered ocular lipid profiles and visual deficits, supporting the enzyme's conserved role in retinal health and disease(Nwagbo et al., 2024).

The variable effects of site-specific mutations suggest that individual residues contribute differently to Elovl4 stability or enzymatic activity. While glycosylation at these Asn residues has not been previously characterized for Elovl4, the results presented in this work provide a first support that these sites influence photoreceptor survival and outer segment organization, possibly by affecting protein folding, localization, or interactions within the VLC-PUFA biosynthesis pathway.

4.5 Pikachurin glycosylation coordinates photoreceptor differentiation and ONL integrity

Loss of *pikachurin* resulted in a markedly thinned photoreceptor layer, often reduced to a single cellular stratum, with a predominance of undifferentiated cells. The identity of individual photoreceptors was difficult to assess, indicating that both rod and cone populations were severely affected. Injection of WT *pikachurin* mRNA partially restored photoreceptor layer thickness and organization, whereas mRNAs harboring mutations at predicted glycosylation sites produced variable phenotypes. In particular, the N50Q mutation elicited the most pronounced morphological defects, with indistinguishable photoreceptor subtypes. The N327Q mutation yielded a more loosely organized outer nuclear layer, with nuclei spaced farther apart, while the N660Q mutation exhibited minimal impact on photoreceptor morphology or subtype composition relative to uninjected controls. These findings demonstrated that specific residues in Pikachurin are critical for photoreceptor layer organization and cellular differentiation.

Pikachurin is an extracellular matrix-like protein localized at photoreceptor terminals, where it contributes to the organization of contacts with postsynaptic retinal cells and the maintenance of proper synaptic positioning (Patil et al., 2023; Sato et al., 2008). Accurate terminal alignment is essential for effective signal transmission and overall retinal function (Patil et al., 2023; Sarria et al., 2015). The phenotypes observed in this study indicate that alterations in *pikachurin*, including potential effects on glycosylation, can compromise photoreceptor differentiation and layer integrity, likely affecting the retinal network.

Although the role of glycosylation on *pikachurin* has not been previously characterized, the variable effects of site-specific mutations suggest that these residues may influence protein folding, stability, extracellular localization, or interactions with synaptic partners such as dystroglycan (Rubio-Fernández et al., 2018; Sato et al., 2008). These results demonstrate the essential role of *pikachurin* in photoreceptor development and outer nuclear layer organization, noting how glycosylation regulates retinal structure and function.

4.6 *In silico* modeling provides mechanistic insight into glycosylation-dependent protein stability

The effects observed across the different variants can be interpreted through two primary contexts: the role of *N*-glycosylation in mediating protein–protein interactions and recognition pathways, and the potential conformational changes at the protein level resulting from Asn>Gln substitutions. Experimentally dissecting these mechanisms is challenging, but predictive computational tools, such as AlphaFold (Jumper et al., 2021; Varadi et al., 2024) and GlycoShape (Ives et al., 2024) provide valuable insights into how specific residues may influence protein folding, structural stability, and surface properties offering a mechanistic framework for interpreting potential functional consequences.

For example, in OPSINS, the *N*-terminal domain contains conserved glycosylation sites critical for folding, chromophore interaction, and engagement in functional recognition pathways (Salom et al., 2019). Simulations suggest that substitutions such as N10Q may not dramatically alter global folding but can modify surface polarity or local domain orientation, potentially affecting interactions with chaperones or other cellular partners (Figure 24A). Conversely, substitutions like N71Q may induce broader conformational changes. Interestingly, GlycoShape predicted that N71 is unlikely to be glycosylated, suggesting that the structural impact arises primarily from the Asn>Gln substitution itself, which could trigger early quality-control mechanisms like ERAD, and contribute to high embryonic lethality (Figure 24B). These *in silico* insights provide a molecular-level rationale for the phenotypic differences observed experimentally: certain glycosylation sites appear essential not simply for structural integrity, but for proper recognition and functional engagement within the photoreceptor, offering the explanation why some mutations lead to severe developmental or survival defects while others show milder effects.

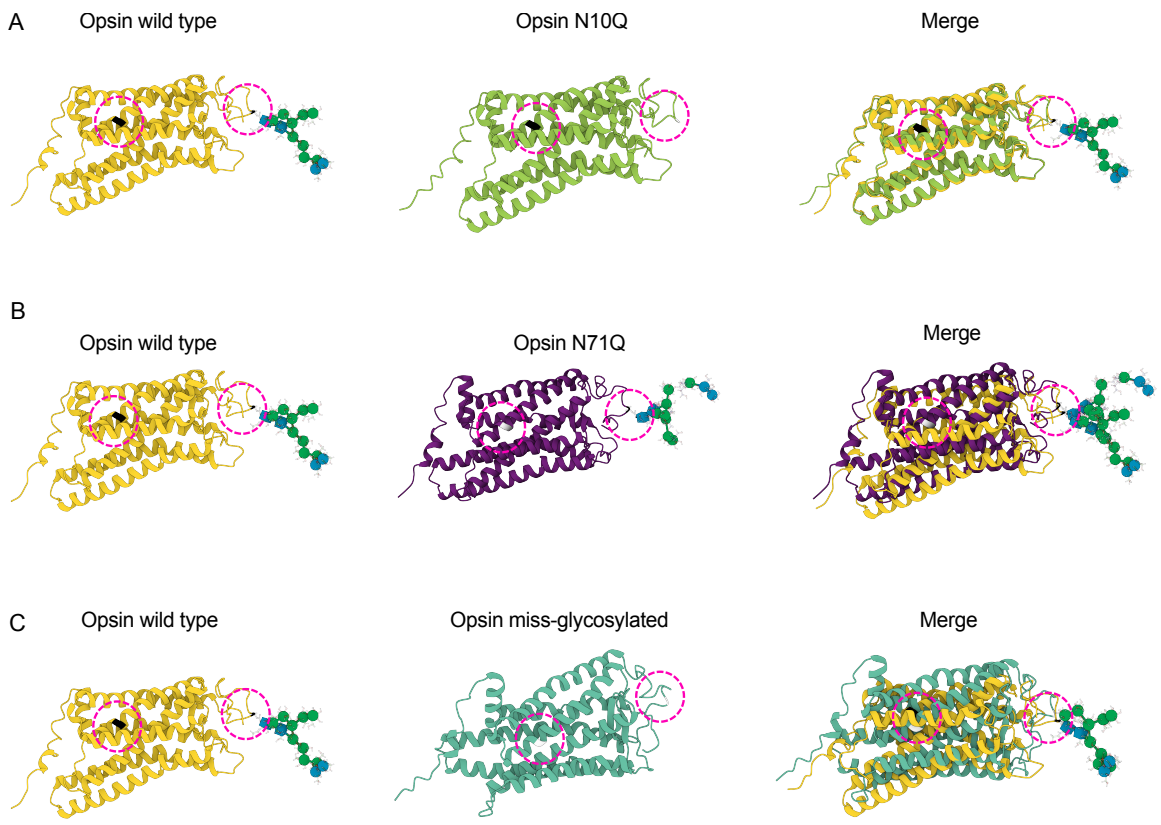

Figure 24. Distinct structural effects of disrupting *N*-linked glycosylation sites in *opn1sw*. Ribbon diagrams depict the WT (yellow), N10Q (green), N71Q (purple), and double mutant N10Q/N71Q (teal) structures. Predicted *N*-linked glycosylation sites, N10 and N71, are highlighted with pink circles; asparagine residues are shown in black and glutamine substitutions in white. (A) Comparison of WT and N10Q shows loss of the glycan at position 10 with minimal change in overall conformation, suggesting that local surface features may be altered without disrupting global folding. (B) WT vs. N71Q indicates that substitution at N71, despite retention of the glycan at N10, produces local polarity changes and detectable conformational shifts, potentially impacting protein. (C) The double mutant exhibits the most pronounced structural divergence relative to WT, highlighting the cumulative effects of multiple site modifications on protein folding and stability.

For Elovl4, simulations indicated effects similar to those observed for Opsin, with Asn>Gln substitutions producing moderate local structural changes while largely preserving overall protein folding (Supplementary Figure 11). Interestingly, Pikachurin simulations revealed that glycosylation at Asn50 depends on the presence of both Asn327 and Asn660, whereas the latter two sites can be glycosylated independently (Supplementary Figure 12). This interdependence would reveal a novel layer of regulation in Pikachurin glycosylation, suggesting that site-specific modifications may be coordinated rather than independent.

Overall, predictive modeling reinforces the concept that *N*-glycosylation is a critical determinant of protein functionality in the retina. Highlighting that the biological consequences of individual site modifications are highly context-dependent,

influencing folding, polarity, interaction potential, and ultimately photoreceptor differentiation and layer organization. While *in silico* predictions cannot replace experimental evidence, they provide mechanistic insight that bridges molecular alterations with the organismal phenotypes observed in knockout and mRNA rescue experiments, allowing a deeper understanding of how specific post-translational modifications govern retinal development.

4.7 Stable knockout lines demonstrate gene-specific contributions to retinal structure and visual function

The generation of stable KO lines for *rho* and *opn1sw* allowed examination of the sustained role of these genes in photoreceptor maintenance and visual function. In *rho* KOs, the progressive loss of rods and the resulting reduction of the ONL emphasized the gene's essential role in rod survival and organization. The observed deficits in light sensitivity and visual tracking, as revealed by ERG and OMR, highlighted that even partial disruption of rod photoreceptors can severely compromise white light vision and behavioral responses. The inability of mutants to follow continuous visual stimuli and the requirement for broader stimuli to elicit a response suggest that rods not only contribute to phototransduction but are critical for coordinated visual processing at the organismal level.

In *opn1sw* KOs, histological analyses suggest a more subtle impact on ONL organization, consistent with partial redundancy or compensation among cone populations. Nevertheless, ERG recordings indicate a specific impairment in UV-sensitive photoreception, demonstrating that even when structural changes are modest, functional deficits can be pronounced.

Taken together, these results emphasize that the role of these candidate genes is not limited to maintaining photoreceptor numbers but extends to shaping retinal circuitry and ensuring effective visual processing. By integrating structural, electrophysiological, and behavioral analyses, a more comprehensive understanding emerged of how specific gene functions support photoreceptor stability and vision. These stable medaka lines thus provide a powerful platform to investigate gene-specific contributions to retinal development, offering opportunities to explore both cellular mechanisms and their impact on visual behavior.

5

Conclusions and Outlook

This study demonstrates that asparagine residues in predicted *N*-glycosylation sites play a critical role in photoreceptor homeostasis, influencing protein folding, stability, and functional interactions. Through a combination of *in silico* modeling, mRNA rescue experiments, and stable knockout lines, I have shown that specific residues in Rhodopsin, Opn1sw, Elovl4, and Pikachurin are essential for maintaining retinal architecture, photoreceptor differentiation, and visual function. Predictive simulations provided mechanistic insight into how Asn>Gln substitutions can disrupt protein conformation and surface properties, offering explanations for observed differences in embryonic lethality and photoreceptor morphology.

Functional analyses of stable KO lines confirmed that loss of these genes can lead to persistent structural defects in the outer nuclear layer and impair vision, as evidenced by ERG recordings and optomotor behavior in *rho* KOs. These results highlight medaka as a model for dissecting gene-specific contributions to retinal development and function, particularly in the context of conserved post-translational modifications.

Overall, this work provides a comprehensive framework linking molecular alterations to cellular phenotypes and organismal outcomes. While experimental limitations remain, particularly in isolating the precise contribution of individual glycosylation sites, these findings advance the understanding of the mechanisms that govern photoreceptor stability and retinal integrity. Future studies leveraging more precise genome editing tools, such as Prime Editors, or more refined behavioral assays, will further elucidate how post-translational modifications and gene function intersect to shape retinal development and visual performance. Nontheless, the candidate list identified in the presented pipeline could be validated for involvement in retina formation and layering, photoreceptor development, maintenance and function. This work strongly supports the prediction for some asparagines to be *N*-glycosylated, which remains to be investigated in future studies.

6 Materials & Methods

6.1 Materials

Medaka fish lines used or created in this thesis are listed in Table 1. The transgenic lines were created either by microinjection of CRISPR/Cas9 or CRISPR/Cas9 base editors in one-cell stage medaka embryos. The respective injection mixes are listed in *Table 20*.

Table 1. Medaka (Oryzias latipes) lines used in this thesis

Fish lines	Internal stock number	Source
Wild-type Cab	#10052, #10346, #10542, #11057, #11332	Lab stock
CR(rho_del9_in41)	#10511, #10860, #11093, #11097, #11472	This thesis
CR(HDR rho N>Q)	#10743, #10949	This thesis
CR(HDR opn1 N>Q)	#10744, #10948, #11270	This thesis
CR(HDR elovl4 N>Q)	#10745, #10947, #11269	This thesis
CR(EGFLAM)	#10994, #11473	This thesis
ABE(00896_N1390)	#10238	This thesis
ABE(25491_	#10239	This thesis
ABE(13140_N228)	#10240	This thesis
ABE(24677_N168)	#10241	This thesis
ABE(opn1_N10K)	#10534, #11249	This thesis

ABE(rho_N15K)	#11248	This thesis

6.1.1 Bacteria

Mach1T1 phage-resistant chemically competent *E.coli* from Thermo Fisher Scientific were used in this thesis.

6.1.2 Plasmids

All plasmids used in this thesis are listed in .

Table 2. Plasmids use in this thesis

Plasmid name	Internal Stock number	Source
pCS2+	#221	Lab stock
GFP	#883	Lab stock
mCherry	#1924	Lab stock
DR274(cr/trRNA_57_Oca2_ex9_T1)	#2327	(Lischik et al., 2019)
evoBE4max	#5797	(Cornean et al., 2022)
ancBE4max	#5811	Addgene #112094, (Koblan et al., 2018)
ABE8e	#5812	Addgene #138489, (Richter et al., 2020)
pCS2(heiCas9)	#6342	(Thumberger et al., 2022)
pUC57(HDR_rho_N2&N15>Q)	#6194	This thesis
pUC57(HDR_opn1_N10&N71>Q)	#6195	This thesis
pUC57(HDR_elov4b_N9/N72&N116>Q)	#6196	This thesis
pCS2+(rho_full-length_cDNA)	#6338	This thesis
pCS2+(opn1_full-length_cDNA)	#6339	This thesis
pCS2+(elovl4b_full-length_cDNA)	#6340	This thesis
pCS2+(pikachurin_full-length_cDNA)	#6341	This thesis
pCS2+(rho_full-length_cDNA_N2&N15>Q))	#6346	This thesis
pCS2+(opn1_full-length_cDNA_N10>Q))	#6347	This thesis
pCS2+(opn1_full-length_cDNA_N71>Q))	#6348	This thesis
pCS2+(opn1_full-length_cDNA_N10&N71>Q))	#6349	This thesis
pCS2+(elovl4b_full-length_cDNA_N9>Q))	#6352	This thesis
pCS2+(elovl4b_full-length_cDNA_N72>Q))	#6350	This thesis
pCS2+(elovl4b_full-length_cDNA_N116>Q))	#6351	This thesis

pCS2+(elovl4b_full-length_cDNA_N9/N72&N116>Q))	#6353	This thesis
pCS2+(pikachurin_full-length_cDNA_N50>Q))	#6354	This thesis
pCS2+(pikachurin_full-length_cDNA_N327>Q))	#6355	This thesis
pCS2+(pikachurin_full-length_cDNA_N660>Q))	#6356	This thesis

6.1.3 Primers

Table 3. Primers used in this thesis

Name	Internal nr.	Sequence (5' to 3' direction)
00896-N1390_seq_F	JW11200	GCAATTAGCAAGACTAGTGCCAA
00896-N1390_seq_R	JW11201	CAGAATTTTCAGAATAAAAGCCTGATAT
00896-N595_seq_F	JW11202	CGCTCATCCCAGCAAGAAAC
00896-N595_seq_R	JW11203	TGTCCCCTCCGTCCGTAG
13140_seq_F	JW11204	TCTCCGTTTGTGAGCCAAA
13140_seq_R	JW11205	CTGCAGAAGTTATGAGGTCCGA
24677_seq_F	JW11206	TTGGATTCTGAGATTAAAAGAATATATAAGGA
24677_seq_R	JW11207	CAAATGCACTTTAAACTGCAGTTT
25491_seq_F	JW11208	ATGTCCACAAATACCTGGAAGAGT
25491_seq_R	JW11209	TATATATGCTGAGAGTCGCTGTGG
rho_seq_F	JW11210	AGTTATGTTTGCAGTGACGGC
rho_seq_R	JW11211	GAAGTTGCTGATGGGCTTGC
24677_OT_F	JW11281	GCTCCATGTTCCGTCTATGC
24677_OT_R	JW11282	TGACATCTGAATGTTTAGCGAGTG
PCDH8 Fwrd	JW11376	TGGCTCAACACCTGGTTCAG
PCDH8 Rv	JW11383	CTGTACGGACACGACCACTT
EGFLAM_Fwrd	JW11384	ACCCCATTGTCTAAGCATGTGA
EGFLAM_Rv	JW11385	GTGGAACAAGGCAGCCAAAG
ELOV4_Fwr	JW11386	ACTAGCGTGCCCTCAACCTA
ELOV4_Rv	JW11387	AGCTTCCTCTTTCCTGGCAG
OPN1S_Fwrd	JW11388	GAAGTAGTAGCCCCTCACGC
OPN1S_RV	JW11389	CGGTTCAGAGCTCAGCTTCA
Tena_Exon1_Fwr	JW11390	TGCACAAAGTCTTCTGGGCT
Tena_Exon1_RV	JW11391	ATTCTACCTGTGACGGGTGC
Tena_Exon16_Fwrd	JW11392	AACCAATAGCAGTGCGGTGA
Tena_Exon16_Rv	JW11393	CAGTGAACTCCTGAGGCTCC
Tena_Exon2_Fwrd	JW11394	GATGCCCAGCTGGTCATACA
Tena_Exon2_Rv	JW11395	CATTTTCCGTCCACGCAGAC
Tenacine like ex1 Fwd	JW11459	GGAAAGGGAGCGATTGGTGA
Tenacine like ex1 Rev	JW11460	CGGGAGTCTGTTATCGGAGC

Name	Internal nr.	Sequence (5' to 3' direction)
Tenacine like ex2 Fwd	JW11461	GGAAAGGGAGCGATTGGTGA
tenacine like ex2 Rev	JW11462	CCGTCCCTTTTAGTCGCCTT
Tenacine like ex2 Fwd	JW11463	ACAGTTAATCATGAACCTCCCTCC
Tnc_like_Fwrd_probe	JW11464	TGCTGTGGTTGTTATCCCCA
TNC_like_Rv_Probe	JW11465	GGTTTTCCTTAGCCCCACCG
TNC_like_RV_II_Probe	JW11466	TGGCTGCCAGTAACATCCAG
PRPH2_Fwrd_Probe	JW11467	CAACTCACAGTCGCAACAGC
PRPH2_Rv_Probe	JW11468	GTGAAGCTCGCTCAGACAGT
EGLAM_Frwd_Probe	JW11469	CATCTCGATCACAGCTGGCT
EGLAM_Rv_Probe_I	JW11470	ATTCCTTCTACCGCCCTCTG
ELOVL4b_Fwrd_Probe	JW11471	TCAGCATGGTGGTCCTCAAC
ELOVL4b_Rv_Probe	JW11472	TTTCTGCGCTGAAGGTTTGC
PRPH2_novel_fwrd_Probe	JW11473	CAACGTGGAGGGGAAGTACC
PRPH2_novel_rv_probe	JW11474	TGCCAGGCTCAGAGTCTTTG
24677_Fwrd_probe	JW11475	CGCTCGGGAGAATGAGATGG
24677_Rv_probe	JW11476	TCGGTAAACGGCTCGAAACA
25491_Fwrd_Probe	JW11477	CATGCAGTAGGTGAGTGGGG
25491_Rv_Probe	JW11478	CATCTGTTGTGGCTCCCTGT
00896_Fwrd_Probe	JW11479	TCCATTATCGGACCCCCAGT
00896_Rv_Probe	JW11480	TGTCCAGGGTTGAGTACAGG
ELOVL4_N9Q_OA1-F	JW11537	TAGGAACTTACCTGCTATAGTA
ELOVL4_N9Q_OA1-R	JW11538	AAACTACTATAGCAGGTAAGTT
ELOVL4_N9Q_OA2-F	JW11539	GTGCTTTATGCAGGACACTGTAGAGTTTTACAAATGGAGCTTGAC TATAGCAGGTACATAATAT
ELOVL4_N9Q_OA2-R	JW11540	ACCCATATTATGTACCTGCTATAGTCAAGCTCCATTTGTAAAACT CTACAGTGTCCTGCATAAA
rho_N2Q_N15Q_OA1-F	JW11546	TAGGGACTCCGGACAATGCCGG
rho_N2Q_N15Q_OA1-R	JW11547	AAACCCGGCATTGTCCGGAGTC
rho_N2Q_N15Q_OA2-F	JW11548	GTGCATGCAGGGCACAGAGGGACCGTACTTTTATGTCCCTATGGT GCAGACAACCGGCATTGTCCGGCTATAATA
rho_N2Q_N15Q_OA2-R	JW11549	ACCCTATTATAGCCGGACAATGCCGGTTGTCTGCACCATAGGGAC ATAAAAGTACGGTCCCTCTGTGCCCTGCAT
OPN1S rv HDR	JW11596	CGGTTCAGAGCTCAGCTTCA
ELOVL4 rv HDR	JW11597	ACGTGAAGGAAGCTGACCTG
EGLAM_insitu probe rv	JW11605	TGATGTTCTTCCCGTCAGCC
00896_probe_rv	JW11607	TCTCCAACGTTGTAGCCCAC
Opn1sw donor rv	JW11617	CGTAAGCTCGTCTTCGGTGT
Rho_Recue_Fwd	JW11942	CAGGATCCGCCAACATGAATGGCACAGAGGGACC
Rho_Resue_rv	JW11943	GCTCTAGATTATGCAGGGGACACAGAGC
Opn_Rescue_Fwd	JW11944	CAGGATCCGCCAACATGGGAAAATACTTCTACCTG
Opn_Rescue_rv	JW11945	GCTCTAGATTAAGAGGCCGTGGACACCT
Elovl4_Rescue_Fwd	JW11946	CAGGATCCGCCAACATGGAGGTTGTAACACATTTTATG
Elovl4_Rescue_rv	JW11947	GCTCTAGATCACTCCCTTTTCGCTCT

Name	Internal nr.	Sequence (5' to 3' direction)
Pika_Rescue_fwd	JW11948	CAGGATCCGCCAACATGGATCATACAAGCAAAGAGAAATG
Pika_Fragment1_rv	JW11949	TCAGTGGACGGAGGGATGAT
Pika_fragment2_Fwd	JW11950	AGTCCCAACTCCGTTCACAC
Pika_fragment2_rv	JW11951	GGAAAGGTAGTTCTGGGGGC
Pika_fragment3_fwd	JW11952	AGCTCTGAGTGGGGCTGATA
Pika_Rescue_rv	JW11953	GCTCTAGATCAGATAGAACAAGTGTTGATGTTCTTCCCGTCAGCC
pikachurin_N50Q_FWD	JW11979	CAGTGTTCTGCCTTCAGTG
pikachurin_N50Q_REV	JW11980	GACAGTCTCTAGCTGG
pikachurin_N327Q_FWD	JW11981	CAGGTCACTGACCCAGCAG
pikachurin_N327Q_REV	JW11982	TGGAAAAGCTCCAGTG
pikachurin_N660Q_FWD	JW11983	CAGGAAACTGTATTTTCCTATGC
pikachurin_N660Q_REV	JW11984	GAAAAGGGGAGAGGAC
OA_rho_N2Q-KpnI-N15Q_F	JW11985	GATCCGCCAACATGCAGGGTACCGAGGGACCATATTTTTATGTCC CTATGGTGCAGACCACCGGCATTGT
OA_rho_N2Q-KpnI-N15Q_R	JW11986	CCGGACAATGCCGGTGGTCTGCACCATAGGGACATAAAAATATGG TCCCTCGGTACCCTGCATGTTGGCG
elovl4_N9Q_FWD	JW11987	CAGGACACTGTAGAGTTTTACAAATG
elovl4_N9Q_REV	JW11988	CATAAAATGTGTTACAACCTC
elovl4_N72Q_FWD	JW11989	CAGTTCAGCATGGTGGTC
elovl4_N72Q_REV	JW11990	GTAGACTATGAGGGTCTTC
elovl4_N116Q_FWD	JW11991	CAGTACTCCAATGATGTCAATG
elovl4_N116Q_REV	JW11992	GACAGGCTGACAAAG
opsin1_N10Q_FWD	JW11993	CAGATCTCCAAAGTGGGC
opsin1_N10Q_REV	JW11994	CTCATACAGGTAGAAGTATTTTC
opsin1_N71Q_FWD	JW11995	CAGATCACCTTTGCTGGTTTC
opsin1_N71Q_REV	JW11996	GACAAGAATGTAGTTGAGC

6.1.4 cr/trRNAs

Table 4. Single guide RNAs used in this thesis

Guide nr.	Target	Target site [PAM]	Source
sg57	*oca2*	GAAACCCAGGTGGCCATTGC[AGG]	(Lischik et al., 2019)
sg58	*oca2*	TTGCAGGAATCATTCTGTGT[GGG]	(Lischik et al., 2019)
cr/trRNA529	*rho_N15*	TGAACACCACCGGCATTGTC[CGG]	This thesis
cr/trRNA530	*00896_N595*	GAAGAACCTGACCTCCCTGA[CGG]	This thesis
cr/trRNA531	*00896_N1390*	GCAGGAAACATCACCACAGA[CGG]	This thesis
cr/trRNA532	*13140_N228*	TCGTGGGAATGTGAGTGAGA[CGG]	This thesis
cr/trRNA533	*24677_N168*	CAACAAGACCCGGATCGA[CGG]	This thesis
cr/trRNA534	*25491_newPAM*	GAGCGACCTGAAGATTGAGG[TGG]	This thesis
cr/trRNA535	*25491-inc1_N54*	TGTAAGAACCGGACAGAGAGCG[AGG]	This thesis
cr/trRNA561	*pcdh8_N575*	GGCGGAGCCGTTGTTGAGCG[GGG]	This thesis
cr/trRNA562	*pcdh8_N425*	ATACAACCTGACGGTGGTGG[CGG]	This thesis
cr/trRNA563	*tnc_N42*	GAGCATAACGCGACGCTCCC[CGG]	This thesis
cr/trRNA564	*tnc_N171*	AACTACAGCTCTGAAACCTG[CGG]	This thesis
cr/trRNA565	*tnc_N189*	TGCTCCGAGCCCGAGTGTCC[CGG]	This thesis
cr/trRNA566	*tnc_N300*	GGCACCTGCTTCTGCGACGA[GGG]	This thesis

Guide nr.	Target	Target site [PAM]	Source
cr/trRNA567	*tnc_N1686*	ATGGTCAAGTTTTCTACTTT[AGG]	This thesis
cr/trRNA568	*opn1sw_N10*	GTATGAGAACATCTCCAAAG[TGG]	This thesis
cr/trRNA569	*egflam_N50*	GTTCTGCCTTCAGTGTACGA[TGG]	This thesis
cr/trRNA570	*elovl4_N9*	ACACTGTAGAGTTTTACAAA[TGG]	This thesis
cr/trRNA571	*elovl4_N72*	TGCTGAAGTTGTAGACTATG[AGG]	This thesis

6.1.5 Antibiotics

Table 5. Antibiotics used in this thesis

Antibiotics	Stock conc.	Working conc.	Comapny
Ampicillin	100 mg/ml	100µg/ml	Roth
Kanamycin	50 mg/ml	50µg/ml	Roth

6.1.6 Enzymes and buffers

Table 6. Enzymes and buffers used in this thesis

Enzyme	Buffer	Source
BamHI-HF (20U/µl)	rCutSmart buffer (10x)	New England Biolabs
BglII (10U/µl)	rCutSmart buffer (10x)	New England Biolabs
BspEI (10U/µl)	rCutSmart buffer (10x)	New England Biolabs
BsrGI-HF (20U/µl)	rCutSmart buffer (10x)	New England Biolabs
DNAase I 1500 U	DNA Digestion Buffer	Zymo Research
DpnI (20U/µl)	rCutSmart buffer (10x)	New England Biolabs
EcoRI-HF (20U/µl)	rCutSmart buffer (10x)	New England Biolabs
Eco0109 (20U/µl)	rCutSmart buffer (10x)	New England Biolabs
HindII (20U/µl)	rCutSmart buffer (10x)	New England Biolabs
HindIII-HF (20U/µl)	rCutSmart buffer (10x)	New England Biolabs
KpnI-HF (20U/µl)	rCutSmart buffer (10x)	New England Biolabs
NheI-HF (20U/µl)	rCutSmart buffer (10x)	New England Biolabs
Not-I-HF (20U/µl)	rCutSmart buffer (10x)	New England Biolabs
Proteinase K (20mg/ml)		Roche
PstI-FD	FastDigest Green buffer (10x)	Thermo Fisher Scientific
Q5 High-Fidelity DNA Polymerase (2 U/µl)	Q5 Reaction buffer (5x)	New England Biolabs
RiboLock (20 U/µl)	Reaction buffer (5x)	Thermo Ficher Scientific
T4 DNA Ligase (5 U/µl)	10x T4 DNA Ligase buffer	Thermo Fisher Scientific
T4 Polynucleotide Kinase (10 U/µl)		New England Biolabs
TURBO DNase (2 U/µl)	DNase I buffer (10x)	Invitrogen
XbaI (20 U/µl)	rCutSmart buffer (10x)	New England Biolabs
XcmI (5 U/µl)	rCutSmart buffer (10x)	New England Biolabs
XmaI (20 U/µl)	rCutSmart buffer (10x)	New England Biolabs

6.1.7 Chemical and reagents

Table 7. Chemical and reagents used in this thesis

Name	Source
4',6-diamidino-2-phenylindole (DAPI)	Sigma-Aldrich
2-Propanol	Sigma-Aldrich
2x RNA loading dye	Life Technologies
6x TriTrack DNA loading dye	Thermo Fisher Scientifics
Acetic acid (96%)	Merck
Agar	VWR
Agarose	Sigma-Aldrich
Alt-R CRISPR-Cas9 crRNA	Integrated DNA Technologies
Alt-R CRISPR-Cas9 tracrRNA	Integrated DNA Technologies
Ampicilin	Roth
CellMaskTM Deep Red Plasma membrane stain	Invitrogen Thermo
Deoxynucleotide triphosphate (dNTPs) (10mM)	Sigma-Aldrich
Dimetil sulfoxide (DMSO)	Roth
Ethanol 70% (EtOH) denatured	Roth
Ethanol 96% (EtOH) denatured	Roth
Ethanol 99% (EtOH)	Sigma-Aldrich
Ethidium Bromide (EtBr) 10% solution	Roth
Ethylenediaminetetraacetic acid (EDTA)	Roth
GeneRuler DNA Ladder Mix	Thermo Fisher Scientifics
Glycerol (Glycerin) ≥99%	Merck
HEPES (4-(2-hydroxyethyl)-1-piperazineethanesulfonic acid)	Roth
Hydrogen chloride (HCl) 37%	Merck
Kanamycin	Roth
Magnesium chloride (MgCl2)	AppiChem
Methanol (MeOH) 100%	Roth
Nail polish	Essence
Normal Goat Serum (NGS)	Gibco
Nuclease-Free Duplex Buffer	Integrated DNA Technologies
Orange G	Sigma-Aldrich
Paraformaldehyde (PFA)	Sigma-Aldrich
Poly(ethylene glycol) (PEG) 4000	Thermo Fisher Scientiics
Sodium acetate NaAc	Roth
Sodium chloride (NaCl)	Sigma-Aldrich
Sodium dodecyl sulphate sodium salt (SDS) 20%	Roth
Sucrose	Sigma-Aldrich
Tricaine (C9H11NO2 · CH4SO3, MS-222)	Sigma-Aldrich
Tris-hydrochloride (Tris-HCl)	Sigma-Aldrich
Tryptone bacteria	Roth
Tween20	Sigma-Aldrich
Yeast extract	Roth
Wheat Germ Agglutinin (Alexa Fluor 594)	Thermo Fisher Scientiics

6.1.8 Antibodies

Table 8. Antibodies used in this thesis

Primary Antibody	**Host**	**Dilution**	**Company**
Zpr1	mouse	1:500	ZIRC
Secondary Antibody	**Host**	**Dilution**	**Company**
Anti-mouseIgG(H+L), alexafluor488	Goat	1:500	Life technologies

6.1.9 Commercial kits

Table 9. Commercial kits used in this thesis

Name	**Source**
MEGAscript T7 Transcription Kit	Life Technologies
mMESSAGE mMACHINE Sp6 Transcription Kit	Life Technologies
Monarch DNA Gel Extraction Kit	New England Biolabs
Monarch PCR & DNA Cleanup Kit	New England Biolabs
QIAGEN Plasmid Mini Kit	Qiagen
QIAquick PCR Purification Kit	Qiagen
RNeasy Mini Kit	Qiagen
RevertAid First Strand cDNA Synthesis Kit	Thermo Fisher Scientific

6.1.10 Buffer and solutions

Table 10. Media and solutions used in this thesis. All buffer are prepares in H_2O if not indicated otherwise

Medium	**Component**	**Concentration**
1.5 % agarose in water	Agarose Boil in water	1,5% w/v
Ampicillin	Ampicillin (100mg/µl) EtOH	100µg/µl 50%
6x DNA Orange G loading dye	Orange G Glycerol	1,2 mg/ml 25% v/v
ERM (Embryos Rearing Medium)	NaCl KCl $CaCl_2 2H_2O$ $MGSO_4 7H_2O$ HEPES pH 7,3 pH 7,1	17 mM 0,4 mM 0,27 mM 0,66 mM 17 mM
70% EtOH	99% EtOH	70% v/v
EtBr bath	EtBr 10mg/ml 1x TAE	0,02%

Medium	Component	Concentration
Fin-Clip Buffer	Tris-HCl pH 8,5	100 mM
	EDTA pH 8	10 mM
	NaCl	200 mM
	SDS	2%
Fin-Clip Buffer with Proteinase K	Fin-Clip buffer	95%
	Proteinase K (20 mg/ml)	5%
Kanamycin	Kanamycin (50mg/ml)	50 µg/µl
LB- bacterial Plates	Bacto- Tryptone	10 g/l
	Yeast extract	5 g/l
	NaCl	10 g/l
	Agar	15 g/l
LB- medium	Bacto- Trytpone	10 g/l
	Yeast extract	5 g/l
	NaCl	10 g/l
Medaka Hatch Medium	NaCl	17 mM
	KCl	0,4 mM
	$CaCl_2$ $2H_2O$	0,27 mM
	$MgSO_4$ $7H_2O$	0,66 mM
	HEPES pH 7,3	17 mM
	Methylene Blue trihydrate	0,0001%
	pH 7,1	
3M NaAc	NaAc	246,1 g/l
	Nuclease-free H_2O	
Oligo annealing buffer	Tris	10 mM
	NaCl	30 mM
	pH 7,5- 8	
1x PBS	NaCl	137 mM
	KCl	2,7 mM
	KH_2PO_4	240 mg/l
	Na_2HPO_4	1,44 g/l
	pH 7,4	
P1 buffer	Glucose	50 mM
	Tris-HCL	20 mM
	EDTA	10 mM
	RNase A	100 µg/ml
	pH 8,0	
P2 buffer	NaOH	0,2 M
	SDS	1% SDS
P3 buffer	KAc	5 M
	pH5,5	
4% PFA	Paraformaldehyde in 1x PBS or 1X PTW	4 %
1x PTW	Tween 20 in 1xPBS	0,05 %
2x RNA loading dye	Xylene cyanol	0,25% w/v
	Bromphenol Blue	0,25% w/v
	SDS	0,025% w/v
	EDTA	5 mM (pH 8,0)
	Formamide	95% (v/v)

Medium	Component	Concentration
1x TAE	Tris-base	242 g/l
	Glacial acetic acid	5,71 %
	EDTA	50 mM
	pH 8,5	
TB-medium	Bacto-Trptone	12 g/l
	Yest extract	24 g/l
	Glycerin	0,4 %
	KH_2PO_4	2,13 g/l
	K_2HPO_4	12,45 g/l
20x Tricaine	Tricaine	4 g/l
	Na_2HPO_4 $2H_2O$	10 g/l
	pH 7-7,5	
50 x Tris-Acetate-EDTA buffer (TAE)	Tris base	242 g/l
	Glacial acetic acid	5,71%
	EDTA	50 mM
	pH 8,5	

6.1.11 Consumables

Table 11. Consumables used in this thesis

Consumable	Company
Cell saver tips 200µl	Biozyum
Cover slips	Roth
Filter paper	Whatman
Filter tips	Starlab
Gel Loading Tips	Thermo Fisher Scientifics
Glass Vials	Roth
Injection molds	House made
Injection needles GC100F-10	Harvard Apparatus
Micro pestles 1.5/ 2.0 ml	Eppedorf
Micro pestles 0.5/1.5 ml	Laborversand Hartmann
Microloader tips	Eppendorf
Nitrile gloves	Starlab
Nitrile gloves	TouchNTuff
Parafilm	Amcor
Pasteur pipettes	Kisker/ Sartedt
PCR stripes and lids	Sarstedt
PCR tubes	Kisker
Petri dished dishes 92mm + 60 mm	Greiner
Pipette tips	Starlab
Reaction tubes 1.5ml, 2ml, 5ml	Sarstedt
Superfrost plus microscope slides	Thermo Fisher Scientifics
Tissue Freezing Medium	Leica
Tubes 15 ml, 50 ml	Sarstedt
Tubes for bacterial cultures, 13 ml PP	Sarstedt
Well plates, 6-well, 12-well, 24-well, 96-well	Roth, Corning

6.1.12 Equipment and Instruments

Table 12. Equipment and Instruments used in this thesis.

Name	Company
Bacterial Shaker INNOVA 44	New Brunswick
Centrifuges 5417C, 5425, 5430R, 5810R	Diagenode
Cold light source for stereomicroscope KL 1500 LCD	Eppendorf
Cryostat CM 3050S	Leica
DIC microscope DB5000	Leica
DeNovix DS-11 spectrophotometer	DeNovix
Electrophoresis chambers and combs	Homemade and Peqlab
FemtoJet express	Eppendorf
Fish incubators	Heraeus instruments and RuMed
Forceps 5, 55 Inox stainless steel	Dumont
Freezer -20 °C	Liebherr
Freezer -80 °C	Thermo Fisher Scientific
Fridge 4 °C	Liebherr
Gel chamber	Custom-made
Incubator 32 °C, 37 °C, 60 °C	Binder
InjectMan NI2	Eppendorf
Leica TCS Sp8	Leica
Macro pipette controller	Brand
Microinjector 5242	Eppedorf
Microwave	Samsung
Mili-Q water filtration station	Millipore Coorporation
Mini centrifuge C1301B	Labnet
Mini centrifuge SU1555	Sunlab
MS1 Minishaker	IKA
Multichannel pipette	Starlab/ VWR
Multipette plus	Eppendorf
MyBlock mini dry bath	Benchmark Scientific
Needle puller P-30	Sutter Instrument Co USA
Nikon SMZ18 stereomicroscope	Nikon
Olympus SZX7	Olympus
PCR C1000 Touch Thermal Cycler	Bio-Rad
pH-meter	Sartorious
Pipettes 10 µl, 20 µl, 200 µl, 1 ml	Gilbson
Power supply PowerPac Basic	Bio-Rad
PowerPac 300	Bio-Rad
Rocking shaker DRS-12	Neolab
Rotating arm	Homemade
Scale	Sartorious
Scale Entris	Sartorious
Scale Extend	Sartorious
Shakers CAT S 20, DRS-12	Neolab
Stereomicroscope Zeiss Stemi 2000	Zeiss
Transferpette® electronic pipette, single channel	Brand
UV table	Vilber Lourmat
UV-Gel Documentation System	Intas
Vortex-Genie 2	Scientific Industries

6.1.13 Sofware and online tools

The software and online tool used in this thesis are listed in Table 13. Claude was used to inprove code writing for Rstudio to provide code suggestions for data plotting. Perplexity was exclusively used for literature research. OpenAI's ChatGPT was used for code suggestions for data plotting and exclusively for proof-reading of selected text passages and no text was generated. DeepL was used to help translating parts of the abstract into German.

Table 13. Sotware and online tools used in this thesis

Software/online tools	Source
ACEofBASEs	(Cornean et al., 2022)
Affinity Designer 2 (v2.6)	Serif (Europe) Ltd
Alphafold	(Varadi et al., 2024)
CCTop	(Stemmer et al., 2015)
ChatGPT	OpenAI
Claude	Anthropic
DeepL	DeepL SE
EditR	(Kluesner et al., 2018)
FileMaker	Filemaker Inc.
Geneious Prime 2019.2.3	Biomatters Limited
GlycoShape	(Ives et al., 2024)
GlyGen	(York et al., 2020)
ImageJ v 2.14.0/1.54f	(Schindelin et al., 2012)
LasX	Leica
Mendeley Reference Manager v. 2.134.	Elsevier
Microsoft Office	Microsoft
NEBaseChanger	New England Biolabs
NEBioCalculator v 1.17.2	New England Biolabs
NetNGlyc	(Gupta & Brunak, 2002)
Perplexity	Perplexity AI
Prism9	Prism
R (v4.4.2)	R Core Team, 2021
Rstudio Version (2024.4.2.764)	Posit team, 2024
Tm Calculator v 1.16.7	New England Biolabs
Tulab Omics data	(Li et al., 2020)
Uniprot	(Bateman et al., 2023)

6.2 Methods

6.2.1 Fish husbandry

Adult medaka fish (*Oryzias latipes*) were breed in close stocks, under control condition, 14 h light and 10 h dark cycle at the Centre for Organismal studies (COS) at Heidelberg Univeristy. The fish husbandry (permit number 35– 9185.64/BH

Wittbrodt) and experiments (permit number 35–9185.81/G-271/20 Wittbrodt) were perfomed in accordance to the local animal welfare standards (Tierschutzgesetz §11, Abs. 1, Nr. 1) and European Union animal welfare guidelines (Bert et al., 2016). The fish facility is under the supervision of the local representative of the animal welfare agency.

6.2.2 Molecular cloning

6.2.2.1 Q5 polymerase PCR

PCR (polymerase chain reaction) were carried out in a total volume of 50µl with, template DNA added by “pipetting without pipetting”: 1µl of DNA was pippeted up and down 15 times in the sample, with the same tip the PCR reaction was aspired 15 times. The standar settings for the thermal cycler are shown in table. he primer annealing temperatures were determined with NEB’s online Tm Calculator and the extension times were estimated from the polymerase extension rate of approximately 1 kb per 20–30 secs.

Table 14. Standar components of PCR Master Mix

Component	50 µl Reaction	Final concentration
Q5 reaction buffer (5x)	10 µl	1 x
sNTPs (10mM)	1 µl	200 µM
Forward Primer (10µM)	2,5 µl	0,5 µM
Reverse Primer (10µM)	2,5 µl	0,5 µM
Template DNA	Variable	< 200 ng
Q5 High-Fidelity DNA Polymerase (2U/µl)	0,2 µl	0,4 U
MilliQ Water	To 50 µl	

Table 15. Standard PCR settings

Step	Temperature	Time
Initial Denaturation	98 ºC	2 min
30x cycles	98 ºC	30 sec
	X ºC	10 sec
	72 ºC	X sec
Final Extention	72 ºC	10 min
Hold	10 ºC	1 min

6.2.2.2 Agarose gel electrophoresis

Gel electrophoresis was performed in agarose gels prepared by heating agarose powder in 1x TAE buffer using a microwave until fully dissolved, and agarose started boiling. Gels with agarose concentrations varying between 1 % and 2 % (w/v) were prepared, depending on the size of DNA or RNA samples. Ones heated up the agarose was poured into a gel casting tray sealed with tape with a comb to form wells.

Once the gel had solidified the comb was removed and the tray was placed into an electrophoresis chamber filled with 1x TAE buffer. DNA or RNA samples were mixed with respective loading dye and together with a DNA Ladder the samples were loaded into the wells. Electrophoresis was first run at 95 V for 5 min followed by 130 V until desired separation was reached. After electrophoresis gels were stained in a 0.2 µg/ml ethidium bromide in 1x TAE solution for 20 min. Visualization was performed under UV illumination. If needed, selected DNA bands were excised from the gel with a scalpel and purified directly or stored at -20 °C.

For RNA gel electrophoresis the comb, gel casting tray and electrophoresis chamber were treated with 0,1 N NaOH for 20 min under a fume hood to minimize RNase contamination. Later rinsed using Milli-Q water directly from the filtration system. The agarose gel was freshly prepared using RNase-free 1x TAE buffer. Moreover, a fresh ethidium bromide staining solution was prepared for each use.

6.2.2.3 DNA gel extraction

DNA from agarose gel was extracted using the Monarch Gel Extraction Kit (NEB) according to manufacturer's protocol. The final elution was always carried out in prewarmed Milli-Q water. The DNA concentration was determined using a Nanodrop spectrophotometer.

6.2.2.4 Restriction digestion

Restriction digests were set in a total volume of 20µl for test digest or 50µl for linearization of plasmid for mRNA templates. All reactions were prepared with the appropriate restriction enzyme and buffer, DNA and nuclease-free water. Test digestions of miniprepped DNA were incubated at the corresponding temperature for

1 hour (high fidelity) or overnight (O/N). Successful digestion was assessed by gel electrophoresis using 200ng of DNA or the entire digestion.

6.2.2.5 DNA Ligation

Ligation reaction was done for 30min at room temperature or O/N at 4°C. The ligation was prepared in a final volume of 10µl, using the components in Table. A 3:1 molar ratio of insert to vector was used and the required DNA mass was calculated using the online NEBioCalculator tool.

Table 16. Ligation reaction components.

Component	10 µl Reaction
10x T4 Ligation buffer	1 µl
Insert	x µl
Vector (40 ng)	y µl
T4 Ligase (5 U/µl)	1 µl
(PEG 4000)	optional
Milli-Q water	z µl

6.2.2.6 Oligo annealing

1 µl of Complementary single-stranded oligonucleotides were diluted with 18µl of water and 20µl of annealing buffer. The mixture was heated to 95 °C for 5 minutes and then gradually cooled to room temperature over 1 hour to allow proper hybridization, forming double-stranded DNA. Resulting DNA was diluted in a concentration of 1:33, using 1µl of this to ligate into 25ng of the receptor vector, followed by transformation as in 6.2.2.8

Table 17. Oligo annealing thermocycler program

Temperature	Time
95ºC	5 min
Ramp down to 70ºC	0.1ºC/sec
Hold	10 min
Ramp down to 65ºC	0.1ºC/sec
Hold	10 min
Ramp down to 60ºC	0.1ºC/sec
Hold	10 min
Ramp down to 10ºC	0.1ºC/sec

6.2.2.7 Q5 directed mutagenesis

Primers for Q5 site-directed mutagenesis were designed using the online tool NEBaseChanger. Standard PCR was performed using the mutagenesis primers. The resulting PCR product was analyzed by gel electrophoresis and the band corresponding to the expected size was excised and purified. KLD (kinase, ligase, DpnI) treatment was then performed according to Table 18.

Table 18. Components of KDL treatment of PCR product.

Component	15 µl Reaction
PCR product	1 µl
Milli-Q water	9,5 µl
rCutSmart buffer (10x)	1,5 µl
ATP (10 mM)	1,5 µl
PNK (NEB)	0,5 µl
T4 Ligase (5U)	0,5 µl
DpnI (10 U/ µl)	0,5 µl

6.2.2.8 Transformation

For transformations chemical component Mach1T1 bacteria were thawed. In 50 µl of bacteria 5 µl of ligation reaction were added, followed by gentle mix by flicking the reaction tube. The mix was incubated on ice for 15 min. the cells were then heat-shocked for 40 sec at 42 ºC and immediately snap cooled on ice for 2 min. Then 300 µl TB medium were added and the cells were then incubated at 37 ºC for either 45 min (ampicillin) or 1 hour (kanamycin), depending in the antibiotic resistance of the plasmid of interest. Meanwhile LB agar plates containing the corresponding antibiotic were prewarmed at 37 ºC for 1 hour. 50 to 250 µ of transformed cells were plated using sterile glass beads, plates were incubated O/N at 37 ºC.

6.2.3 Plasmid Preparation

6.2.3.1 Minipreparation

Single *E. coli* colonies were picked from agar plates, for minipreparation, using autoclaved toothpicks and incubated in 3 ml of LB medium with the corresponding antibiotic. The cultures were incubated O/N at 37 ºC while shaking at 175 rpm. The following day 2 ml of each bacterial culture was transfer to 2 ml microcentrifuge tubes

and centrifuge at 1400 rpm for 2 min at room temperature. The remaining bacterial cultures were stored at 4 ºC as backup and for BigMini preparations.
Bacterial pellets were resuspended 200 µl of P1 buffer by sliding the tubes across a rack. To lysate the cells 200 µl of P2 buffer were added and tubes were inverted 5-6 times. Neutralization of the solution was done by adding 200 µl of P3 buffer and the tubes were inverted ones again 5-6 times. Samples were then centrifuge for 10 min at 14000 rpm and 4°C. Supernatants were transfer to fresh 1,5ml tubes.
To precipitate the plasmid DNA, 500 µl of isopropanol were added to the supernatant and tubes were vortexed. After 15 min centrifugation at 14000 rpm and 4°C the supernatant was discarded, and DNA pellets were washed with 500 µl of 70% EtOH, followed by centrifugation at 14000 rpm and room temperature, for 5 min, the ethanol was removed and the DNA pellet was air dried for ~ 10 min. Finally, the DNA pellet was dissolved in 50 µl of Mill-Q water.

6.2.3.2 Big Minipreparation

Around 100µll from the O/N bacterial culture were inoculated in 20 ml of LB medium with the corresponding antibiotic (ampicillin and kanamycin) in a 300 Erlenmeyer flask. The cultures were incubated O/N at 37 ºC while shaking at 175 rpm. Next 8 ml of each culture were collected and centrifuge for 2 min at 8000 rpm and room temperature to pellet the cells. DNA was subsequently extracted using the QIAprep Spin Miniprep Kit (QIAGEN) following the manufacturer's protocol. The purified DNA was eluted in 50 µl Milli-Q water.

6.2.4 mRNA *in vitro* synthesis

The mRNAs for micro injections were in vitro transcribed from the plasmids listed in *Table 19*.
Of each plasmid, 5–10 µg was linearized O/N at 37°C. After verification of linearization on an agarose gel, digestions were either purified using the QIAquick PCR Purification Kit (Qiagen) or recovered from an agarose gel using the Monarch® DNA Gel Extraction Kit (NEB). mRNA synthesis was performed using the mMESSAGE mMACHINE SP6 or T7 Transcription Kit (Invitrogen) following the manufacturer's instructions, and RNA was purified with the RNeasy Mini Kit (Qiagen). The mRNA quality was evaluated by running an RNA test gel.

Table 19. Plasmids used for in vitro mRNA synthesis are listed together with the corresponding enzymes used for linearization and promoters leading transcription.

mRNA	Plasmid nr.	Enzyme	Promotor
evoBE4max	#5797	NotI	SP6
ancBE4max	#5811	SapI	T7
ABE8e	#5812	SapI	T7
elovl4b_WT	#6340	NotI	SP6
elovl4b_N9Q	#6350	NotI	SP6
elovl4b_N72Q	#6351	NotI	SP6
elovl4b_N116Q	#6352	NotI	SP6
elovl4b_N9Q-N72Q-N116Q	#6353	NotI	SP6
heiCas9	#6342	NotI	SP6
opn1sw_WT	#6339	NotI	SP6
opn1sw_N10Q	#6347	NotI	SP6
opn1sw_N71Q	#6348	NotI	SP6
opn1sw_N10Q-N71Q	#6349	NotI	SP6
Rho_WT	#6338	NotI	SP6
rho_N2Q-N15Q	#6346	NotI	SP6
Pikachurin_WT	#6341	NotI	SP6
pikachurin_N50Q	#6354	NotI	SP6
pikachurin_N327Q	#6355	NotI	SP6
pikachurin_N660Q	#6356	NotI	SP6

6.2.5 crRNA

CRISPR RNAs (crRNA) were analysed for potential off-target effects using CCTop (Stemmer et al., 2015) and ACEofBASES (Cornean et al., 2022) using standard settings. The gRNAs designed in this thesis are listed in Table 4. Synthetic crRNAs and tracrRNA (custom Alt-R crRNA) were ordered from IDT. To prepare crRNA and tracrTRA both were resuspended in nuclease-free duplex buffer (IDT) to a final concentration of 100 µM and stored at -20 °C. Duplex mixture of 40 µM crRNA:tracrRNA was prepared by mixing 4µl of each RNA with 2 µl of nuclease-free duplex buffer. The mixture was incubated at 95 ºC for 5 min, and cooled down at room temperature, later stored at -20 ºC. For injections, 1 µl was used in a 10 µl injection mix, with a final concentration of 4 µM.

6.2.6 Microinjections and phenotypes

Microinjections were performed in wild-type Cab embryos with listed mixes in table. The night prior to injections, adult medaka fish were separated and paired the next morning for mating. After 15 min, freshly fertilize eggs were collected in ice-cold 1x ERM and separated with forceps. The eggs were aligned in the grooves of a 1,5% agarose in water mold covered in cold 1x ERM.

Injections needles were pulled from glass capillaries with needler puller. Approximately 3µl of injection mix waws loaded into the needle and opened by scratching the chorion. The injection parameters were 1000 hPa for injection pressure and 180 hPa for holding pressure, individual adjustment were performed during the injections to adapt to needle conditions. Embryos were injected at the one-cell stage with the corresponding mix. Injection volumes were estimated visually, approximately 10% of the cell volume. After injection, embryos were transfer to fresh 1x ERM and incubated at 28ºC. Embryos were screened for GFP presence 7-10 hours after injection. If phenotypes emerged, embryos were imaged with a stereomicroscope equipped with a Nikon DXM1200 digital camera, for hatchlings imaging, they were anesthetized in 1x Tricaine prepared in 1x ERM.

Table 20. List of injection mixes used in this thesis.

Injection mix	Injection mix components	Final concentration
00896_N595-ABE	*ABE8e* mRNA	150 ng/µl
	00896_N595 cr/trRNA	4 µM
	GFP mRNA	10 ng/µl
00896 -KO	*heiCas9* mRNA	150 ng/µl
	00896_N595 cr/trRNA	4 µM
	GFP mRNA	10 ng/µl
00896_N1390-ABE	*ABE8e* mRNA	150 ng/µl
	00896_N1390 cr/trRNA	4 µM
	GFP mRNA	10 ng/µl
00896- KO	*heiCas9* mRNA	150 ng/µl
	00896_N1390 cr/trRNA	4 µM
	GFP mRNA	10 ng/µl
13140_N469-ABE	*ABE8e* mRNA	150 ng/µl
	13140_N469 cr/trRNA	4 µM
	GFP mRNA	10 ng/µl
13140-KO	*heiCas9* mRNA	150 ng/µl
	13140_N469 cr/trRNA	4 µM
	GFP mRNA	10 ng/µl
24677_N186-ABE	*ABE8e* mRNA	150 ng/µl
	24677_N186 cr/trRNA	4 µM
	GFP mRNA	10 ng/µl

Injection mix	Injection mix components	Final concentration
24677 -KO	*heiCas9* mRNA	150 ng/µl
	24677_N186 cr/trRNA	4 µM
	GFP mRNA	10 ng/µl
25491_N59-ABE	*ABE8e* mRNA	150 ng/µl
	25491_new-PAM cr/trRNA	4 µM
	25491 N59	4 µM
	GFP mRNA	10 ng/µl
25491-KO	*heiCas9* mRNA	150 ng/µl
	25491_new-PAM cr/trRNA	4 µM
	GFP mRNA	10 ng/µl
elovl4b_N9-ABE	*ABE8e* mRNA	150 ng/µl
	elovl4b_N9 cr/trRNA	4 µM
	GFP mRNA	10 ng/µl
elovl4b_N9-KO	*heiCas9* mRNA	150 ng/µl
	elovl4b_N9 cr/trRNA	4 µM
	GFP mRNA	10 ng/µl
elovl4b_N72-ABE	*ABE8e* mRNA	150 ng/µl
	elovl4b_N72 cr/trRNA	4 µM
	GFP mRNA	10 ng/µl
elovl4b_N72 -KO	*heiCas9* mRNA	150 ng/µl
	elovl4b N72 cr/trRNA	4 µM
	GFP mRNA	10 ng/µl
elovl4b -WT rescue	*heiCas9* mRNA	150 ng/µl
	elovl4b_N9 cr/trRNA	4 µM
	elovl4b_WT mRNA	100 ng/µl
	GFP mRNA	10 ng/µl
elovl4b -N9Q rescue	*heiCas9* mRNA	150 ng/µl
	elovl4b_N9 cr/trRNA	4 µM
	elovl4b_N9Q mRNA	100 ng/µl
	GFP mRNA	10 ng/µl
elovl4b -N72Q rescue	*heiCas9* mRNA	150 ng/µl
	elovl4b_N9 cr/trRNA	4 µM
	elovl4b_N72Q mRNA	100 ng/µl
	GFP mRNA	10 ng/µl
elovl4b-N116Q rescue	*heiCas9* mRNA	150 ng/µl
	elovl4b_N9 cr/trRNA	4 µM
	elovl4b_N116Q mRNA	100 ng/µl
	GFP mRNA	10 ng/µl
oca2-CBE	*ancBE4max* mRNA	150 ng/µl
	oca2 sgRNA (58)	15 ng/µl
	GFP mRNA	10 ng/µl
oca2-KO	*heiCas9* mRNA	150 ng/µl
	oca2 sgRNA (57)	15 ng/µl
	GFP mRNA	10 ng/µl
opn1sw_N10-ABE	*ABE8e* mRNA	150 ng/µl
	opn1sw_N10 cr/trRNA	4 µM
	GFP mRNA	10 ng/µl
opn1sw-KO	*heiCas9* mRNA	150 ng/µl
	opn1sw_N10 cr/trRNA	4 µM
	GFP mRNA	10 ng/µl

Injection mix	Injection mix components	Final concentration
opn1sw -WT rescue	*heiCas9* mRNA	150 ng/μl
	opn1sw_N10 cr/trRNA	4 μM
	opn1sw_WT mRNA	100 ng/μl
	GFP mRNA	10 ng/μl
opn1sw -N10Q rescue	*heiCas9* mRNA	150 ng/μl
	opn1sw_N10 cr/trRNA	4 μM
	elovl4b_N9Q mRNA	100 ng/μl
	GFP mRNA	10 ng/μl
opn1sw -N71Q rescue	*heiCas9* mRNA	150 ng/μl
	opn1sw_N10 cr/trRNA	4 μM
	opn1sw_N71Q mRNA	100 ng/μl
	GFP mRNA	10 ng/μl
opn1sw-N10QN71Q rescue	*heiCas9* mRNA	150 ng/μl
	opn1sw_N10 cr/trRNA	4 μM
	opn1sw_N10Q-N71Q mRNA	100 ng/μl
	GFP mRNA	10 ng/μl
opn1sw -WT control	*opn1sw_WT* mRNA	100 ng/μl
	GFP mRNA	10 ng/μl
opn1sw-N10QN71Q control	*opn1sw_N10Q-N71Q* mRNA	100 ng/μl
	GFP mRNA	10 ng/μl
PCDH8_N425-ABE	*ABE8e* mRNA	150 ng/μl
	PCDH8_N425 cr/trRNA	4 μM
	GFP mRNA	10 ng/μl
PCDH8_N425-KO	*heiCas9* mRNA	150 ng/μl
	PCDH8_N425 cr/trRNA	4 μM
	GFP mRNA	10 ng/μl
PCDH8_N575-ABE	*ABE8e* mRNA	150 ng/μl
	PCDH8_N575 cr/trRNA	4 μM
	GFP mRNA	10 ng/μl
PCDH8_N575-KO	*heiCas9* mRNA	150 ng/μl
	PCDH8_N575 cr/trRNA	4 μM
	GFP mRNA	10 ng/μl
pikachurin_N50-CBE	*evoBE4max* mRNA	150 ng/μl
	pikachurin_N50 cr/trRNA (58)	4 μM
	GFP mRNA	10 ng/μl
pikachurin-KO	*heiCas9* mRNA	150 ng/μl
	pikachurin_N50 cr/trRNA	4 μM
	GFP mRNA	10 ng/μl
pikachurin-WT recue	*heiCas9* mRNA	150 ng/μl
	pikachurin_N50 cr/trRNA	4 μM
	pikachurin_WT mRNA	100 ng/μl
	GFP mRNA	10 ng/μl
pikachurin-N50Q recue	*heiCas9* mRNA	150 ng/μl
	pikachurin_N50 cr/trRNA	4 μM
	pikachurin_N50Q mRNA	100 ng/μl
	GFP mRNA	10 ng/μl
pikachurin-N327Q recue	*heiCas9* mRNA	150 ng/μl
	pikachurin_N50 cr/trRNA	4 μM
	pikachurin_N327Q mRNA	100 ng/μl
	GFP mRNA	10 ng/μl

Injection mix	Injection mix components	Final concentration
pikachurin-N660Q recue	*heiCas9* mRNA	150 ng/µl
	pikachurin_N50 cr/trRNA	4 µM
	pikachurin_N660Q mRNA	100 ng/µl
	GFP mRNA	10 ng/µl
rho_N15-ABE	*ABE8e* mRNA	150 ng/µl
	rho_N15 cr/trRNA	4 µM
	GFP mRNA	10 ng/µl
rho-KO	*heiCas9* mRNA	150 ng/µl
	rho_N15 cr/trRNA	4 µM
	GFP mRNA	10 ng/µl
rho -WT rescue	*heiCas9* mRNA	150 ng/µl
	rho_N15 cr/trRNA	4 µM
	rho_WT mRNA	100 ng/µl
	GFP mRNA	10 ng/µl
rho -N2QN15Q rescue	*heiCas9* mRNA	150 ng/µl
	rho_N15 cr/trRNA	4 µM
	rho_N2QN15Q mRNA	100 ng/µl
	GFP mRNA	10 ng/µl
rho -WT control	*rho_WT* mRNA	100 ng/µl
	GFP mRNA	10 ng/µl
rho -N2QN15Q control	*rho_N2QN15Q* mRNA	100 ng/µl
	GFP mRNA	10 ng/µl
tnc_N42-ABE	*ABE8e* mRNA	150 ng/µl
	tnc_N42 cr/trRNA	4 µM
	GFP mRNA	10 ng/µl
tnc_N42-KO	*heiCas9* mRNA	150 ng/µl
	tnc_N42 cr/trRNA	4 µM
	GFP mRNA	10 ng/µl
tnc_N171-ABE	*ABE8e* mRNA	150 ng/µl
	tnc_N171 cr/trRNA	4 µM
	GFP mRNA	10 ng/µl
tnc_N171-KO	*heiCas9* mRNA	150 ng/µl
	tnc_N171 cr/trRNA	4 µM
	GFP mRNA	10 ng/µl
tnc_N186-CBE	*evoBE4max* mRNA	150 ng/µl
	tnc_N186 cr/trRNA	4 µM
	GFP mRNA	10 ng/µl
tnc_N186-KO	*heiCas9* mRNA	150 ng/µl
	tnc_N186 cr/trRNA	4 µM
	GFP mRNA	10 ng/µl
tnc_N300-ABE	*ABE8e* mRNA	150 ng/µl
	tnc_N300 cr/trRNA	4 µM
	GFP mRNA	10 ng/µl
tnc_N300-KO	*heiCas9* mRNA	150 ng/µl
	tnc_N42 cr/trRNA	4 µM
	GFP mRNA	10 ng/µl
tnc_N1686-ABE	*ABE8e* mRNA	150 ng/µl
	tnc_N1686 cr/trRNA	4 µM
	GFP mRNA	10 ng/µl

Injection mix	Injection mix components	Final concentration
tnc_N1686-CBE	*evoBE4max* mRNA	150 ng/µl
	tnc_N1696 cr/trRNA	4 µM
	GFP mRNA	10 ng/µl
tnc_N1686-KO	*heiCas9* mRNA	150 ng/µl
	tnc_N1686 cr/trRNA	4 µM
	GFP mRNA	10 ng/µl

6.2.7 Sanger sequence genotyping of crispants and editants

To genotype the injected embryos with the cr/trRNAs and *heiCas9* mRNA (Table 20), genotyping was performed on pooled samples, of five embryos randomly selected. If the embryos showed phenotypes, gDNA was extracted from individual embryos. To extract gDNA embryos were grounded with a plastic pestle, and then lysed in 100 µl of fin-clip buffer with Proteinase K. Samples were then incubates at 60ºC O/N, on the following day, the samples were diluted 1:2 with nuclease-free water. To inactivate Proteinase K, samples were then incubated at 95ºC for 20 min. Samples were then stored at 4ºC.

To amplify regions of interest of the targeted genes, primers were design surrounding it. PCR was performed using Q5 High-Fidelity DNA polymerase and specific primers per gene shown in *Table 3*.

PCR products were visualized by agarose gel electrophoresis, cut out of the gel and purified using the Monarch DNA Gel Extraction Kit following the manufacturer's indications and sent for Sanger sequencing (Eurofins Genomics).

6.2.8 Functional and behavioural analysis of mutant stable lines

Sample preparation and analysis for OMR assays were performed by Dr. Risa Suzuki (Wittbrodt lab, Heidelberg university). For the ERG experiments, retina extraction, ERG experiments and analysis were done by Dr. Jingjing Zang (Nehauss lab, Zurich University). Genotyping and further experiments were executed by me.

6.2.8.1 OptoMotor Response analysis (OMR)

To study the visual acuity and swimming behaviour of the *rho* mutant medaka line, infinity pool OMR was performed. Exposing the specimens to a black and white stripe stimulus, as *rho* is responsible to contrast vision.

After hatching, specimens were transfer to individual plates with fresh 1x ERM at 28ºC, until the following day when OMR was performed. Before OMR hatchlings were

transfer to experimental setup, described in (Suzuki, Wittbrodt, 2025; unpublished). The OMR experiment started with an acclimatation phase of 5 min: 1 min black background, 4 min of the first stipe pattern with no movement. Then the exposure to moving stimuli started, each set of stimuli consisted on 2,5 min clockwise motion, 30 sec pause, 2,5 min counterclockwise motion and one more pause. This sequence was repeated with progressive increase in the thickness of the stripes 1.2, 1.6, 2.0, 2.4, 2.8, 3.2, 3.7, 4.0, 4.4, 4.7, 5.2, 5.7, 6.0, 6.3, 6.7, 7.1, 7.6, 8.1, 8.1, 16.2, and 16.2 mm. Stripe motion speed was set to 20.6°/s, except for the second round of the 8.1 mm and 16.2 mm conditions, which were presented at 61.8°/s.
Ones the experiments finished, hatchlings were sacrifice in 20x tricaine, and later fix individually in 4% PFA in 1x PBS, to analyse the retinal structure.
OMR recordings were analysed with a Custom Python-based detection software and Custom R script (Risa, Wittbrodt, 2025; unpublished).

6.2.8.2 Electroretinography (ERG)

To determine the functionality of the different photoreceptors in the mutant lines, ERG was performed, using UV/ green light for *opn1sw* mutant line and white light for the *rho* mutant line.
ERGs were recorded on 1dph medaka hatchlings' eyes, as previously described (Sirisi et al., 2014). In brief, hatchlings were dark-adapted for a minimum of 30 min before recordings. Preparatory steps, including eye dissection, positioning the eye, and recording pipette, were done under a dim red light to prevent bleaching of photopigments. The eye was removed and placed on a filter paper on top of an agarose gel. The reference electrode was inserted into the agarose gel, and the recording electrode, a glass capillary with a tip diameter of 20-30 µm filled with E3 medium, was positioned on top of the cornea. ERG light generation and measurement were done as previously described in (Niklaus et al., 2024). A series of five white light stimuli of decreasing light intensities (log 0 to log -5) were presented to the eyes. Each stimulus lasted 100 milliseconds, with a 15-second interval between stimuli. ERG recordings were analysed using Excel and MATLAB, with b-wave amplitudes used as an indicator of ON-bipolar cell depolarization. The first 50 milliseconds of each recording were averaged to establish baseline values, and b-wave amplitudes were statistically analysed using Prism9.

6.2.8.3 Genotyping of the mutant stable lines

To identify the genotype of each specimen that was analyse with ERG and OMR, hatchlings tails were used for DNA extraction, following the steps described in 6.2.2.3 For the *rho* stable line primers *rho fwd* (5'-AGTTATGTTTGCAGTGACGGC-3') and *rho rv* (5'-GAAGTTGCTGATGGGCTTGC-3') were used. PCR were run with standard settings as described in Table 15, annealing at 68ºC and 20 sec extension. For the *opn1sw* stable line, the primers used were *opn1sw fwd* (5'-GAAGTAGTAGCCCCTCACGC-3') and *opn1sw rv* (5'-CGGTTCAGAGCTCAGCTTCA -3'), using standard PCR setting, annealing at 68ºC for 10 sec.

PCR products were separated by electrophoresis on 2% agarose gels. Genotype could be confirmed by fragment size as shown in Figure 12 and Figure 14.

6.2.9 mRNA rescue injections

6.2.9.1 Cloning of constructs

Wild type mRNA of the candidate genes *rho, opn1sw, elovl4 and pikachurin* were cloned from stage 40 wild type Cab cDNA using PCR. Primers were designed to introduce restriction enzyme sites for XbaI (fwrd) and EcoRI (rv) (Table 3). The resulting PCR product were digested with *XbaI* and *EcoRI*, and ligated in the the pCS2+ vector backbone, previously digested with the same two enzymes. All the steps were followed as described in 6.2.2.5.

To create the different variants two different techniques were used, oligo annealing 6.2.2.6 and Q5 mutagenesis 6.2.2.7 The creation of the plasmids containing the variants cDNA was done Ellie Pusher (Master Rotation at Wittbrodt Lab, Heidelberg University).

To generate the corresponding mRNA of the wild type cDNA and the variants *in vitro* mRNA synthesis was performed as described in 6.2.4.

6.2.9.2 mRNA injections

Wild type Cab embryos were injected in the 1-cell stage with 100ng of mRNA final volume. The injection mix used are described in Table 20. Injected embryos were incubated at 28ºC until hatching. 1dph Self-hatched and normal looking hatchlings were fixed in 4%PFA in 1xPBS for histological analysis of the retina. To determine the

efficiency of the CRISPR/Cas9, siblings, looking similar to those fixed, were pooled for DNA extraction and PCR amplification, to send samples for Sanger sequencing as described in 6.2.7.

6.2.10 Immunohistochemistry of medaka hatchlings retina

6.2.10.1 Sample preparation

To perform cryosections, samples: medaka hatchlings, and head, were prepared to performed the sections.

Samples were fixed in 4%PFA/1xPBS O/N at 4ºC. To remove fixative excess, samples were washed 3 times with 1x PBS and transfer to 30% sucrose/1x PBS for O/N incubation at 4°C. Next day the samples were washed 3 times before cryoprotection in 1:1 30%sucrosse/x1PBS and tissue freezing media (TFM), for at least one night at 4ºC.

6.2.10.2 Cryosections

To perform cryosections, samples were transfer to plastic moulds, and arranged so the heads would be facing the bottom surface of the mould. The moulds were then filled with TFM and deep freeze in liquid nitrogen, and immediately after place inside the cryostat for at least 10 min, to equilibrate. Cryosections of 16µm thickness were done using a Leica cryostat (Leica CM 3050S) collecting the resulting sections in Superfrost plus microscope slides, and then dried O/N at 4ºC.

6.2.10.3 Immunohistochemistry on retinal sections and imaging

To rehydrate the samples, they were incubated for 30min in 1x PBS at room temperature, using a pipette tip box as a moisturise chamber. Samples were blocked in 10%BSA in x1PBS at room temperature, for 2 hours and covered with parafilm to avoid evaporation. After blocking, solution was removed and the slides were washed 2 times for 5 min in with 1xPBS. Samples were incubated with primary antibodies, in the corresponding concentration (Table 8), diluted in 1%BSA in 1xPBS, and covered with parafilm O/N at 4°C in darkness. To remove unbonded antibodies, the slides were washed 6 times for 5 min with 1x PBS. The corresponding secondary antibodies (Table 8) were applied in 1%BSA in 1xPBS, combined with DAPI (1:500) O/N at 4ºC in darkness. Next day, the slides were washed again 3 times for 5 min un 1x PBS, and

mounted in 100µl of 60% glycerol in 1xPBS, after which a coverslip was place slowly on top and sealed with nail polish. Slides were kept at 4°C in darkness until imaging was performed. Samples were imaged using a Leica SP8 confocal microscope. Obtained images were process and analyzed with ImageJ.

6.2.10.4 Image analysis and quantification

Retinal images were analysed in ImageJ by manually defining regions of interest of 54 µm wide spanning the full thickness of the retina, from the centre of the lens to the RPE (Figure 5). For each ROI, nuclei were counted across all retinal layers. One representative optical section within the 16 µm stack was selected where all nuclear layers were complete and well defined. The total number of nuclei per layer was manually counted using the Cell Counter plugin, and cells in the outer nuclear layer were classified according to types described in Figure 17. Proportions of each cell type were calculated to the total number of cells per region of interest.

Statistical analyses were performed in R. Data were first assessed for normality (Shapiro-Wilk or Anderson-Darling test) and for homogeneity of variance (Levene's test). Comparisons between experimental conditions and the control group (Uninjected) were then conducted using two-tailed t-tests, with p-values corrected for multiple comparisons using the Bonferroni method. Each experimental condition was compared individually against Uninjected for each combination of gene, retinal region, and cell type. Statistical significance was represented using asterisks (* $p<0.05$, ** $p<0.01$, *** $p<0.001$, **** $p<0.0001$, ns = not significant).

7 Appendix

7.1 Supplementary data

Supplementary Table 1. Genes analyzed in this thesis

Gene	GeneID	UniProt Medaka ID	PTM Medaka	Human GeneID	Gene	UniProt Human ID	PTM Human
novel gene	**ENSORLG00000000896**	**H2L5MO**	**no signal peptide**				
rom1b	ENSORLG00000002572	H2LBD3	no PTM	ENSG00000149489	ROM1	Q03395	No glycosylation
novel gene	ENSORLG00000003634	H2LF05	no PTM				
kfharr-r2	ENSORLG00000006701	Q9W7R1	no PTM	ENSG00000130561	SAG	P10523	No glycosylation
novel gene	ENSORLG00000006731	H2LQV4		ENSG00000167325	RRM1	P23921	No glycosylation
rgra	ENSORLG00000006925	A0A3B3HT59	no PTM	ENSG00000148604	RGR	P47804	1 Glycosylation site
sec31b	ENSORLG00000009277	A0A3B3HLA1	no PTM	ENSG00000075826	SEC31B	Q9NQW1	No glycosylation
novel gene	ENSORLG00000009919	H2M208	no sidnal peptide	ENSG00000131051	RBM39	Q14498	
novel gene	ENSORLG00000010067	A0A3B3HCP5	peptide signal	ENSG00000185008	ROBO2	Q9HCK4	Glycosylation and N-linked asparagine
rho1	**ENSORLG00000010599**	**KFH-Rh**		**ENSG00000163914**	**RHO**		
novel gene	ENSORLG00000010644	H2M4H8	no PTM	ENSG00000122786	CALD1	Q05682	No glycosylation
rom1a	ENSORLG00000010774	H2M4Z1	no PTM	ENSG00000149489	ROM1	Q03395	
novel gene	ENSORLG00000010880	H2M5C0	peptide signal	ENSG00000205832	C14orf96	A6NNT2	No glycosylation
novel gene	**ENSORLG00000013140**	**H2MD32**	**peptide signal**	**ENSG00000148702**	**HABP2**	**Q14520**	**2 Glycosylation sytes**
novel gene	ENSORLG00000014225	H2MGV2	no PTM				
novel gene	ENSORLG00000014933	A0A3B3IFV5	no PTM				
novel gene	ENSORLG00000016348	A0A3B3HP81	no PTM	ENSG00000127824	TUBA4A	P68366	No glycosylation
novel gene	ENSORLG00000017308	H2MSC4	no PTM	ENSG00000136068	FLNB	O75369	No glycosylation
novel gene	ENSORLG00000017377	H2MSJ7	no PTM				
novel gene	ENSORLG00000022891	A0A3B3IMD1	no PTM	ENSG00000100345	MYH9		
novel gene	**ENSORLG00000024677**	**A0A3B3HLL0**	**no PTM**	**ENSG00000132639**	**SNAP25**	**P60880**	**No glycosylation**
novel gene	**ENSORLG00000025491**	**A0A3B3I291**	**no PTM**	**ENSG00000102003**	**SYP**	**P08247**	**1 Glycosylation site**
novel gene	ENSORLG00000026256	A0A3B3HW25	no PTM	ENSG00000126803	HSPA2	P35579	No glycosylation

Gene	GeneID	UniProt Medaka ID	PTM Medaka	Human GeneID	Gene	UniProt Human ID	PTM Human
novel gene	ENSORLG00000027417	A0A3B3H6H3	no PTM	ENSG00000078018	MAP2	P11137	No glycosylation
novel gene	ENSORLG00000027727	A0A3B3HBQ8	no PTM				
novel gene	ENSORLG00000028255	A0A3B3ID86	no PTM	ENSG00000126803	HSPA2	P54652	No glycosylation
novel gene	ENSORLG00000028379	A0A3B3I310	no PTM	ENSG00000146676	PURB	Q96QR8	No glycosylation
novel gene	ENSORLG00000029511	A0A3B3HDP6	no PTM	ENSG00000144674	GOLGA4	Q13439	N-linked asparagine
novel gene	ENSORLG00000030114	A0A3B3HRI9	no PTM				
ppp3cca	ENSORLG00000016121	H2MN74	NO				
elovl4b	**ENSORLG00000017019**	**H2MRB5**	**NO**	**ENSG00000118402**	**ELOVL4**	**Q9GZR5**	**Glycosylation site by publication**
tmem106a	ENSORLG00000018866	H2MX97	NO				
rpl23	ENSORLG00000019162	H2MY25	NO	ENSG00000125691	RPL23	P62829	No PTM
plekhg5b	ENSORLG00000019281	H2MYE3		ENSG00000171680	PLEKHG5	O94827	No PTM
opn1sw	**ENSORLG00000019293**	**Q2L6A1**	**Desulfide bond**	**ENSG00000128617**	**OPN1SW**	**P03999**	**Glycosylation curated; related with cones**
ENSORLG00000019978	ENSORLG00000019978	A0A3B3HJU5	NO	ENSG00000135097	MSI1	O43347	No PTM
ENSORLG00000020890	ENSORLG00000020890	H2N316	NO				
ENSORLG00000021792	ENSORLG00000021792	A0A3B3IMW2	NO				
snca	ENSORLG00000022195	A0A3B3H770	No	ENSG00000145335	SNCA	P37840	No PTM
ENSORLG00000022333	ENSORLG00000022333	A0A3B3HAP6	NO	ENSG00000104237	RP1	P56715	No PTM, photoreceptor differentiation
ENSORLG00000022456	ENSORLG00000022456	A0A3B3HF69	NO				
ENSORLG00000022474	ENSORLG00000022474	A0A3B3IL27	Methylation				
atp5f1e	ENSORLG00000022838	A0A3B3HDJ9					
si_dkey-283b15.2	ENSORLG00000022932	A0A3B3II30	NO				
rpl18a	ENSORLG00000024868	A0A3B3IJY7	NO	ENSG00000105640	RPL18A	Q02543	No PTM
hsp90aa1.1	ENSORLG00000025267	H2M8S8	NO				
fam131a	ENSORLG00000025673	A0A3B3HKT2	NO	ENSG00000175182	FAM131A	Q6UXB0	No PTM
ENSORLG00000025815	ENSORLG00000025815	A0A3B3IBY4	NO				
rgs3a	ENSORLG00000026253	A0A3B3HLW7	NO	ENSG00000138835	RGS3	P49796	No PTM
ENSORLG00000026953	ENSORLG00000026953	A0A3B3H9U8					
zbtb18	ENSORLG00000027425	A0A3B3H8K2	NO	ENSG00000179456	ZBTB18	Q99592	No PTM
neurod1	ENSORLG00000027657	A0A3B3H7Y2	NO	ENSG00000162992	NEUROD1	Q13562	No PTM
pde6ha	ENSORLG00000028008	A0A3B3H759	NO				
otx1	ENSORLG00000028142	A0A3B3IA06		ENSG00000115507	OTX1	P32242	No PTM
gngt2b	ENSORLG00000028846	A0A3B3HF80	no signal peptide	ENSG00000167083	GNGT2	O14610	No PTM
fkbp1ab	ENSORLG00000029721	H2LAX8					
rpl39	ENSORLG00000030471	A0A3B3HGM1	NO	ENSG00000198918	RPL39	P62891	No PTM

Gene	GeneID	UniProt Medaka ID	PTM Medaka	Human GeneID	Gene	UniProt Human ID	PTM Human
rpl14	ENSORLG00000030613	A0A3B3I146	NO	ENSG00000188846	RPL14	P50914	No PTM
ENSORLG00000000594	ENSORLG00000000594	H2L4N5	NO	ENSORLG00000000594			
zgc_112294	ENSORLG00000000848	H2L5G6	NO	ENSORLG00000000848			
arr3b	ENSORLG00000001830	H2L8U8	NO	ENSORLG00000001830	ARR3	P36575	No PTM
arr3	ENSORLG00000001983	H2L9D0	NO	ENSORLG00000001983	ARR3	P36575	No PTM
NDUFA4	ENSORLG00000002522	H2LB63	NO	ENSORLG00000002522	NDUFA4	O00483	Phosphoserine and N-acetylation
tnc	**ENSORLG00000002627**	**A0A3B3HLP6**	**signal peptide**	**ENSORLG00000002627**	**TNC**	**P24821**	**Glycosylation several from publications**
LAPTM4B	ENSORLG00000002899	A0A3B3HN64	NO	ENSORLG00000002899	LAPTM4B	Q86VI4	No PTM
CKMT2	ENSORLG00000003211	H2LDJ4	NO	ENSORLG00000003211	CKMT2	P17540	No PTM
casz1	ENSORLG00000005173	A0A3B3I9D7	NO	ENSORLG00000005173	CASZ1	Q86V15	No PTM
rpl31	ENSORLG00000005178	H2LKH3	NO	ENSORLG00000005178	RPL31	P62899	No PTM
EGFLAM	**ENSORLG00000005499**	**A0A3B3HC55**	**Desulfide bond**	**ENSORLG00000005499**	**EGFLAM**	**Q63HQ2**	**Glycosylation only by sequence analysys**
ssx2ipb	ENSORLG00000006011	H2LND2	NO	ENSORLG00000006011	SSX2IP	Q9Y2D8	No PTM
rpl26	ENSORLG00000007374	A0A3B3HTG6		ENSORLG00000007374	RPL26	P61254	No PTM
rps3a	ENSORLG00000007681	O73813	methilation	ENSORLG00000007681	RPS3A	P61247	No PTM
six7	ENSORLG00000007974	H2LV74	NO	ENSORLG00000007974	ANHX	E9PGG2	No PTM
itm2bb	ENSORLG00000008253	H2LW72	Desulfide bond	ENSORLG00000008253	ITM2B	Q9Y287	No PTM
fabp11b	ENSORLG00000008282	H2LWA3	NO	ENSORLG00000008282	PMP2	P02689	No PTM
ENSORLG00000009309	ENSORLG00000009309	H2LZV3	no signal peptide	ENSORLG00000009309			
ENSORLG00000009507	ENSORLG00000009507	H2M0J5	NO	ENSORLG00000009507			
kif19	ENSORLG00000010994	H2M5Q9	NO	ENSORLG00000010994	KIF19	Q2TAC6	No PTM
pcdh8	**ENSORLG00000011123**	**H2M662**	**signal peptide**	**ENSORLG00000011123**	**PCDH8**	**O95206**	**Glycosylation only by sequence analysys**
chl1b	ENSORLG00000011220	A0A3B3IG98		ENSORLG00000011220			
ENSORLG00000011582	ENSORLG00000011582	A0A3B3I8P1	Phosphoprotein	ENSORLG00000011582	TACC2	O95359	no PTM
atp5l	ENSORLG00000012113	H2M9H4	NO	ENSORLG00000012113	ATP5MGL	Q7Z4Y8	no PTM
fabp7a	ENSORLG00000013475	H2ME97	NO	ENSORLG00000013475			
soul3	ENSORLG00000014505	H2MHQ9	NO	ENSORLG00000014505			

Gene	GeneID	UniProt Medaka ID	PTM Medaka	Human GeneID	Gene	UniProt Human ID	PTM Human
ppdpfa	ENSORLG00000014723	H2MIH5	NO	ENSORLG00000014723	PPDPFL	Q8WWR9	no PTM
ENSORLG00000014931	ENSORLG00000014931	H2MJ78	NO	ENSORLG00000014931			
ENSORLG00000015002	ENSORLG00000015002	A0A3B3HRL4	NO	ENSORLG00000015002			

NetNGlyc analysis to identify the glycosylation sequons all candidates

```
Output for 'sec31b'

    Warning: This sequence may not contain a signal peptide!!

Name:  sec31b  Length:  1215
MRLKEIQRTAHQAWSPSGHHPIFLALGTSAQQLDASFNTTAAIEIFQMDFTDPSLEMQLKGSIPTPNRLHSIVWVDFGMG      80
ADETGGRLICGSENGLLTVYKPEAIMNSGADALVGQSDKHTGPVGALDFNPFQSNLLASGANDSEIFIWDLNNFNSPMTP     160
GAKTQPAEDISVVSWNRQVQHILASATPSGKAVVWDLRKNEPIIKISDHSNRMHCSGMLWHPDVATQLVLASEDDRLPVI     240
QMWDLRFATSPLKVFENHTRGILSISWSQADSELLLSSAKDNRILCWNPNTGEVIYELPTTNQWCFDVQWCPRNPALLST     320
ASFDGRISVYSVMGGSLKAQQQSTAEKISSSFDTMDPFGTGQVLPPLQVPLPHMQDTIVPPLKKPPKWVRRPVGASFAFG     400
GKLITFENPKQPSVQSPQPVPRQVFMSQVTTETELLQRSRELQAALQSGSFNTYCQTKIQNATSDTEQDIWKFLLVNFED     480
EARVKFLKLLGFSKDELERKISKCLGKSCQPNGLGVDAKDLAEKMQRLSTERCEEGAESRTSGSVSPADFFSDTPKDTPN     560
FQIPVSCDSDGLISQALLVGNFEGAVELCLNDGRYAEAILLSISGGEELLKKTQQKYLSKRKNSISMLISSVVTQNWRDI     640
VQCCELDNWKEALAALLTYAHPEDFAFLCDILGNRLEHEGTEKRCLQACLCYICSGNIEKLVECWALHRDCSSPLGLEDL     720
VEKVMMLRKSIERLRNNEVAIQSPILAEKLTSYAGILAAEGSLSTAMAYLPENSDQPAITMLRDRLFHAQEEASVQPQIT     800
HPSKVALSTANAIPAPKAPFMNQFQPPAPSPVAPPQQPQIPSVFTPQAPPPNPGPGLPPTSHVHHPSSPPSAMRPSYPQH     880
PSMPPGIPSHQPFQPQPVSAGGPFPPTVPSIPAPSLSGPQLPPSSSTPGGLPPMPSPGVPPTGFMPSTSLPSGFMPPNSQ     960
PGAPVPMYPGNFPNQGPPAPLMSPGHFTPAGPGYPQGGPGAPAVKPFPAPVVAPPPTGFFPWLTSQSDSQGPQEGWNDPP    1040
TVRGGPRKTKVSSNYTPPVPITAPVMGFPVESQQPHDPTQVPPGAPQEPSVQLLQQLPAERVEQKEIPPEHVILKTTFDS    1120
LVQRCQLAAGDPQTKRKLDDAGKRLGHLYDKLREQSLSPNILNGLHEISRCVSSQNYQRALEVHTQVVSSSNFSEISAFM    1200
PILKVVITTANKLGV
................................................................................      80
.....................................................N..........................     160
................................................................................     240
................N...............................................................     320
................................................................................     400
.....................................................N..........................     480
................................................................................     560
................................................................................     640
................................................................................     720
................................................................................     800
................................................................................     880
................................................................................     960
................................................................................    1040
................................................................................    1120
................................................................................    1200
.............                                                                       1280

(Threshold=0.5)
--------------------------------------------------------------------------
SeqName      Position  Potential    Jury    N-Glyc
                             agreement result
--------------------------------------------------------------------------
sec31b         38 NTTA   0.4672      (5/9)   -
sec31b        142 NDSE   0.5944      (8/9)   +
sec31b        257 NHTR   0.5224      (5/9)   +
sec31b        461 NATS   0.6559      (6/9)   +
sec31b       1054 NYTP   0.1381      (9/9)   ---
sec31b       1192 NFSE   0.4178      (6/9)   -
--------------------------------------------------------------------------
```

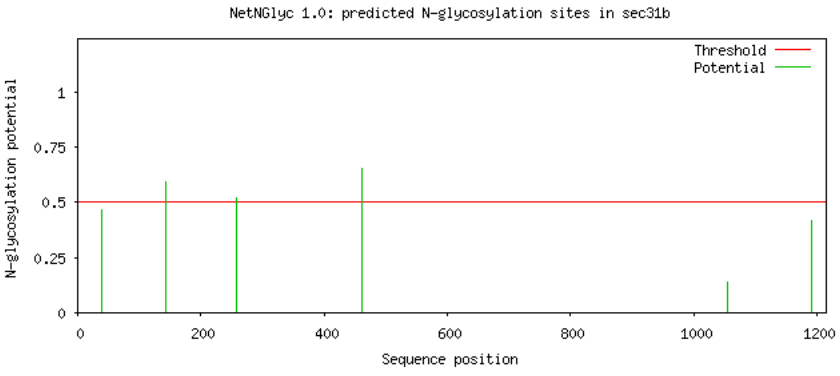

```
Output for 'rgra'

    Warning: This sequence may not contain a signal peptide!!


Name:  rgra    Length:  295
MATSYPLPEGFSEFDVFSLGSCLLVEGLLGIFLNSVTIVAFLKVRELRTPSNFLVFSLAMADIGISMNATIAAFSSFLRY      80
WPYGSEGCQTHGFHGFLTALASIHFIAAIAWDRYHQYCTRTKLQWSTAITLAVLVWIFTAFWAAMPLIGWGEYDYEPLRT     160
CCTLDISKGDRNYVSYVIPMSIFNMGIQVFVVMSSYQSIAQKFQKTGNPRFNASTPLKTLLFCWGPYGILAFYAAVADAN     240
LVSPKIRMIAPILAKTSPTFNPLLYALGNENYRGGIWQFLTGEKIHVPQDDNKSK
.............................................................N.............      80
................................................................................     160
................................................N...............................     240
................................................N...                                320

(Threshold=0.5)
--------------------------------------------------------------------------------
SeqName      Position  Potential    Jury    N-Glyc
                                  agreement result
--------------------------------------------------------------------------------
rgra          68 NATI   0.6149     (7/9)    +
rgra         212 NAST   0.5016     (5/9)    +
rgra         292 NKSK   0.5254     (5/9)    +
--------------------------------------------------------------------------------
```

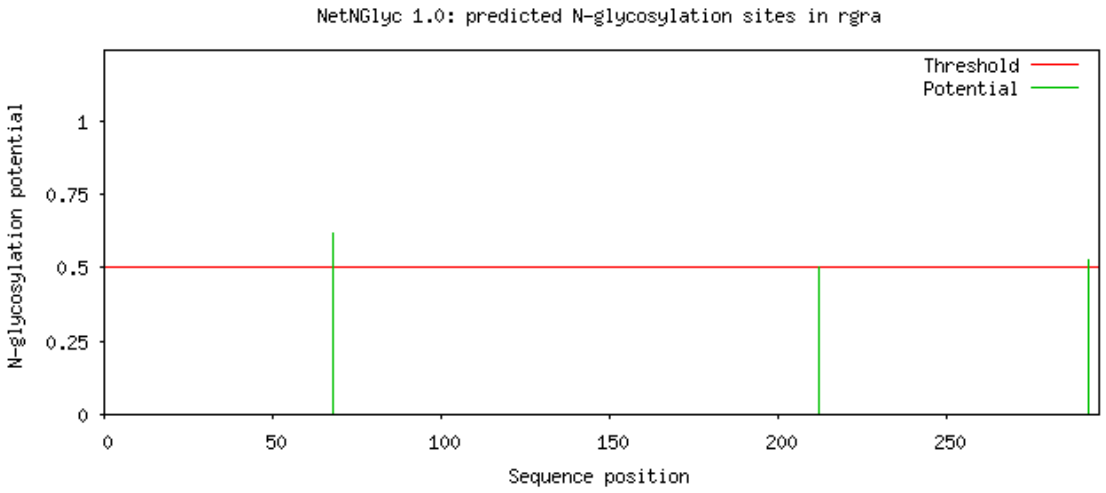

```
Output for 'H2LF05'

    Warning: This sequence may not contain a signal peptide!!

Name:  H2LF05  Length:  768
MATQSDLMELDMALGDSKAAVSQWQQQSYLDSGIQSGVTTTAPSLSGKGNPDIEEEDPTLYDWEFSQPFTPEPTDIEGYA      80
MTRAQRVRAAMFPETLEEGLQIPPTQLDAAHPTAVQRLAEPSQMLKHAVVNLINYQDDAELATRAIPELTKLLNDEDQVV     160
VNKAAVMVHQLSKKEASRHALMRSPQMVSAVVRAMQNTGDVETARCSAGTLHNLSHHREGLLAIFKSGGIPALVKMLGSP     240
VDSVLFYAITTLHNLLLHQEGAKMAVRLAGGLQKMVALLSNTNVKFLAITTDCLQILAYGNQESKLIILASGGPQALVNI     320
MRTFTYEKLLWTTSRVLKVLSVCSSNKPAIVEAGGMQALGLHLTDPSQRLVQNCLWTLRNLSDAATKQEGMEGLLGTLVQ     400
LLGSDDINVVTCAAGILSNLTCNNYSNKLMVCQVGGIEALVRTVLRAGDREDITEPAVCALRHLTSRHQDAEMAQNAVRL     480
HYGLPVVVKLLHPPSHWPLIKATVGLIRNLALCPANHSALREQGAIPRLVQLLVRAHQDTQRRTSMGGNQQQFVEGVRME     560
EIVEGCTGALHILARDVHNRIVIRGLNTIPLFVQLLYSPVENIQRVAAGVLCELAQDKEAAEAIEAEGATAPLTELLHSR     640
NEGVATYAAAVLFRMSEDKPQDYKKRLSVELTSSLFRTEPMAWNDTGDLGLDIGAQGDPLAYRPDDGAYRAYPANYGPDA     720
LLDPMMEGADYHTDALPDLGHHTDPLPDLGHTQDLMDSNQLAWFDTDL
................................................................................      80
................................................................................     160
.....................................................N..........................     240
................................................................................     320
.........................................................N......................     400
..................N....N........................................................     480
................................................................................     560
................................................................................     640
.............................................N..................................     720
...........................................                                    800

(Threshold=0.5)
--------------------------------------------------------------------------------
SeqName      Position  Potential    Jury    N-Glyc
                                  agreement result
--------------------------------------------------------------------------------
H2LF05       213 NLSH   0.6614     (8/9)    +
H2LF05       380 NLSD   0.5628     (7/9)    +
H2LF05       419 NLTC   0.7017     (9/9)    ++
H2LF05       424 NYSN   0.5476     (6/9)    +
H2LF05       516 NHSA   0.2399     (9/9)    ---
H2LF05       684 NDTG   0.5892     (8/9)    +
--------------------------------------------------------------------------------
```

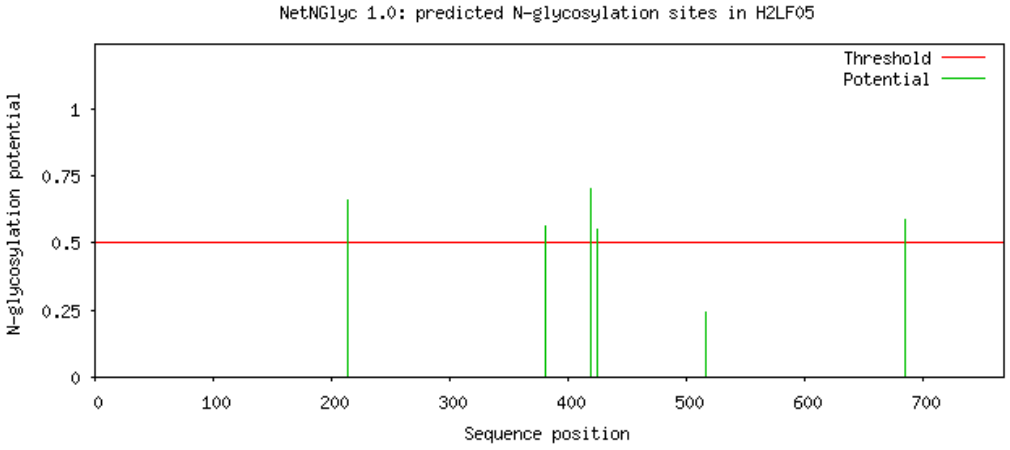

```
Output for 'H2L5M0'
Name:  H2L5MO  Length:  1869
MQSSVTPSLCLLGCILILALLPNSAQGQVSSPRRFRARILSPTKLDVAWKEPKGEFEGFKVSYIMNPGGRQKMVELSKQKT      80
NLLIEDFDSTKEYVFKITAVGGGRESKPLHGKLKAQRSTLESTQSQRGQSGSAIQENNEISEDMEGFMCKTPAIADIVIL     160
VDGSWSIGRINFRLVRTFLENLVRAFSVDFDKTRIGLAQYSGDPRIEWHLNTHSSKEAVIEAVKNLPYKGGNTLTGLALT     240
FILENSFKPESGSRPGVPKIGILITDGKSQDDVIPPAQSLKDAGIELFAIGVKNADENELKAIASPPEETHVYNVADFSV     320
MSDIVEGLTKGVCDRVDQLDKQIKGGGESAPPPDSLAPPRDLVIADITARSFRVTWTHATGQVEKYRVVYYPASGGQPEE     400
KVVQGTDNSVELNYLNSLTEYQVAVFAIYRSSASQALRGSATTLALPTVNNLELHDITHSTMRVRWRAAIGATGYMILYA     480
PLTEGESADEKEVKVADSVNEVELEGLSPDTEYTVTVYAMYGEEASDPMTSQETTLPLIPARNLRFSEVDHSSARLTWES     560
TSRLVRGYRVMYVKTNGVQTTEVDVGKVTTYLLKNLTSLTEYTVGVFAIYDEGEAEAVTESFTTKVVPDPLDLRSSDITA     640
ESFRVSWQHPATDVTLYRITWTPTDGGDSKDVLVDSNVNTYKITGLSPDSEYEVLLAAIYANEIESDEVILVENTAKRTT     720
TVATTSSKPSPRHGVRNMKIDDETTFSLRVSWQPVDSRNVRQYRLSYISMRGDRATETRTVPPAQNSIVLQPLLSDTEYK     800
ITLIPVYPDGDGPVASQVGRTLPLSAPKNLRVSEEWYNRFRISWDVPPSPTMGYRVVYQPLSAPGPALETFVGEDVNTML     880
IVNLLSGTEYSVKVIASYTTGSSEALSGRAKTLYLGVTNLSTYQVRMTSVCAQWLTHRHASAYRVVIQPLLGSQKQEIRL     960
GAGSNLHCFSNLKPNTEYKISVYAQLQDGTEGPAATATVKTLPVPTQAPTKPPATTPLPTIPSAKEVCRAAKADLVFLVD    1040
GSWSIGDDNFLKIIRFLYSTVGALDRIGPDGTQVAIAQFSDDARTEFKLNSYTNKERLLDAVNKISYKGGNTKTGRAIQH    1120
VKENIFTAEGGVRRGIPNVLVVLTDGRSQDDVNKVSKEMQMEGYIVFAIGFADADYGELVSIASKPSDRHVFFVDDLDAF    1200
QKIEEKLVTFVCEAATATCPSVPMSGSTTPGFRMMELFGLVEDRYNSIYGVSMVPGTFNAFPSFHLHSNALLAQPTRFIH    1280
PEGLPSDYTVSLLFRLLHDTPEEPFALWEILNNNNEPLAGVILDNGGKTLTFFNNDYKGDFQTVTFEGPEIKKLFFGSFH    1360
KLHVAISKTSAKVFVDCKMVSERAINAAGNITTDGLEVLGRMVRSRGNKDNSAPFQLQNFDIVCSTSWASRDKCCELPGL    1440
RKEAECPALPKACTCTQDSKGPPGPPGVPGGPGIRGARGDRGEPGPVGPAGAVGDMGVPGPQGPPGPQGPSGRSIIGPPG    1520
SPGERGQKGDPGQQGQQGIPGRPGAPGREGPPGPRGLVGKDGPQGRQGPPGSMGTPGAPGSPGSTGPPGKQGELGPPGSP    1600
GSRGEKGDRGDVQSTASVQAIARQVCEQLIQSHMARYNTLLTQVPSPPVSIRTVPGPPGEPGRQGSPGPQGEQGPPGRPG    1680
FPGQNGQNGNPGERGQPGEKGEKGSQGVGVQGPRGPPGPPGAAGQGRPGSQGQSGRPGNPGAPGRPGVPGPVGPPGPQGY    1760
CDQNSCVGYNVGEGEDVTDRGAVSAVQLPPNVFQNYGEVEEDDPYRYYQPNYPAPQPVSPEDPSLAYGDIELRSPGVHRS    1840
SRSVGSEGEKVGPKRRRKSRAKELPGLTN                                                        1869
```

```
(Threshold=0.5)
--------------------------------------------------------------------------------
SeqName      Position  Potential    Jury    N-Glyc
                                  agreement result
--------------------------------------------------------------------------------
H2L5MO        595 NLTS   0.6919     (9/9)   ++
H2L5MO        919 NLST   0.6021     (7/9)   +
H2L5MO       1390 NITT   0.6247     (9/9)   ++
--------------------------------------------------------------------------------
```

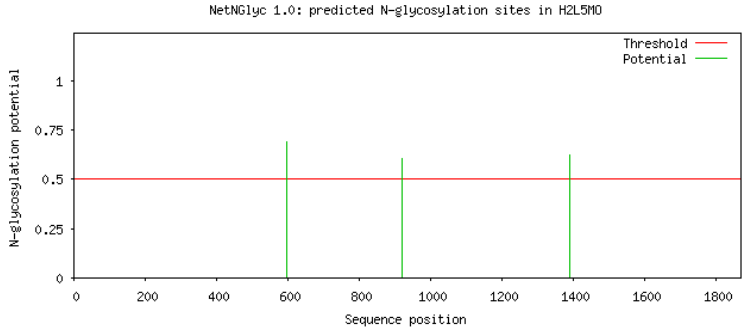

Output for 'H2LQV4'

Warning: This sequence may not contain a signal peptide!!

Name: H2LQV4 Length: 794

```
MMYVIKRDGRQERVMFDKITSRIQKLCYGLNSEFVDPAQITMKVIQGLYSGVTTVELDTLAAEIAATLTTKYPDYAILAA      80
RIAVSNLHKETKKVFSEVMEDLYSYVNPLNKCHSPMISKETLDIVLENKDRLNSAIIFDRDFSYNFFGFKTLERSYLLKI     160
NGKVAERPQHMLMRVAVGIHGRNIDAAIETYNLLSEKWFTHASPTLFNAGTNRPQLSSCFLLAMKDDSIEGIYDTLKQCA     240
LISKSAGGIGVAVSCIRSTGSYIAGTNGNSNGLVPMLRVYNNTARYVDQGGNKRPGAFAMYLEPWHFDVFDFLELKKNTG     320
KEEQRARDLFYALWIPDLFMKRVESNQDWSLMCPNECPGLDECWGVEFEELYTKYEREGRVKRVVKAQQLWHAVIESQTE     400
TGTPYMLYKDACNKKSNQQNLGTIKCSNLCTEIVEYTSHDEVAVCNLASIALNMYVTPERTFDFKKLASVTKVIVKNLNK     480
IIDINYYPVPEAEKSNKRHRPIGIGVQGLADAFILMRYPFESPEAQLLNIQIFETIYYAALEASCELAAELGPYETYDGC     560
PVSRGVLQYDMWEKTPTDLWDWKLLKEKIAKHGVRNSLLLAPMPTASTAQILGNNESIEPYTSNIYTRRVLSGEFQIVNP     640
HLLKDLTERGLWSEEMKNKLIGNNGSIQDIAEIPNDLKQLYKTVWEISQKTVLKMAADRGAFIDQSQSLNIHIAEPNYGK     720
LTSMHFYGWKQGLKTGMYYLRTKPAANPIQFTLNKEKLKEGQSSKMPEQDAKERNTAAMVCSLENRDDCLMCGS
.....................................................................................      80
.....................................................................................     160
.....................................................................................     240
.....................................N...............................................     320
.....................................................................................     400
.....................................................................................     480
.....................................................................................     560
.....................................................................................     640
.....................N...............................................................     720
.....................................................................                 800
```

(Threshold=0.5)

SeqName	Position	Potential	Jury agreement	N-Glyc result
H2LQV4	281 NNTA	0.6146	(8/9)	+
H2LQV4	615 NESI	0.4014	(9/9)	--
H2LQV4	664 NGSI	0.5713	(7/9)	+

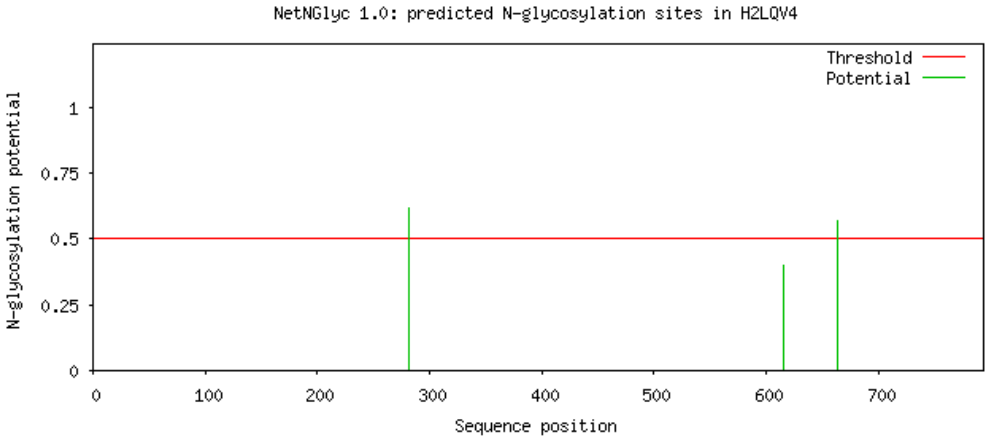

Output for 'A0A3B3HRI9'

Warning: This sequence may not contain a signal peptide!!

Name: A0A3B3HRI9 Length: 120

```
MVHLQTNSKSVKLHFNFERCALSEADLEDFFSLVSHSQGGRLDEQRCVLNVSPQTTTKHQLDSEQFFSLLSNVQSRRLDD      80
QRISLPSLPGIQNGDESWCPAPSLAPQPSWQPERDNRCLI
................................................................................      80
........................................                                              160
```

(Threshold=0.5)

No sites predicted in this sequence.

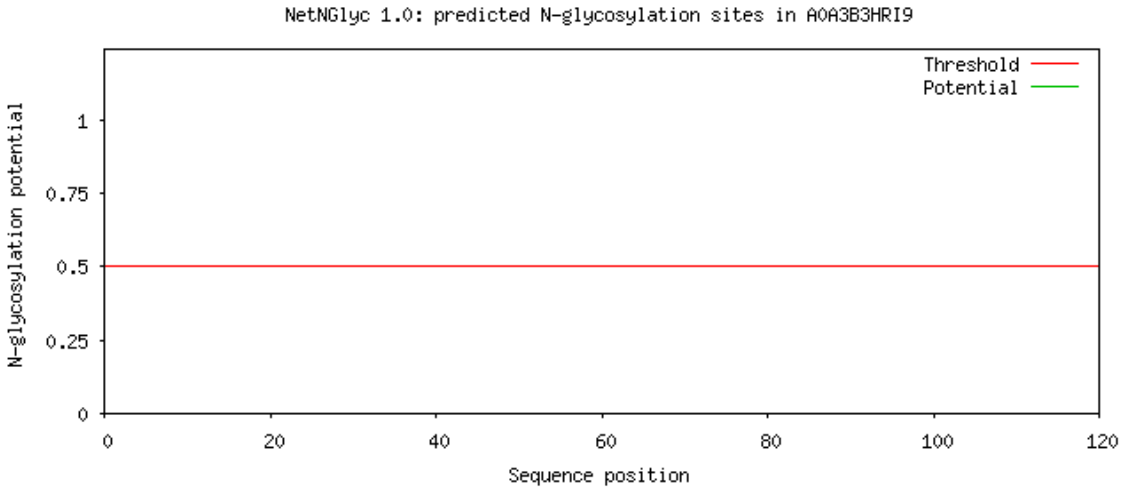

Output for 'H2MGV2'

Warning: This sequence may not contain a signal peptide!!

Name: H2MGV2 Length: 428

```
MDEQPRMMLSHTPGMAAHAGLPQHVHEGGTAPDGDARKQELGEILQQIMTITDQSLDEAQARKHGLNCHRMKPALFNVLC      80
EIKEKTVLSIRGAQEEEPLDPQLMRLDNMLLAEGVSGPDKGGGSVAAAAAAAASGGVGADNSAEHSDYRAKLSQIRQIYH     160
TELEKYEQACNEFTTHVMNLLREQSRTRPISPKEIERMVNIIHRKFSSIQMQLKQSTCEAVMILRSRFLDARRKRRNFNK     240
QATEILNEYFYSHLSNPYPSEEAKEELAKKCSITVAQVSNWFGNKRIRYKKNIGKFQEEANMYAARTAVNAANASSHGSQ     320
ANSPSTPNSAGSAASFNVSNSGDLFMSVHALNGDSFQGAQVGANVQSQVDTLRHVISQTGAFSEGVVASHMYSPQGINAN     400
GGWQDAPTPSSVTSPTEGPGSVHSDTSN
.....................................................................................      80
.....................................................................................     160
.....................................................................................     240
.....................................................................................     320
.....................................................................................     400
.............................                                                              480
```

(Threshold=0.5)

No sites predicted in this sequence.

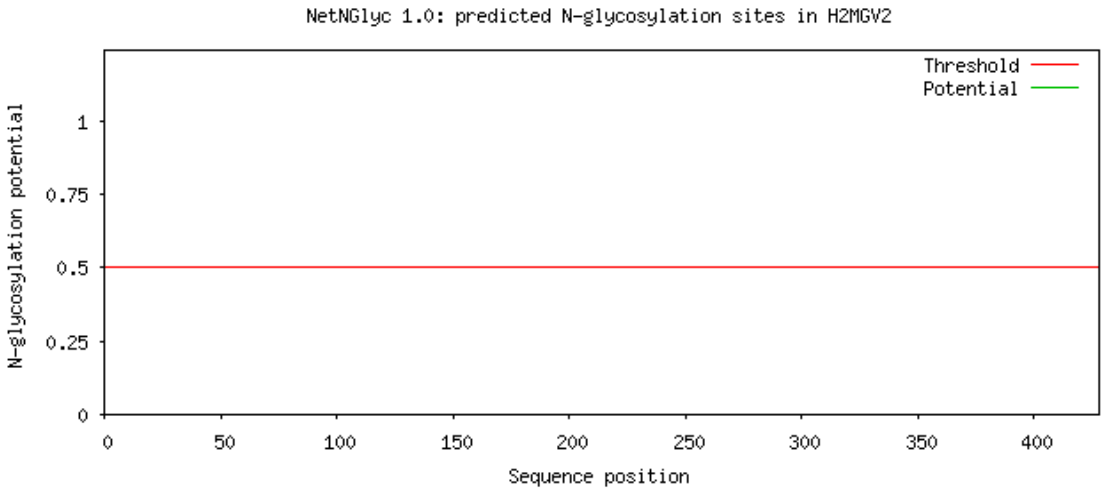

```
Output for 'rom1a'

    Warning: This sequence may not contain a signal peptide!!

Name:  rom1a   Length:  348
MVVMKMKFPFQKRVKLAQGLWLLSWCATVAGATTFTLGCLLKTELLRRAEVMDNADIHIVPNTLMIVGLASLGINYFASK      80
ICQDALDAGRFPRWKNFLKPYFAVSCFFTVLMLLSVIMSYAMKGSLESSLKAGLRNGIRFYKDTDTPGRCFQKQNIDRLQ     160
MEFECCGNNDFRDWFEVQWISNRYLDFSSKEVKDRVKSNVDGRYLVDGVPFSCCNPRSPRPCIQYQLTNNSAHYNYDYLT     240
EELNIYLRGCREALVHYYMGLMNTIGAGVLSIFILQGSVLVSLRFLQTAMEAVAGKENTEIETEGYLLEKGVKDTIMEYL     320
DPVLKFFLLKNGGKVEEGDAAEKPPAVP
.....                                                                                  80
.....                                                                                 160
.....                                                                                 240
.....                                                                                 320
.....                                                                                 400

(Threshold=0.5)

No sites predicted in this sequence.
```

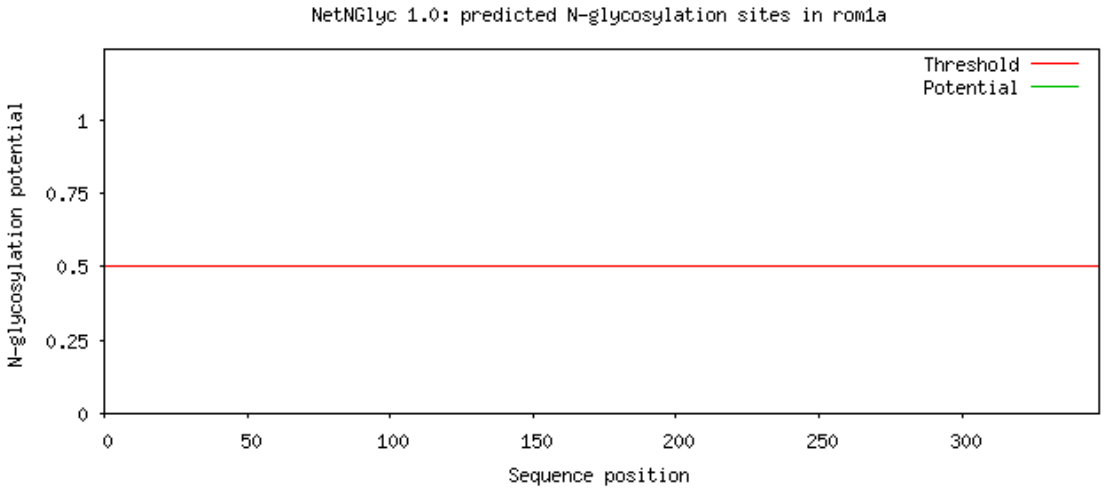

Output for 'A0A3B3HBQ8'

Warning: This sequence may not contain a signal peptide!!

Name: A0A3B3HBQ8 Length: 193

```
MSAIRKKLVIVGDGACGKTCLLIVFSKDQFPEVYVPTVFENYVADIEVDGRQVELALWDTAGQEDYDRLRPLSYPDTDVI      80
LMCFSVDSPDSLENIPEKWTPEVKHFCPNVPIILVGNKKDLRHDEHARRELAKMKQEPVKFEDGREMANRISAYGYQECS     160
AKTKDGVREVFEMATRAALQAKRNRKKAACILL
................................................................................      80
................................................................................     160
................................                                                     240
```

(Threshold=0.5)

No sites predicted in this sequence.

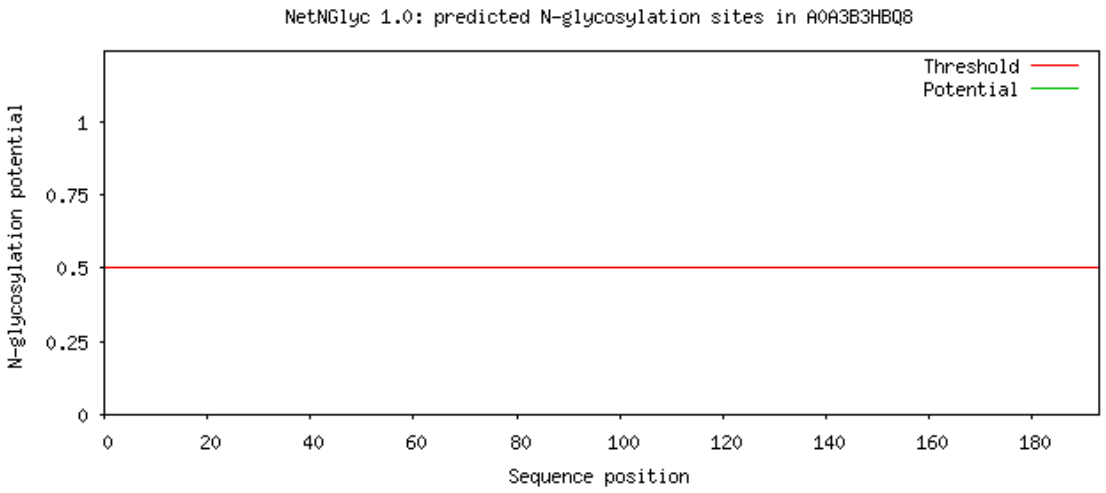

```
Output for 'A0A3B3H6H3'

    Warning: This sequence may not contain a signal peptide!!


Name:  A0A3B3H6H3      Length:  539
MADGRQPDEHWTANGQENGENGYSSYSYRENGYHGGAAAGTTADDSANLPPSPPPSPSAEQTGPVAQEGKVEVVRQPHDE      80
KAGANQEEVESEQPGNSLLKERDSLTQSQDLGFKQAQIPDIFNGGSHAHSPSNQGGEHHHPLSVAQQPRERPTSPTRAVL     160
LKMAAQRGGGSLRPSSACSLKRSPLVEAELRQPRPNSACSQPPPHSGKWAGRGKERTYRSPEKRSSLPRPAKSLTRHIPA     240
SEQEDNGTPSRPTSIRTEPRGDNRSGRASSVAGTDSARSRSARSGASTPGAVTPGTPPSYSCRTPGSRTPGSHTPKSFSV     320
LQEKKVAVIRTPPKSPSSVQRQLKVINQPLPDLKNVKSKIGSTSNLKHQPKGGQVMIPSVKLDFSHVQAKCGSLDKVNYT     400
ASGGNVQIQSKKIDLSHITSKCGSMSNIHHRPGGGNVRIENVKLDFKDKAHAKVGSLDNATHTPGGGNIVIESHKLSFRE     480
TAKARVDHGAEIIITHSPGMETGGTSPRLSSAGSINMMDSPQLSTLAQDVTAALAKQGL
.....................................................................................      80
.....................................................................................     160
.....................................................................................     240
.....................N...............................................................     320
.....................................................................................     400
.....................................................N...............................     480
.....................................................                                  560

(Threshold=0.5)
--------------------------------------------------------------------------------
SeqName      Position  Potential    Jury    N-Glyc
                                   agreement result
--------------------------------------------------------------------------------
A0A3B3H6H3   246 NGTP   0.1888     (9/9)   ---
A0A3B3H6H3   263 NRSG   0.5692     (8/9)   +
A0A3B3H6H3   398 NYTA   0.5993     (6/9)   +
A0A3B3H6H3   459 NATH   0.6257     (8/9)   +
--------------------------------------------------------------------------------
```

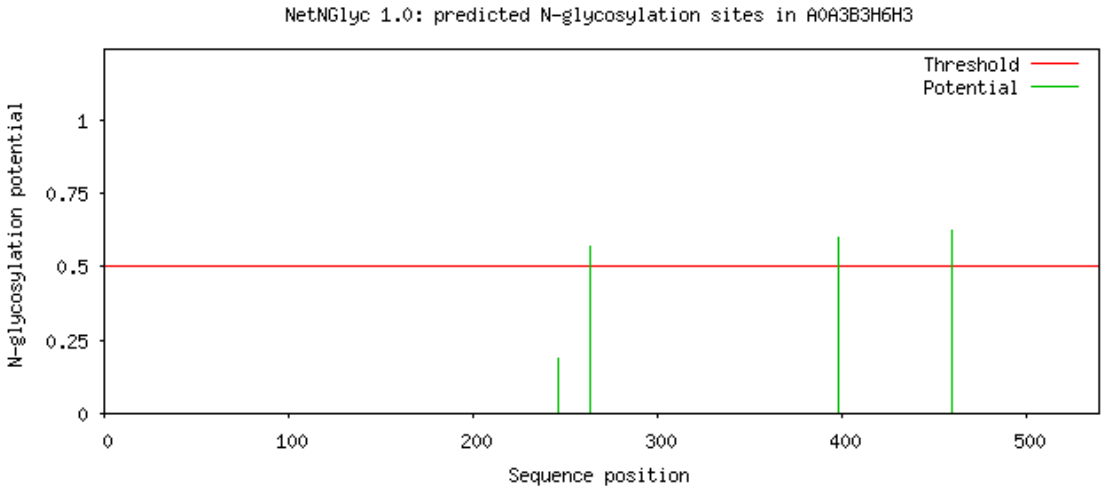

```
Output for 'kfharr-r2'

    Warning: This sequence may not contain a signal peptide!!


Name:  kfharr-r2       Length:  399
MSPKNVIFKKTCKDKSVGVFMGKRDFVDRVDSVDPVDGVILIDPEVLAGRKVFVTLSCTFRYGRDDMDVMGIAFRRELYL      80
VTRQVYPPMQDRDKTVHTRVQAKLLRKLGNNAYPFFFEFPDNLPCSVALQPAPNDVGKQCAVEFEIKAFSAESQDAKVRK     160
RSTVKLMIRKVQYAPESQEVAPSVEITKDFVMSDKPLHVQATLDKELYYHGEPIKVHVNVTNNSNKNIKNIIVSVDQVAT     240
VVLFSNDSYTKCVDYEDNGDSVSAGATLKKVYTLLPLLANNRERRGIALDGKLKHEDTNLASSSVVKEGVLKEVMGIMVS     320
YRVMVKLIVGGMMGSSEVGLEVPFRLMHPKPDAVRESEMEDEMVFEEFKRSYLRGIIAGDDDDEEGNVSGGDDITPKEK
.................................................................................      80
.................................................................................     160
.....................................................N...........................     240
.................................................................................     320
.....................................................................N...........     400

(Threshold=0.5)
--------------------------------------------------------------------------------
SeqName      Position  Potential    Jury    N-Glyc
                                  agreement result
--------------------------------------------------------------------------------
kfharr-r2    219 NVTN    0.6914     (9/9)    ++
kfharr-r2    222 NNSN    0.2656     (9/9)    ---
kfharr-r2    246 NDSY    0.4377     (5/9)    -
kfharr-r2    387 NVSG    0.5437     (7/9)    +
--------------------------------------------------------------------------------
```

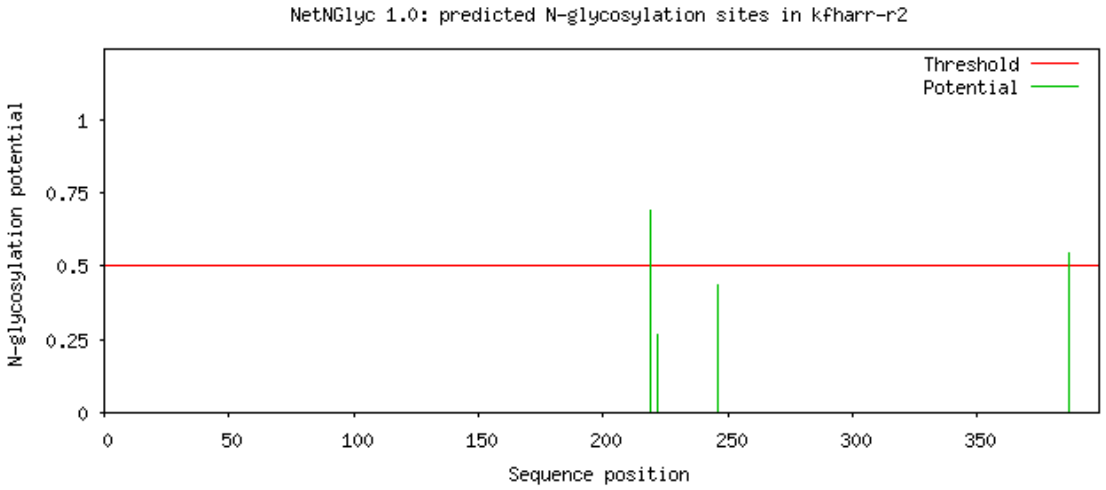

```
Output for 'A0A3B3HP81'

    Warning: This sequence may not contain a signal peptide!!

Name:  A0A3B3HP81      Length:  514
MPALCLTGGVTMESGGAISTAELCSSGRFLCRSSTSAAGFAIMVSVCIHELERFKNDLTSPTPFQRECISIHIGQAGVQM      80
GNACWELYCLEHGIQPDGQMPSDKTISGGDDSFNTFFSETGAGKHVPRAVFVDLEPSVVDEVRTGTYRQLFHPEQLITGK     160
EDAANNYARGHYTIGKEIIDLVLDRIRKLADQCTGLQGFLIFHSFGGGTGSGFTSLLMERLSVDYGKKSKLEFAVYPAPQ     240
VSTAVVEPYNSILTTHTTLEHSDCAFMVDNEAIYDLCRRNLDIERPSYTNLNRLIGQIVSSITASLRFDGALNVDLTEFQ     320
TNLVPYPRIHFPLVTYAPVISAEKAYHEQLSVAEITNACFEPANQMVKCDPRHGKYMACCLLYRGDVVPKEVNAAIATIK     400
TKRSIQFVDWCPTGFKVGINYQPPTVVPGGDLAKVQRAVCMLSNTTAIAEAWARLDHKFDLMYAKRAFVHWYVGEGMEEG     480
EFSEAREDMAALEKDYEEVGTDSVGEGEEEGAEQ
.....................................................................................      80
.....................................................................................     160
.....................................................................................     240
.....................................................................................     320
.....................................................................................     400
.........................................N.......................................     480
.................................                                                      560

(Threshold=0.5)
-------------------------------------------------------------------------
SeqName      Position  Potential    Jury    N-Glyc
                                  agreement result
-------------------------------------------------------------------------
A0A3B3HP81   444 NTTA   0.5944     (8/9)   +
-------------------------------------------------------------------------
```

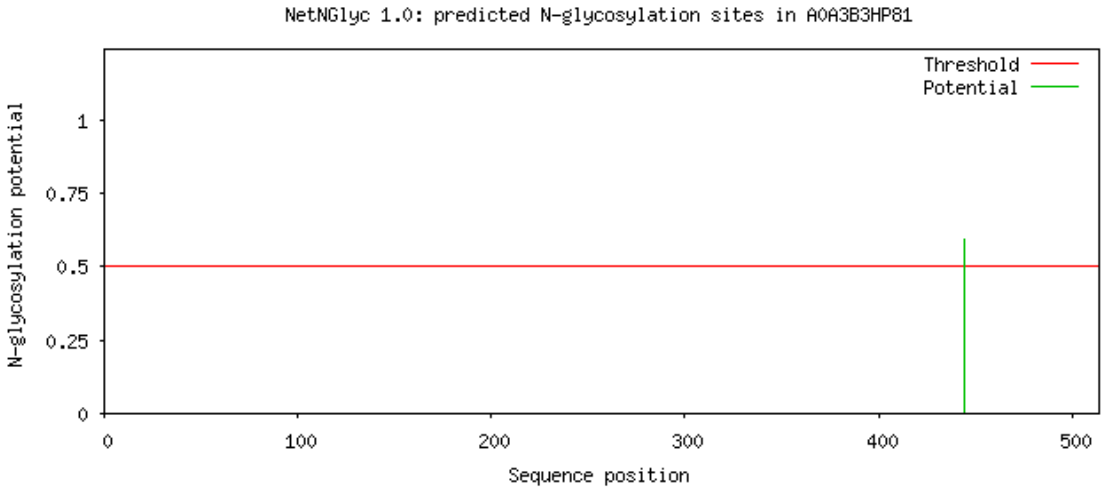

```
Output for 'A0A3B3HW25'

    Warning: This sequence may not contain a signal peptide!!

Name:  A0A3B3HW25      Length:  707
MSAAKSVSIGIDLGTTYSCVGVFQHGKVEIIANDQGNRTTPSYVAFTDTERLIGDAAKNQVALNPSNTVFDAKRLIGRRF      80
DEPVVQADMKHWPFKVVSEGGKPKIQVDYKGENKTFFPEEISSMVLVKMKEIAEAYLGHKVSNAVITVPAYFNDSQRQAT     160
KDAGVIAGLNVQRIINEPTAAAIAYGLDKGKSGERNVLIFDLGGGTFDVSILTIEDGIFEVKATAGDTHLGGEDFDNRMV     240
NHFVEEFKRKHKKDISQNKRALRRLRTACERAKRTLSSSSQASIEIDSLFEGIDFYTSVTRARFEELCSDLFRGTLEPVE     320
KALRDAKMDKGQIHDVVLVGGSTRIPKIQKLLQDFFNGRELNKSINPDEAVAYGAAVQAAILSGDTSGNVQDLLLLDVAP     400
LSLGIETAGGVMTALIKRNTTIPTKQTQVFSTYADNQPGVLIQVYEGERAMTKDNNLLGKFDLTGIPPAPRGVPQIEVTF     480
DIDANGILNVSAVDKSTGKENKITITNDKGRLSKEDIERMVQEAEKYKAEDEQQRDKIAAKNSLESLAFNLKSSAQDDSL     560
KDKISQEDRKRAMVSSHFSTTLFLSSWLILSFKLSSCALLFRLKAKDSREFLAAILSLCCSSSALYFSASCTILSMSSLL     640
RRPLSLVMVILFSLPVLLSTADTFKMPLASMSKVTSICGTPRGAGGIPVRSNLPSRLLSLVMALSPS
.....................................N.........................N.................      80
................................N.....................................N.......     160
................................................................................     240
................................................................................     320
.........................................N......................................     400
..................N.............................................................     480
........N.....................................................................     560
................................................................................     640
.............................................................                  720

(Threshold=0.5)
--------------------------------------------------------------------------------
SeqName      Position  Potential    Jury    N-Glyc
                                  agreement result
--------------------------------------------------------------------------------
A0A3B3HW25     37 NRTT    0.6446     (8/9)    +
A0A3B3HW25     64 NPSN    0.7742     (9/9)    +++  WARNING: PRO-X1.
A0A3B3HW25    113 NKTF    0.7459     (9/9)    ++
A0A3B3HW25    153 NDSQ    0.5940     (8/9)    +
A0A3B3HW25    362 NKSI    0.5942     (8/9)    +
A0A3B3HW25    419 NTTI    0.5660     (8/9)    +
A0A3B3HW25    489 NVSA    0.7491     (9/9)    ++
--------------------------------------------------------------------------------
```

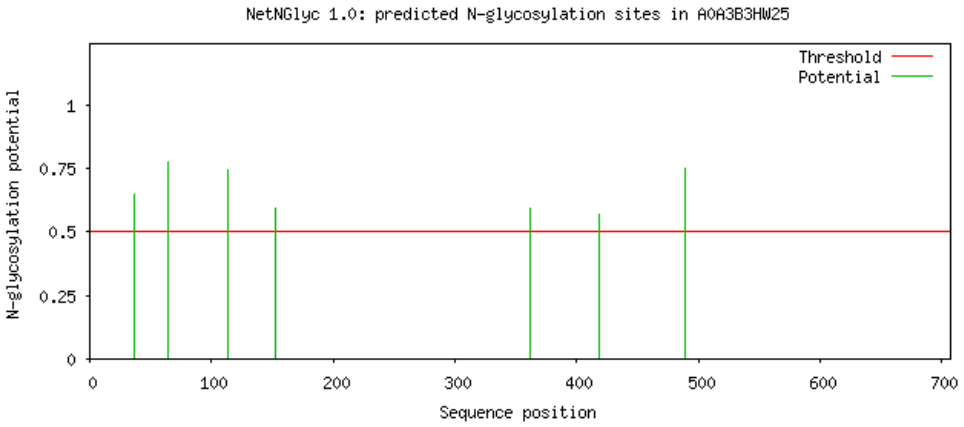

```
Output for 'A0A3B3ID86'

    Warning: This sequence may not contain a signal peptide!!

Name:  A0A3B3ID86      Length:  604
MFSVSIGIDLGTTYSCVGVFQHGKVEIIANDQGNRTTPSYVAFTDTERLIGDAAKNQVALNPSNTVFDAKRLIGRRFDEP      80
VVQADMKHWPFKVMKEIAEAYLGHKVSNAVITVPAYFNDSQRQATKDAGVIAGLNVQRIINEPTAAAIAYGLDKGKSGER     160
NVLIFDLGGGTFDVSILTIEDGIFEVKATAGDTHLGGEDFDNRMVNHFVEEFKRKHKKDISQNKRALRRLRTACERAKRT     240
LSSSSQASIEIDSLFEGIDFYTSVTRARFEELCSDLFRGTLEPVEKALRDAKMDKGQIHDVVLVGGSTRIPKIQKLLQDF     320
FNGRELNKSINPDEAVAYGAAVQAAILSGDTSGNVQDLLLLDVLPLSLGIETAGGVMTALIKRNTTIPTKQTQVFSTYAD     400
NQPGVLIQVYEGERAMTKDNNLLGKFDLTGIPPAPRGVPQIEVTFDIDANGILNVSAVDKSTGKENKITITNDKGRLSKE     480
DIERMVQEAEKYKAEDEQQRDKIAAKNSLESLAFNLKSSAQDDSLKDKISQEDRKRVVEKCDETIAWLENNQLADKDEFQ     560
HKQKELEKVCNPIISKLYQGGMPSGSCREQARADSQGPTIEEVD
.................................N.........................N..................      80
.....................................N.........................................     160
................................................................................     240
................................................................................     320
......N.....................................................N.................     400
.....................................................N..........................     480
................................................................................     560
.....................................                                          640

(Threshold=0.5)
--------------------------------------------------------------------------------
SeqName      Position  Potential    Jury    N-Glyc
                                agreement result
--------------------------------------------------------------------------------
A0A3B3ID86     34 NRTT    0.6464      (8/9)    +
A0A3B3ID86     61 NPSN    0.7749      (9/9)    +++  WARNING: PRO-X1.
A0A3B3ID86    118 NDSQ    0.6009      (8/9)    +
A0A3B3ID86    327 NKSI    0.5921      (8/9)    +
A0A3B3ID86    384 NTTI    0.5612      (8/9)    +
A0A3B3ID86    454 NVSA    0.7449      (9/9)    ++
--------------------------------------------------------------------------------
```

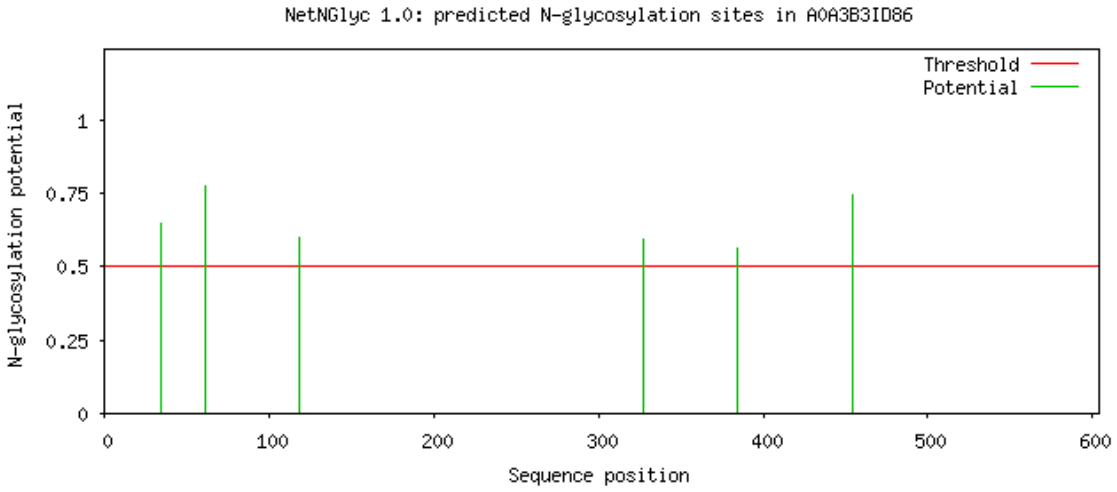

```
Output for 'H2M5C0'
Name:  H2M5C0  Length:  651
MARHWSITVFSALALLCSFLGTEVDAQKGNPQDPKVPYPPYYPQPKPQDPQHVSPPYYPGKPQNPPQKPSNPQYPSYPQT      80
PQNPQVPQNPQVPQNPQYPSYPQNPSYPQNPSYPQNPKLFQDGKPSNPQQPQVPQYPSKPQPPQNPQVPQYPSKPQPPQN     160
PQVPQYPSKPQPPQNPQVPQYPSKPQPPQNPQVPQYPSKPQPPQNPQVPQYPSKPQPPQNPQVPQYPSKPQPPQNPQVPQ     240
YPSKPQNPQYPSKPQYPQAPQQPQNPQYPSKPQDPGKNPNTPPIGPPPPKSCEVPRDVRVPCGVPDISPSACDAIDCCHD     320
GQSCYFGTGATVQCTKDGHFIVVVAKDVTLPHIDLETISLLGQGQDCGPADSNSAFAIYYFPVTYCGTVVMEEPGVIVYE     400
NRMTSSYEVGVGPLGAITRDSSFELLFQCRYRATSVETLVVEVQPPDSPLSIAELGPLNVYLQIANGQCQTKGCDEAAAA     480
YTSFYTDADYPVTKVLRDPVYVDVQILGRTDPNLVLTLGRCWATTSPNAFSLPQWDILIDGCPYADDRYLSALVPIDHSS     560
GLPFPTHHSRFLFKMFTFVDPHSMEPLREKVYIHCSTAACVPGQGVSCEPSCSRRKGRDTEAVAIRTDERRVVVSSGEVL     640
MLAAADEPSEQ
.....                                                                                  80
.....N.....N.....                                                                     160
.....                                                                                  240
.....                                                                                  320
.....                                                                                  400
.....                                                                                  480
.....                                                                                  560
.....                                                                                  640
.....                                                                                  720

(Threshold=0.5)
--------------------------------------------------------------------------------
SeqName      Position  Potential    Jury    N-Glyc
                                  agreement result
--------------------------------------------------------------------------------
H2M5C0       104 NPSY   0.5399     (6/9)   +     WARNING: PRO-X1.
H2M5C0       110 NPSY   0.5240     (6/9)   +     WARNING: PRO-X1.
--------------------------------------------------------------------------------
```

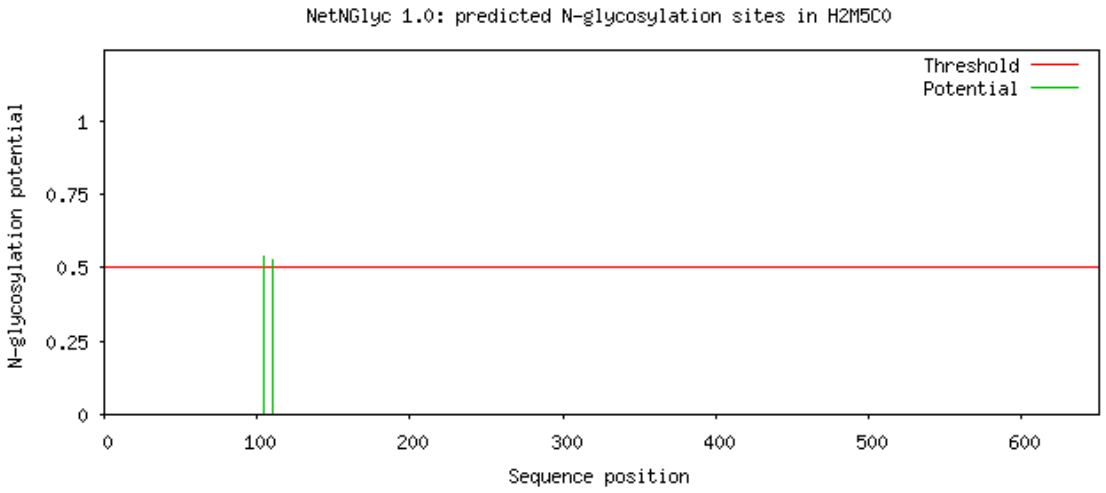

```
Output for 'A0A3B3HCP5'
Name:  A0A3B3HCP5      Length:  1434
MGPLLYLFLCGLLCIRTEASRLRQEDSPPRIVEHPSDLIVSKGEPATLNCKAEGRPIPSVEWYKDGERVETDRDNPRSHR      80
MLLPSGSLFFLRIVHGRRSKPDDGNYVCVARNYMGEAVSRNASLEVALLRDDFRQNPQDVVVAVGETATFECQPPRGHPE     160
PVTFWRKDKTRLDLSDDRITVRGGKLTISNTKKSDSGIFVCVASNMVGERESEKAQLSVFEKPSFVQRPVNQVVLVDESV     240
EFRCQVHGDPPPVLRWKKEDVDIPRGRYEIRYEKEDFLLRIKKASVSDQGTFTCSAENRVGKTEASAYLTIREAPQFVVR     320
PRDQIVAQGRTATFPCETRGKPQPTVFWQREGSKDLLFPNQSAQGDSRVSVSVNGELTISSVQRSDAGYYICQALTVAGS     400
IMAKAQLEVADALKDRPPPIIRQGPSNQTQALGAVSVFRCQASGDPEPTVTWRKNGANLLGKDPRFSVLEHGSLQIQNSR     480
LSDAGLYTCVATSSSGETSWSAYLDVRGLFHWKQIKSNILLVYSTSHCLVFFAFYNVISICLASPDSMDPIDFVFHNSTT     560
LPGPPSKPEVTNVTKSSISLSWEPGPEAGSPVSSYVIEAFGQSVSNSWQTVADHVKTTEFTVTDLRPKTVYLFIIRAVNA     640
QGLGDPSPMSDPVRTQDISPTGQGVDHRRVQKELGDVVVTMHNPVVLSSTSVQVTWAVENPSQFIQGYRVLYRQTSGLPS     720
PGPWQIQDLRVASERDITLSDLKKGIVYEIKVRPYFNEFQGADSESMTTRTMEEAPSAPPQQVTVLTVGSHNSTSISVSW     800
DPPPPEQQNGIIQEYKIWCLANDTRFHVNKSVDATIRSVVVGGLQTGVHYSVEVAASTSAGVGAKSKPQLIILGAELKDV     880
MTGSESNNSISDVVKQPAFIAGLGGACWIVLMGFSAWLYWRRKKRKGLSNYAVQSFTFTRAVTFQRDRGLIRNGSRPGLL     960
KAGDPGLPWLADSWPSTSLPANGGMGSPKGGSNFGRGDVLPSAAVEKTGTMLSDGAIYSSIDFMGKGGYSSPARGSQPTP    1040
YATTQILQSNSFHELAVDRPDARWKASLQAQQEMANMGYSLTDRRPGGGSKVGKKKKVKGATKTTKSNGTCWANIPLPPP    1120
PMHPLPGTEVNLDRYLQENHTGGYDNNSWAPAMSVHTYHHQNLDSEEDRERGPTPPLRGKSSSPAGASFSQPSASSLSSA    1200
HHEEMQSILQAHLDELTRAYQYEVAKQAWHLKSSPSVSGTPIDFMSSTLGSDLGATLLSEEDEEEDEEREDDRYAVVSKN    1280
VCGFDYTPGHSMDSLDGSGKTTYSDGFGAADRAGQGTHSLGHKRAPLTGHKPQTDKVGTLPRRRDTNTDAHTTAVKPLNS    1360
MGSHMHSSWATAASDQSEECMVTVSTLERQHMASWSGTTSSGRATMNMGSQKRPGTDFSHNGHHSTHGTEKREH
.....................................................................................      80
.....................................N...............................................     160
.....................................................................................     240
.....................................................................................     320
.....................................N...............................................     400
.......................N.............................................................     480
.....................................................................................     560
..........N..........................................................................     640
.....................................................N...............................     720
.....................................................................................     800
....................N.....N..........................................................     880
.....................................................................................     960
.....................................................................................    1040
.....................................................N...............................    1120
................N....................................................................    1200
.....................................................................................    1280
.....................................................................................    1360
.....................................................................                    1440

(Threshold=0.5)
--------------------------------------------------------------------------------
SeqName      Position  Potential    Jury    N-Glyc
                                agreement result
--------------------------------------------------------------------------------
A0A3B3HCP5    121 NASL    0.5909      (6/9)    +
A0A3B3HCP5    360 NQSA    0.5982      (6/9)    +
A0A3B3HCP5    427 NQTQ    0.7017      (9/9)    ++
A0A3B3HCP5    557 NSTT    0.5214      (6/9)    +
A0A3B3HCP5    572 NVTK    0.7283      (9/9)    ++
A0A3B3HCP5    700 NPSQ    0.5101      (3/9)    +     WARNING: PRO-X1.
A0A3B3HCP5    792 NSTS    0.6483      (8/9)    +
A0A3B3HCP5    822 NDTR    0.5163      (4/9)    +
A0A3B3HCP5    829 NKSV    0.6751      (9/9)    ++
A0A3B3HCP5    887 NNSI    0.4071      (7/9)    -
A0A3B3HCP5    953 NGSR    0.6200      (9/9)    ++
A0A3B3HCP5   1108 NGTC    0.5591      (5/9)    +
A0A3B3HCP5   1139 NHTG    0.5319      (6/9)    +
A0A3B3HCP5   1146 NNSW    0.4739      (7/9)    -
--------------------------------------------------------------------------------
```

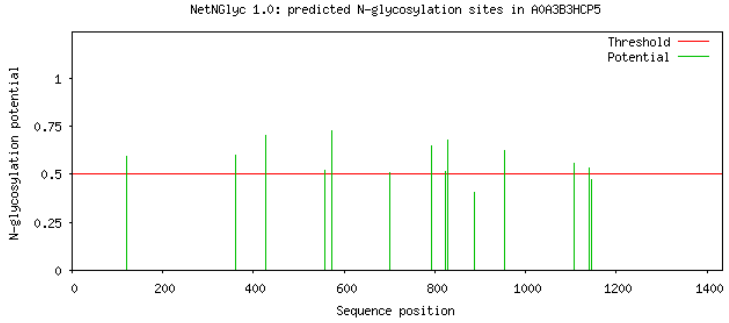

```
Output for 'H2MD32'
Name:  H2MD32  Length:  603
MKLKLLLLCLFLAALFCKAEPKKKDKNGHDNEEVHGQRGRHGNHGRHGNHSRHGMKKIKRMKYEDIIKDVFFVAENTGDD      80
EEDDDQGNQDWLFDLQDPDGKCNPNPCLNEGVCKEKGKRNYKCDCPKPFKGRRCQKGPKICRMGLCGHGECVLTSASPFY     160
ECKCKEPFQPPNCRRLSVCEPNPCRNGGKCIMDGNNFDCVCPEGFSGRFCRVGPNDCYLDDGESYRGNVSETDDGDDCLH     240
WNSHFILAHGVNPFKSFEDKDGLGPHNFCRNPDGEPKPWCFFRRGRRLLWDYCDVTPCPQPTTVGPTGVPPSPQPTSAKP     320
LFTTLPPRPSAGPASPTEAAASQFLTCGVPQPKKAITRIFGGLKVSPGAIPWQVSLQQKPKNSNLPYRHVCGGVLIKSCW     400
VLTAGHCIDKSKDMQVLMGSLSLDKTDPSAQTLPVENAIVHQRYRETSGAVYNDIALLRLRGTRGLCANETQFVKTACLP     480
DAQLPDGMECTISGWGATEESQYGSSHLLEANVLLINQGKCSEPAIYGSKLDSTMFCAGHLQGGVDSCQGDSGGPLTCKN     560
NNSSVIYGLVSWGDQCGKQNSPGVYTRVTHYLDWIKSTIQSNP
.............................................N..............................      80
.............................................................................     160
.....................................................................N.......     240
.............................................................................     320
.............................................................................     400
.....................................................................N.......     480
.............................................................................     560
.N...................................                                         640

(Threshold=0.5)
-------------------------------------------------------------------------
SeqName      Position  Potential    Jury    N-Glyc
                                agreement result
-------------------------------------------------------------------------
H2MD32         49 NHSR   0.5568     (8/9)   +
H2MD32        228 NVSE   0.7453     (9/9)   ++
H2MD32        469 NETQ   0.6888     (9/9)   ++
H2MD32        561 NNSS   0.4000     (7/9)   -
H2MD32        562 NSSV   0.5419     (7/9)   +
-------------------------------------------------------------------------
```

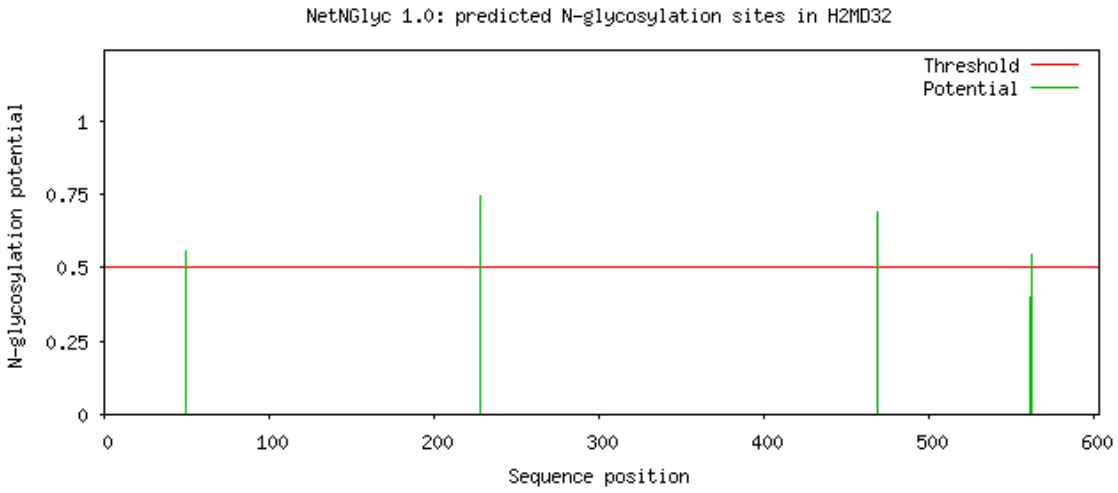

```
Output for 'A0A3B3HLL0'

    Warning: This sequence may not contain a signal peptide!!


Name:  A0A3B3HLL0      Length:  204
MADEADMRNELADLQTRADQITDESLESTRRMLAMVEESKDAGIRTLVMLDEQGEQLERIEEGMDQINKDMMDAEKNLNN      80
LGQFCGLCSCPCNKIKGGGQAWGGNQDGVVNSQPGARVMDEREQMAISGGFIRRVTDDARENEMDENLEQVGGIIGNLRH     160
MALDMGQEIDTQNRQIDRIMDKADSNKTRIDEANQRATKMLGSG
................................................................................      80
................................................................................     160
.......................N..................                                     240

(Threshold=0.5)
--------------------------------------------------------------------------------
SeqName      Position  Potential    Jury    N-Glyc
                                 agreement result
--------------------------------------------------------------------------------
A0A3B3HLL0   186 NKTR   0.5364     (7/9)   +
--------------------------------------------------------------------------------
```

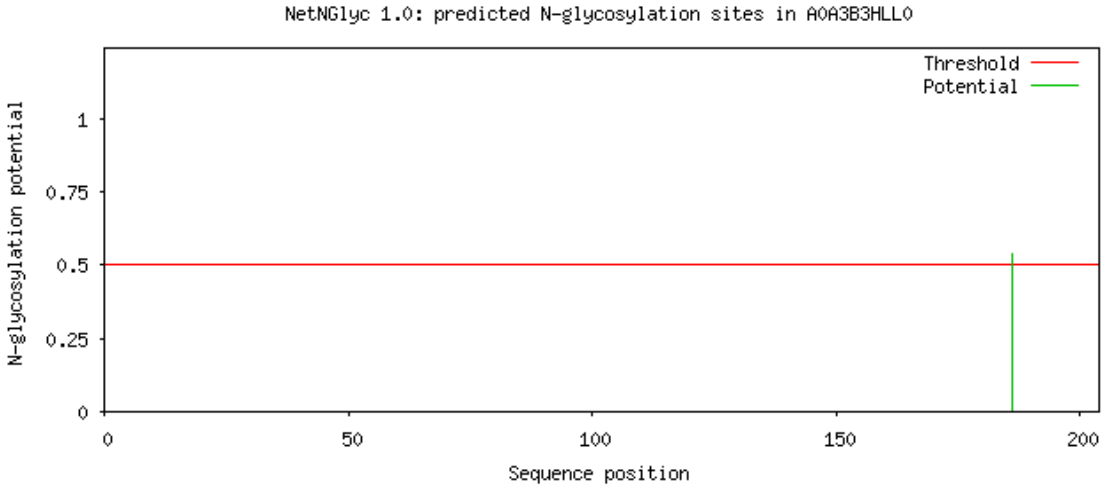

```
Output for 'rom1b'

    Warning: This sequence may not contain a signal peptide!!


Name:  rom1b   Length:  362
MVLLKMKFNQQRRVRLAQGLWLLSWLAVMCGAFIFCLGVYLKTELLRRDEVEKESFMDIHVVPNILMMVGLASIGTNWVA      80
TRVCQDSLDASRFPRWKVLLLAWFVVAALLCCLLLAVVVLSYVLQGRLEESLKVGLRNGIRFYKDTDVPGRCFQKETIDR     160
LQMEFRCCGNNNFKDWFEVQWVSGRFLDYTAQEVKDRIRSNVDGRYLLDGVPFSCCNPASPRPCLQYHLTDNRAHFNYDY     240
LSEDLNLYSRGCRQALTDYYMGLMNSTGPGVLSVILIQVGNFHLRYLQTAVEGAMALEDPEGDSEGYILEKGVKETFEEV     320
KVKVLTMMKLAQVDPEGVPVDAEAEKAADTTAEKAASPTPAS
.....................................................................................      80
.....................................................................................     160
.....................................................................................     240
.....................N.....................................................          .     320
.....................................                                               .     400

(Threshold=0.5)
---------------------------------------------------------------------------
SeqName      Position  Potential    Jury    N-Glyc
                                  agreement result
---------------------------------------------------------------------------
rom1b        265 NSTG   0.6962      (9/9)    ++
---------------------------------------------------------------------------
```

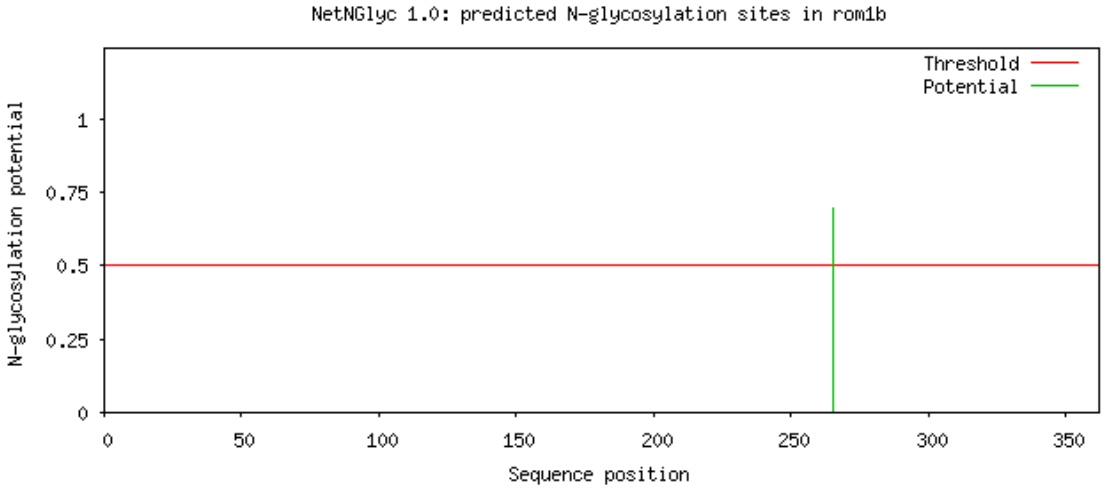

Output for 'A0A3B3IFV5'

Warning: This sequence may not contain a signal peptide!!

Name: A0A3B3IFV5 Length: 184

```
MREYKLVVLGSGGVGKSALTVQFVQGIFVEKYDPTIEDSYRKQVEIDGQQCMLEILDTAGTEQFTAMRDLYMKNGQGFAL      80
VYSITAQSTFNDLQDLREQILRVKDTEDVPMILVGNKCDLEDERVVGKEQGQNLARQWNNCAFLETSAKSKINVNEIFYD     160
LVRQINRKSPPEKKTKKKSGCTLL
.....                                                                                   80
.....                                                                                  160
.....                                                                                  240
```

(Threshold=0.5)

No sites predicted in this sequence.

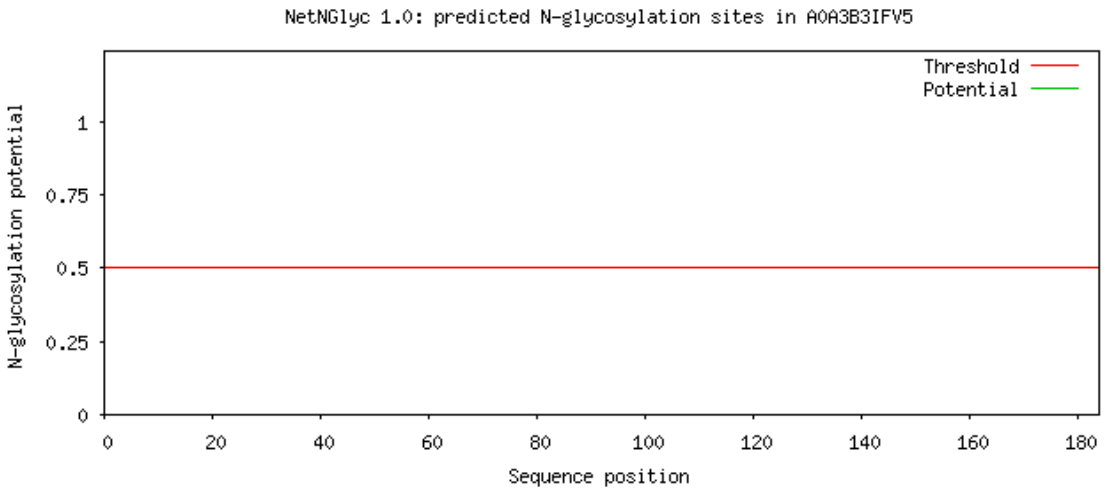

Output for 'A0A3B3I310'

Warning: This sequence may not contain a signal peptide!!

```
Name:  A0A3B3I310      Length:  363
MFEFAAWFFDRQLQWPIRARRQAVVLLLPRQSRGEERRGGEGLGVKDTQRNGLLVAKMADGDSGSERGGSSGGGGGGGSG      80
FQHYQREPETQELASKRLDIQNKRFYLDVKQNAKGRFIKIAEVGAGGSKSRLTLSMSVAAEFRDYLGDFIEHYAQLGPST     160
PEQIAQSSGGDDTGPRRALKSEFLVRENRKYYLDLKENQRGRFLRIRQTVNRGPGFGVGVGGIPGAGLQAGQTIALPAQG     240
LIEFRDALAKLIDDYGGDDEDLAGGGGGAGAYSELPEGTSIMVDSKRFFFDVGSNKYGVFLRVSEVKPSYRNSITIPFKA     320
WSKFGGAFSRYAEEMKEIQERHRDKMYERRTADESEGDDVDDD
.................................................................................      80
.................................................................................     160
.................................................................................     240
.................................................................................     320
........................................                                              400
```

(Threshold=0.5)

No sites predicted in this sequence.

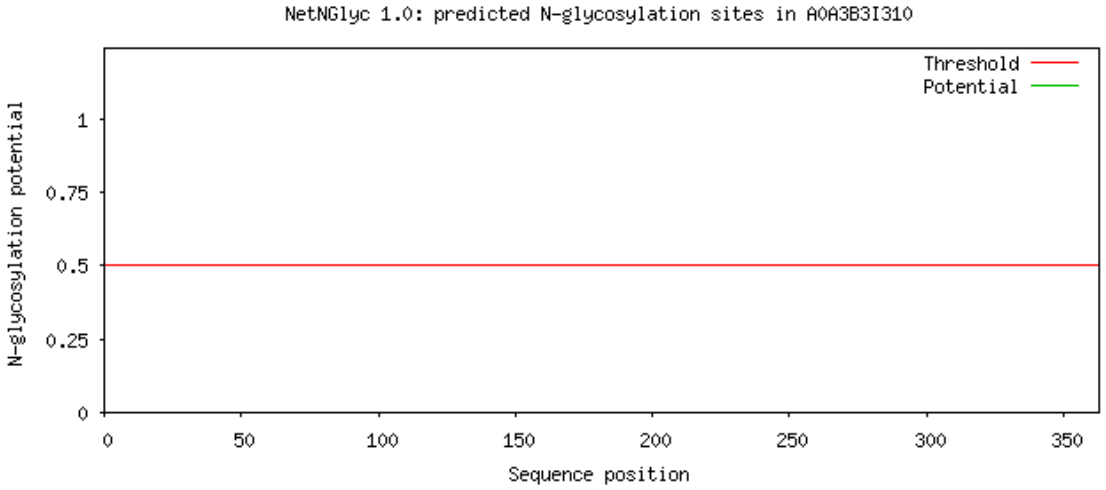

```
Output for 'H2M208'

    Warning: This sequence may not contain a signal peptide!!

Name:  H2M208  Length:  503
MADDLDIEALLDAPFRKEDKSQSPNGQEDRSKRPEKKRRSRSRSRDKKRSRSRERKRSRSRERKRSRSKDRRRSRSRERR      80
RSRERGGRYKDHHKHRRWSKSKSPVKKEKSPIRMPNDNLTPEERDGRTVFCMQLAARIRPRDLEEFFSAVGKVRDVRMIS     160
DRNSRRSKGIAYIEFVEASSVPLAIGLTGQRLLGVPIIVQASQAEKNRAAAAAAANNLQRGLTGPMRLYVGSLHFNITED     240
MLRGIFEPFGRIENIQLMMDSETGRSKGYGFITFSDAECAKKALEQLNGFELAGRPMKVGHVTERTDPSSAPSILDNDEL     320
ERSGIDLGTTGRLQLMARLAEGTGLQIPPAAQQALQMSGAIAIGAMAAVSAAMNPSLNVNMNSGALNLPSQPLATHCFQL     400
SNMFNPSSENTFGWEVDIQRDVIEECNKHGGVVHIYVDKNSAEGNVYVKCPSIPAAMSAVNALHGRFFGGKMITAAYVPL     480
PTYHKLFPESVTATQLLVPPLRR
.................................................................................      80
.................................................................................     160
.....................................................................N...........     240
.................................................................................     320
.........................................................N.......................     400
.................................................................................     480
....................                                                            560

(Threshold=0.5)
---------------------------------------------------------------------------
SeqName      Position  Potential    Jury    N-Glyc
                                agreement result
---------------------------------------------------------------------------
H2M208       118 NLTP   0.3320     (7/9)   -
H2M208       236 NITE   0.7038     (9/9)   ++
H2M208       374 NPSL   0.5371     (6/9)   +    WARNING: PRO-X1.
H2M208       405 NPSS   0.4248     (6/9)   -
---------------------------------------------------------------------------
```

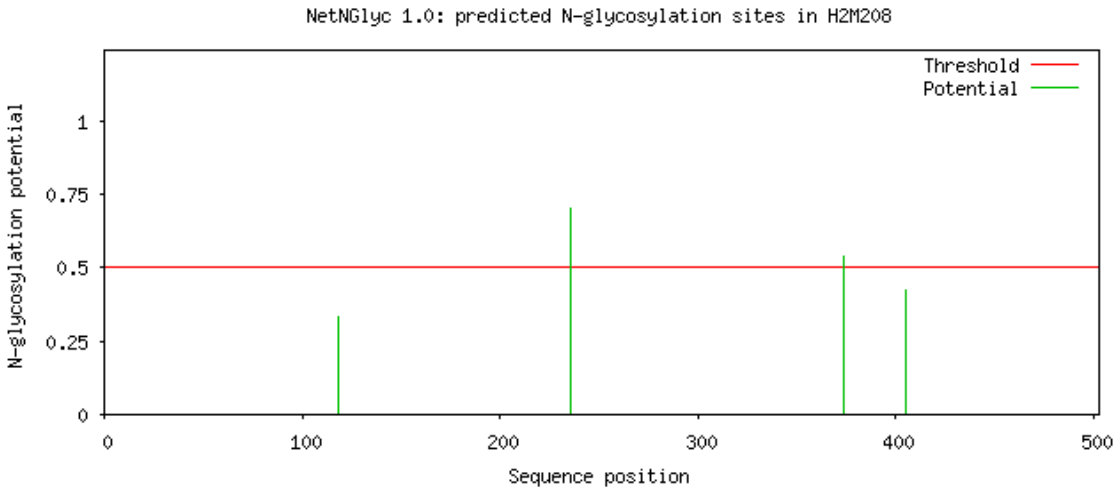

```
Output for 'A0A3B3HDP6'

    Warning: This sequence may not contain a signal peptide!!


Name:  A0A3B3HDP6      Length:  211
MDQQAKKHLQEEFDAALEEKDQMITVLQTQVRGWKRNDVPQSELAADPTSASQTPSEEQKLEPEIGNSDPAKLLETLQKR      80
VTRQENLLQKCKDVIRTHKDRSAQLSSENETLHQQLQERLQELEKMKELHTTEKTKLITQLRDAKNLIEQLEQDKGMVIA     160
ETKRQMHETLEMKEDEIAQLRSRLQQVTAQKEEIQDQREKGEKSGVCWAMF
................................................................................      80
............................N................................................     160
................................................                                      240

(Threshold=0.5)
--------------------------------------------------------------------------------
SeqName      Position  Potential    Jury    N-Glyc
                                  agreement result
--------------------------------------------------------------------------------
A0A3B3HDP6   109 NETL   0.5886     (6/9)   +
--------------------------------------------------------------------------------
```

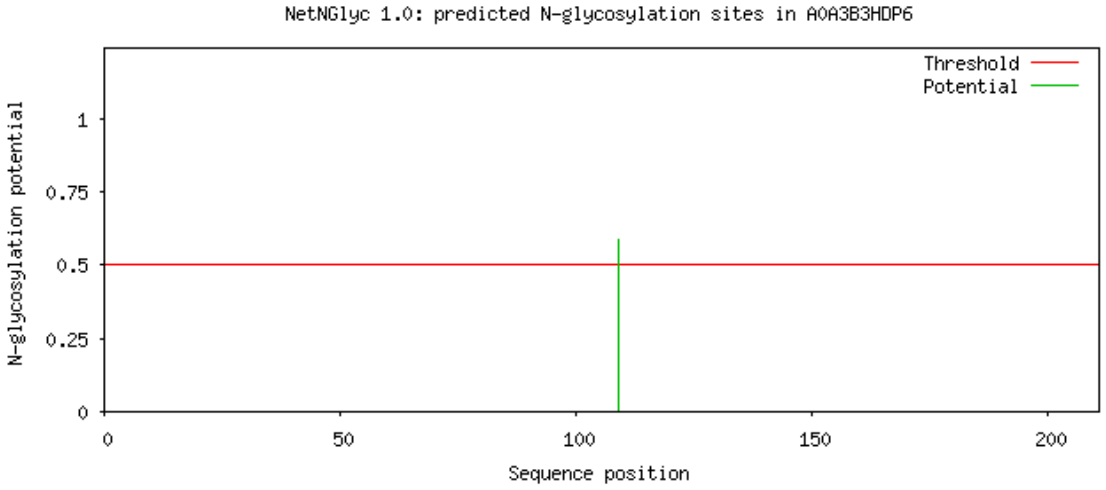

```
Output for 'H2MSC4'

    Warning: This sequence may not contain a signal peptide!!

Name:  H2MSC4  Length:  771
CSEAAEEPLKLVSSQNGVFSYEYYPSSPGRYSVSITWGGQHIPKSPFDVAVGAKAGPQQIRAWGPGLEGGIVGKAATFVV      80
ESIGPDAGVLGFAIEGPSQAKIECEDQNDGSCDVRYWPTEPGEYAIRVTCDEEDIELSPFMAHIVPDTNVNHPEKVRTAD     160
GPAARPPLDLSPSQRAVPCNVRPQAGRADASVVRYTPTEEGVHAVKVSYDGHPVPGSPFPVEASLLIPPFASQVKAFGPG     240
LEGGLVGNPAEFTIDTTGAGTGGLGLTVEGPTEAKIECSDNGDGTCSVSYLPTEPGDYLVNILFENAHVPGSPFRADIQM     320
PFDPSKVVASGSGLKRAKVRGRLPERGSCSLLQKAVPVCPSSDGDAPLCVPGRKAKTEVISNNDGTFTVTYVPTTAGMYT     400
LLLKYGDQTVPGFPAKVPVDPAVDTSRVKVFGPGVDGQGKVWGAGIGGLGITVEGPSESKMSCKDNKDGSCSVEYVPFTP     480
GLYDVNITYGGEHIPGESRLADGHGKLSAIFVRLKGSPFKVQVKDIVDPSKVKVSGPGVGSGVRANIPQSFTVDCRKAGV     560
APLAVAVTDPDGNPKQPRIHDNGGGTYLVSYIPDRTGRYTIVIKYGGDDIPASPFRVRATATGDASKCSVSGTEKVRERE     640
SEREKRQAERPFLHSGVGPTVAIGQEMSLAVNTKGAGKGKVCCVVVQPDGSEVEAEVVENPDGTFDIFYTAPAPGNYVIF     720
VRFGGENIPRSPFKVMVRTAFLPLPVPSCSQHQPEEPFPKRNGRKYSIHSA
.....     80
.....     160
.....     240
.....     320
.....     400
.....     480
.....N.....     560
.....     640
.....     720
.....     800

(Threshold=0.5)
-------------------------------------------------------------------------
SeqName      Position  Potential    Jury    N-Glyc
                                agreement result
-------------------------------------------------------------------------
H2MSC4       486 NITY   0.5499     (6/9)   +
-------------------------------------------------------------------------
```

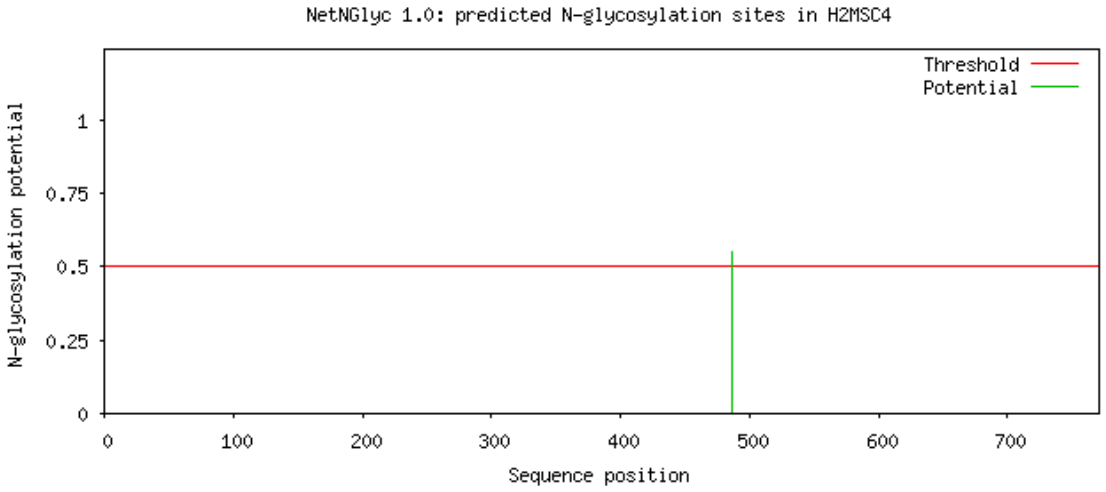

Output for 'H2M4H8'

Warning: This sequence may not contain a signal peptide!!

```
Name:  H2M4H8  Length:  486
MAKNDDDEEEAARERRRRARQERLRSRESEDPSSQSDKLCVLSPLSVTENVSVSGSYGDGGDDEEQALLDRMAKREERRQ      80
RRMKEALERQKQLDPAASEASEGVALEKNNMEEERPSSWRKGRYRDSMDEDEKTFSSRQEKEQDWPTGDTKAATEEEEEE     160
EEQKTTEVEVIPRRSIFREQDCNVDNSTLNRNMLLSNDTEEDFEVSEILHAMDNEDENARLEAERKLEELKRRRDDAESE     240
EFERMRQKQQEAEAELEELKRKREERRKILEEEERQRKQEEEERKAREEEEKRKMKEEIERRRAEAAEKRQKVDDTMDGE     320
GKPFKCVSPRGSSLKAAHSPVVSKIDNRLEQYTSARENKESRSPRAGAVDLPVVTDSIRNIKSMWEKGSVFNAPGNGGSA     400
FKEAAVIKTGVAGRINDWLNKTPDGGRTPGGKPTDLKPVDVTNKRSLWENKGGASTKVKLLISALAPMLIDITPAKKADF     480
FLSLHW
..................................................N.............................      80
................................................................................     160
.........................N..........N............................................     240
................................................................................     320
................................................................................     400
................................................................................     480
......                                                                               560

(Threshold=0.5)
--------------------------------------------------------------------------------
SeqName      Position  Potential    Jury    N-Glyc
                                  agreement result
--------------------------------------------------------------------------------
H2M4H8         50 NVSV   0.7046     (9/9)    ++
H2M4H8        186 NSTL   0.5562     (6/9)    +
H2M4H8        197 NDTE   0.7102     (9/9)    ++
H2M4H8        420 NKTP   0.1672     (9/9)    ---
--------------------------------------------------------------------------------
```

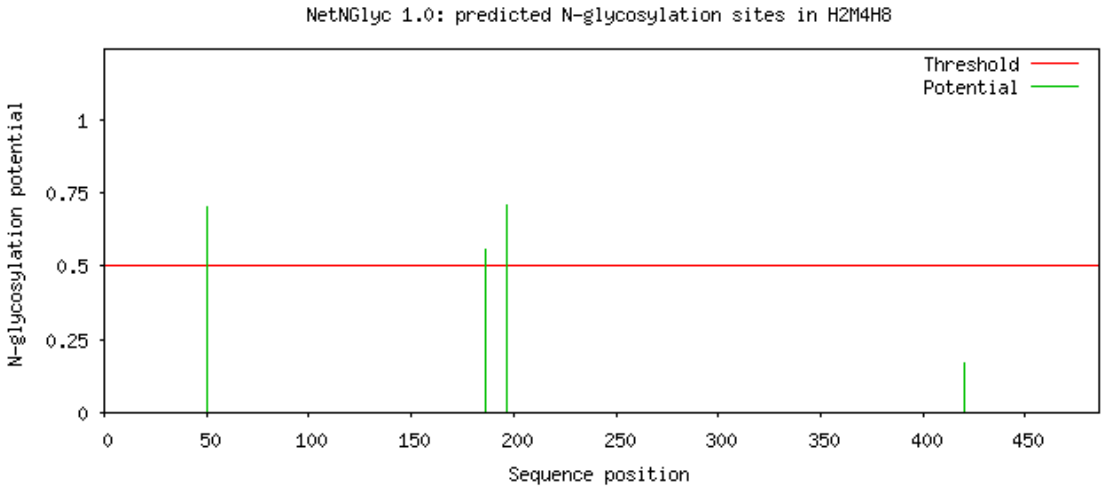

```
Output for 'A0A3B3IMD1'

    Warning: This sequence may not contain a signal peptide!!


Name:  A0A3B3IMD1      Length:  298
MTDADKFLYGDRGAVSNPLAQADWATKKLVWVPNEKLGFEVGSLKEEQGDECVVELVDSGKKVKINKDDIQKMNPPKFNK      80
VEDMAELTCLNEASVLHNLKERYYSGLIYTYSGLFCVVINPYKHLPIYSEEIVNMYKGKKRHEMPPHIYAITDSAYRSMM     160
QDREDQSILCTGESGAGKTENTKKVIQYLAHVASSFKSKKDQGELEKQLLQANPILEAFGNAKTVKNDNSSRFGKFIRIN     240
FDVTGYIVGANIETCILFPAFASFKCFHHYFFSLVCSLLLNWTLRSAGEIPRHQTSQR
.....                                                                                  80
.....                                                                                 160
.....N.....                                                                           240
.....N.....                                                                           320

(Threshold=0.5)
--------------------------------------------------------------------------------
SeqName      Position  Potential    Jury    N-Glyc
                                   agreement result
--------------------------------------------------------------------------------
A0A3B3IMD1   229 NSSR   0.5710     (8/9)   +
A0A3B3IMD1   281 NWTL   0.5730     (7/9)   +
--------------------------------------------------------------------------------
```

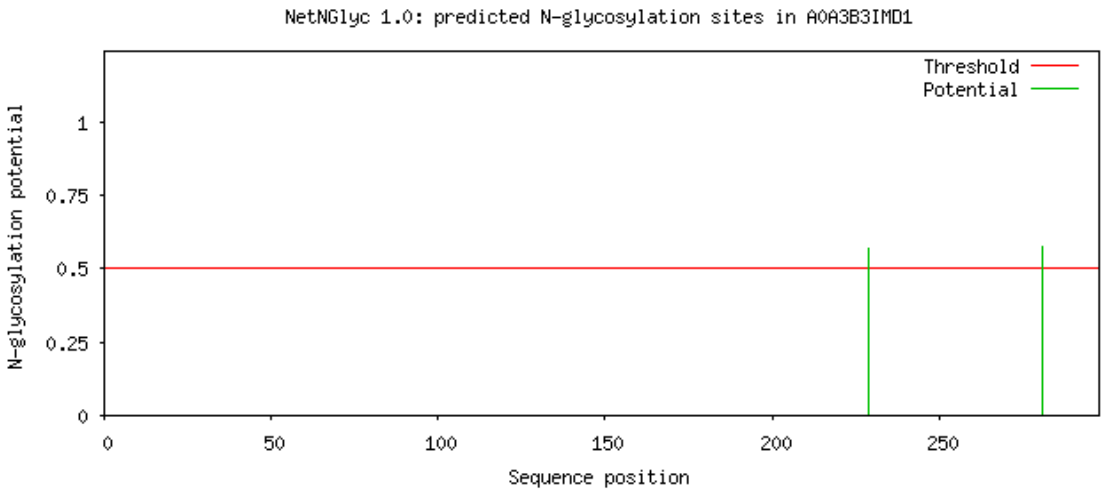

```
Output for 'H2MSJ7'

    Warning: This sequence may not contain a signal peptide!!


Name:  H2MSJ7  Length:  181
MGALISSIFSRFVSKDPFRILMVGLDGAGKTTILYKLKLGEVVTTIPTIGFNVETVEYKNISFTVWDVGGQNRIRLLWRH      80
YLVNTQGLIFVVDSIDPERFKEAAEDFHLAEHELRDAAVLIFANKQDLPGAAAVHDITEGLGLLGVHQPWHVQPCCAVSG     160
AGLAEGLDWLSSQIQSRQRPQ
.............................................................N.....................      80
................................................................................     160
.....................                                                             240

(Threshold=0.5)
---------------------------------------------------------------------------
SeqName      Position  Potential    Jury    N-Glyc
                                agreement result
---------------------------------------------------------------------------
H2MSJ7         60 NISF   0.5409     (5/9)   +
---------------------------------------------------------------------------
```

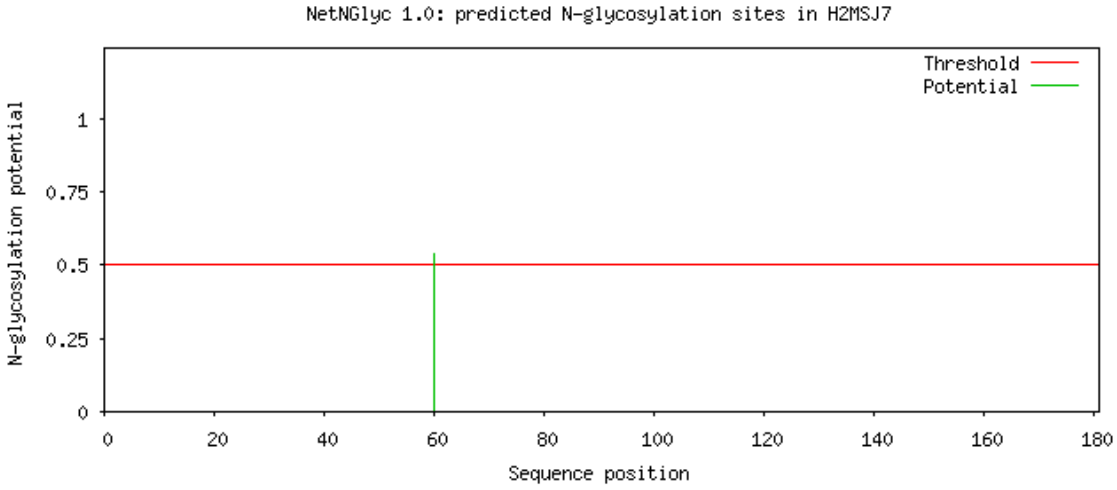

```
Output for 'A0A3B3I291'

    Warning: This sequence may not contain a signal peptide!!

Name:  A0A3B3I291      Length:  289
MMDVVNQLVAQGQFRVLKVPLGFIKVLQWFFAVFAFSTCGSYSGLLRVAVDCKNRTESDLKIEVEFEYPFRLHQEYFDAP      80
TCKDGEKEQVFLIGDHSSSAEFFVTIAVFAFLYSTATLSIYIFFFEKYKENNKGPLIDLAVTAVFAFMWLVSSAAWAKGL     160
SDVKTATDPDKVIMMIPACKKEENRCREVHDPVMSGLNTSVAFGFINLVLWVGNLWFVFKETGIIAPFMRAPPPQQKPAP     240
DAYGQQGVYEQDPYASNQGSYQPEFSQQGYNQDAEYGQQGAPTSFSNQM
.....................................................N..........................      80
................................................................................     160
.....................................N..........................................     240
.................................................                                    320

(Threshold=0.5)
----------------------------------------------------------------------
SeqName      Position  Potential   Jury    N-Glyc
                                agreement  result
----------------------------------------------------------------------
A0A3B3I291    54 NRTE    0.5748    (8/9)    +
A0A3B3I291   198 NTSV    0.5981    (6/9)    +
----------------------------------------------------------------------
```

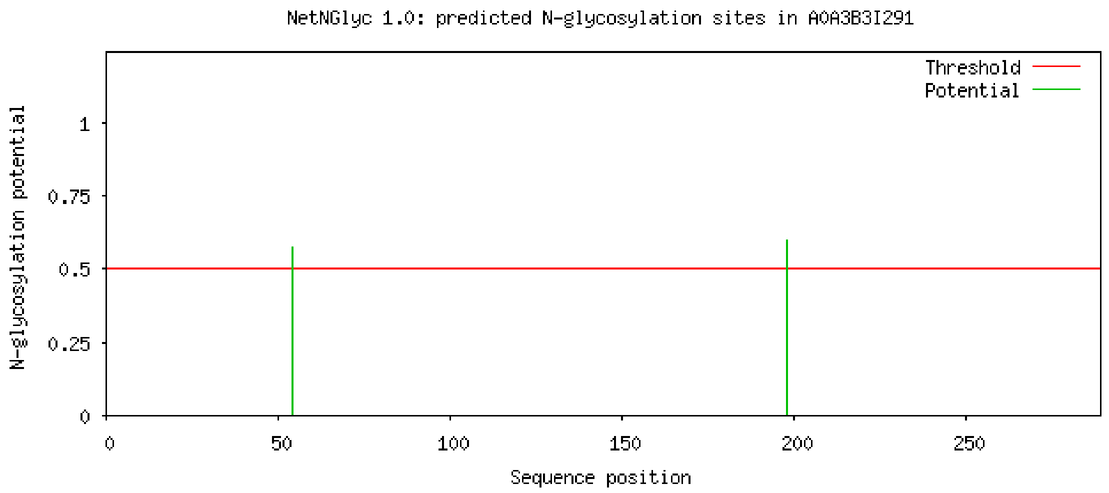

7.2 Supplementary figures

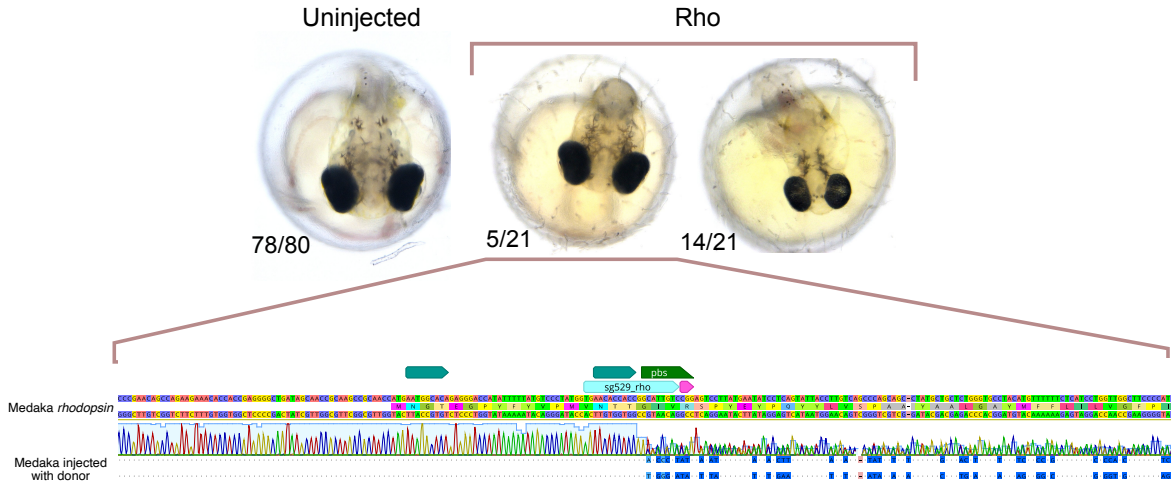

Supplementary Figure 1. HDR-mediated donor insertion targeting *N*-glycosylation sites in *rho*. Representative embryos from control (uninjected) and donor injected groups. While some injected embryos were phenotypically similar to controls, others exhibited severe developmental defects (microcephaly) which were incompatible with survival. Sanger sequencing of one phenotypically normal injected embryo showed no donor integration but clear evidence of double strand breaks (DSBs).

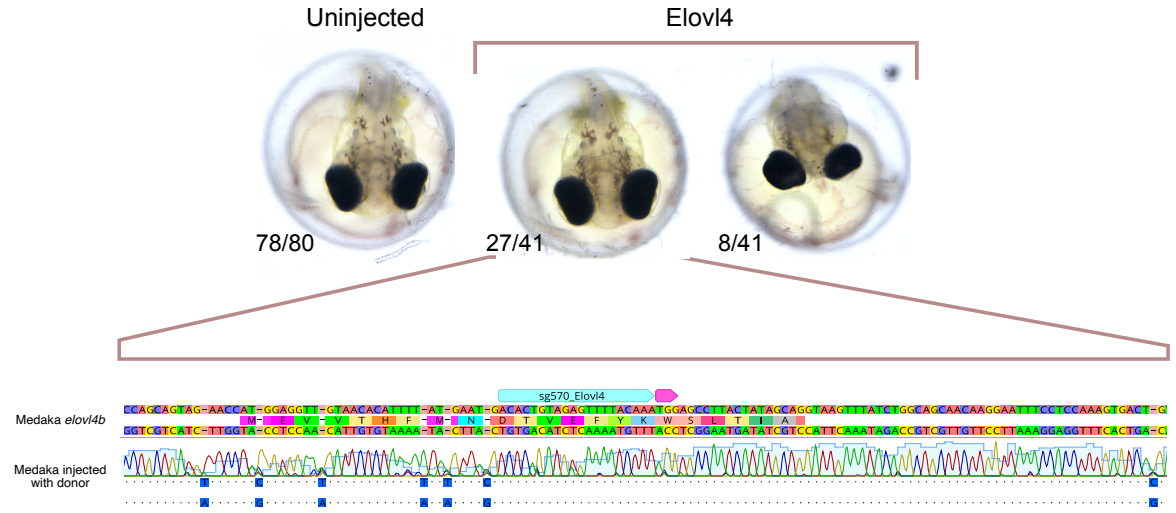

Supplementary Figure 2. HDR-mediated donor insertion targeting *N*-glycosylation sites in *elovl4*. Representative embryos from control (uninjected) and donor injected groups. While some injected embryos were phenotypically similar to controls, others exhibited severe developmental defects (microcephaly and oedema) which were incompatible with survival. Sanger sequencing of one phenotypically normal injected embryo showed no donor integration but clear evidence of double strand breaks (DSBs).

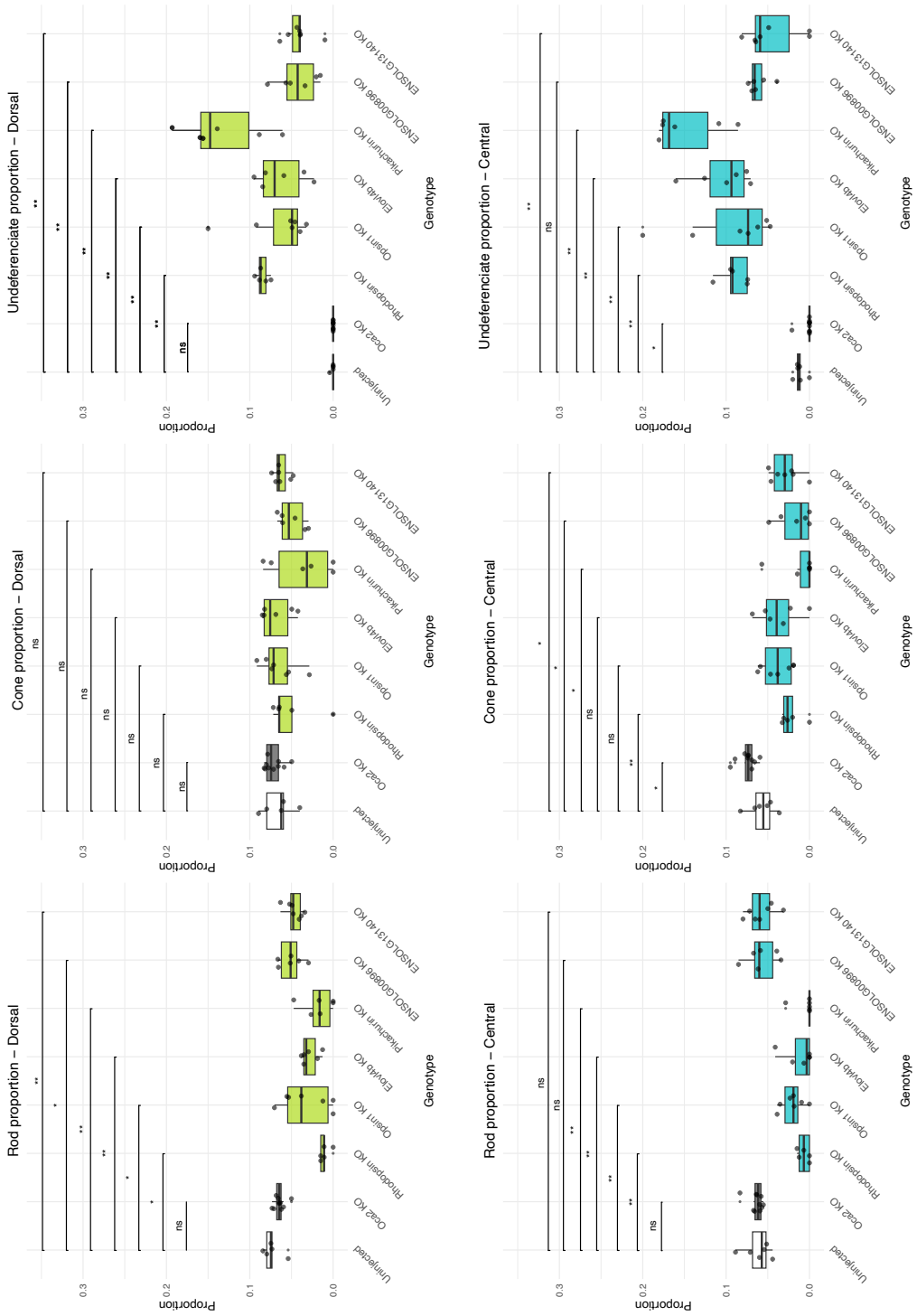

Supplementary Figure 3. Candidates knockout effect in photoreceptors population in the retina. Boxplot depicting the proportion of all photoreceptor populations, relative to the total number of cells, in dorsal and central retina for all knockout (KO) candidates generated using CRISPR/Cas9. Comparisons were made between knockout larvae and uninjected siblings at 0 days post hatch (dph). *Oca2* was used as injection control altering eye pigmentation but not the retinal cell composition. Asterisks indicate statistical significance compared with uninjected siblings. Statistical analysis was performed with two-tailed t-tests, corrected with Bonferroni, $p < 0.05$.

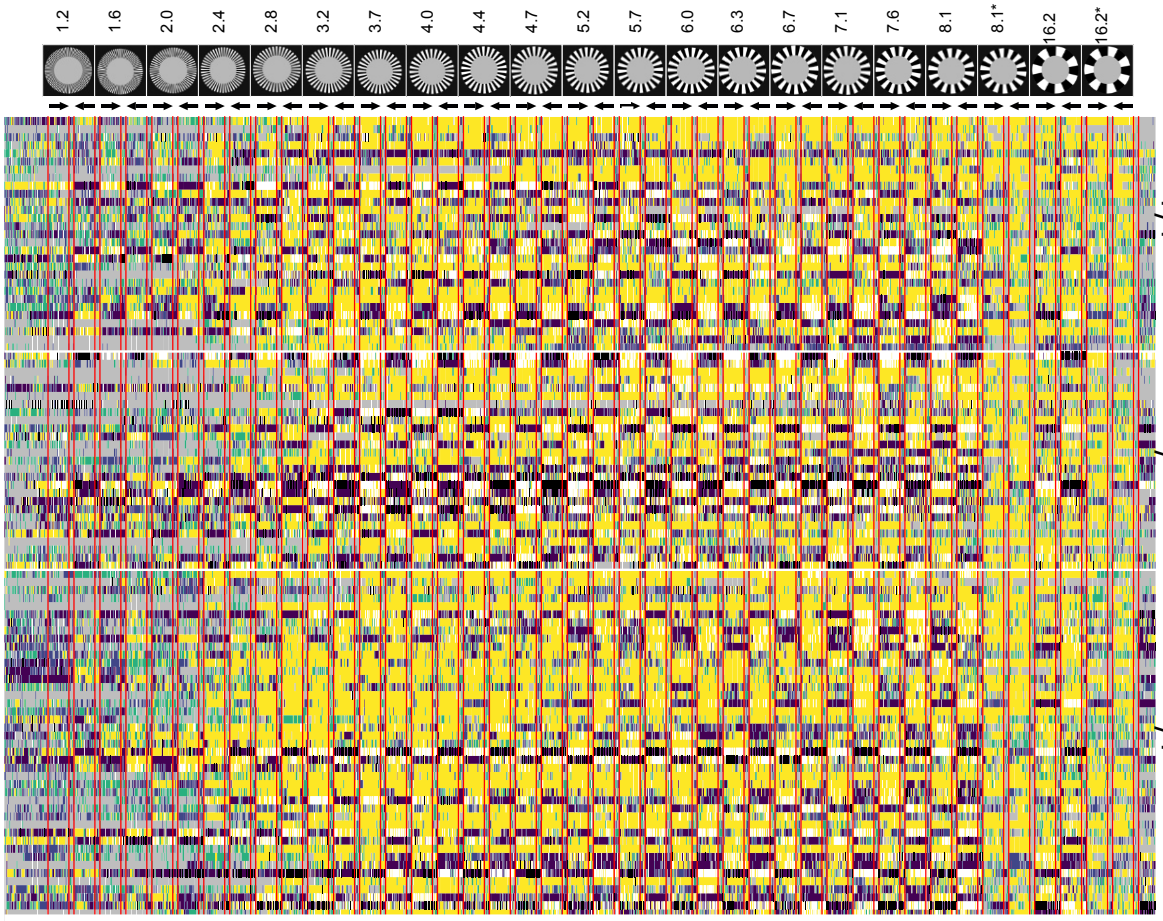

Supplementary Figure 4. OMR analysis of the *rho* knockout line to study swimming behaviour. Heatmap showing response values (every 5 second as a column) of each individual hatchlings (row) at each stripe motion in each direction (top arrows). Sections where neither clock wise (CW) nor counter clock wise (CCW) is indicated represent periods when stripe motion was paused (red). Stripe width is shown on x axis. The color of the blocks indicates, the response values: white (>1.75) and yellow (0.5 to 1.75) indicate hatchlings following the stripe motion; green (0.2 to 0.5), gray (0.2 to 0.2), and blue (-0.5 to -0.2) represent non-responsive behavior; while purple (-1.75 to -0.5) and black (<-1.75) denote hatchlings swimming in the direction opposite to the stripe motion.

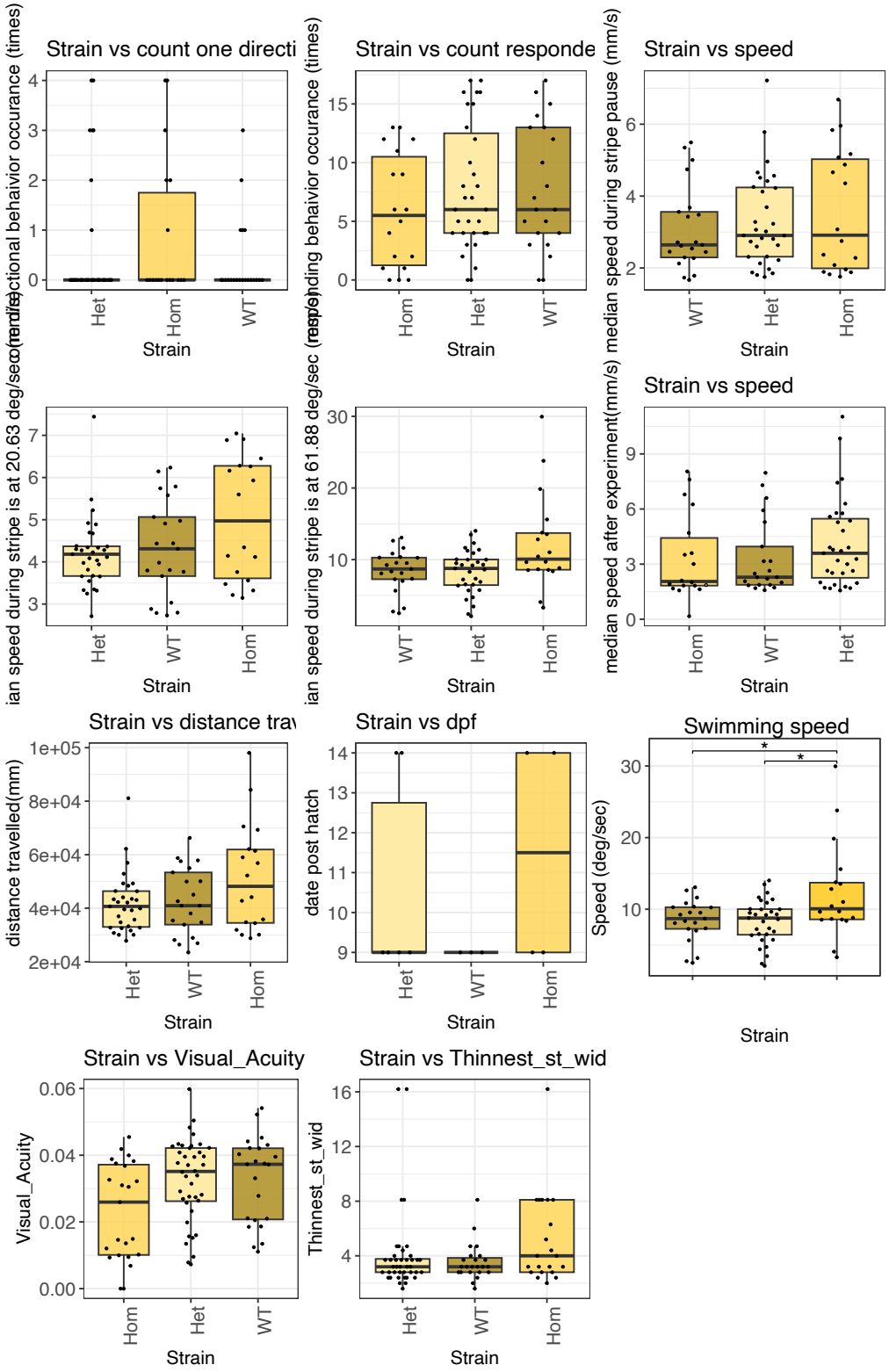

Supplementary Figure 5. OMR as a tool to understand more than visual acuity. Box plots showing obtained data from the OMR as the minimum stripe width to which the hatchlings of each strain responded,visual acuity for the different genotypesBox plots showing median swimming speed (in mm/s) during and (l) after completion of all stripe motion phases or the count of one-directional swimming and the total distance swum (in mm) during the experiment.

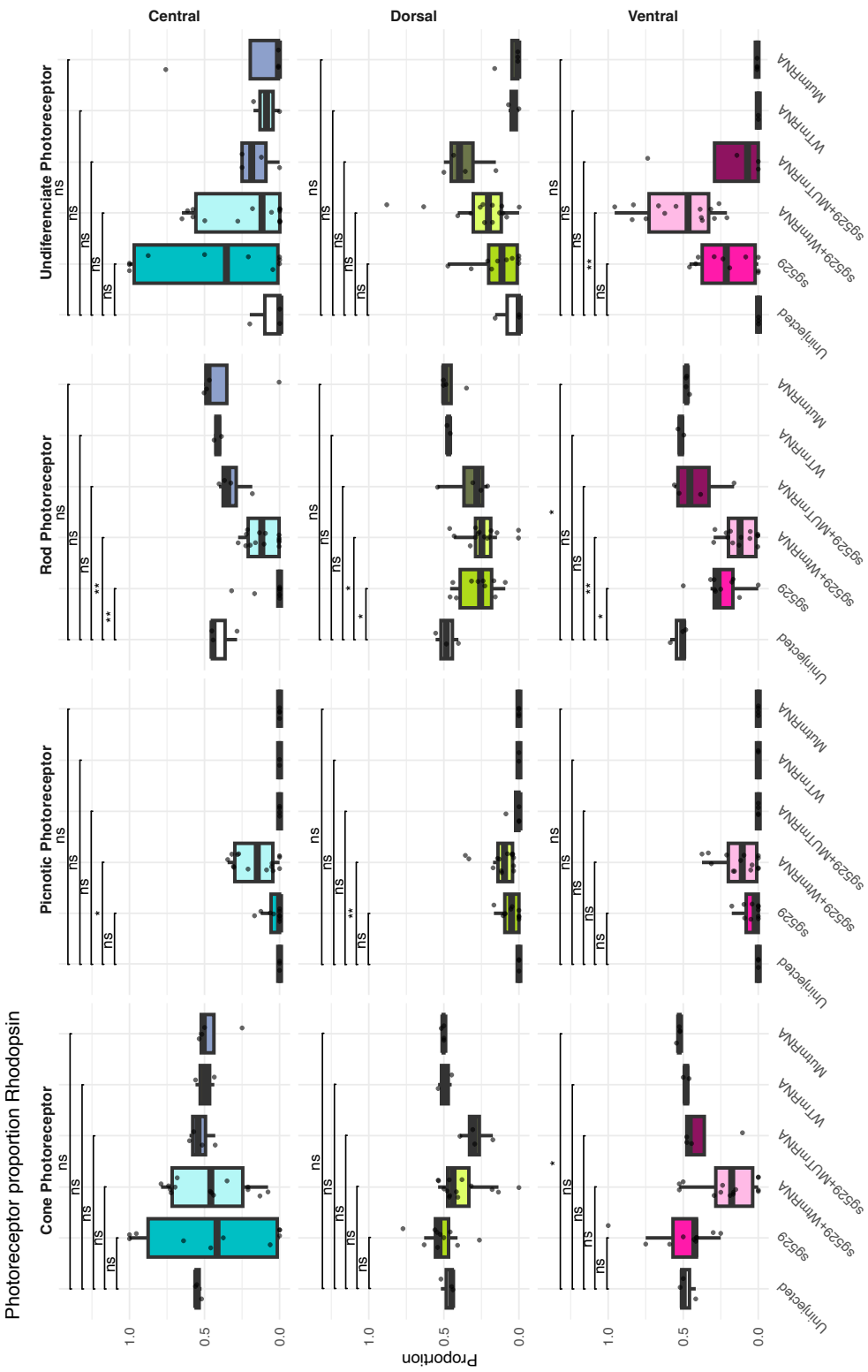

Supplementary Figure 6. Comparative analyses of the photoreceptor population in rhodopsin mRNA rescue. Comparative analysis if the different identified photoreceptor populations (top x axis) comparing each condition (KO, KO+WTmRNA; KO+variants mRNA) to the uninjected siblings, in the different regions of the retina (y right axis) (blue= central; dorsal= green; ventral= pink). Statistical analysis was performed with two-tailed t-tests, corrected with Bonferroni, $p < 0.05$.

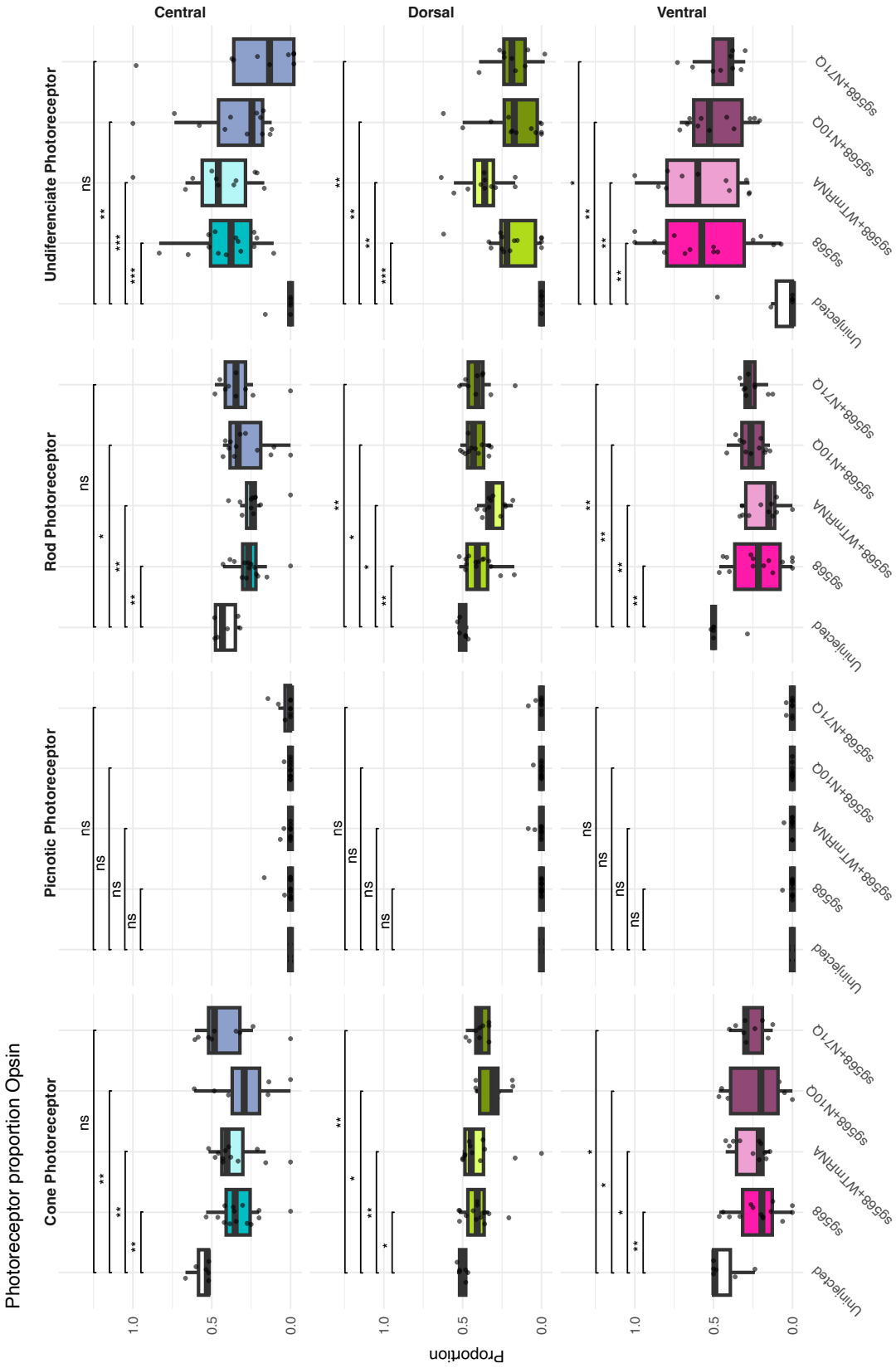

Supplementary Figure 7. Comparative analyses of the photoreceptor population in opn1sw mRNA rescue. Comparative analysis if the different identified photoreceptor populations (top x axys) comparing each condition (KO, KO+WTmRNA; KO+variants mRNA) to the uninjected siblings, in the different regions of the retina (y right axis) (blue= central; dorsal= green; ventral= pink). Statistical analysis was performed with two-tailed t-tests, corrected with Bonferroni t, $p < 0.05$.

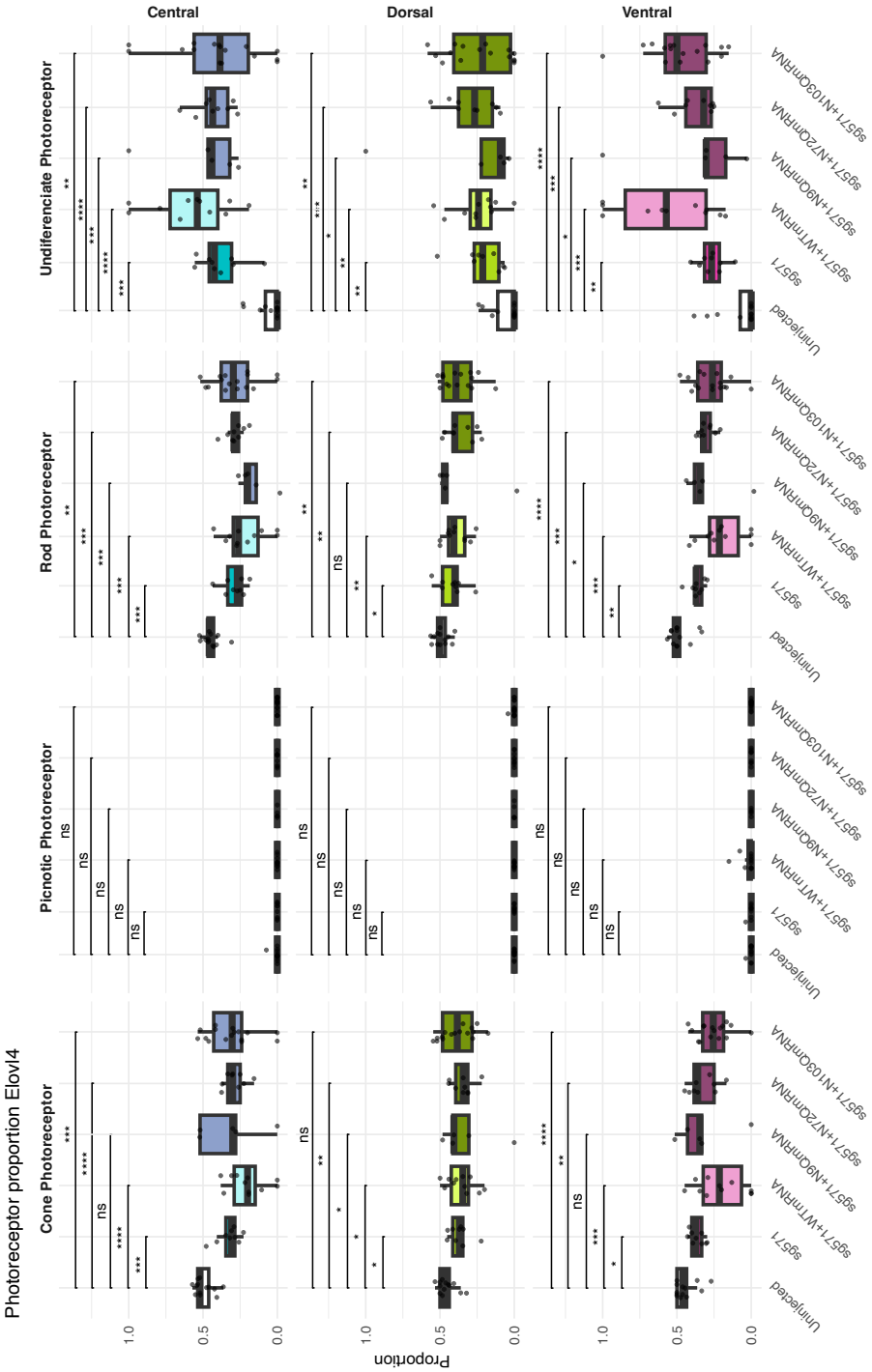

Supplementary Figure 8. Comparative analyses of the photoreceptor population in *elvl4b* mRNA rescue.Comparative analysis if the different identified photoreceptor populations (top x axys) comparing each condition (KO, KO+WTmRNA; KO+variants mRNA) to the uninjected siblings, in the different regions of the retina (y right axis) (blue= central; dorsal= green; ventral= pink). Statistical analysis was performed with two-tailed t-tests, corrected with Bonferroni, $p < 0.05$.

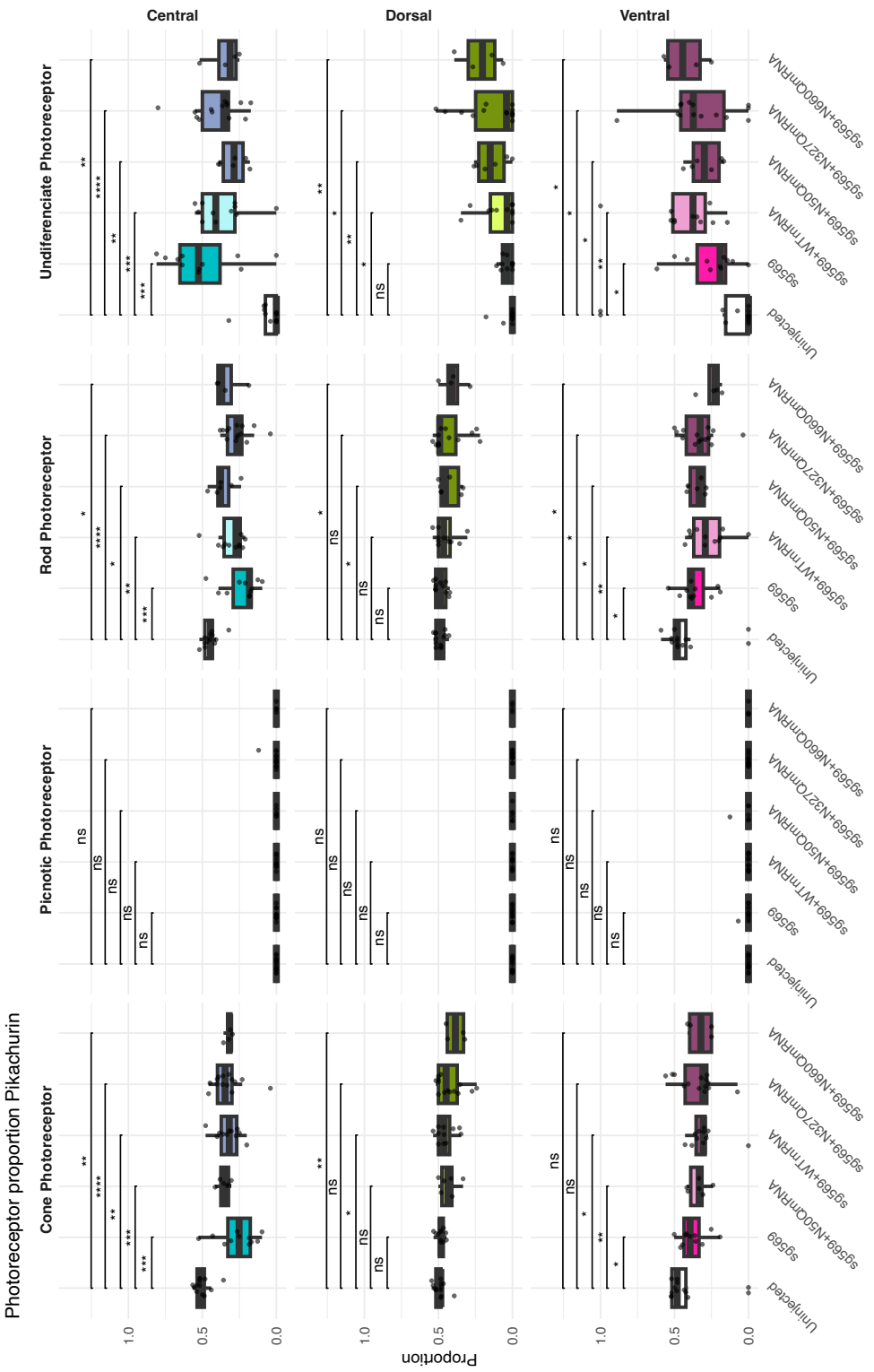

Supplementary Figure 9. Comparative analyses of the photoreceptor population in *pikachurin* mRNA rescue. Comparative analysis if the different identified photoreceptor populations (top x axys) comparing each condition (KO, KO+WTmRNA; KO+variants mRNA) to the uninjected siblings, in the different regions of the retina (y right axis) (blue= central; dorsal= green; ventral= pink). Statistical analysis was performed with two-tailed t-tests, corrected with Bonferroni, $p < 0.05$.

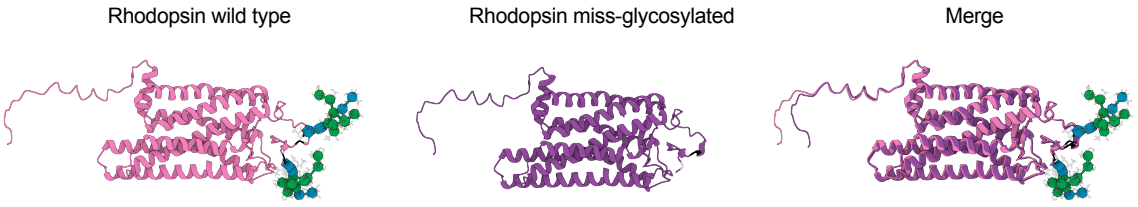

Supplementary Figure 10. Structural effects of *N*-linked glycosylation disruption in Rhodopsin (Rho). Ribbon diagrams compare the WT (pink) with the miss-glycosylated variant (purple) carrying the substitution Asn>Gln, asparagine residues are shown in black and glutamine substitutions in white. This changes lead to subtle changes in the conformation of the protein.

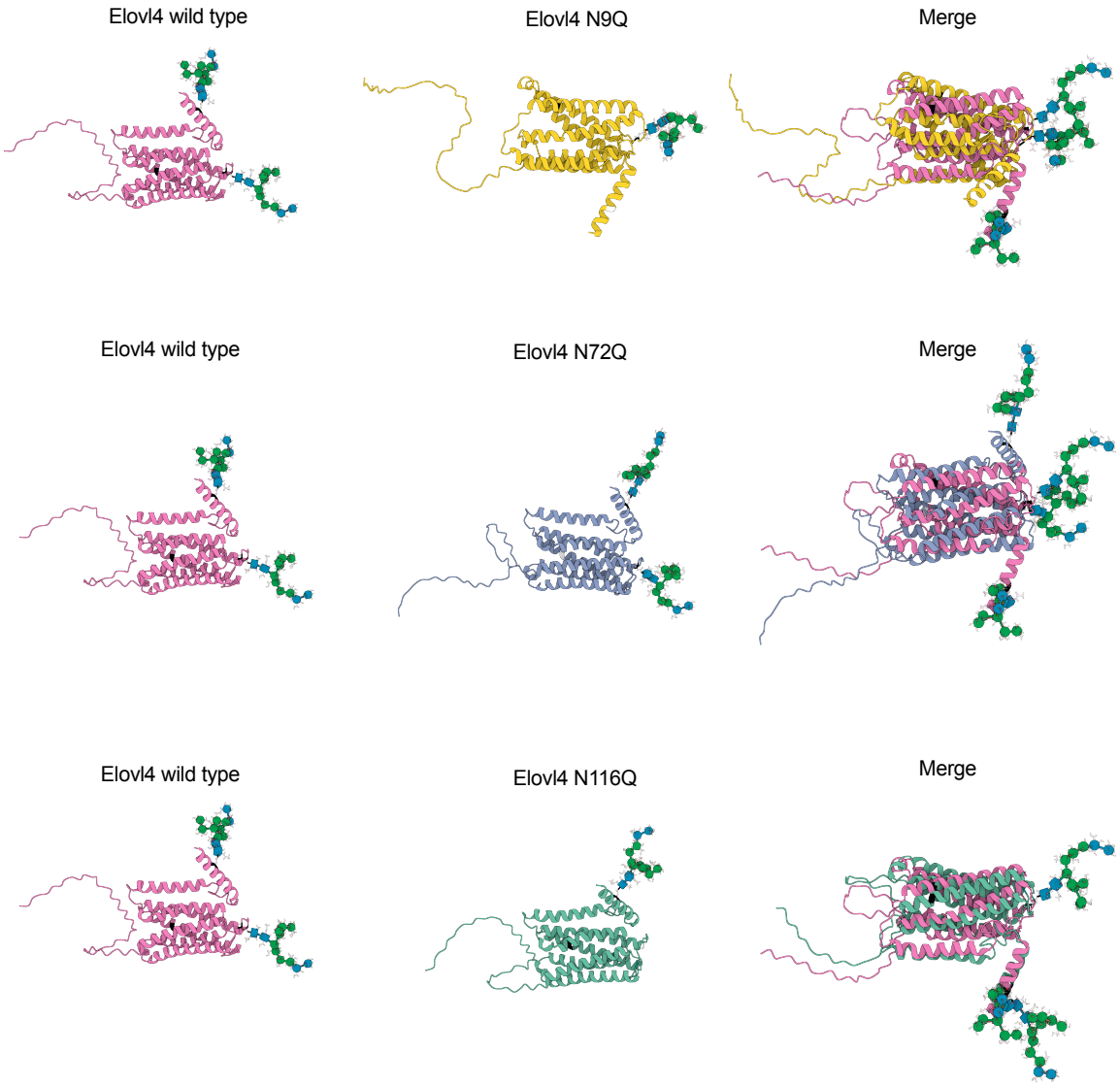

Supplementary Figure 11. Predicted structural consequences of *N*-linked glycosylation site substitutions in Elovl4. Ribbon diagrams compare the WT (pink)with the miss-glycosylated variants (N9Q yellow, N72Q lila and N116Q tiel) carrying the substitution Asn>Gln, asparagine residues are shown in black and glutamine substitutions in white. N9Q and N72 changes show strong misalignment with the WT simulation indicating a high change in protein polarity, while N116 seemed not to affect the polarity of the protein in a strong manner.

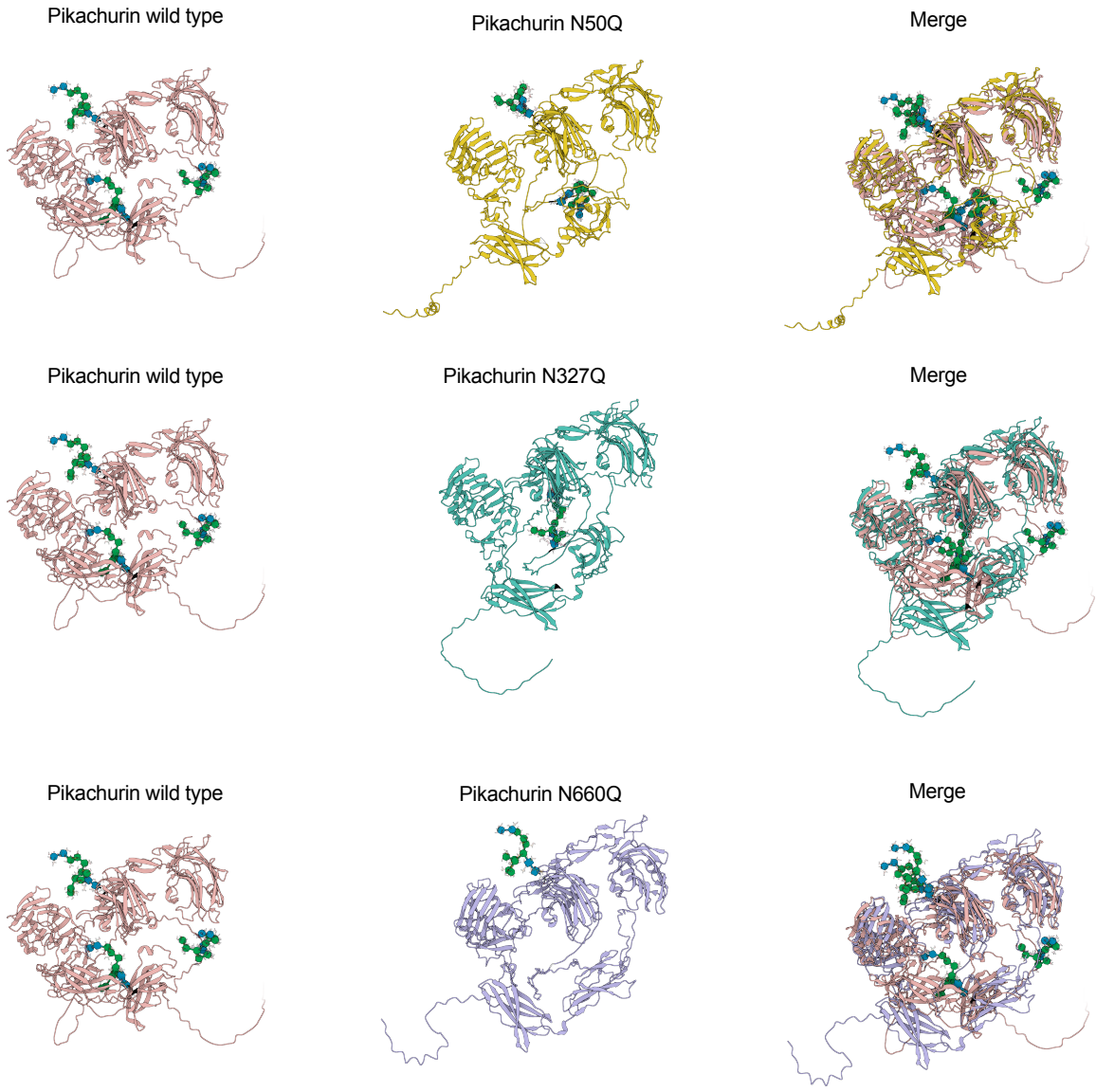

Supplementary Figure 12. Predicted structural consequences of *N*-linked glycosylation site substitutions in Pikachurin. Ribbon diagrams compare the WT (pink) with the miss-glycosylated variants (N50Q yellow, N327Q tiel and N660Q lila) carrying the substitution Asn>Gln, asparagine residues are shown in black and glutamine substitutions in white. N50Q seemed not to affect the polarity of the protein in a strong manner while N327Q and N660Q presented less compact structure in the simulations due to the changes. Interestingly these simulations show a co-dependency on the glycosylation of pikachurin as each variant only present one point mutation, in the cases of N327Q and N660Q, simulations to install the glycan at position 50 failed.

8

References

Abu Bakar, N., & Hamzan, N. I. (2025). Advancement in Clinical Glycomics and Glycoproteomics for Congenital Disorders of Glycosylation: Progress and Challenges Ahead. *Biomedicines*, *13*(8). https://doi.org/10.3390/BIOMEDICINES13081964

Abu Bakar, N., Lefeber, D. J., & van Scherpenzeel, M. (2018). Clinical glycomics for the diagnosis of congenital disorders of glycosylation. *Journal of Inherited Metabolic Disease*, *41*(3), 499. https://doi.org/10.1007/S10545-018-0144-9

Agbaga, M. P., Tam, B. M., Wong, J. S., Yang, L. L., Anderson, R. E., & Moritz, O. L. (2014a). Mutant ELOVL4 that causes autosomal dominant Stargardt-3 macular dystrophy is misrouted to rod outer segment disks. *Investigative Ophthalmology and Visual Science*, *55*(6), 3669–3680. https://doi.org/10.1167/IOVS.13-13099

Agbaga, M. P., Tam, B. M., Wong, J. S., Yang, L. L., Anderson, R. E., & Moritz, O. L. (2014b). Mutant ELOVL4 that causes autosomal dominant Stargardt-3 macular dystrophy is misrouted to rod outer segment disks. *Investigative Ophthalmology and Visual Science*, *55*(6), 3669–3680. https://doi.org/10.1167/IOVS.13-13099

Aoki-Kinoshita, K. F., Akune-Taylor, Y., Ando, H., Angata, K., Fujita, M., Furukawa, J. I., Kaji, H., Kato, K., Kitajima, K., Kizuka, Y., Matsui, Y., Nakajima, K., Nishihara, S., Okajima, T., Sakamoto, K., Sato, C., Thaysen-Andersen, M., Togayachi, A., Yagi, H., … Kadomatsu, K. (2024). The Human Glycome Atlas project for cataloging all glycan-related omics data in human. *Glycobiology*, *34*(11), cwae052. https://doi.org/10.1093/GLYCOB/CWAE052

Apweiler, R., Hermjakob, H., & Sharon, N. (1999). On the frequency of protein glycosylation, as deduced from analysis of the SWISS-PROT database. *Biochimica et Biophysica Acta*, *1473*(1), 4–8. https://doi.org/10.1016/S0304-4165(99)00165-8

Badawi, A. H., Al-Muhaylib, A. A., Al Owaifeer, A. M., Al-Essa, R. S., & Al-Shahwan, S. A. (2019). Primary congenital glaucoma: An updated review. *Saudi Journal of*

Ophthalmology : Official Journal of the Saudi Ophthalmological Society, *33*(4), 382–388. https://doi.org/10.1016/J.SJOPT.2019.10.002

Bandyopadhyay, M., & Rohrer, B. (2010). Photoreceptor structure and function is maintained in organotypic cultures of mouse retinas. *Molecular Vision*, *16*, 1178. https://pmc.ncbi.nlm.nih.gov/articles/PMC2901185/

Barabas, P., Liu, A., Xing, W., Chen, C. K., Tong, Z., Watt, C. B., Jones, B. W., Bernstein, P. S., & Križaj, D. (2013). Role of ELOVL4 and very long-chain polyunsaturated fatty acids in mouse models of Stargardt type 3 retinal degeneration. *Proceedings of the National Academy of Sciences of the United States of America*, *110*(13), 5181–5186. https://doi.org/10.1073/PNAS.1214707110/SUPPL_FILE/PNAS.201214707SI.PDF

Barrangou, R., Fremaux, C., Deveau, H., Richards, M., Boyaval, P., Moineau, S., Romero, D. A., & Horvath, P. (2007). CRISPR provides acquired resistance against viruses in prokaryotes. *Science*, *315*(5819), 1709–1712. https://doi.org/10.1126/SCIENCE.1138140/SUPPL_FILE/BARRANGOU.SOM.PDF

Bateman, A., Martin, M. J., Orchard, S., Magrane, M., Ahmad, S., Alpi, E., Bowler-Barnett, E. H., Britto, R., Bye-A-Jee, H., Cukura, A., Denny, P., Dogan, T., Ebenezer, T. G., Fan, J., Garmiri, P., da Costa Gonzales, L. J., Hatton-Ellis, E., Hussein, A., Ignatchenko, A., … Zhang, J. (2023). UniProt: the Universal Protein Knowledgebase in 2023. *Nucleic Acids Research*, *51*(D1), D523–D531. https://doi.org/10.1093/NAR/GKAC1052

Bert, F., Gualano, M. R., Camussi, E., Pieve, G., Voglino, G., & Siliquini, R. (2016). Animal assisted intervention: A systematic review of benefits and risks. *European Journal of Integrative Medicine*, *8*(5), 695–706. https://doi.org/10.1016/J.EUJIM.2016.05.005

Bloomfield, S. A., & Dacheux, R. F. (2001). Rod vision: pathways and processing in the mammalian retina. *Progress in Retinal and Eye Research*, *20*(3), 351–384. https://doi.org/10.1016/S1350-9462(00)00031-8

Brodsky, J. L., & Skach, W. R. (2011). Protein folding and quality control in the endoplasmic reticulum: Recent lessons from yeast and mammalian cell systems. *Current Opinion in Cell Biology*, *23*(4), 464–475. https://doi.org/10.1016/J.CEB.2011.05.004

Cacheiro, P., Westerberg, C. H., Mager, J., Dickinson, M. E., Nutter, L. M. J., Muñoz-Fuentes, V., Hsu, C. W., Van den Veyver, I. B., Flenniken, A. M., McKerlie, C., Murray, S. A., Teboul, L., Heaney, J. D., Lloyd, K. C. K., Lanoue, L., Braun, R. E., White, J. K., Creighton, A. K., Laurin, V., … Smedley, D. (2022). Mendelian gene identification through mouse embryo viability screening. *Genome Medicine*, *14*(1), 119. https://doi.org/10.1186/S13073-022-01118-7

Cardozo, M. J., Sánchez-Bustamante, E., & Bovolenta, P. (2023). Optic cup morphogenesis across species and related inborn human eye defects. *Development (Cambridge, England)*, *150*(2), dev200399. https://doi.org/10.1242/DEV.200399

Castle, A. M. R., Salian, S., Bassan, H., Sofrin-Drucker, E., Cusmai, R., Herman, K. C., Heron, D., Keren, B., Johnstone, D. L., Mears, W., Morlot, S., Nguyen, T. T. M., Rock, R., Stolerman, E., Russo, J., Burns, W. B., Jones, J. R., Serpieri, V., Wallaschek, H., … Campeau, P. M. (2021). Expanding the Phenotypic Spectrum of GPI Anchoring Deficiency Due to Biallelic Variants in GPAA1. *Neurology: Genetics*, *7*(6), e631. https://doi.org/10.1212/NXG.0000000000000631/ASSET/AEEA04C0-32D4-4A1A-A8C0-376205AD71DC/ASSETS/GRAPHIC/NXG.0000000000000631TU1.GIF

Chapple, J. P., & Cheetham, M. E. (2003). The Chaperone Environment at the Cytoplasmic Face of the Endoplasmic Reticulum Can Modulate Rhodopsin Processing and Inclusion Formation. *Journal of Biological Chemistry*, *278*(21), 19087–19094. https://doi.org/10.1074/JBC.M212349200

Chen, C., Ma, B., Wang, Y., Cui, Q., Yao, L., Li, Y., Chen, B., Feng, Y., & Tan, Z. (2023). Structural insight into why S-linked glycosylation cannot adequately mimic the role of natural O-glycosylation. *International Journal of Biological Macromolecules*, *253*, 126649. https://doi.org/10.1016/J.IJBIOMAC.2023.126649

Cheng, H., Nair, G., Walker, T. A., Kim, M. K., Pardue, M. T., Thulé, P. M., Olson, D. E., & Duong, T. Q. (2006). Structural and functional MRI reveals multiple retinal layers. *Proceedings of the National Academy of Sciences of the United States of America*, *103*(46), 17525–17530. https://doi.org/10.1073/PNAS.0605790103/SUPPL_FILE/05790FIG8.PDF

Chrispell, J. D., Rebrik, T. I., & Weiss, E. R. (2015). Electroretinogram analysis of the visual response in zebrafish larvae. *Journal of Visualized Experiments : JoVE*, *2015*(97). https://doi.org/10.3791/52662

Christianson, J. C., & Carvalho, P. (2022). Order through destruction: how ER-associated protein degradation contributes to organelle homeostasis. *The EMBO Journal*, *41*(6). https://doi.org/10.15252/EMBJ.2021109845/ASSET/024E6054-3A75-48A3-B35E-F3F8B1DE650F/ASSETS/GRAPHIC/EMBJ2021109845-FIG-0005-M.PNG

Christianson, J. C., Jarosch, E., & Sommer, T. (2023). Mechanisms of substrate processing during ER-associated protein degradation. *Nature Reviews Molecular Cell Biology 2023 24:11*, *24*(11), 777–796. https://doi.org/10.1038/s41580-023-00633-8

Conroy, L. R., Hawkinson, T. R., Young, L. E. A., Gentry, M. S., & Sun, R. C. (2021). Emerging roles of N-linked glycosylation in brain physiology and disorders. *Trends in Endocrinology & Metabolism*, *32*(12), 980–993. https://doi.org/10.1016/J.TEM.2021.09.006

Cornean, A. (2022). *The role of the medaka protein O-mannosyltransferase 2 across tissues, development and dystroglycanopathies*. https://doi.org/10.11588/HEIDOK.00032151

Cornean, A., Gierten, J., Welz, B., Mateo, J. L., Thumberger, T., & Wittbrodt, J. (2022). Precise in vivo functional analysis of DNA variants with base editing using ACEofBASEs target prediction. *ELife*, *11*. https://doi.org/10.7554/ELIFE.72124

Dabsan, S., Twito, G., Biadsy, S., & Igbaria, A. (2024). Less is better: various means to reduce protein load in the endoplasmic reticulum. *The Febs Journal*, *292*(5), 976. https://doi.org/10.1111/FEBS.17201

Daiger, S. P., Bowne, S. J., & Sullivan, L. S. (2007). Perspective on genes and mutations causing retinitis pigmentosa. *Archives of Ophthalmology (Chicago, Ill. : 1960)*, *125*(2), 151–158. https://doi.org/10.1001/ARCHOPHT.125.2.151

De Graef, D., Mousa, J., Waberski, M. B., & Morava, E. (2022). Mannose treatment improves immune deficiency in mannose phosphate isomerase–congenital disorder of glycosylation: case report and review of literature. *Therapeutic Advances in Rare Disease*, *3*, 26330040221091284. https://doi.org/10.1177/26330040221091283

Del Medico, G., Ferri, L., Procopio, E., Annibalini, G., Barbieri, E., Barone, R., Guerrini, R., Morrone, A., & Stagi, S. (2025). Phosphomannomutase 2-congenital disorder of glycosylation: exploring the role of N-glycosylation on the endocrine axes. *Frontiers in Endocrinology*, *16*, 1594118. https://doi.org/10.3389/FENDO.2025.1594118/BIBTEX

den Hollander, A. I., Roepman, R., Koenekoop, R. K., & Cremers, F. P. M. (2008). Leber congenital amaurosis: genes, proteins and disease mechanisms. *Progress in Retinal and Eye Research*, *27*(4), 391–419. https://doi.org/10.1016/J.PRETEYERES.2008.05.003

Dobson, C. M., Hempel, S. J., Stalnaker, S. H., Stuart, R., & Wells, L. (2013). O-Mannosylation and human disease. *Cellular and Molecular Life Sciences*, *70*(16), 2849–2857. https://doi.org/10.1007/S00018-012-1193-0

Doudna, J. A., & Charpentier, E. (2014). The new frontier of genome engineering with CRISPR-Cas9. *Science*, *346*(6213). https://doi.org/10.1126/SCIENCE.1258096

Elbashir, S. M., Harborth, J., Lendeckel, W., Yalcin, A., Weber, K., & Tuschl, T. (2001). Duplexes of 21-nucleotide RNAs mediate RNA interference in cultured mammalian cells. *Nature*, *411*(6836), 494–498. https://doi.org/10.1038/35078107

Esfandiari, H., Mets, M. B., Kim, K. H., & Kurup, S. P. (2019). Ocular abnormalities in a patient with congenital disorder of glycosylation type Ig. *Ophthalmic Genetics*, *40*(6), 549–552. https://doi.org/10.1080/13816810.2019.1692361

Fisher, P., Thomas-Oates, J., Wood, A. J., & Ungar, D. (2019). The N-Glycosylation Processing Potential of the Mammalian Golgi Apparatus. *Frontiers in Cell and Developmental Biology*, *7*, 462669. https://doi.org/10.3389/FCELL.2019.00157/BIBTEX

Freeze, H. H., Eklund, E. A., Ng, B. G., & Patterson, M. C. (2015). Neurological Aspects of Human Glycosylation Disorders. *Annual Review of Neuroscience*, *38*(Volume 38, 2015), 105–125. https://doi.org/10.1146/ANNUREV-NEURO-071714-034019/1

GAPDH glyceraldehyde-3-phosphate dehydrogenase [Homo sapiens (human)] - Gene - NCBI. (n.d.). Retrieved August 27, 2025, from https://www.ncbi.nlm.nih.gov/gene/2597

Garg, A., & Tsang, S. H. (2024). Retinal Dystrophies. *Microperimetry and Multimodal Retinal Imaging*, 137–142. https://doi.org/10.1007/978-3-642-40300-2_14

Gaudelli, N. M., Komor, A. C., Rees, H. A., Packer, M. S., Badran, A. H., Bryson, D. I., & Liu, D. R. (2017). Programmable base editing of A•T to G•C in genomic DNA without DNA cleavage. *Nature 2017 551:7681*, *551*(7681), 464–471. https://doi.org/10.1038/nature24644

Goth, C. K., Petäjä-Repo, U. E., & Rosenkilde, M. M. (2020). G Protein-Coupled Receptors in the Sweet Spot: Glycosylation and other Post-translational Modifications. *ACS Pharmacology & Translational Science*, *3*(2), 237. https://doi.org/10.1021/ACSPTSCI.0C00016

Grünewald, S. (2009). The clinical spectrum of phosphomannomutase 2 deficiency (CDG-Ia). *Biochimica et Biophysica Acta (BBA) - Molecular Basis of Disease*, *1792*(9), 827–834. https://doi.org/10.1016/J.BBADIS.2009.01.003

Gücüm, S. (2021). *Modeling hypo-N-glycosylation in medaka, Oryzias latipes, to decipher mechanisms of Congenital Disorders of Glycosylation*. https://doi.org/10.11588/HEIDOK.00030086

Gücüm, S., Sakson, R., Hoffmann, M., Grote, V., Becker, C., Pakari, K., Beedgen, L., Thiel, C., Rapp, E., Ruppert, T., Thumberger, T., & Wittbrodt, J. (2021). A patient-based medaka alg2 mutant as a model for hypo-N-glycosylation. *Development (Cambridge, England)*, *148*(11). https://doi.org/10.1242/DEV.199385

Gupta, R., & Brunak, S. (2002). Prediction of glycosylation across the human proteome and the correlation to protein function. *Pacific Symposium on Biocomputing. Pacific Symposium on Biocomputing*, 310–322. https://doi.org/10.1142/9789812799623_0029

Gutierrez-Triana, J. A., Tavhelidse, T., Thumberger, T., Thomas, I., Wittbrodt, B., Kellner, T., Anlas, K., Tsingos, E., & Wittbrodt, J. (2018). Efficient single-copy HDR by 5’ modified long dsDNA donors. *ELife*, *7*. https://doi.org/10.7554/ELIFE.39468

Haltiwanger, R. S., & Lowe, J. B. (2004). Role of glycosylation in development. *Annu. Rev. Biochem.*, *73*, 491–537. https://doi.org/10.1146/annurev.biochem.73.011303.074043

Hang, J., Wang, J., Lu, M., Xue, Y., Qiao, J., & Tao, L. (2022). Protein O-mannosylation across kingdoms and related diseases: From glycobiology to glycopathology. *Biomedicine & Pharmacotherapy*, *148*, 112685. https://doi.org/10.1016/J.BIOPHA.2022.112685

Hao, C., Zou, Q., Bai, X., & Shi, W. (2025). Effect of glycosylation on protein folding: From biological roles to chemical protein synthesis. *IScience*, *28*(6). https://doi.org/10.1016/J.ISCI.2025.112605

Harms, H. K., Zimmer, K. P., Kurnik, K., Bertele-Harms, R. M., Weidinger, S., & Reiter, K. (2002). Oral mannose therapy persistently corrects the severe clinical symptoms and biochemical abnormalities of phosphomannose isomerase deficiency. *Acta Paediatrica, International Journal of Paediatrics*, *91*(10), 1065–1072. https://doi.org/10.1080/080352502760311566

Hartong, D. T., Berson, E. L., & Dryja, T. P. (2006). Retinitis pigmentosa. *Lancet*, *368*(9549), 1795–1809. https://doi.org/10.1016/S0140-6736(06)69740-7

Haynes, P. A. (1998). Phosphoglycosylation: a new structural class of glycosylation? *Glycobiology*, *8*(1), 1–5. https://doi.org/10.1093/GLYCOB/8.1.1

Heermann, S., Schütz, L., Lemke, S., Krieglstein, K., & Wittbrodt, J. (2015). Eye morphogenesis driven by epithelial flow into the optic cup facilitated by modulation of bone morphogenetic protein. *ELife*, *4*(4). https://doi.org/10.7554/ELIFE.05216

Helenius, A., & Aebi, M. (2004). Roles of N-linked glycans in the endoplasmic reticulum. *Annual Review of Biochemistry*, *73*, 1019–1049. https://doi.org/10.1146/ANNUREV.BIOCHEM.73.011303.073752

Helleday, T., Lo, J., van Gent, D. C., & Engelward, B. P. (2007). DNA double-strand break repair: from mechanistic understanding to cancer treatment. *DNA Repair*, *6*(7), 923–935. https://doi.org/10.1016/J.DNAREP.2007.02.006

Hetz, C., Zhang, K., & Kaufman, R. J. (2020). Mechanism, regulation and functions of the unfolded protein response. *Nature Reviews. Molecular Cell Biology*, *21*(8), 421. https://doi.org/10.1038/S41580-020-0250-Z

Howe, K., Clark, M. D., Torroja, C. F., Torrance, J., Berthelot, C., Muffato, M., Collins, J. E., Humphray, S., McLaren, K., Matthews, L., McLaren, S., Sealy, I., Caccamo, M., Churcher, C., Scott, C., Barrett, J. C., Koch, R., Rauch, G. J., White, S., … Stemple, D. L. (2013). The zebrafish reference genome sequence and its relationship to the human genome. *Nature 2013 496:7446*, *496*(7446), 498–503. https://doi.org/10.1038/nature12111

Hsu, P. D., Lander, E. S., & Zhang, F. (2014). Development and applications of CRISPR-Cas9 for genome engineering. *Cell*, *157*(6), 1262–1278. https://doi.org/10.1016/J.CELL.2014.05.010/ATTACHMENT/DCDA5CE7-B3A3-46A9-B89D-CCD4D57F0BCD/MMC1.MP4

Huo, J., Ren, S., Gao, P., Wan, D., Rong, S., Li, X., Liu, S., Xu, S., Sun, K., Guo, B., Wang, P., Yu, B., Wu, J., Wang, F., & Sun, T. (2020). ALG13 participates in epileptogenesis via regulation of GABAA receptors in mouse models. *Cell Death Discovery 2020 6:1*, *6*(1), 1–11. https://doi.org/10.1038/s41420-020-00319-6

Hyer, J., Kuhlman, J., Afif, E., & Mikawa, T. (2003). Optic cup morphogenesis requires pre-lens ectoderm but not lens differentiation. *Developmental Biology*, *259*(2), 351–363. https://doi.org/10.1016/S0012-1606(03)00205-7

Ichinose, T., & Habib, S. (2022). On and off signaling pathways in the retina and the visual system. *Frontiers in Ophthalmology*, *2*, 989002. https://doi.org/10.3389/FOPHT.2022.989002

Ives, C. M., Singh, O., D'Andrea, S., Fogarty, C. A., Harbison, A. M., Satheesan, A., Tropea, B., & Fadda, E. (2024). Restoring protein glycosylation with GlycoShape. *Nature Methods 2024 21:11*, *21*(11), 2117–2127. https://doi.org/10.1038/s41592-024-02464-7

Iwamatsu, T. (2004). Stages of normal development in the medaka Oryzias latipes. *Mechanisms of Development*, *121*(7–8), 605–618. https://doi.org/10.1016/J.MOD.2004.03.012

Jaeken, J. (2013). Congenital disorders of glycosylation. *Handbook of Clinical Neurology*, *113*, 1737–1743. https://doi.org/10.1016/B978-0-444-59565-2.00044-7

Jahncke, J. N., & Wright, K. M. (2023). The many roles of dystroglycan in nervous system development and function. *Developmental Dynamics*, *252*(1), 61–80. https://doi.org/10.1002/DVDY.516

Jay, M. (1982). On the heredity of retinitis pigmentosa. *Br J Ophthalmol*, *66*(7), 405–416. https://doi.org/10.1136/bjo.66.7.405

Jean, D., Ewan, K., & Gruss, P. (1998). Molecular regulators involved in vertebrate eye development. *Mechanisms of Development*, *76*(1–2), 3–18. https://doi.org/10.1016/S0925-4773(98)00117-8

Jinek, M., Chylinski, K., Fonfara, I., Hauer, M., Doudna, J. A., & Charpentier, E. (2012). A programmable dual-RNA-guided DNA endonuclease in adaptive bacterial immunity. *Science*, *337*(6096), 816–821. https://doi.org/10.1126/SCIENCE.1225829/SUPPL_FILE/JINEK.SM.PDF

Jumper, J., Evans, R., Pritzel, A., Green, T., Figurnov, M., Ronneberger, O., Tunyasuvunakool, K., Bates, R., Žídek, A., Potapenko, A., Bridgland, A., Meyer,

C., Kohl, S. A. A., Ballard, A. J., Cowie, A., Romera-Paredes, B., Nikolov, S., Jain, R., Adler, J., … Hassabis, D. (2021). Highly accurate protein structure prediction with AlphaFold. *Nature 2021 596:7873*, *596*(7873), 583–589. https://doi.org/10.1038/s41586-021-03819-2

Kamarus Jaman, N., Rehsi, P., Henderson, R. H., Löbel, U., Mankad, K., & Grunewald, S. (2021). SRD5A3-CDG: Emerging Phenotypic Features of an Ultrarare CDG Subtype. *Frontiers in Genetics*, *12*, 737094. https://doi.org/10.3389/FGENE.2021.737094/FULL

Kasahara, M., Naruse, K., Sasaki, S., Nakatani, Y., Qu, W., Ahsan, B., Yamada, T., Nagayasu, Y., Doi, K., Kasai, Y., Jindo, T., Kobayashi, D., Shimada, A., Toyoda, A., Kuroki, Y., Fujiyama, A., Sasaki, T., Shimizu, A., Asakawa, S., … Kohara, Y. (2007a). The medaka draft genome and insights into vertebrate genome evolution. *Nature 2007 447:7145*, *447*(7145), 714–719. https://doi.org/10.1038/nature05846

Kasahara, M., Naruse, K., Sasaki, S., Nakatani, Y., Qu, W., Ahsan, B., Yamada, T., Nagayasu, Y., Doi, K., Kasai, Y., Jindo, T., Kobayashi, D., Shimada, A., Toyoda, A., Kuroki, Y., Fujiyama, A., Sasaki, T., Shimizu, A., Asakawa, S., … Kohara, Y. (2007b). The medaka draft genome and insights into vertebrate genome evolution. *Nature 2007 447:7145*, *447*(7145), 714–719. https://doi.org/10.1038/nature05846

Kim, P. (2024). Understanding the Unfolded Protein Response (UPR) Pathway: Insights into Neuropsychiatric Disorders and Therapeutic Potentials. *Biomolecules & Therapeutics*, *32*(2), 183. https://doi.org/10.4062/BIOMOLTHER.2023.181

Kirchmaier, S., Naruse, K., Wittbrodt, J., & Loosli, F. (2015). The Genomic and Genetic Toolbox of the Teleost Medaka (Oryzias latipes). *Genetics*, *199*(4), 905. https://doi.org/10.1534/GENETICS.114.173849

Kitamura, N., & Galligan, J. J. (2023). A global view of the human post-translational modification landscape. *Biochemical Journal*, *480*(16), 1241. https://doi.org/10.1042/BCJ20220251

Kluesner, M. G., Nedveck, D. A., Lahr, W. S., Garbe, J. R., Abrahante, J. E., Webber, B. R., & Moriarity, B. S. (2018). EditR: A Method to Quantify Base Editing from Sanger Sequencing. *The CRISPR Journal*, *1*(3), 239–250. https://doi.org/10.1089/CRISPR.2018.0014

Koblan, L. W., Doman, J. L., Wilson, C., Levy, J. M., Tay, T., Newby, G. A., Maianti, J. P., Raguram, A., & Liu, D. R. (2018). Improving cytidine and adenine base editors by expression optimization and ancestral reconstruction. *Nature Biotechnology*, *36*(9), 843–848. https://doi.org/10.1038/NBT.4172

Komor, A. C., Kim, Y. B., Packer, M. S., Zuris, J. A., & Liu, D. R. (2016). Programmable editing of a target base in genomic DNA without double-stranded DNA cleavage. *Nature 2015 533:7603*, *533*(7603), 420–424. https://doi.org/10.1038/nature17946

Koopman, M., Hetz, C., & Nollen, E. A. A. (2019). Saved by the Matrix: UPR Independent Survival under ER Stress. *Cell*, *179*(6), 1246–1248. https://doi.org/10.1016/J.CELL.2019.11.012

Kumari, D., & Brodsky, J. L. (2021). The Targeting of Native Proteins to the Endoplasmic Reticulum-Associated Degradation (ERAD) Pathway: An Expanding Repertoire of Regulated Substrates. *Biomolecules*, *11*(8), 1185. https://doi.org/10.3390/BIOM11081185

Lachke, S. A., & Maas, R. L. (2010). Building the Developmental Oculome: Vertebrate Eye Development and Disease. *Wiley Interdisciplinary Reviews. Systems Biology and Medicine*, *2*(3), 305. https://doi.org/10.1002/WSBM.59

Lefeber, D. J., Freeze, H. H., Steet, R., & Kinoshita, T. (2022). Congenital Disorders of Glycosylation. *Physician's Guide to the Diagnosis, Treatment, and Follow-Up of Inherited Metabolic Diseases, Second Edition*, 1335–1396. https://doi.org/10.1101/GLYCOBIOLOGY.4E.45

Lefeber, D. J., Morava, E., & Jaeken, J. (2011). How to find and diagnose a CDG due to defective N-glycosylation. *Journal of Inherited Metabolic Disease*, *34*(4), 849–852. https://doi.org/10.1007/S10545-011-9370-0

Li, Y., Liu, Y., Yang, H., Zhang, T., Naruse, K., & Tu, Q. (2020). Dynamic transcriptional and chromatin accessibility landscape of medaka embryogenesis. *Genome Research*, *30*(6), 924–937. https://doi.org/10.1101/GR.258871.119

Lingam, G., Sen, A. C., Lingam, V., Bhende, M., Padhi, T. R., & Xinyi, S. (2021). Ocular coloboma—a comprehensive review for the clinician. *Eye 2021 35:8*, *35*(8), 2086–2109. https://doi.org/10.1038/s41433-021-01501-5

Lischik, C. Q., Adelmann, L., & Wittbrodt, J. (2019). Enhanced in vivo-imaging in medaka by optimized anaesthesia, fluorescent protein selection and removal of pigmentation. *PLOS ONE*, *14*(3), e0212956. https://doi.org/10.1371/JOURNAL.PONE.0212956

Lolley, R. N., & Lee, R. H. (1990). Cyclic GMP and photoreceptor function. *FASEB Journal : Official Publication of the Federation of American Societies for Experimental Biology*, *4*(12), 3001–3008. https://doi.org/10.1096/FASEBJ.4.12.1697545

Lopez, M. A., Klotz, J., & Cardon, M. (2025). Neuromuscular disorders. *Capute and Accardo' s Neurodevelopmental Disabilities in Infancy and Childhood*, 403–425. https://doi.org/10.1016/B978-0-12-824060-1.00039-0

Lu, S., Liang, S., Wu, Y., Liu, J., Lin, L., Huang, G., & Ning, H. (2023). Mannose phosphate isomerase gene mutation leads to a congenital disorder of glycosylation: A rare case report and literature review. *Frontiers in Pediatrics*, *11*, 1150367. https://doi.org/10.3389/FPED.2023.1150367/BIBTEX

Ma, X., Sechrest, E. R., Fajardo, D., Zhu, P., Dyka, F., Wang, Y., Lobanova, E., Boye, S. E., Baehr, W., & Deng, W. T. (2022). Gene Therapy in Opn1mw−/−/Opn1sw−/− Mice and Implications for Blue Cone Monochromacy Patients with Deletion Mutations. *Human Gene Therapy*, *33*(13–14), 708. https://doi.org/10.1089/HUM.2021.298

Magalhães, C. G. De, Cvekl, A., Jaeger, R. G., & Yan, C. Y. I. (2024). Lens Placode Modulates Extracellular Matrix Formation During Early Eye Development. *BioRxiv*, 2023.11.30.569417. https://doi.org/10.1101/2023.11.30.569417

Mahabadi, N., & Khalili, Y. Al. (2023). Neuroanatomy, Retina. *StatPearls*. https://www.ncbi.nlm.nih.gov/books/NBK545310/

Marquardt, T., & Gruss, P. (2002). Generating neuronal diversity in the retina: one for nearly all. *Trends in Neurosciences*, *25*(1), 32–38. https://doi.org/10.1016/S0166-2236(00)02028-2

Martinez-Morales, J. R., & Wittbrodt, J. (2009). Shaping the vertebrate eye. *Current Opinion in Genetics & Development*, *19*(5), 511–517. https://doi.org/10.1016/J.GDE.2009.08.003

Mendes, H. F., Van Der Spuy, J., Chapple, J. P., & Cheetham, M. E. (2005). Mechanisms of cell death in rhodopsin retinitis pigmentosa: implications for therapy. *Trends in Molecular Medicine*, *11*(4), 177–185. https://doi.org/10.1016/J.MOLMED.2005.02.007

Mikula Mrstakova, S., & Kozmik, Z. (2024). Genetic analysis of medaka fish illuminates conserved and divergent roles of Pax6 in vertebrate eye development. *Frontiers*

in Cell and Developmental Biology, *12*, 1448773. https://doi.org/10.3389/FCELL.2024.1448773/FULL

Miles, A., & Tropepe, V. (2021). Retinal Stem Cell 'Retirement Plans': Growth, Regulation and Species Adaptations in the Retinal Ciliary Marginal Zone. *International Journal of Molecular Sciences*, *22*(12), 6528. https://doi.org/10.3390/IJMS22126528

Minakata, S., Manabe, S., Inai, Y., Ikezaki, M., Nishitsuji, K., Ito, Y., & Ihara, Y. (2021). Protein C-Mannosylation and C-Mannosyl Tryptophan in Chemical Biology and Medicine. *Molecules*, *26*(17), 5258. https://doi.org/10.3390/MOLECULES26175258

Molday, R. S., & Moritz, O. L. (2015). Photoreceptors at a glance. *Journal of Cell Science*, *128*(22), 4039–4045. https://doi.org/10.1242/JCS.175687/-/DC1

Morava, E., Wosik, H. N., Sykut-Cegielska, J., Adamowicz, M., Guillard, M., Wevers, R. A., Lefeber, D. J., & Cruysberg, J. R. M. (2009). Ophthalmological abnormalities in children with congenital disorders of glycosylation type I. *The British Journal of Ophthalmology*, *93*(3), 350–354. https://doi.org/10.1136/BJO.2008.145359

Moremen, K. W., Tiemeyer, M., & Nairn, A. V. (2012a). *Vertebrate protein glycosylation: diversity, synthesis and function*. https://doi.org/10.1038/nrm3383

Moremen, K. W., Tiemeyer, M., & Nairn, A. V. (2012b). Vertebrate protein glycosylation: diversity, synthesis and function. *Nature Reviews Molecular Cell Biology 2012 13:7*, *13*(7), 448–462. https://doi.org/10.1038/nrm3383

Moulton, J. D., & Yan, Y. L. (2008). Using Morpholinos to Control Gene Expression. *Current Protocols in Molecular Biology*, *83*(1), 26.8.1-26.8.29. https://doi.org/10.1002/0471142727.MB2608S83

Murray, A. R., Fliesler, S. J., & Al-Ubaidi, M. R. (2009). Rhodopsin: the Functional Significance of Asn-Linked Glycosylation and Other Post-translational Modifications. *Ophthalmic Genetics*, *30*(3), 109. https://doi.org/10.1080/13816810902962405

Murray, A. R., Vuong, L., Brobst, D., Fliesler, S. J., Peachey, N. S., Gorbatyuk, M. S., Naash, M. I., & Al-Ubaidi, M. R. (2015). Glycosylation of rhodopsin is necessary for its stability and incorporation into photoreceptor outer segment discs. *Human Molecular Genetics*, *24*(10), 2709. https://doi.org/10.1093/HMG/DDV031

Neubert, P., & Strahl, S. (2016). Protein O-mannosylation in the early secretory pathway. *Current Opinion in Cell Biology*, *41*, 100–108. https://doi.org/10.1016/J.CEB.2016.04.010

Ng, B. G., & Freeze, H. H. (2018). Perspectives on Glycosylation and its Congenital Disorders. *Trends in Genetics : TIG*, *34*(6), 466. https://doi.org/10.1016/J.TIG.2018.03.002

Ng, B. G., Freeze, H. H., Himmelreich, N., Blau, N., & Ferreira, C. R. (2024). Clinical and biochemical footprints of congenital disorders of glycosylation: Proposed nosology. *Molecular Genetics and Metabolism*, *142*(1), 108476. https://doi.org/10.1016/J.YMGME.2024.108476

Niklaus, S., Glasauer, S. M. K., Kovermann, P., Farshori, K. F., Cadetti, L., Früh, S., Rieser, N. N., Gesemann, M., Zang, J., Fahlke, C., & Neuhauss, S. C. F. (2024). Glutamate transporters are involved in direct inhibitory synaptic transmission in the vertebrate retina. *Open Biology*, *14*(7). https://doi.org/10.1098/RSOB.240140

Norden, C. (2023). A Fish Eye View: Retinal Morphogenesis from Optic Cup to Neuronal Lamination. *Annual Review of Cell and Developmental Biology*, *39*(Volume 39, 2023), 175–196. https://doi.org/10.1146/ANNUREV-CELLBIO-012023-013036/CITE/REFWORKS

Nwagbo, U., Parvez, S., Maschek, J. A., & Bernstein, P. S. (2024). Elovl4b knockout zebrafish as a model for ocular very-long-chain PUFA deficiency. *Journal of Lipid Research*, *65*(3), 100518. https://doi.org/10.1016/J.JLR.2024.100518

Ohno, M. (2014). Roles of eIF2α kinases in the pathogenesis of Alzheimer's disease. *Frontiers in Molecular Neuroscience*, *7*(1 APR), 83350. https://doi.org/10.3389/FNMOL.2014.00022/BIBTEX

Okamoto, N., Kadoya, M., & Wada, Y. (2025). Clinical and Molecular Features of Patients With Congenital Disorders of Glycosylation in Japan. *JIMD Reports*, *66*(3), e70011. https://doi.org/10.1002/JMD2.70011

Oommen, D., Kizhakkedath, P., Jawabri, A. A., Varghese, D. S., & Ali, B. R. (2020). Proteostasis Regulation in the Endoplasmic Reticulum: An Emerging Theme in the Molecular Pathology and Therapeutic Management of Familial Hypercholesterolemia. *Frontiers in Genetics*, *11*, 570355. https://doi.org/10.3389/FGENE.2020.570355/XML

Otaki, M., Hirane, N., Natsume-Kitatani, Y., Nogami Itoh, M., Shindo, M., Kurebayashi, Y., & Nishimura, S. I. (2022). Mouse tissue glycome atlas 2022 highlights inter-organ variation in major N-glycan profiles. *Scientific Reports 2022 12:1*, *12*(1), 1–15. https://doi.org/10.1038/s41598-022-21758-4

Pakari, K., Jakab, S., Salvador, E. S., Thiel, C., Wittbrodt, J., & Thumberger, T. (2025). Establishing an auxin-inducible GFP nanobody-based acute protein knockdown system to mimic hypomorphic mutations during early medaka embryogenesis. *BioRxiv*, 2025.05.23.655727. https://doi.org/10.1101/2025.05.23.655727

Palczewski, K. (2006). G protein-coupled receptor rhodopsin. *Annual Review of Biochemistry*, *75*, 743–767. https://doi.org/10.1146/ANNUREV.BIOCHEM.75.103004.142743

Panda, S. K., Sanchez-Pajares, I. R., Rehman, A., Del Vecchio, V., Mele, L., Chipurupalli, S., Robinson, N., & Desiderio, V. (2025). ER stress and/or ER-phagy in drug resistance? Three coincidences are proof. *Cell Communication and Signaling : CCS*, *23*(1), 223. https://doi.org/10.1186/S12964-025-02232-W

Paprocka, J. (2023). Neurological Consequences of Congenital Disorders of Glycosylation. *Advances in Neurobiology*, *29*, 219–253. https://doi.org/10.1007/978-3-031-12390-0_8

Paprocka, J., Jezela-Stanek, A., Tylki-Szymańska, A., & Grunewald, S. (2021). Congenital Disorders of Glycosylation from a Neurological Perspective. *Brain Sciences*, *11*(1), 1–25. https://doi.org/10.3390/BRAINSCI11010088

Park, C., & Zhang, J. (2011). Genome-Wide Evolutionary Conservation of N-Glycosylation Sites. *Molecular Biology and Evolution*, *28*(8), 2351. https://doi.org/10.1093/MOLBEV/MSR055

Parmeggiani, F., S. Sorrentino, F., Ponzin, D., Barbaro, V., Ferrari, S., & Di Iorio, E. (2011). Retinitis Pigmentosa: Genes and Disease Mechanisms. *Current Genomics*, *12*(4), 238. https://doi.org/10.2174/138920211795860107

Patil, D. N., Pantalone, S., Cao, Y., Laboute, T., Novick, S. J., Singh, S., Savino, S., Faravelli, S., Magnani, F., Griffin, P. R., Singh, A. K., Forneris, F., & Martemyanov, K. A. (2023). Structure of the photoreceptor synaptic assembly of the extracellular matrix protein pikachurin with the orphan receptor GPR179. *Science Signaling*, *16*(795), eadd9539. https://doi.org/10.1126/SCISIGNAL.ADD9539

Pérez-Núñez, D., García-Belmonte, R., Riera, E., Fernández-Sesma, M. H., Vigara-Astillero, G., & Revilla, Y. (2023). Signal peptide and N-glycosylation of N-

terminal-CD2v determine the hemadsorption of African swine fever virus. *Journal of Virology*, *97*(10), e01030-23. https://doi.org/10.1128/JVI.01030-23

Praissman, J. L., & Wells, L. (2014). Mammalian O-mannosylation pathway: Glycan structures, enzymes, and protein Substrates. *Biochemistry*, *53*(19), 3066–3078. https://doi.org/10.1021/BI500153Y/ASSET/IMAGES/LARGE/BI-2014-00153Y_0007.JPEG

Puller, C., Ivanova, E., Euler, T., Haverkamp, S., & Schubert, T. (2013). OFF bipolar cells express distinct types of dendritic glutamate receptors in the mouse retina. *Neuroscience*, *243*, 136–148. https://doi.org/10.1016/J.NEUROSCIENCE.2013.03.054

Ramachandra Rao, S., Skelton, L. A., Wu, F., Onysk, A., Spolnik, G., Danikiewicz, W., Butler, M. C., Stacks, D. A., Surmacz, L., Mu, X., Swiezewska, E., Pittler, S. J., & Fliesler, S. J. (2020). Retinal Degeneration Caused by Rod-Specific Dhdds Ablation Occurs without Concomitant Inhibition of Protein N-Glycosylation. *IScience*, *23*(6), 101198. https://doi.org/10.1016/J.ISCI.2020.101198

Ran, F. A., Hsu, P. D., Wright, J., Agarwala, V., Scott, D. A., & Zhang, F. (2013). Genome engineering using the CRISPR-Cas9 system. *Nature Protocols*, *8*(11), 2281–2308. https://doi.org/10.1038/NPROT.2013.143

Rees, H. A., & Liu, D. R. (2018). Base editing: precision chemistry on the genome and transcriptome of living cells. *Nature Reviews Genetics 2018 19:12*, *19*(12), 770–788. https://doi.org/10.1038/s41576-018-0059-1

Reily, C., Stewart, T. J., Renfrow, M. B., & Novak, J. (2019). Glycosylation in health and disease. *Nature Reviews. Nephrology*, *15*(6), 346. https://doi.org/10.1038/S41581-019-0129-4

Richter, M. F., Zhao, K. T., Eton, E., Lapinaite, A., Newby, G. A., Thuronyi, B. W., Wilson, C., Koblan, L. W., Zeng, J., Bauer, D. E., Doudna, J. A., & Liu, D. R. (2020). Phage-assisted evolution of an adenine base editor with improved Cas domain compatibility and activity. *Nature Biotechnology*, *38*(7), 883–891. https://doi.org/10.1038/S41587-020-0453-Z

Roller, R. F., Malik, A., Carillo, M. A., Garg, M., Rella, A., Raulf, M. K., Lepenies, B., Seeberger, P. H., & Varón Silva, D. (2020). Semisynthesis of functional glycosylphosphatidylinositol-anchored proteins. *Angewandte Chemie International Edition*, *59*(29), 12035–12040. https://doi.org/10.1002/ANIE.202002479

Rubio-Fernández, M., Uribe, M. L., Vicente-Tejedor, J., Germain, F., Susín-Lara, C., Quereda, C., Montoliu, L., De La Villa, P., Martín-Nieto, J., & Cruces, J. (2018). Impairment of photoreceptor ribbon synapses in a novel Pomt1 conditional knockout mouse model of dystroglycanopathy. *Scientific Reports 2018 8:1*, *8*(1), 1–15. https://doi.org/10.1038/s41598-018-26855-x

Salom, D., Jin, H., Gerken, T. A., Yu, C., Huang, L., & Palczewski, K. (2019). Human red and green cone opsins are O-glycosylated at an N-terminal Ser/Thr–rich domain conserved in vertebrates. *The Journal of Biological Chemistry*, *294*(20), 8123. https://doi.org/10.1074/JBC.RA118.006835

Sarria, I., Pahlberg, J., Cao, Y., Kolesnikov, A. V., Kefalov, V. J., Sampath, A. P., & Martemyanov, K. A. (2015). Sensitivity and kinetics of signal transmission at the first visual synapse differentially impact visually-guided behavior. *ELife*, *4*(4), e06358. https://doi.org/10.7554/ELIFE.06358

Sato, S., Omori, Y., Katoh, K., Kondo, M., Kanagawa, M., Miyata, K., Funabiki, K., Koyasu, T., Kajimura, N., Miyoshi, T., Sawai, H., Kobayashi, K., Tani, A., Toda, T., Usukura, J., Tano, Y., Fujikado, T., & Furukawa, T. (2008). Pikachurin, a dystroglycan ligand, is essential for photoreceptor ribbon synapse formation. *Nature Neuroscience 2008 11:8*, *11*(8), 923–931. https://doi.org/10.1038/nn.2160

Schindelin, J., Arganda-Carreras, I., Frise, E., Kaynig, V., Longair, M., Pietzsch, T., Preibisch, S., Rueden, C., Saalfeld, S., Schmid, B., Tinevez, J. Y., White, D. J., Hartenstein, V., Eliceiri, K., Tomancak, P., & Cardona, A. (2012). Fiji: an open-source platform for biological-image analysis. *Nature Methods 2012 9:7*, *9*(7), 676–682. https://doi.org/10.1038/nmeth.2019

Schjoldager, K. T., Narimatsu, Y., Joshi, H. J., & Clausen, H. (2020). Global view of human protein glycosylation pathways and functions. *Nat. Rev. Mol. Cell Biol.*, *21*(12), 729–749. https://doi.org/10.1038/s41580-020-00294-x

Schneider, N., Sundaresan, Y., Gopalakrishnan, P., Beryozkin, A., Hanany, M., Levanon, E. Y., Banin, E., Ben-Aroya, S., & Sharon, D. (2022). Inherited retinal diseases: Linking genes, disease-causing variants, and relevant therapeutic modalities. *Progress in Retinal and Eye Research*, *89*. https://doi.org/10.1016/j.preteyeres.2021.101029

Sheeladevi, S., Lawrenson, J. G., Fielder, A. R., & Suttle, C. M. (2016). Global prevalence of childhood cataract: a systematic review. *Eye*, *30*(9), 1160. https://doi.org/10.1038/EYE.2016.156

Sinn, R., & Wittbrodt, J. (2013). An eye on eye development. *Mechanisms of Development*, *130*(6–8), 347–358. https://doi.org/10.1016/J.MOD.2013.05.001

Sirisi, S., Folgueira, M., López-Hernández, T., Minieri, L., Pérez-Rius, C., Gaitán-Peñas, H., Zang, J., Martínez, A., Capdevila-Nortes, X., De La Villa, P., Roy, U., Alia, A., Neuhauss, S., Ferroni, S., Nunes, V., Estévez, R., & Barrallo-Gimeno, A. (2014). Megalencephalic leukoencephalopathy with subcortical cysts protein 1 regulates glial surface localization of GLIALCAM from fish to humans. *Human Molecular Genetics*, *23*(19), 5069–5086. https://doi.org/10.1093/HMG/DDU231

Snellman, J., Kaur, T., Shen, Y., & Nawy, S. (2008). Regulation of ON Bipolar Cell Activity. *Progress in Retinal and Eye Research*, *27*(4), 450. https://doi.org/10.1016/J.PRETEYERES.2008.03.003

Sparks, S. E., & Krasnewich, D. M. (2017). Congenital Disorders of N-Linked Glycosylation and Multiple Pathway Overview. *GeneReviews®*. https://www.ncbi.nlm.nih.gov/books/NBK1332/

Stemmer, M., Thumberger, T., Del Sol Keyer, M., Wittbrodt, J., & Mateo, J. L. (2015). CCTop: An Intuitive, Flexible and Reliable CRISPR/Cas9 Target Prediction Tool. *PLOS ONE*, *10*(4), e0124633. https://doi.org/10.1371/JOURNAL.PONE.0124633

Stevens-Sostre, W. A., & Hoon, M. (2024). Cellular and Molecular Mechanisms Regulating Retinal Synapse Development. *Annual Review of Vision Science*, *10*(1), 377–402. https://doi.org/10.1146/ANNUREV-VISION-102122-105721

Sung, C. H., Makino, C., Baylor, D., & Nathans, J. (1994). A rhodopsin gene mutation responsible for autosomal dominant retinitis pigmentosa results in a protein that is defective in localization to the photoreceptor outer segment. *Journal of Neuroscience*, *14*(10), 5818–5833. https://doi.org/10.1523/JNEUROSCI.14-10-05818.1994

Sung, C. H., Schneider, B. G., Agarwal, N., Papermaster, D. S., & Nathans, J. (1991). Functional heterogeneity of mutant rhodopsins responsible for autosomal dominant retinitis pigmentosa. *Proceedings of the National Academy of Sciences of the United States of America*, *88*(19), 8840–8844. https://doi.org/10.1073/PNAS.88.19.8840

Suzuki, R. (2025). *Genetic Variation Shapes Visual-Motor Behavior: Insights from High-Throughput Optomotor Response Screening in Medaka Inbred Population*. https://doi.org/10.11588/HEIDOK.00037319

Tam, B. M., & Moritz, O. L. (2009). The role of rhodopsin glycosylation in protein folding, trafficking, and light-sensitive retinal degeneration. *Journal of Neuroscience*, *29*(48), 15145–15154. https://doi.org/10.1523/JNEUROSCI.4259-09.2009

Taniguchi, Y., Takeda, S., Furutani-Seiki, M., Kamei, Y., Todo, T., Sasado, T., Deguchi, T., Kondoh, H., Mudde, J., Yamazoe, M., Hidaka, M., Mitani, H., Toyoda, A., Sakaki, Y., Plasterk, R. H. A., & Cuppen, E. (2006). Generation of medaka gene knockout models by target-selected mutagenesis. *Genome Biology*, *7*(12), R116. https://doi.org/10.1186/GB-2006-7-12-R116

Taniuchi, S., Miyake, M., Tsugawa, K., Oyadomari, M., & Oyadomari, S. (2016). Integrated stress response of vertebrates is regulated by four eIF2α kinases. *Scientific Reports 2016 6:1*, *6*(1), 1–11. https://doi.org/10.1038/srep32886

Thiel, C., Lübke, T., Matthijs, G., von Figura, K., & Körner, C. (2006). Targeted disruption of the mouse phosphomannomutase 2 gene causes early embryonic lethality. *Molecular and Cellular Biology*, *26*(15), 5615–5620. https://doi.org/10.1128/MCB.02391-05

Thompson, D. A., Lyons, R. J., Liasis, A., Russell-Eggitt, I., Jägle, H., & Grünewald, S. (2012). Retinal On-Pathway Deficit in Congenital Disorder of Glycosylation Due to Phosphomannomutase Deficiency. *Archives of Ophthalmology*, *130*(6), 712–719. https://doi.org/10.1001/ARCHOPHTHALMOL.2012.130

Thoreson, W. B., & Mangel, S. C. (2012). Lateral interactions in the outer retina. *Progress in Retinal and Eye Research*, *31*(5), 407. https://doi.org/10.1016/J.PRETEYERES.2012.04.003

Thumberger, T., Tavhelidse-Suck, T., Gutierrez-Triana, J. A., Cornean, A., Medert, R., Welz, B., Freichel, M., & Wittbrodt, J. (2022). Boosting targeted genome editing using the hei-tag. *ELife*, *11*. https://doi.org/10.7554/ELIFE.70558

Tikidji-Hamburyan, A., Reinhard, K., Storchi, R., Dietter, J., Seitter, H., Davis, K. E., Idrees, S., Mutter, M., Walmsley, L., Bedford, R. A., Ueffing, M., Ala-Laurila, P., Brown, T. M., Lucas, R. J., & Münch, T. A. (2017). Rods progressively escape saturation to drive visual responses in daylight conditions. *Nature Communications 2017 8:1*, *8*(1), 1–17. https://doi.org/10.1038/s41467-017-01816-6

Uribe, M. L., Haro, C., Ventero, M. P., Campello, L., Cruces, J., & Martín-Nieto, J. (2016). Expression pattern in retinal photoreceptors of POMGnT1, a protein

involved in muscle-eye-brain disease. *Molecular Vision*, *22*, 658. https://pmc.ncbi.nlm.nih.gov/articles/PMC4911909/

van Overbeek, M., Capurso, D., Carter, M. M., Thompson, M. S., Frias, E., Russ, C., Reece-Hoyes, J. S., Nye, C., Gradia, S., Vidal, B., Zheng, J., Hoffman, G. R., Fuller, C. K., & May, A. P. (2016). DNA Repair Profiling Reveals Nonrandom Outcomes at Cas9-Mediated Breaks. *Molecular Cell*, *63*(4), 633–646. https://doi.org/10.1016/J.MOLCEL.2016.06.037

Varadi, M., Bertoni, D., Magana, P., Paramval, U., Pidruchna, I., Radhakrishnan, M., Tsenkov, M., Nair, S., Mirdita, M., Yeo, J., Kovalevskiy, O., Tunyasuvunakool, K., Laydon, A., Žídek, A., Tomlinson, H., Hariharan, D., Abrahamson, J., Green, T., Jumper, J., … Velankar, S. (2024). AlphaFold Protein Structure Database in 2024: providing structure coverage for over 214 million protein sequences. *Nucleic Acids Research*, *52*(D1), D368–D375. https://doi.org/10.1093/NAR/GKAD1011

Varki, A. (2017). Biological roles of glycans. *Glycobiology*, *27*(1), 3–49. https://doi.org/10.1093/GLYCOB/CWW086

Varki, A., Cummings, R. D., Esko, J. D., Stanley, P., Hart, G. W., Aebi, M., Mohnen, D., Kinoshita, T., Packer, N. H., Prestegard, J. H., Schnaar, R. L., & Seeberger, P. H. (2022). Essentials of Glycobiology [Internet]. *Cold Spring Harbor (NY)*, 892. https://doi.org/10.1101/9781621824213

Vasireddy, V., Wong, P., & Ayyagari, R. (2010). Genetics and molecular pathology of Stargardt-like macular degeneration. *Progress in Retinal and Eye Research*, *29*(3), 191–207. https://doi.org/10.1016/J.PRETEYERES.2010.01.001

Wang, Q., Groenendyk, J., & Michalak, M. (2015). Glycoprotein Quality Control and Endoplasmic Reticulum Stress. *Molecules 2015, Vol. 20, Pages 13689-13704*, *20*(8), 13689–13704. https://doi.org/10.3390/MOLECULES200813689

Wang, S., He, Q., Ye, J., Kang, Z., Zheng, Q., Liu, S., He, J., & Sun, L. (2020). N-linked Glycosylation and its Potential Application in Drug Development. *Health Science Journal*, *14*(5), 0–0. https://doi.org/10.36648/1791-809X.14.5.743

Weixel, T., Wolfe, L., & Macnamara, E. F. (2024). Genetic counseling for congenital disorders of glycosylation (CDG). *Journal of Genetic Counseling*, *33*(6), 1358. https://doi.org/10.1002/JGC4.1856

Wittbrodt, J., Shima, A., & Schartl, M. (2002). Medaka — a model organism from the far east. *Nature Reviews Genetics 2001 3:1*, *3*(1), 53–64. https://doi.org/10.1038/nrg704

Wu, D., Huang, L. F., Chen, X. C., Huang, X. R., Li, H. Y., An, N., Tang, J. X., Liu, H. F., & Yang, C. (2023). Research progress on endoplasmic reticulum homeostasis in kidney diseases. *Cell Death & Disease 2023 14:7*, *14*(7), 1–12. https://doi.org/10.1038/s41419-023-05905-x

Wu, J., Lu, K., Xie, R., Zhu, C., Luo, Q., & Liang, X. F. (2025). The Beneficial Role of the Thyroid Hormone Receptor Beta 2 (thrb2) in Facilitating the First Feeding and Subsequent Growth in Medaka as Fish Larval Model. *Cells*, *14*(5), 386. https://doi.org/10.3390/CELLS14050386/S1

Xu, J., Meng, X., Wu, F., Deng, H., & Fu, S. (2019). *ER stress drives ER-to-Golgi trafficking of ATF6 by blocking its membrane insertion*. https://doi.org/10.1101/822965

Xu, W., Liu, X., Han, W., & Zhao, L. (2022). Editorial: Genetic features contributing to eye development and disease. *Frontiers in Cell and Developmental Biology*, *10*, 1008907. https://doi.org/10.3389/FCELL.2022.1008907/BIBTEX

Yau, K. W., & Hardie, R. C. (2009). Phototransduction Motifs and Variations. *Cell*, *139*(2), 246. https://doi.org/10.1016/J.CELL.2009.09.029

Yoon, H., Ringland, A., Anderson, J. J., Sran, S., Elziny, S., Huynh, C., Shinagawa, N., Badertscher, S., Corrigan, R. R., Mashburn-Warren, L., Amari, F., Chen, M., Coppola, V., Crino, P. B., & Bedrosian, T. A. (2024). Mouse models of Slc35a2 brain mosaicism reveal mechanisms of mild malformations of cortical development with oligodendroglial hyperplasia in epilepsy. *Epilepsia*, *65*(12), 3717. https://doi.org/10.1111/EPI.18166

York, W. S., Mazumder, R., Ranzinger, R., Edwards, N., Kahsay, R., Aoki-Kinoshita, K. F., Campbell, M. P., Cummings, R. D., Feizi, T., Martin, M., Natale, D. A., Packer, N. H., Woods, R. J., Agarwal, G., Arpinar, S., Bhat, S., Blake, J., Castro, L. J. G., Fochtman, B., … Zhang, W. (2020). GlyGen: Computational and Informatics Resources for Glycoscience. *Glycobiology*, *30*(2), 72–73. https://doi.org/10.1093/GLYCOB/CWZ080

Zhao, Z., Shang, P., Mohanraju, P., & Geijsen, N. (2023). Prime editing: advances and therapeutic applications. *Trends in Biotechnology*, *41*(8), 1000–1012. https://doi.org/10.1016/J.TIBTECH.2023.03.004

Acknowledgements

This thesis marks the end of a long and challenging, but also deeply rewarding, journey. I could never have reached this point without the generous support, guidance, and friendship of so many people over these four years.

First and foremost, I would like to thank Jochen for giving me the incredible opportunity to join your lab. Thanks to you, I have learned so much, not only about science but also about myself. Your advice has shaped the way I think as a scientist in so many ways. Thank you for being there when things became complicated; your ability to turn problems into new perspectives is truly inspiring.

It is impossible to continue without thanking Thomas. You gave me an opportunity I never thought I would have. Your enthusiasm for science is exemplary, and you have always been ready for heated discussions about the “impossibilities” of science — and to share a mutual coffee addiction. I have learned lessons from you on so many levels that it is hard to put them into words. I will always remember that during my first three months in the lab, although you barely knew me, when you found out I might have to spend Christmas in Germany alone, you offered me your home so I wouldn’t feel lonely at that time of the year.

Britta, thank you for your support over these years as part of my committee, always showing empathy and patience.

Lázaro, I am so grateful for your help during the committee meetings. I always felt I could turn to you to discuss any topic, even if, in your own words, you “had no clue what I was doing.” Our little chats in Spanish became moments of reflection and gave rise to some of the best anecdotes.

Sergio, thank you for stepping in and adapting to the circumstances to serve as an examiner for this defense.

To my dear Glyco Club, I could not have asked for a better team to work with. I especially want to thank Phoebe, it was a genuine pleasure to supervise you and see you grow as a scientist (complaints included!). You were my right hand in these last months, and I can never thank you enough. But especially Kaisa, I could not have asked for a better benchmate. Together we have grown, laughed, and cried a lot in these four years, but we forged a relationship of mutual support in which I always knew

you had my back. I am sure that wherever life takes us, what we built here is stronger than gluten.

To everyone on the fifth floor, I can't choose just a few, so I will mention you as we often do when taking attendance: by bays.

At the heart of our floor, our wonderful administration team, Eva and Frederike, you are the light and support for all of us. You have always been there for any issue, whether administrative or helping us find a knitting pattern. You've saved more than one day with your improvised "bars," and I hope you never change and always continue to brighten every place you go.

Although not a bay themselves, I have to give special mention to our amazing technicians, Claudia, Rebecca, and especially Beate, always attentive to our needs and fostering a good atmosphere in the lab; and my dear Tanja, who knows how everything works. Working with you has been wonderful, and I will carry with me what I learned from seeing how the gears of the lab truly turn.

To my second bay in the lab, Bay 1, my little confessional, Risa, my girl of a thousand moves, you stand out for your perseverance and dedication, but for me it was your ability to always notice and care for those around you despite being busy with a thousand things.

And my dear Rashi, what can I say, you were the first person I connected with when I arrived. You are an example of hard work and kindness. Thank you for always taking care of me and for answering my eight million questions a day.

Where it all started, Bay 2, even as it transitions, will always be where I picture the MIKK team. Bettina, always ready to smile and patiently go over the logic of transcription to synthesize in situ probes, and Philip, running around building his own army of PhD students in medaka, always with coffee in hand and dad jokes in training. Thank you for the laughs and the discussions.

The antibacterial (organoid) bay, Lucie, you are an example of how passion for the lab can drive everything; a true multitasking mom whose curiosity is inspiring. Christina, one of the great discoveries in the lab, you are the definition of a ray of sunshine, please never change. You embody resilience, adaptability, and proof that the sugar rush is real. And my favorite Dr. Dr., Cassian, the person with the clearest opinions I know; somehow you became the person I confided my problems in and also had the most random conversations with.

The former immune bay (Bay 4), Joergen, thank you for the heated discussions about the retina (or anything else, as long as there was coffee and a few bad jokes), and for now being ready to psychoanalyze us all with your UMAPs in hand.
And my dear Jana, mi Alemana reggaetonera , thank you for always being there when I needed you, for cheering me up, and for officially giving me permission for my little mental breakdowns. Words fall short to describe how much I admire you, both personally and scientifically. I know you will go far.
To the most recent addition, who floats between bays, Laura, in the short time we have shared, you have become very important to me. Your passion for your work is amazing, and I hope you keep it up because people like you make a difference both personally and professionally.
Thanks also to the other labs on the fifth floor, the Lemke Lab: Steffen, Verena, Andreas, Girish, for the great conversations and shared coffees; the Centanin Lab Jasmin, Karen, and all their students, especially Javi, thank you for listening to my rants that started as five-minute chats and turned into hours, you have been an incredible support throughout these years; and the Wienhardt Lab, Venera, you are an example of perseverance, it has been a great pleasure sharing discussions with you and learning new perspectives in lab meetings; Kristaps and Fariha, our time together wasn't long but always pleasant; Natalia, thank you for looking out for me so I wouldn't work at unreasonable hours (even if I didn't always listen) and for sharing one of my favorite experiences in Germany, the CONCERT.
Last but not least, my dear Anthi, thank you for being truly amazing, a woman always at the forefront while caring for those around you. You have always been there to talk and to look out for me despite the distance. I cannot wait to see what life has in store for you.
I also owe thanks to those not on the fifth floor but essential to our work , the wonderful fish facility team, Marzena, Antonino, Erik, and Crysta, for taking care of our beloved fish so we could continue with our "crazy things," and Gero, almost an extension of the lab, a key figure for our research to move forward.
I must also thank my dear friends Sara, Jaione, Irene, Ana, and Déborah. Even across the distance, you always knew when to call and have supported me in everything I do , you have believed in me more than I ever imagined.
To my therapist Marta, thank you for helping me so much in this last year; without your guidance and support, I'm not sure this thesis would have come to fruition.

Finally, but by no means least, to my family, my aunts Virginia and María, examples of strong, caring women, always sending love even from afar; my beloved cousins Clara, María and Tamara, like sisters to me, always supporting me I love you dearly. I also want to remember those who always believed in me but are no longer here. My grandparents Adolfo, Francisca, and Encarnita, my uncle Eloy, and my dear cousin Jesús Domingo.

And most of all, my core family. My parents Isabel and Manolo and my little brother Adolfo. You are essential to who I am. Thank you for always supporting me, believing in me, and encouraging me to fight for what I want without you, none of this would have been possible.

Mamá, you have always been an example to me of a strong, resilient woman.

Papá, you taught me from an early age to think for myself and not let anything break me.

Adolfo, you have always been a fighter, and I know you will achieve everything you set your mind to.

To all those mentioned here thank you so much for your guidance, patience, and unwavering support. I will always carry you with me.

Publication

Manuscripts in peer review

Deep learning predicts tissue outcomes in retinal organoids. Cassian Afting, Norin Bhatti, Christina Schlagheck, Encarnación Sánchez Salvador, Laura Herrera-Astorga, Rashi Agarwal, Risa Suzuki, Nicolaj Hackert, Hanns-Martin Lorenz, Lucie Zilova, Joachim Wittbrodt, Tarik Exner
https://doi.org/10.1101/2025.02.19.639061

Establishing an auxin-inducible GFP nanobody-based acute protein knockdown system to mimic hypomorphic mutations during early medaka embryogenesis. Kaisa Pakari, Sevinç Jakab, Encarnación Sánchez Salvador, Christian Thiel, Joachim Wittbrodt, Thomas Thumberger
https://doi.org/10.1101/2025.05.23.655727

Declaration

I herewith declare that I have written the PhD thesis “The importance of *N*-glycosylation in photoreceptor maintenance and degeneration in medaka” on my own with no other sources and aids than quoted.

Heidelberg, 2025

List of Figures

Figure 1. Schematic overview of major glycosylation types. 2
Figure 2. Schematic representation of the *N*-glycosylation pathway. 6
Figure 3. ER-associated degradation (ERAD) of misfolded polypeptides. 8
Figure 4. *N*-linked glycosylation in neuronal signaling. 11
Figure 5. Layered architecture of the camera-type retina. 14
Figure 6. CRISPR-Cas genome editing mechanisms..... 17
Figure 7. alg2 mutants in medaka reveal systemic and retina-specific defects. 21
Figure 8. Methodological pipeline for glycoprotein-related candidate genes selection in retinal degeneration. 27
Figure 9. Design and outcome of base editing to disrupt NXS/T motifs reveal a trade-off between editing efficiency and embryonic viability. 29
Figure 10. Base editor-mediated targeting of glycosylated Asn residues causes severe developmental delays. 30
Figure 11. Experimental design for HDR-mediated donor insertion targeting *N*-glycosylation sites. 32
Figure 12. No gross morphological phenotype in *opn1sw* homozygous mutants..... 33
Figure 13. Characterization of a stable CRISPR/Cas9 edited *opn1sw* line. 35
Figure 14 No gross morphological phenotype in *rhodopsin* homozygous mutants. . 36
Figure 15. Loss of rod photoreceptors physiologically impacts on light sensitivity in rhodopsin mutants. 37
Figure 16. Optomotor response as a functional analysis for visual acuity in *rhodopsin* mutant line. 38
Figure 17. Image acquisition and cell quantification strategy for photoreceptor analysis. 40
Figure 18. Knockout of candidate genes affects rod photoreceptor proportion in Medaka retina. 43
Figure 19. Experimental design for mRNA rescue assays. 45
Figure 20. Reconstitution of wildtype but mutant Rhodopsin rescues knockout induced photoreceptor loss 47
Figure 21. Histological and morphological evaluation of opsin mRNA rescue in medaka hatchlings. 50

Figure 22. Histological and morphological evaluation of Elovl4 mRNA rescue in medaka hatchlings. 52
Figure 23. Histological and morphological evaluation of Pikachurin mRNA rescue in medaka hatchlings. 54
Figure 24. Distinct structural effects of disrupting *N*-linked glycosylation sites in *opn1sw* 65

Supplementary Figure 1. HDR-mediated donor insertion targeting *N*-glycosylation sites in *rho*..... 129
Supplementary Figure 2. HDR-mediated donor insertion targeting *N*-glycosylation sites in *elovl4*. 129
Supplementary Figure 3. Candidates knockout effect in photoreceptors population in the retina. 130
Supplementary Figure 4. OMR analysis of the *rho* knockout line to study swimming behaviour. 131
Supplementary Figure 5. OMR as a tool to understand more than visual acuity. ... 132
Supplementary Figure 6. Comparative analyses of the photoreceptor population in rhodopsin mRNA rescue. 133
Supplementary Figure 7. Comparative analyses of the photoreceptor population in opn1sw mRNA rescue. 134
Supplementary Figure 8. Comparative analyses of the photoreceptor population in *elvl4b* mRNA rescue. 135
Supplementary Figure 9. Comparative analyses of the photoreceptor population in *pikachurin* mRNA rescue. 136
Supplementary Figure 10. Structural effects of *N*-linked glycosylation disruption in Rhodopsin (Rho). 137
Supplementary Figure 11. Predicted structural consequences of *N*-linked glycosylation site substitutions in Elovl4. 138
Supplementary Figure 12. Predicted structural consequences of *N*-linked glycosylation site substitutions in Pikachurin. 139

List of Tables

Table 1. Medaka (Oryzias latipes) lines used in this thesis 69
Table 2,. Plasmids use in this thesis 70
Table 3. Primers used in this thesis 71
Table 4. Single guide RNAs used in this thesis 73
Table 5. Antibiotics used in this thesis 74
Table 6. Enzymes and buffers used in this thesis 74
Table 7. Chemical and reagents used in this thesis 75
Table 8. Antibodies used in this thesis 76
Table 9. Commercial kits used in this thesis 76
Table 10. Media and solutions used in this thesis. All buffer are prepares in H_2O if not indicated otherwise 76
Table 11. Consumables used in this thesis 78
Table 12. Equipment and Instruments used in this thesis. 79
Table 13. Sotware and online tools used in this thesis 80
Table 14. Standar components of PCR Master Mix 81
Table 15. Standard PCR settings 81
Table 16. Ligation reaction components. 83
Table 17. Oligo annealing thermocycler program 83
Table 18. Components of KDL treatment of PCR product. 84
Table 19. Plasmids used for in vitro mRNA synthesis are listed together with the corresponding enzymes used for linearization and promoters leading transcription. 86
Table 20. List of injection mixes used in this thesis. 87

Supplementary Table 1. Genes analyzed in this thesis 97